The University Of Sheffield.

Aromatic Selection for Surrogate Jet Fuel

By

James Cronly

Supervisors

Dr Bhupendra Khandelwal
Prof Bill Nimmo
Dr Kevin Hughes

A thesis submitted to the Department of Mechanical Engineering in partial fulfilment of the requirements for the degree of "Doctor of Philosophy".

Department of Mechanical Engineering
University of Sheffield
United Kingdom
January 2023

Abstract

The aromatic component of jet fuel is limited to 25% by volume in the current aviation specification for commercial flight. Aromatic hydrocrabons present in petroleum fuels are acknowledged to contribute to the formation of polycyclic aromatic hydrocarbons (PAH) and subsequently high levels of soot. Non-volatile particulate matter in the form of soot, or black carbon, contributes significantly to global warming, contrail formation, the degradation of combustion liner walls and has an adverse effect on human health. There is significant interest in minimising the emission levels of non-volatile particulate matter and smoke by varying the source and chemical composition of Jet fuel. While the overall volumetric proportion of aromatics is currently regulated, there is no indication as to the effect of the molecular composition of the aromatic component. The composition of conventional and surrogate fuels with specific focus on the variation of aromatic type and composition is investigated in this work with the goal of reducing the emission of nVPM in the aviation sector. In this report, a metadata analysis of the correlation between aromatic and naphthalene content and the smoke point of fuel samples finds a week correlation between the two variables as determined by the Jet fuel specification. The composition of Jet fuel is then discussed as is the contemporary understanding of the various formation mechanisms of non-volatile particulate matter. A literature review of the effect of molecular composition of the aromatic component on soot formation found a correlation with total aromatic volume, naphthalene volume, hydrogen mass proportion and the proportion of ring carbon present, although no individual factor agreed consistently with experimental results. A knowledge gap was identified as to

the effect of varying individual aromatic species in an aviation context. This report presents experimental data collected using a Rolls Royce Tay single can combustor using extractive laser induced incandescence to measure the mass concentration of black carbon emitted by thirteen different aromatic species in four blend proportions (7.5%, 12.5%, 17.5%, 22.5% vol/vol) in an alkene paraffinic surrogate for Jet-A. Data for the same configuration is also presented using a differential mobility analyser to determine the size distribution and total number concentration when combusting sixteen aromatics in three blend proportions (8%, 13%, 18% vol/vol). Fuel global density and the aggregate Unified YSI were found to be of statistical significance and regression models were developed to estimate black carbon mass and number exhaust concentrations with high accuracy. Meta-analysis indicates that, on balance of beneficial properties, p-Cymene is a strong potential candidate for inclusion as an aromatic component in sustainable jet fuel.

Acknowledgements

Firstly, I'd like to thank my main supervisor, Dr. Bhupendra Khandelwal for his encouragement and support throughout my time at the University of Sheffield. Despite many setbacks and complications, he was a constant source of reassurance. I'd also like to thank Prof. Bill Nimmo and Dr. Kevin Hughes for taking over my supervision under difficult circumstances and getting me over the finishing line. I'd also like to thank Dr. Simon Blakey for his advice and stewardship of the Low Carbon Combustion Centre during his time there.

The skills and expertise of the staff of the LCCC were invaluable to me and I would not have been able to complete my body of work without their support. I'd like to express my sincere gratitude to Ihab Ahmed, Tim Haycock, Andrew Hemstock and fuels specialist David Dunstan. I'd like to acknowledge my fellow doctoral students, both past and current; Dr. Emamode Ubogo, Dr. Jonathan Knapton, Dr. Lukai Cheng, Dr. Charith Wijesinghe, Huanrong Lei and Chenxing Ling.

I'd like to thank my parents, John and Trish, my wife's parents, Steve and Linda, my brothers, Tom and Luke, and friends, James, Ian, Duncan, Jake, Matt, Dave, John, Sacha, Gary and Rod, all of whom refused to let their eyes glaze over when I discussed fuel. Finally, and most importantly, I'd like to acknowledge the love and support of my wife, Laura, and sons, Elliott and Miles. My wife knows nothing of fuel, but has known what to say and when to say it during every setback over the years to get me back on course.

Publications to Date

Under Construction

- **Cronly J, Zheng L, Ubogu E A, Ahmed I, Knapton J N, Zhang Y & Khandelwal** (2023) - *Optimisation of aromatic content and black carbon emissions in formulated jet fuel*

In Review

- **Khandelwal B, Zheng L, Boylu R, Cronly J, Ahmed I & Zhang Y** (2023) - *Imaging based investigation on alternative jet fuels flames near lean blowout conditions in a gas turbine combustor* Fuel

Published to Date of Submission

- **Zheng L, Boylu R, Cronly J, Ahmed I, Ubogu E & Khandelwal B** (2022) - *Experimental study on the impact of alternative jet fuel properties and derived cetane number on lean blowout limit* The Aeronautical Journal 1-20

- **Zheng L, Singh P, Cronly J, Ubogu A, Ahmed I, Ling C, Zhang Y & Khandelwal B** (2021) - *Impact of Aromatic Structures and Content in Formulated Fuel for Jet Engine Applications on Particulate Emissions.* Journal of Energy Resources Technology, Vol 143/122301-1, ASME

- **Kauffmann M, Cronly J, Ahmed I S & Khandelwal B** (2019) - *An investigation of varying fuel sources used in jet engines on particulate matter.* An investigation of varying fuel sources used in jet engines on particulate matter

- **Khandelwal B, Cronly J, Ahmed I S, Wijesinghe C J & Lewis C** (2019) - *The effect of alternative fuels on gaseous and Particulate Matter (PM) emission performance in an Auxiliary Power Unit.* The Aeronautical Journal 1-19

- **Zheng L, Cronly J, Ubogu E, Ahmed I, Zhang Y & Khandelwal B** - *Experimental investigation on alternative fuel composition performance using a gas turbine combustor.* Applied Energy 238 pp.1530-1542

- **Ubogu E A, Cronly J, Khandelwal B & Roy S** (2018) - *Determination of the effective density and fractal dimension of PM emissions from an aircraft auxiliary power unit.* Journal of Environmental Sciences 74 pp.11-18

- **Zheng L, Ling C, Ubogu E A, Cronly J, Ahmed I, Zhang Y & Khandelwal B** (2018) - *Effects of alternative fuel properties on particulate matter produced in a gas turbine combustor.* Energy and Fuels 32(9) pp.9883-9897

- **Khandelwal B, Cronly J & Okai K** (2017) *Testing alternative fuels, solar thermal systems* - Aerospace America 55(11) pp.6-64

- **Zheng L, Ubogu E A, Ahmed I, Cronly J, Knapton J N & Khandelwal B** (2017) *Test and Analysis of Alternative Jet Fuel Combustion Performance.* - Federal Aviation Administration Report

Abbreviations

LCCC	Low Carbon Combustion Centre
nvPM	Non-Volatile Particulate Matter
BC	Black Carbon
EC	Elemental Carbon
HACA	Hydrogen Abstraction Acetylene Addition
PAC	Phenyl Addition Cyclization
RQL	Rich-Quench-Lean Combustor
GCMS	Gas Chromatography Mass Spectrometry
LACF	Low Aromatic Content Fuel
SN	Smoke Number
ASTM	American Society for Testing and Materials
UK MOD	United Kingdom Ministry of Defence
CIS	Confederation of Independent States
AQSIQ	General Administration of Quality, Supervision, Inspection and Quarantine
SP	Smoke Point
ICAO	International Civil Aviation Organisation
GCxGC	Two-Dimensional Gas Chromatography
PAH	Polycyclic Aromatic Hydrocarbon
TSI	Threshold Sooting Index
YSI	Yield Sooting Index
H/C	Hydrogen to Carbon Ratio

DMF	Diesel Marine Fuel
UV	Ultra-violet
FIA	Flow Injection Analysis
LII	Laser Induced Incandescence
DMS	Differential Mobility Scanner
CPMA	Centrifugal Particle Mass Analyser
FTIR	Fourier Transform Infrared Spectroscopy
MEL	Mobile Emissions Laboratory
RC	Ring Carbon

Contents

List of Figures

List of Tables

Chapter 1

Introduction

1.1 Context of Proposed Thesis

Gas turbine engines utilised for the purposes of aviation propulsion, commonly referred to as jet engines, use liquid fuel as a propellant to provide the energy necessary to power the Brayton cycle. While gas turbine cycles can and do operate using gaseous fuel for terrestrial power generation, the lower energy density of gaseous fuel currently renders it impractical for aviation purposes due to the reduced operating range [20]. The ease with which liquid fuel can be transported and handled in comparison to solid and gaseous fuels is also advantageous. The ongoing availability and relative low cost of liquid fuel has also provided a groundwork for the successful proliferation of the jet engine. Liquid fuel has been used in jet engines since their original inception. The reciprocating engines of the proceeding generation of piston aircraft could operate using aviation gasoline similar to that used in automobiles of the time. One of the key attributes of the gas turbine engine is the ability to use a wide range of fuels. While it was perfectly feasible for initial jet engines to operate using aviation gasoline, it's use for non-aviation military and civilian operations during World War II and over the post-war years was prioritised. Instead, kerosene would become the mainstay fuel used for the newly developed gas turbine. Kerosene is derived from petroleum and is obtained by fractional distillation and is composed of hydrocarbons with boiling points of approximately $150°C$-$300°C$.

Combustion continues to play an important role in power generation, heating, and automotive and aerospace transportation. The composition of the fuel used in combustion is of significant interest and represents the focus of this study, with

a specific focus on aerospace applications. Figure 1.1.1 shows the anticipated fuel consumption of commercial airlines between 2005 and 2050, showing the anticipated effect of moving from conventional to various proportions of alternative fuels [1].

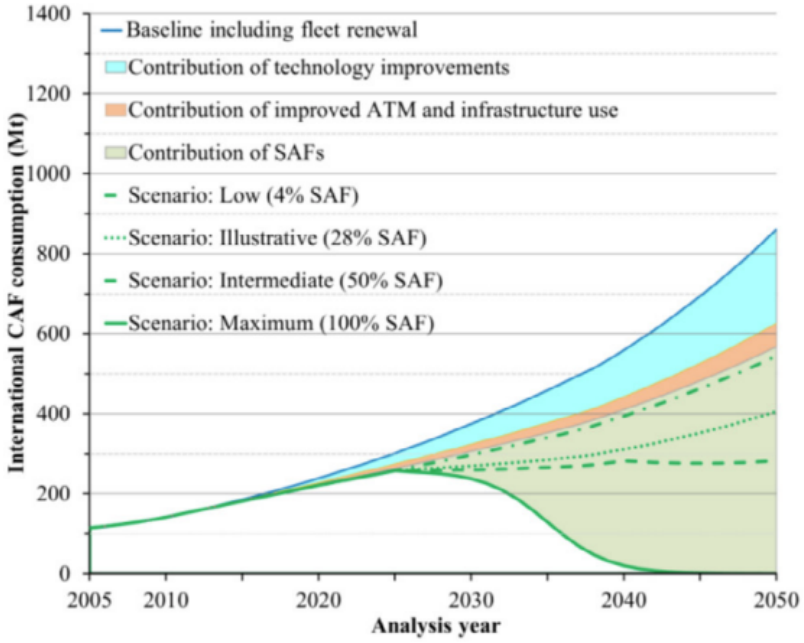

Figure 1.1.1: Total anticipated fuel consumption of global aviation between 2005 and 2050 [1]

It should be noted that Covid-19 pandemic significantly reduced the consumption of jet fuel. The total number of commercial flights only regularly exceeded pre-pandemic levels in mid-2022, and the demand for jet fuel is not expected to reach pre-pandemic levels of 8 million barrels a day until around 2027 [21].

While there has been increased interest in utilising alternative sources of energy in recent years, with a particular emphasis on sustainability, combustion is still expected to represent a large proportion of total energy use in aviation for decades to come [22, 23, 24], predominantly due to its higher specific energy density compared to current and proposed battery concepts, and the general availability of petroleum sources. As a consequence, there is demand for cleaner, more environmentally friendly combustion technologies and techniques to mitigate the negative side effects of combustion, with a particular focus on minimising the emission of greenhouse gases and harmful particulates [24, 25, 26]. In the wider research community, there also is incentive to understand the fundamental combustion mechanics that determine the occurrence of particulate emissions which will help in providing

models for other combustion applications away from aerospace applications.

Aviation fuel for use in commercial gas turbine engines is primarily composed of kerosene obtained by the fractional distillation of crude oil. Kerosene must pass a series of specification tests after which it can then be referred to as Jet Fuel. Jet Fuel is composed of many different hydrocarbon types which can be sub-categorised based on their molecular structure and behaviour. Fuel will behave differently depending on the relative proportion of each hydrocarbon group present. There has been significant industrial and research interest in recent years in diversifying the sources of Jet Fuel away from solely relying on petroleum sources obtained from crude oil supplies [26, 27]. These fuels have come to be called alternative fuels and many, dependent on the feed-stock and production process used, have been approved for use in supplementing petroleum derived jet fuel [27, 28] up to 50% by volume [29]. The diversification of fuel sources away from kerosene introduces fuel with highly variable molecular compositions and has raised questions as to compatibility with existing infrastructure, legacy engines, fuel supply systems, and also regarding the potential for optimisation and the development of fuel idealised for a particular application. Conventional fuels are typically composed of hydrocarbons of various molecular masses and configurations and the proportion of each type present has various effects on the combustion performance and emissions profile of a particular platform. An important component of conventional liquid fuel is the proportion and type of aromatic content included. The impact of the aromatic content of Jet Fuel is well established in the literature and Jet Fuel specification. There is a strong association between the proportion of aromatic content in a fuel and its emissions profile, in particular with regard to the size and mass of non- volatile particulate matter (nvPM) produced, with aromatic content known to contribute to the formation black carbon (BC) or smoke. Consequently, the aromatic content of jet fuel is typically limited to no more than 25% of the total volume and under certain circumstances, polycyclic aromatics (napthalenes) are limited to 3% of the total volume. These upper limits have been arrived at somewhat arbitrarily however, as the is no evidential basis for these specific values. The production of nvPM in the form of BC and smoke, is generally considered an undesirable consequence of the combustion process and there is significant interest in reducing their emission

levels [30]. BC is uniquely a by-product of the combustion process and its fine, carbonaceous particles have a strong radiative effect, and subsequently, contribute to anthropomorphic global warming [22, 31]. BC is estimated to be the second greatest contributor to global warming, second only to carbon dioxide. This radiative effect also adversely affects engine longevity, as radiative heat transfer is increased which damages combustor wall linings.

For automotive and aerospace applications, fuel has a secondary role as a coolant and a promoter of seal swell, which prevents leaks between joined fuel lines. Secondary considerations such as these, amongst others, place additional constraints on the composition of fuels as further performance requirements must be met. Aromatics generally promote swell in the seals used to join fuel lines [32], and its inclusion is mandated by volume in alternative fuels to meet this requirement to prevent leaks. This is especially a concern for legacy vehicles due to potential decades of operation. Aromatics also generally have a higher volumetric energy density than other forms of hydrocarbon, which negatively affects the gravimetric energy density as required by the specification, but can be useful in optimising the range of a fully fuelled aircraft where mass is not a consideration, such as military application. The introduction of drop-in fuels has also led to the introduction for a lower limit of aromatic content of 8% to mitigate the concerns of a potentially statistically low content kerosene base blended in equal proportion with a low or no aromatic content fuel.

For civilian aviation purposes, the various factors create a limit between 8% and 25% by volume of aromatic content. These limits however, have been arrived at somewhat arbitrarily without empirical evidence to provide justification for their inclusion. There is also a gap in the literature as to the performance of different types and combinations of aromatic content, which may affect these limits significantly.

1.2 Kerosene

Kerosene derived fuels obtained from petroleum contain a significant number of molecular components, with as many as a 1000 different organic compounds present [5, 33]. The specification method for determining the aromatic component of jet fuel using ASTM D 1319 [34] is capable of resolving the proportion of hydrocarbon

components into three types; aromatics, olefins and saturates, although only the aromatic proportion is required to be reported. Table 1.1 qualitatively summarises the relative contributions of each hydrocarbon type to key metrics of fuel performance [35, 18].

Table 1.1: Potential contribution of each hydrocarbon class to selected Jet Fuel properties [18]

Jet Fuel Property	Hydrocarbon Class			
	n-Paraffin	Isoparaffin	Napthene	Aromatic
Gravimetric Energy Content	+	+	0	-
Volumetric Energy Content	-	-	0	+
Combustion Quality	+	+	+	-
Low Temperature Fluidity	–	0/+	+	0/-

"+" indicates beneficial effect, "0" a neutral effect and "-" is a detrimental effect

For a given boiling range of Kerosene from around $150°C$-$300°C$, there are potentially hundreds, if not thousands of various molecular species of hydrocarbons [36]. An exact determination of the number and type is very difficult to ascertain due to the current limitations of technologies used to categorise hydrocarbons.

Generally, there is no one hydrocarbon type that is universally beneficial to every metric in isolation as each has its own relative merit to contribute. There is no intent or consideration however, using conventional routes for producing Jet Fuel, as to predetermining the optimum presence of each type due to the economics and practicalities of the refining process. In contrast to automotive gasoline, there is no differentiation between the various grades or types of Jet Fuel at the point of purchase in commercial aviation, omitting consideration of military grades. Due to the homogeneity of the commercial aviation fuel market, there is little incentive for a producer to optimise a fuel compared to its competitors, as there is no mechanism in the market for their fuel to be rewarded as superior. It might be assumed that a given refinery's main goal is to meet the specification as determined by regulation without significant regard as to its exact composition.

Due to the substantial volume of aviation fuel consumed each year, and the limited requirements of reporting composition for certification, the exact makeup of the vast majority of jet fuel by hydrocarbon type is not certain. The introduction of alternative blends of known composition has led to increased interest in determining the exact components and proportions present in petroleum derived Jet Fuels.

While there are a variety of analytical techniques outside the specification that can be used to sub-categorise hydrocarbon types, the current method which provides the greatest insight is through the use of comprehensive two-dimensional gas chromatography (GCxGC). A GCxGC [2] breakdown of a given fuel sample is shown in Figure 1.2.1.

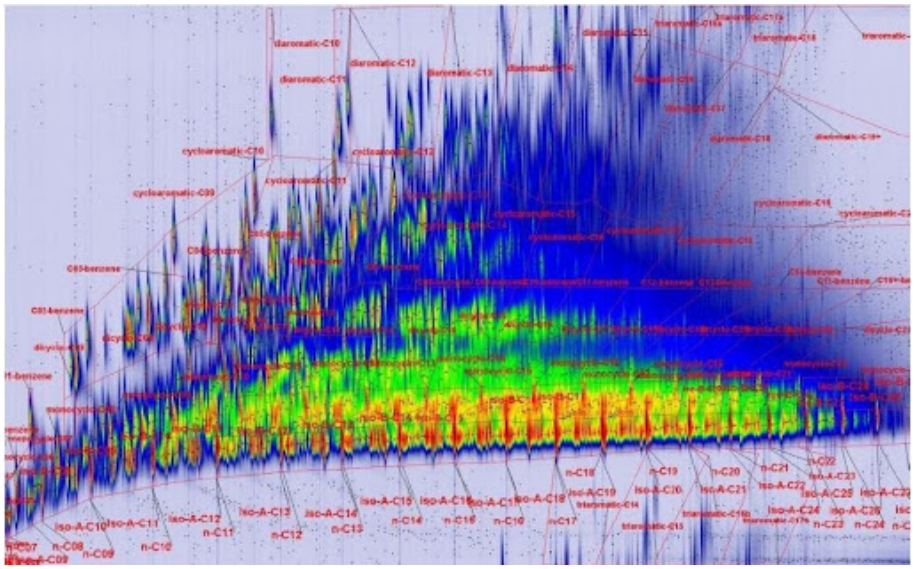

Figure 1.2.1: GCxGC Hydrocarbon Group Type Analysis [2]

This technique allows categorisation of fuel components into relevant groups based on hydrocarbon type and mass, and perhaps provides the most comprehensive overview currently available for analysing Jet Fuel composition. For a given result however, the technique is unable to accurately resolve the various isomers of a given group. For example, a C2-alkylbenzene category of 3.5% by mass potentially includes three separate isomers, m-xylene, o-xylene and p-xylene, each of which has its own propensity to produce soot. This absence of clarity is particularly problematic for groups with a higher molecular mass, such as C5-alkylbenzenes, which may contain hundreds of specific isomers, each with their own soot forming propensity. So, while each category can be quantified, the technology is not currently available to individually isolate each specific molecule present. It is not unreasonable to suggest that any aromatic molecule with a boiling point in the given specification range may be assumed to potentially included in a given sample of petroleum derived Jet Fuel.

1.3 Jet Fuel Specification

Kerosene obtained via fractional distillation must pass through a series of specification tests before it can be classified and approved for use as a Jet Fuel. There are four primary bodies that determine the specifications which producers and users must adhere to in order to meet the criteria for approval in order to ensure regional and global uniformity of commercial fuel supply.

1.3.1 ASTM International (formerly American Society for Testing and Materials)

ASTM international is an international standards organisation that determines the specification for Jet A and Jet A-1. The organisation operates independently of government but in many US state and federal authorities its standards are regulated as mandatory. The current specification standard for Jet A and Jet A-1 is contained in ASTM D1655 [37]. Jet A is predominantly produced and used exclusively within the USA and as such, ASTM D1655 is generally considered the standard for American jet fuel.

1.3.2 United Kingdom Ministry of Defence.

The UK MOD determines the jet fuel specification for commercial and military use. The current specification, Defence Standard 91-91 (DEF STAN 91-91) [35] is used for Jet A-1, which is widely used outside of the United States. While ASTM D 1655 contains its own specification for Jet A-1, DEF STAN 91-91 is considered the main specification for Jet A-1 internationally. In practical terms there is very little difference between D1655 and 91-91 and they are considered as synonymous by most national governing bodies.

1.3.3 Russian Federation

The use of commercial aviation fuel in the Commonwealth of Independent States (CIS), which is primarily comprised of eastern Europe and much of the Middle East, is determined by the Russian government. GOST 10227 is the standard used to classify TS-1, the main fuel used for commercial applications.

1.3.4 AQSIQ - General Administration of Quality Supervision, Inspection and Quaranteen of the People's Republic of China

The AQSIQ uses GB 6537-2006 to determine the specification for No.3 Jet Fuel, the main commercial jet fuel used in the People's Republic of China.

1.3.5 Specification

Each specification is extensive, and while many of the relevant properties are interrelated, a significant proportion are of no relevance to the scope of this work. As such, relevant abbreviated specification summaries are presented in Table 1.2

Table 1.2: Abbreviated Kerosene Derived Jet Fuel Specifications

	Jet A	*Jet A-1*	*TS-1*	*No.3 Fuel*
Specification	ASTM D 1655	DEF STAN 91-91	GOST 10227	GB 6537-2019
Aromatics [% vol, max]	25	25	22 [% mass]	20[% mass]
Distillation [oC]				
Initial Boiling Point	-	Report	150	Report
10% recovered, max	205	205	165	Report
50% recovered, max	Report	Report	195	232
90% recovered, max	Report	Report	230	Report
End Point	300	300	250	300
Density $[kgm^{-3}15^oC]$	775-840	775-840	min 774 @ 20^oC	775-830
Viscosity $[mm^2s^{-1}20^oC, max]$	8.0	8.0	8.0 @ -40^oC	8.0
Net Heat of Combustion $[MJkg^{-1}min]$	42.8	42.8	42.9	42.8
Smoke Point [mm, min]	25/18 with *	19	25	25
***Napthalenes [vol%,max]**	3.0	3.0	N/A	3.0

The specification for each governing body are generally homogeneous with slight variation, excepting for regional requirements predominantly based on environmental conditions, such as the local climate affecting the freezing point. Both western specifications limits the total proportion of aromatic hydrocarbons to 25% by total volume. The exception is TS-1 and No.3 Fuel, which limits 22% and 20% by mass, repectively. Taking into account the typical density of aromatics of around 0.800

kgm^{-3} however, this essentially brings GOST 10227 and GB 6537-2019 in line with western specification with regard to aromatic content restrictions.

Aromatics are the only type of hydrocarbon to be specifically regulated in the specification, which also includes the naphthalene component. Aromatic hydrocarbons are a naturally occurring component of kerosene, whose structure and prevalence is discussed in detail later in this chapter (Section 1.8). Their proportion in a given fuel has been long known to have an effect on the likelihood of a fuel to produce visible smoke. The initial emission limits for commercial aircraft were implemented in order to limit visible smoke from an exhaust plane [5] in order to alleviate public concern. The occurrence of BC emissions without visible smoke can be significant however, and has significant impact on other factors such as engine life and anthropogenic global warming. The aromatic content of a fuel is measured using the specification methods which are summarised in Table 1.3. A given fuel sample must pass either of these tests by showing a volume percentage of less than 25% [34].

Table 1.3: Summary of Aromatic Volume Tests for Kerosene Derived Jet Fuel Specification

Standard Test Method	Test Description
ASTM D 1319/IP 156	Hydrocarbon Types in Liquid Petroleum Products by Fluorescent Indicator Absorption
ASTM D 6379/IP436	Aromatic Hydrocarbon Types in Aviation Fuels – High Performance Liquid Chromatography with Refractive Index Detection

1.4 Gas Turbine Combustion

All gas turbine engines operate on the Brayton thermodynamic cycle, based on the principles of compression of incoming air, the addition of an appropriate fuel source and subsequent combustion, and expansion through a turbine apparatus in order to provide the energy required to run the compressor. The remaining energy is used to provide mechanical work to a generator, in the case of power generation, or mechanical work for applications for such as helicopter turboshaft. For Jet Engine applications, once the required enthalpy required for compressor work is extracted, the remaining enthalpy is uninhibited and exits the vehicle as propellant after being

expanded to near-atmospheric pressure. For Turbofan applications, the necessary enthalpy is also extracted to provide the mechanical work necessary to drive the fan to displace the air as propellant.

The heat addition phase in Gas Turbine combustion is incredibly flexible, as the cycle can hypothetically operate on a wide range of fuels. Ground based applications typically use gaseous fuel such as natural gas, while Jet Engines use liquid fuel due to the higher energy density requirements for storing the required fuel onboard.

Air leaving the compressor of a jet engine does so at significant pressure and velocity and initially is too fast for a stable flame to be established in the combustion chamber. The air velocity is slowed significantly before fuel is introduced through air assist or pressure nozzles where it mixes with the incoming air. In the presence of a pre-established stable flame, fuel is injected into the combustion chamber and the combustion maintains a steady state.

Soot is formed in any part of the combustor where there is inadequate mixing between fuel rich vapour pockets and oxygen deficient gas. In combustors that feature pressure blast fuel injectors, combustion by-products, deficient of oxygen by nature, recirculate and move upstream into the path of the incoming fuel vapour. The resulting effect creates fuel rich zones which undergo pyrolysis in the absence of oxygen and form significant quantities of soot as a result.

1.5 What is Black Carbon?

Black Carbon is a form of nVPM that is formed during combustion of carbon containing fuels, which are typically fossil fuel based. The combustion reaction of carbonaceous fuel is represented by Equation 1.1.

$$a.C_nH_m + b.O_2 \rightarrow x.H_2O + y.CO_2 + z.C \tag{1.1}$$

Where

C = atomic carbon H = atomic hydrogen O = atomic oxygen n = atomic proportion of carbon m = atomic proportion of hydrogen a, b, x, y, z = the molar proportion of the associated molecules

While a more detailed description of the current theory behind practical soot

formation is included later (Section 2.1), a conceptual outlay of incomplete combustion is described here. In an idealised reaction, a hydrocarbon fuel, in the presence of oxygen, reacts to form water, usually in the form of vapour, and carbon dioxide. Complete combustion can be said to occur when there is sufficient atomic oxygen available to fully oxidise the atomic carbon proportion in the given fuel. Using the coefficients described in Equation 1.1, and balancing for the carbon, hydrogen and oxygen terms respectively yields Equations 1.2, 1.3 and 1.4.

$$a \times n = y \tag{1.2}$$

$$a \times m = 2x \tag{1.3}$$

$$2b \geqslant x + 2y \tag{1.4}$$

As the reactant products are dependant upon relative proportion of the reagents, substituting Equations 1.2 and 1.3 into Equation 1.4 and rearranging for b yields Equation 1.5.

$$b \geqslant \frac{a}{4}(m + 4n) \tag{1.5}$$

The relative proportion of the reagents, in this case, carbonaceous fuel and oxygen, determines the stoichiometry of the reaction, which allows for the quantification of the combustion products following the principle of the conservation of mass. In a situation for hexane, where the equality expressed in Equation 1.5 is satisfied, yields the following reaction as shown in Equation 1.6.

$$C_6H_8 + 8O_2 \rightarrow 4H_2O + 6CO_2 \tag{1.6}$$

This leads to the conclusion that the hypothetical complete combustion stoichiometry for hexane occurs when the available molar proportion of oxygen is eight times that of hexane. When the coefficient, b, drops below the requisite value, incomplete combustion occurs as there is no longer sufficient oxygen available to only form water and carbon dioxide in the reagents. This is shown in Equation 1.7.

$$C_6H_8 + 7O_2 \rightarrow 4H_2O + 5CO_2 + C \tag{1.7}$$

The stoichiometry of the reaction can now be said to be fuel rich as there is a greater proportion of fuel to oxygen for complete combustion to occur. This leads to a third reagent term, that is purely carbonaceous, conceptually explaining the idealised emergence of BC, or soot, due to incomplete combustion.

Combustion occurring in an abundance of oxygen, however, is experimentally observed to produce soot, in contrast to a conceptually stoichiometric mixture in which reagents and products are balanced. Real world chemical reactions are not ideal and do not involve perfect mixing of reagents. A combustion reaction that produces zero Black Carbon would, even in an abundance of oxygen, would have one hundred percent efficiency and is impractical. Reactions such as combustion do not take place on a macroscopic single-step scale, but instead feature microscopic multi-step component elementary reactions. The combustion of hydrogen in pure oxygen in contemporary models is thought to be comprised of twenty individual step reactions, each with their own reaction rates described by the Arrhenius equation of that specific reaction [38]. In certain molecules, certain reaction pathways dominate, which potentially lead to BC precursors regardless of the global stoichiometry.

In practical industrial applications, combustion does not take place in pure oxygen, but in air, which is a multi-component medium where oxygen is not even the predominant molecule. Improper mixing on a macroscopic scale can lead to local combustion conditions where the stoichiometry is fuel rich, regardless of the abundance of oxygen on a global scale. The concept of improper fuel/air mixing in an aerospace combustion context is examined further in Section 1.6. The ideal combustion described above also features the use of integers for the proportion of hydrogen and carbon in homogeneous fuel such as hexane. Practically, fuels rarely have a singular molecular component, and Jet Fuel in particular, potentially contains hundreds of different hydrocarbon molecules each with its own proportion of hydrogen to carbon, which may vary significant based on position in the boiling range and hydrocarbon type. A blended fuel such as kerosene, may yield an aggregate H/C ratio that is not reflected by a significant proportion of the components present, which may have a lower H/C ratio that leads to increased carbon formation in parts

of the flame where their presence dominates. The mechanisms of BC formation are discussed further in Chapter 2.

Where soot occurs, it takes the form of purely carbonaceous spheres with a primary particle diameter of 10-30 nm [39], although particle size is normally distributed between a range of 10 nm and 1000 nm when including agglomerated particles [40, 41]. Larger soot particles do not appear to be comprised of larger spheres however, as these larger particles are instead comprised of an agglomeration of smaller particles into fractal aggregates of variable geometry. An example of a range of soot morphologies obtained using transmission electron topography (TEM) from a Jet Engine exhaust is shown in Figure 1.5.1. In these images, primary soot particles are conjoined in complex arrangements leading to the measurement of larger soot molecules. Certain techniques for classifying the effective density of soot aggregates have been carried out to date [42].

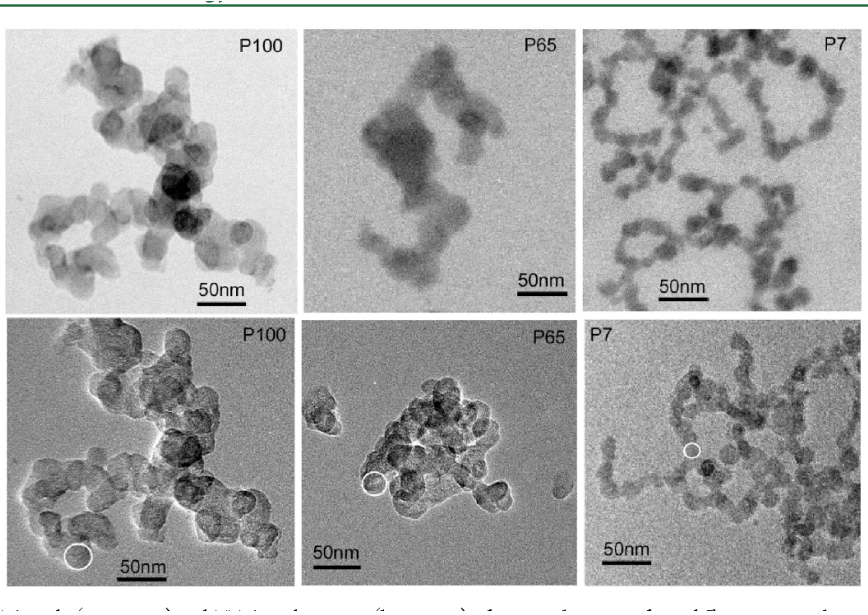

Figure 1.5.1: Electron microscopic study of soot particulate matter emissions from aircraft turbine engine [3]

Figure 1.5.2 shows the typical distribution of soot particle exhaust sizes from a Jet Engine exhaust burning various fuels, including Jet A-1 [3].

The majority of particles, irrespective of the fuel source, have an electrical mobility diameter between 10nm and 110nm. It should be noted that even though these smaller particles predominate, they represent a very small proportion of the overall mass of a given fuels exhaust, with most of the mass being contained within

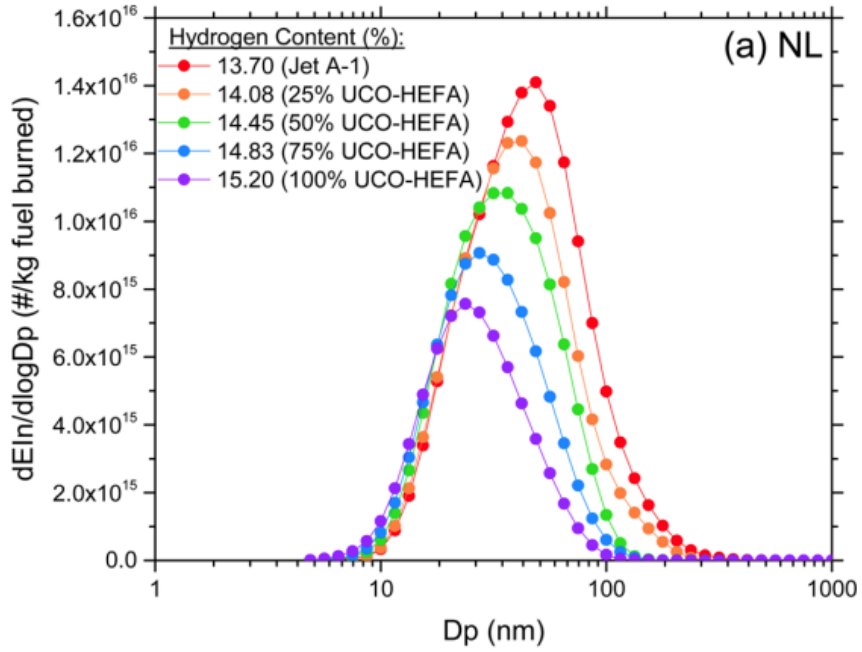

Figure 1.5.2: nvPM EIn size distributions for selected fuels at No-Load Condition [3]

the larger aggregates of around 1000nm. This does not make the smaller particles insignificant however, as their number and geometric mean diameter have significant repercussions on human health, climate change, and radiative heat transfer within combustion chambers due to a high proportion of surface area per unit mass for smaller particles. All of these influences are discussed further in Sections 1.10 and 1.11. For these reasons, the full classification of the mass, size, number and shape of soot emissions is of significant interest to a range of shareholders and is an ongoing area of research, despite only the smoke point of a given fuel sample being currently regulated.

1.6 Smoke Point

According to the fuel specification [35], a given Jet Fuel sample's propensity to produce soot is determined by measuring its Smoke Point. The sample being measured is placed within a cylindrical vial which is then attached below the chamber of a smoke point meter, which is also known as a lamp. A wick is inserted into the liquid sample and then protrudes into the chamber of the lamp. Fuel diffuses into the body of the wick and the operator lights the wick and titrates the flow rate of the fuel

until visible smoke is emitted from the flame, while observing a ruler measure on the back of the chamber wall. The height at which the flame begins to produce visible smoke, as determined by the observer, is known as the Smoke Point. There are both manual and automated methods validated by the specifications ASTM D 1322 [4] and IP 57 [43]. An illustration of the automated test method for this standard is shown in Figure 1.6.1. The optical resolution of the observer is claimed to be 0.1 mm using the manual method according to the specification.

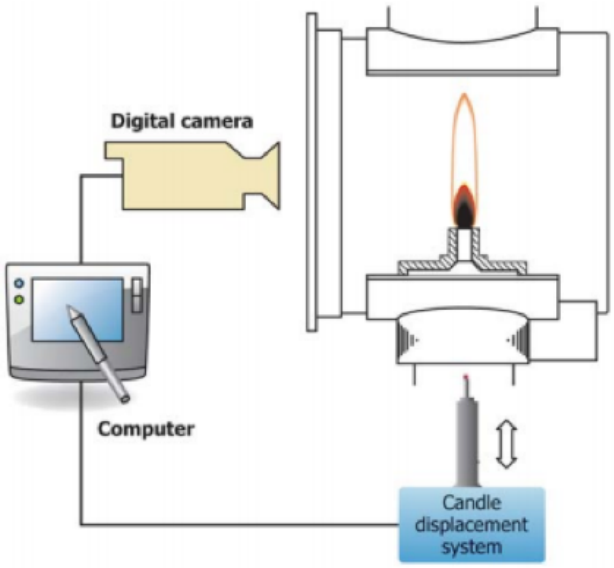

Figure 1.6.1: Automated SP Method [4]

A cleaner burning fuel will typically have a higher smoke point and conversely, a smokier fuel with have a lower smoke point. Examples of the typical observations encountered during this test are shown in Figure 1.6.2. In the furthest left picture there is a prominent smoky tail, which declines in size in the subsequent pictures for samples with a lower smoke point. These four images from left to right represent fuels that are increasingly “smoky”, as there is an inverse relationship between a fuels propensity to produce smoke and its smoke point.

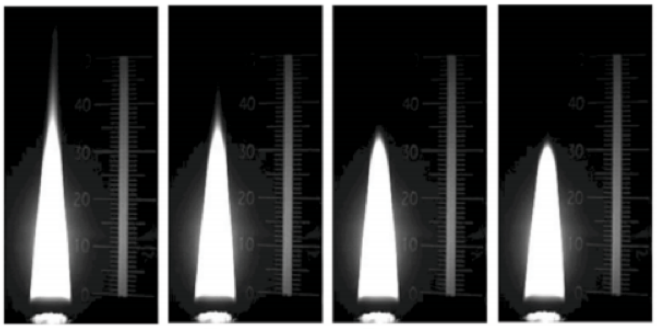

Figure 1.6.2: Variation in flame height in order to obtain smoke point [4].

As shown in table 1.2, the specification requires a smoke point at least 25 mm high for certification as Jet Fuel. If a fuel fails to meet this threshold, the requirement is lowered to 18 mm provided that the naphthalene content, which is a form of aromatic, comprises no more than 3% of the total fuel volume. The molecular composition of napthalenes is discussed later in this chapter. The naphthalenes volume is measured using ASTM D 1840 [44]. The ongoing industry consensus is that napthalenes are a special class of aromatic that have an especially high-sooting propensity, and this relationship is explored further in Chapters 2 and 3 of this thesis.

There are several techniques for assessing a fuels sooting propensity, but the SP method has become ubiquitously used for assessing fuel purposed specifically for aviation. This is primarily due to the method being required by the specification, although there are specific advantages to using this method regardless of necessity. It does not require the use of expensive equipment as the lamp apparatus is relatively rudimentary and inexpensive. While SP operators need to be trained to take effective readings, the method does not require expertise greater than that of a proficient technician. As what may be considered a legacy test, it provides a comparable metric that can be used to compare a wide range of fuels years of research data is available as the smoke point has been collected for decades and as the test has remained consistent, if not overly simplistic..

The major disadvantage of the SP method is its poor repeatability and reproducibility. Repeatability is the degree to which experimental results are consistent given the same operator, equipment, environment, and in this context; the same fuel sample. Reproducibility is the degree to which the experiment agrees with pre-

vious results, on the same fuel but in a different local, with a different operator and different equipment. Figure 1.6.3 shows the repeatability and reproducibility of the ASTM D 1322 method of determining SP's between 15 mm and 42 mm. In the range of the Jet Fuel specification, the manual method has a repeatability of approximately +/- 2.25 mm at SP's of 18 mm and +/- 2.8 mm at 25 mm.

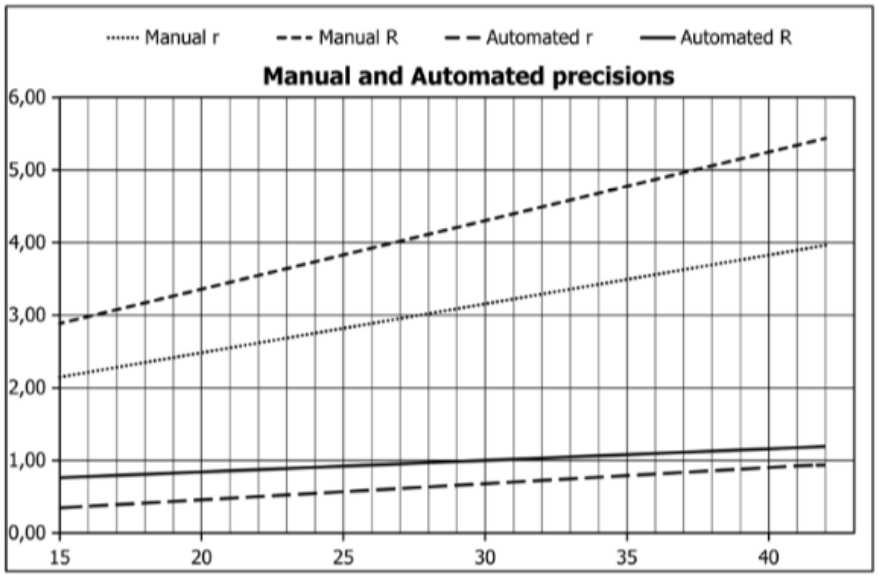

Figure 1.6.3: Repeatability (r) and reproducability (R) for the manual and automated methods for determining SP. [4]

This can be problematic for refiners, as a prospective fuel may give high variance results around the limits of the specification, and a fuel that may have been tested multiple times in-house may provide values around a mean of 25mm, for example, but due to the inconsistencies of the test, may have an SP lower than 23 mm when sent for specification testing, and subsequently require that sample to have a naphthalene content of less than 3%. The manual reproducibility is worse, with a value of approximately +/- 3.1 mm at 18mm and +/- 3.84 mm at 25 mm. This is due to the significant variability in the setup of the apparatus, the ambient conditions under which the test takes place, and the subjectivity, or bias, of the observer. This again increases the uncertainty of correct certification of a given fuel initially tested on in-house equipment when it is then sent to be tested at a different facility. To mitigate these concerns, an automated method for determining SP was proposed in 2012 and was subsequently incorporated into the ASTM D 1322 specification. The automated SP meter uses an integrated digital camera attached to a computer

built into the housing of the apparatus. Three individual SP measurements are taken and the average is then reported. The method removes the necessity for active supervision during the test and removes the potential bias and subjectivity of the observer. The automated method has now become the gold standard for SP measurement although as the manual method is not precluded, there is no available data to assess how widespread its use has become. Regardless, the automated reproducibility and reproducibility is significantly better than the manual method, as can be seen in Figure 1.6.3. Both metrics are seen to have improved, as the reproducibility is between five and six times less, and the reproducibility is around four times less. The advantages and disadvantages of the SP method in a research context are discussed further in Chapter 2, and a large volume of SP data is assessed in Chapter 3.

1.7 Other BC Detection Methods

While Smoke Point is a specific requirement of fuel, there are other requirements that the gas turbine configurations themselves must pass. Commercial aircraft engines are regulated by measuring the Smoke Number (SN) of a particular engine which must meet a certain standard based on its engine rated thrust [5] as shown in Figure 1.7.1

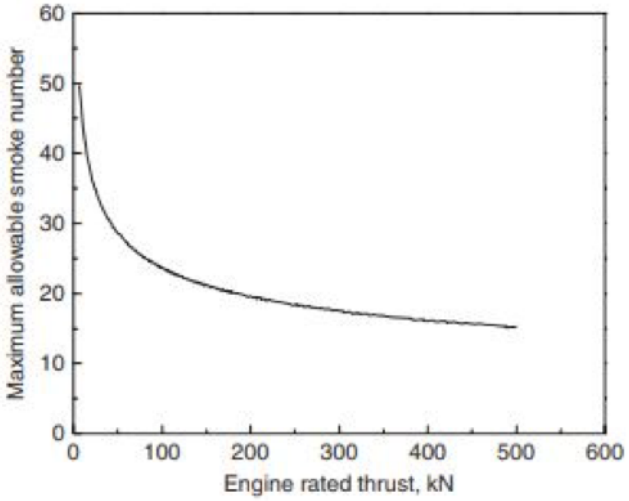

Figure 1.7.1: ICAO/CAEP Smoke Number Limit [5]

1.7.1 Smoke Number

An engine's Smoke Number is determined by passing a given exhaust volume through a Whatman #4 Filter paper and measuring its reflective characteristics before and after exposure. An empirical Smoke Number can then be used to determine whether an engine meets certification requirements. Individual engine model performance however, is incredibly dependant on the geometry and design of each engine and introduce other variables other than the composition of the fuel being used. As such, a given engine's Smoke Number is specific to that particular engine. In contrast, the measurement of the Smoke Point uses a much simpler configuration that does not reflect the complex flame dynamics and processes encountered in a gas turbine configuration. The Smoke Point is also a test where the only true variable is the fuel itself, the result of which will predominantly be determined by not only its bulk physical properties, but the nature of its chemical composition. There is evidence however, that a fuel's smoke point is an appropriate test when considering the molecular structure of a fuel when burnt in a more practical configuration [15]. This may suggest that it is appropriate to infer relations from this lab scale test when considering the performance of fuels in terms of composition. The aromatic content, naphthalene content and smoke point are specifically included in each specification to limit the amount of soot produced by a given fuel and a lab scale test such as determining the smoke number for a large number of samples gives the strongest, most independent indication as to the reliability of using these metrics to assess a fuels likelihood to produce significant BC.

1.7.2 Threshold Sooting Index

Calcote and Manos [45] developed an empirical scale for assessing the sooting potential of individual fuels using the following formula show in Equation 1.8

$$TSI = a\frac{MW}{h} + b \tag{1.8}$$

Where MW is the molecular weight of the fuel, h is the smoke point, and a and b are constants specific to the apparatus being used. This comparative scale places hexane at the bottom with a score of 2 and 1-methylnapthalene at the high end with

a score of 100, with a higher number denoting a greater propensity to produce soot. This metric has been used successfully to predict the sooting propensity of multi-component blends by using the proportion of the relevant TSI for each component as a mole fraction of the total mixture. The strengths and weaknesses of the TSI method are discussed further in Chapter 2.

1.7.3 Yield Sooting Index

McNally and Pfefferle [46, 47] developed a method of empirically quantifying the sooting propensity of purely aromatic substances. This approach uses a given quantity of the substance is diffused into a methane flame and its soot volume fraction is measured using Laser Induced Incandescence. The YSI is quantified using the formula shown in Equation 1.9.

$$YSI = Cf_{v,max} + D \tag{1.9}$$

Where C and D are apparatus specific constants and $f_{v,max}$ is the soot volume fraction. The empirical scale creates a lower bound with benzene on a YSI of 30 and 1,2-dihydronapthalene at 100. It is possible to use YSI values of multiple substituted aromatics, such as trimethylbenzene and the YSI values of single substituted aromatics to obtain an accurate aggregate. The strengths and weaknesses of the YSI method are discussed further in Chapter 2.

1.8 Particulate Matter Terminology

The various methods for characterising particulate matter emissions has given rise to a panoply of terms, many of which are used in this thesis. While some of these terms are interchangeable, many are not, and refer specifically to a certain metric or classification of particulate matter emissions. The following are general descriptions of the terms used in this thesis and their specific meaning.

- **Particulate Matter (PM)** - PM, refers to solid particles and liquid droplets found in the air. This encompasses dust, dirt, soot, smoke, water droplets, and unburnt fuel.

- **Black Carbon BC** - As discussed in Section 1.5, describes the carbonaceous remainder of incomplete combustion. Also referred to more colloquially and in various literature as **soot**. These terms are interchangeable.

- **Non-Volatile Particulate Matter (nvPM)** - nvPM, according to the ICAO definition [48], includes:

  "Emitted particles that exist in a gas turbine engine exhaust nozzle exit plane that do not volatilise when heated to a temperature of 350^oC*"*

  For a gas turbine exhaust, most, but not all of the particulate matter that meets this criteria will be carbonaceous, in the form of soot or black carbon. All black carbon is nvPM, but not all nvPM is black carbon, and so the terms are not interchangeable.

- **Smoke** - According to the ICAO definition [49], Smoke is:

  "The product of burning materials made visible by the presence of small particles."

  In an aviation context using hydrocarbon based fuel, the visibility of smoke is determined by its soot content. The important distinction between soot and smoke, however, is it's visibility. All jet engine emissions will emit soot, but not all of it, if any, will be visible.

All sub-sonic engines manufactured after 1983 need to meet the standards for smoke, as discussed in Section 1.7. Since ICAO Annex 16 Volume II [50] in 2017 all in production engines with a rated thrust of 26.7kN or more have had to meet standards for maximum nvPM mass and number concentration. As of 1st January 2023 [48], these standards are as shown in Figure 1.8.1 [6].

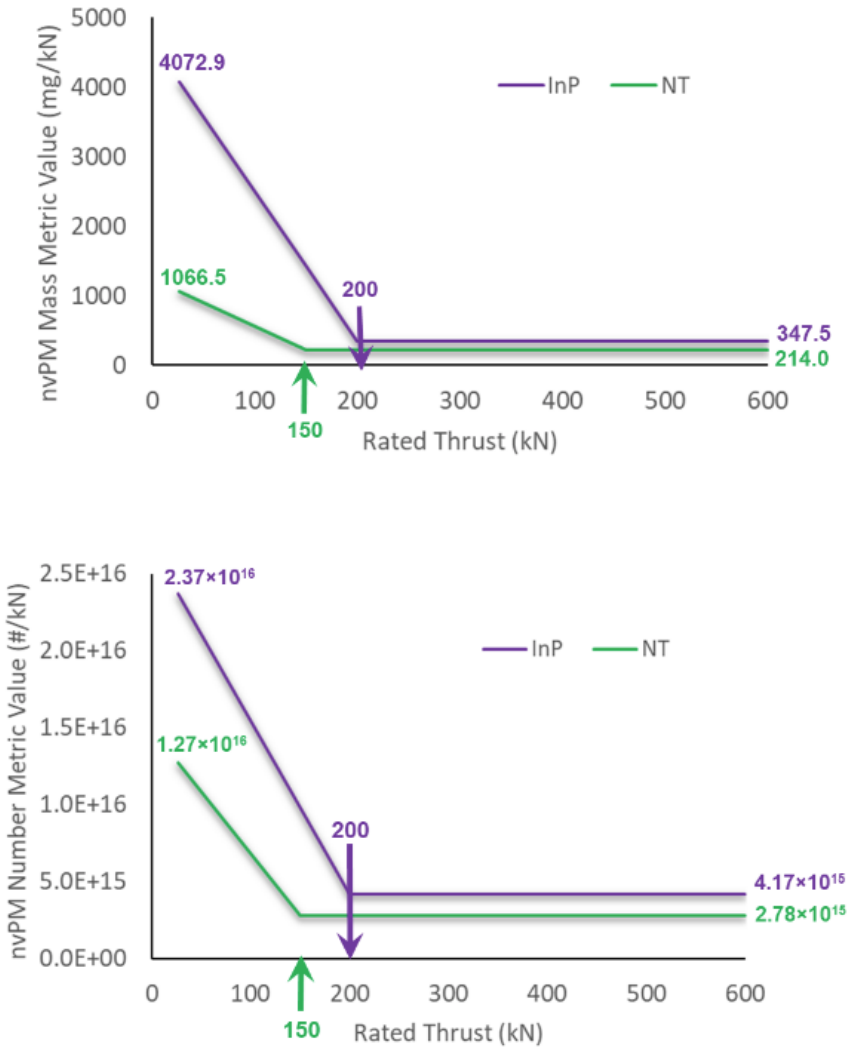

Figure 1.8.1: ICAO nvPM Mass and Number Concentration Standards [6]

1.9 Hydrocarbon Types & Classification

As modern conventional fuels are rarely comprised of a single molecular component, it is important to establish the various forms of hydrocarbon types that may be present. The nomenclature for hydrocarbon types can vary dependant on the specialism concerned. This section aims to clarify the various terms currently in use by various research and industrial interests.

1.9.1 Alkanes

Alkanes, also known as Paraffins, are the simplest molecular form of hydrocarbon, the main characteristics being their non-cyclic, saturated structure. Their general

formula is given by C_nH_{2n+2}. Alkanes have a comparatively high hydrogen to carbon ratio that decreases with increasing carbon number. The simplest alkane, methane is shown in Figure 1.9.1 as well as a hexane, containing six carbon atoms.

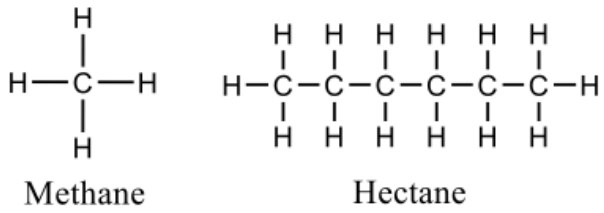

Figure 1.9.1: Illustrative bonding arrangement of methane and hexane molecules

Alkanes can be further subcategorised into normal alkanes (n-Paraffin) and iso alkanes (Isoparaffin), whereby the former is a completely straight carbon chain, whereas the later features branches of functional groups arranged non-linearly.

1.9.2 Alkenes

Alkenes, also known as Olefins, are unsaturated hydrocarbons, as they have further potential to form covalent bonds with additional hydrogen atoms. This gives alkenes their characteristic double carbon-carbon bond. The simplest alkene, ethene (ethylene), is shown in Figure 1.9.2 alongside butane. Despite the presence of only one double carbon bond, butene is classed as an alkene, as is any uncyclic molecule that contains a double bond. Alkenes have the general formula C_nH_{2n}.

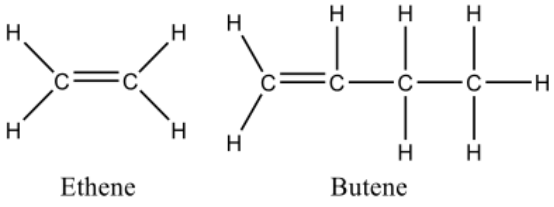

Figure 1.9.2: Illustrative bonding arrangement of ethene and butene molecules

1.9.3 Nathenes

Hydrocarbons may form cyclical structures instead of chains. Two examples of this form are cyclopropane and cyclohexane, as shown in Figure 1.9.3. The general form

of a cyclohexane is $C_nH_{2(n+1-r)}$, where r is the number of rings present. Cycloalkenes follow a similar structural pattern but are comprised of at least one carbon double bond with general formula $C_nH_{2(n-m)}$, where m refers to the number of double bonds present.

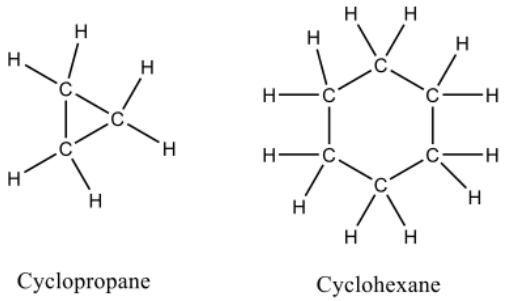

Figure 1.9.3: Illustrative bonding arrangement of cyclopropane and cyclohexane

1.9.4 Arenes

Arenes are commonly referred to as aromatics hydrocarbons. This term arose due to the characteristic smell encountered with many aromatic species and the term 'aromatic' came into being before the advent of modern molecular chemistry and therefore before their full chemical behaviour and structure was determined. While many aromatics do have a distinctive aroma, this is not specifically true for all aromatics, which are more accurately described as arenes. Due to its ubiquitous use in the aerospace research community, the term aromatic is used throughout this work outside of this sub-chapter.

Arenes feature the cyclic structure of cycloalkanes but are unsaturated as they have the potential to form more covalent bonds with additional hydrogen atoms. As each carbon atom has valences to form, one of these four is bonded to a hydrogen atom, two are shared with each neighbouring carbon atom, creating a carbon single bond, leaving one remaining electron that disassociates from its parent atom to form a de-localised pi orbital above and below the plane of the molecule. As a result of this complex bonding arrangement, aromatic structures in the form of phenyl rings can be represented in various ways, as shown in Figure 1.9.4.

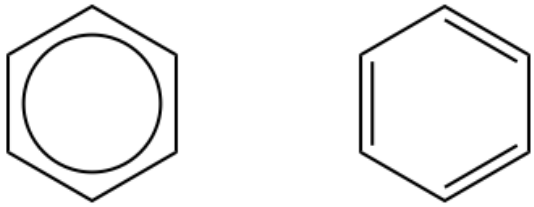

Figure 1.9.4: Alternative representations of benzene ring (phenyl group)

1.9.5 Arene Classification

Arenes can be further sub-classified into various types based on their configuration.

- Neutral Homocyclics – most annulenes (conjugated monocyclic hydrocarbons), with the general formula C_nH_n, display aromatic properties. The simplest aromatic neutral homocyclic is benzene.
- Heterocyclics – at least one atom in the aromatic ring has been substituted with an atom other than carbon. This tends to reduce the aromaticity of the molecule and increase its reactivity due to the decrease in electrons available to contribute to the pi bond.
- Polycyclic Aromatic Hydrocarbons – one or more phenyl rings are joined together by interatomic carbon-carbon bonds. Examples of this type of molecule include napthalene and phenathrene are shown in Figure 1.9.5.

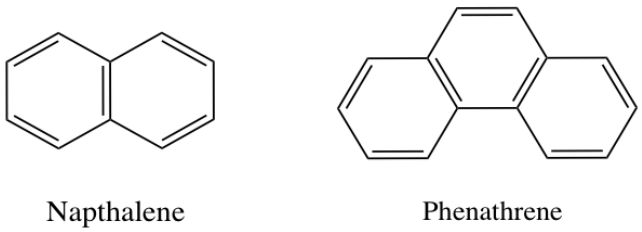

Figure 1.9.5: Napthalene and Phenathrene molecules

- Substituted Aromatics – the aromatic ring is left intact and is bonded with other functional groups in place of a carbon-hydrogen bond. Two examples of this structure are toluene and cumene as shown in Figure 1.9.6. In the case of

substituted aromatics, the aromatic ring is commonly referred to as the phenyl ring and the terms are used interchangeably as appropriate throughout this thesis.

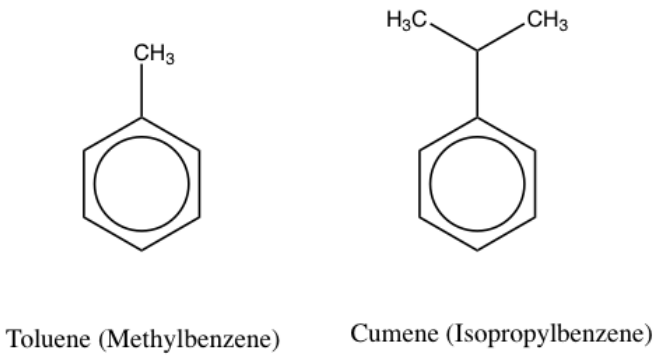

Figure 1.9.6: Examples of Substituted Aromatics - Toluene and Cumene molecules

- Cycloaromatics – a term predominantly used by the National Jet Fuels Combustion Program, an organisation discussed further in Chapter 2, when classifying compounds of a certain structure. Cycloaromatics are composed of one unsaturated ring and one unsaturated, or partially unsaturated ring. Common examples are Tetralin and Indan, whose structure can be seen in Figure 1.9.7.

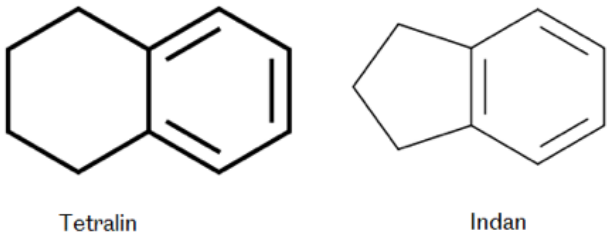

Figure 1.9.7: . Examples of Cycloaromatics - Tetralin and Indan molecules

A semantic summary of hydro-carbon classification terms is shown in Table 1.4.

1.10 Alternative Fuels & Certification Process

The first alternative fuel to be proposed for aviation use arose from necessity rather than a concerted attempt to combat global warming. In the mid-1990's, O.R. Tambo

Table 1.4: Summary of Aromatic Volume Tests for Kerosene Derived Jet Fuel Specification

Hydrocarbon Group	Chemical Classification	Aerospace Nomenclature
Aliphatics	Alkanes	Normal Paraffin
		Iso Paraffin
	Alkenes	Olefins
	Cycloalkanes	Napthenes
Arenes	Monocyclic Aromatics	Alkylbenzenes
	Dicyclic Aromatics	Cycloaromatics
	Polycyclic Aromatics	Napthalenes

Airport, then known as Johannesburg International Airport, was experiencing difficulty in obtaining enough jet fuel to meet demand as a busy hub for commercial travel. This was predominantly due to a shortage of local refineries in southern Africa available to provide kerosine. Sasol, a South African energy and chemical company, proposed alternatively produced Jet Fuel obtained through the Fischer-Tropsch process, by which carbon dioxide and hydrogen or water vapour is converted into larger hydrocarbons at temperatures of $150°C$-$300°C$ under pressures between one and ten bar [51]. This synthetic fuel, known as Fischer-Tropsch Synthetic Parrafinic Kersosene, or FT-SPK, met the requirements of the ASTM D 1655 standard at the time, and was proposed to regulators for approval for use in commercial aviation [52].

The proposal that a non-petroleum derived fuel, meeting all specification limits, initially caused concern amongst OEM's, regulators and policymakers due to the potential unforeseen effects of using a fuel with parameters outside the experiential limits of traditional kerosene Jet Fuel. While a given group of hydrocarbons may satisfy the parameters of a given specification, there may be other necessary parameters for normal operation that remain unknown to date or taken for granted, such as a diverse range of hydrocarbons present over the boiling range of kerosene. After consultation and review, the use of FT-SPK was approved as a 'drop-in' fuel, where the synthetic fuel was approved for blending with refined kerosene obtained via fractional distillation up to 50% by volume.

Since the introduction into the market of FT-SPK in 2009, seven technical pathways (eight including the two ATJ routes) have been approved for the production of

synthetic fuel used as a drop-in to kerosene. These routes are summarised in Table 1.5.

Table 1.5: Approved SAF's to date [19]

Acronym	**ASTM Approval Process**	**Date of Approval**	**Feedstock**	**Blending Ratio by Volume**
FT-SPK	Fischer-Tropsch hydro-processed synthesised paraffinic kerosene	2009	Lignocellulosic biomass, Agricultural and forestry residues and municipal waste	< 50%
HEFA-SPK	Synthesised paraffinic kerosene produced from hydro-processed esters and fatty acids	2011	Oils and Fats - Camelina, jatropha, castor oil, palm oil, animal fats and used cooking oil	< 50%
HFS-SIP	Synthesised isoparaffins produced from hydro-processed fermented sugars	2014	Microbial conversion of sugars to hydrocarbons - Sugarcane, cassava, sorghum and corn	< 10%
FT-SPK/A	Synthesised kerosene with aromatics derived by alkylation of light aromatics from non-petroleum sources	2015	Lignocellulosic biomass - Agricultural and forestry residues and municipal waste	< 50%
ATJ-SPK (isobutanol)	Alcohol-to-jet synthetic paraffinic kerosene	2016	Biomass used for sugar production and lignocellulosic biomass - Sugarcane, cassava, sorghum, corn and ethanol	< 50%
ATJ-SPK (ethanol)	Alcohol-to-jet synthetic paraffinic kerosene	2018	Biomass used for sugar production and lignocellulosic biomass - Sugarcane, cassava, sorghum, corn and ethanol	< 50%
CHJ	Catalytic hydrothermolysis synthetic jet fuel	2020	Triglyceride-based feedstocks - Waste oils, algae, soybean, jatropha, camelina and carinata	< 50%
HHC-SPK	High hydrogen content synthetic parrafinic kerosene	2020	Biologically derived hydrocarbons - Algae	< 10%

No fuel approved to date may comprise more than 50% by volume of synthetic content, and two can be present only up to 10% by volume. There is still concern that approval of a jet fuel whose largest component is synthetic may lead to unforeseen circumstances and is reflected in the specification. The relevant specifications governing the approval, production and use of alternative fuels are summarised in Table 1.6.

Table 1.6: Summary of Aromatic Volume Tests for Kerosene Derived Jet Fuel Specification

Specification	**Description**
ASTM D 1655	Standard Specification for Aviation Turbine Fuels
ASTM D 4054	The Standard Practice for Qualification and Approval of New Aviation Turbine Fuels and Fuel Additives
ASTM D 7566-09	Standard Specification for Aviation Turbine Fuel Containing Synthesised Hydrocarbons

ASTM D 1655, as discussed previously, is the specification governing fuel from conventional sources. Due to the concern over the potential complications of non-conventional fuels, the Coordinating Research Council (CRC) integrated additional requirements for alternative fuels which included a range of recommended additional parameters that have become known as "fit-for-purpose" tests. These additional parameters were integrated into the introduction of a new standard, ASTM D 4054 [53], which specifies the process by which a new alternative fuel is approved for use. It should be noted that these fit-for-purpose tests are not additional specification tests that each sample must meet, as in ASTM D 1655, but tests that must be met for approval of the technical process by which the fuel is produced. ASTM D 7566-09 [54] is the standard governing individual specification tests of production blends and is analogous to ASTM D 1655 for alternative fuels in that it's used to test individual samples for subsequent use.

The potential of introducing larger ranges and quantities of alternative fuels along with an increasing interest in reducing greenhouse gas emissions from the aviation sector led to the concept of Sustainable Alternative Fuels, or SAF's. Petroleum

derived fuels release greenhouse gas emissons into the atmosphere from previously terrestrial bound sources, and are therefore a net contributor to the global warming effect. There is a conceptual cycle, shown in Figure 1.10.1, where jet fuel is obtained from renewable sources such as biomass to obtain synthetic jet fuel whose emissions, predominantly CO_2, are reabsorbed by the chemical or biological process that led to development of the feedstock initially [7]. Such a process could ideally approach carbon neutrality and would effectively mean that fuel has a near zero net carbon contribution to the atmosphere. Any alternative fuel that meets these requirements can be labelled as an SAF.

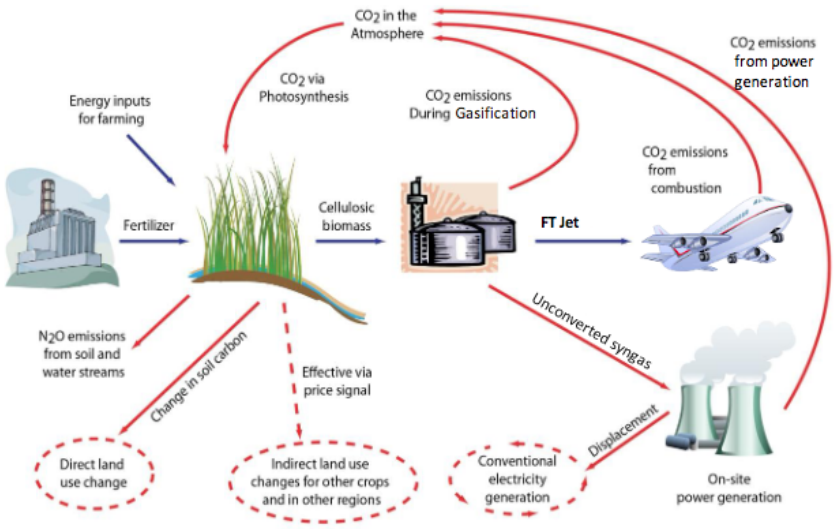

Figure 1.10.1: Carbon lifecycle diagram for biofuels [7]

The use of alternative drop in fuels has proliferated since their introduction and as of 2020, 650,000 commercial flights using 6 billion litres classified as SAF [55] have flown. While this progress is significant, SAF currently represents around 0.01% of global supply, although this is expected to increase to 2% by 2025 depending on production capacity. The combination of environmental concern over climate change and an interest in increased diversity of supply away from petroleum sources suggests there will be significant demand for SAF fuels in the future. Jet fuel regulations are constantly reviewed and iterated and it is highly likely that in future, commercial flights may be able to operate using 100% SAF. Technical demonstration flights have been conducted under these conditions with no adverse effects [56].

The introduction of SAF's have raised concerns and opportunities regarding the

aromatic proportion of Jet Fuel. As discussed previously, a desire to stay within experiential limits requires no more than 50% of synthetic fuel to be blended with paraffinic kerosene. This is also required in order to maintain a significant proportion of the final blend as aromatic, which is currently 8% vol/vol as specified. Of the eight SAF pathways approved to date as summarised in Table 1.5, all of them produce little or negligible amounts of aromatic hydrocarbons. When blended with petroleum kerosene, the only aromatic component that remains is at least 50% of the original amount, depending on the blend proportion. As discussed previously, the aromatic component is necessary to ensure the correct amount of seal swell in conjoining fuel lines and to raise the volumetric energy content of the fuel. Low and no aromatic fuels can cause the polymers found in O-rings to shrink and therefore cause leaks [57]. There are potential production pathways that could be added to FT and HEFA methods that produce their own aromatic hydrocarbons without having to rely on those inherent to paraffinic kerosene [58]. It is possible however, that these Aromatic Synthetic Aviation Fuels (ASAF) fuels are mono-aromatic, in that rather than containing a diverse range of aromatic types over the boiling range of a typical fuel, they instead only contain one or several types of aromatic, such as toluene, xylene or ethylbenzene. As each aromatic has its own propensity to produce soot, differences that were negligible when present individual hydrocarbon types represented up to 1% of the final blend, could now potentially dominate in a hypothetical ASAF comprised of 8-25% vol/vol under the current specification. It would therefore, be beneficial for ASAF producers of the future to be forearmed with the knowledge of preferential aromatic components to be included or avoided in hypothetical blends.

1.11 Effects of BC on Atmosphere

The latter half of the 20th century and early 21st century has seen an increased focus on mitigating the impact of human society and industry on the environment. Anthropogenic global warming is a specific point of concern and there is an increased incentive to eliminate or reduce the production of emissions that contribute to this phenomenon.

The greenhouse effect is a proposed mechanism where the molecular composition of the atmosphere has a direct effect on the proportion of heat received from the sun that is retained. The Sun emits electromagnetic radiation which passes through space and into the Earth's atmosphere, and is subsequently reflected back into space by the Earth's surface. Certain molecules within the atmosphere interact more strongly with this radiation and absorb a higher proportion of energy, which translates on a macroscopic scale to an increase in heat energy. The proportion of these molecules in the atmosphere, known as greenhouse gases, inhibit this thermal radiation to space and the result is an increase in ambient global temperatures.

The population of the earth has increased significantly in the last century and has increased the consumption of fossil fuels using combustion technologies. The subsequent release of carbon dioxide, is then released into the atmosphere and increases the relative proportion of greenhouse gases. The automotive industry has traditionally relied on petroleum products as a power source for the internal combustion engine, but has made significant efforts to switch to battery technology in recent years. It is likely that the sale of vehicles using hydrocarbons will be prohibited beyond 2030 and the preponderance of electric automobiles will become ubiquitous [59]. Aviation, however, is somewhat reliant on hydrocarbon fuel sources for the foreseeable future, due to the greater energy density of liquid fuel compared to batteries. There is also the fact that an aeroplane uses its fuel source also as a propellant, and each unit is expelled after use, therefore reducing the mass of the vehicle and energy required to provide the necessary force to propel it forwards and increasing overall fuel efficiency. Discounting for rapid advances in battery technology, hydrocarbon-based fuels are likely to remain in use for the foreseeable future.

The term greenhouse gases has become synonymous with the effect of carbon dioxide in the mind of the public and certain legislators. This is an oversimplification however, as carbon dioxide is one of a wide range of atmospheric components that contribute to the global warming effect. All of the inherent emission types from gas turbine combustion are greenhouse gases, including water vapour. Figure 1.11.1 shows estimates of the total contribution of each component towards radiative forcing; a measure of the change in energy flux in the atmosphere used to model climate change.

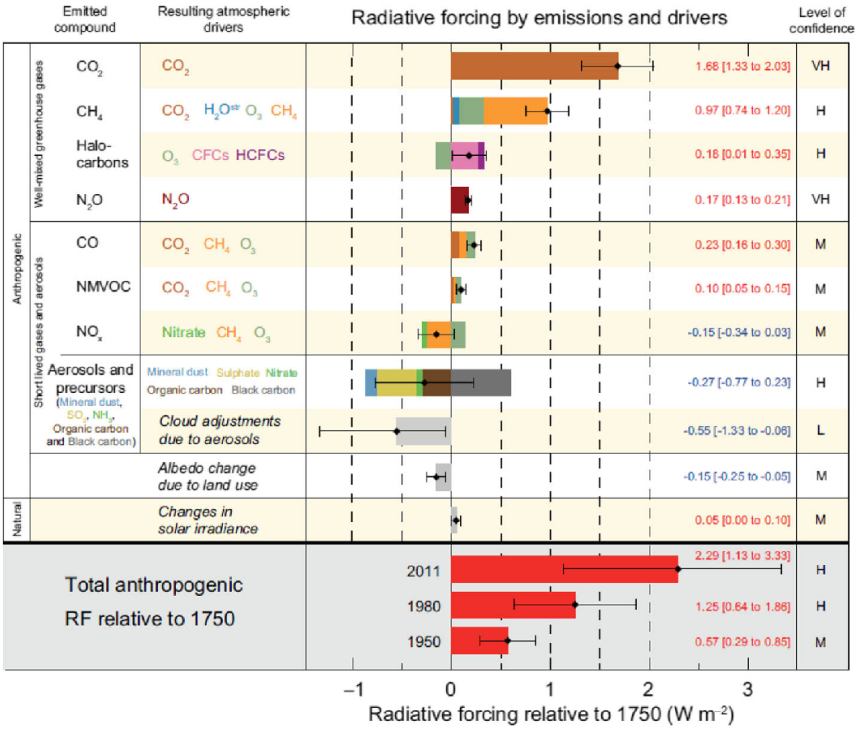

Figure 1.11.1: Global radiative forcing by emissions and drivers [8]

Carbon dioxide is seen to have the highest value for radiative forcing of around 4690 Wm^{-2}, while the contribution of soot, relevant to the topic of this thesis, is around 2800 Wm^{-2}; approximately 43.2% of the CO_2 contribution. The role of soot in atmospheric science is complex and is an ongoing area of interest. In recent years, the role of soot as a contributor to anthropogenic global warming was found to be underestimated [60]. Soot is a near black body and as a result, is a strong absorber of all wavelengths of direct incident light. It also plays a significant role in the mechanisms of cloud formation [61] depending on its presence within the atmosphere. This is significant as clouds inhibit heat loss and are the largest natural contributor to global warming. The effect of increased soot in the atmosphere acts to induce more cloud formation which potentially contributes indirectly to anthropogenic global warming [62]. It should be noted that the estimated values included in Figure 1.11.1 are not industry specific, and so the soot estimate includes non-aerospace sources such as forest fires, coal fire power generation and automotive diesel emissions. Currently, all transport is thought to contribute around 12% to total anthropogenic global warming, with aviation directly contributing around 2%. This means that aviation global warming emissions represent 14% of total travel emissions.

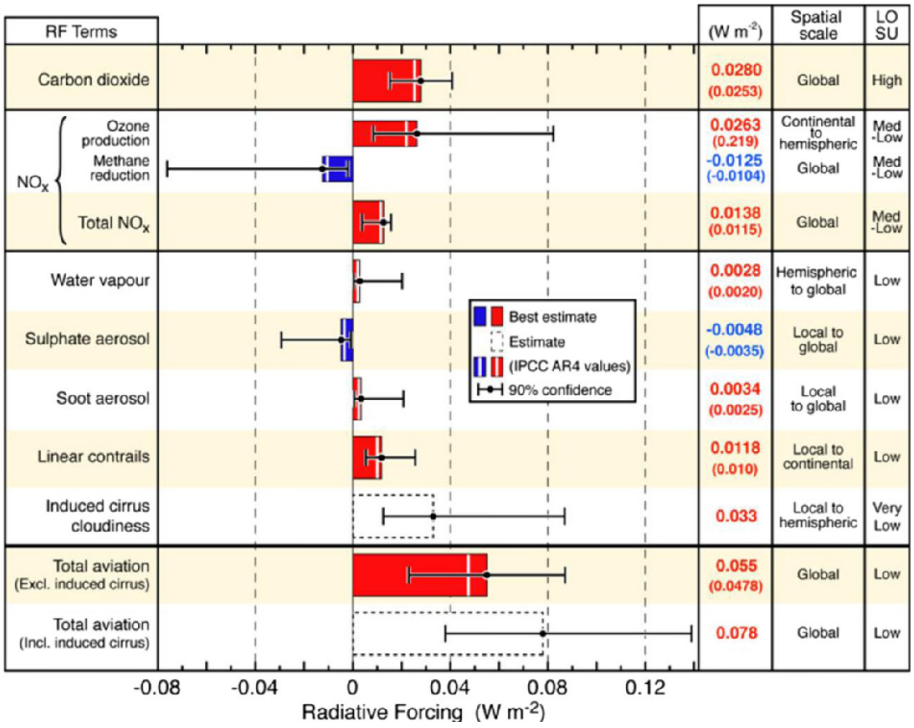

Figure 1.11.2: Global radiative forcing by emissions and drivers due to aviation [8]

Figure 1.11.2 shows estimates of emissions specific to aviation. In terms of radiative forcing, soot has around 12% of the contribution compared to that of carbon dioxide. The 90% confidence interval for these results gives a wide range of values for each potential contribution. For soot, this means that the contribution could be up to 7 times higher than the best estimate. The effect of induced cirrus cloud formation is also quantified in Figure 1.11.2 and it's potential effect on radiative forcing is estimated to be significant. The impact of soot suggests that the direct effects on radiative forcing, while not insignificant, may be of secondary importance compared to their ability to induce cirrus cloud formation at altitude.

The operation of a commercial jet covers a full height range from ground based when idling, taxing and taking off through to cruise at altitudes of up to 14 km (45,000 ft). As combustion occurs during the range of operation, soot emissions can be deposited at any altitude. Cruise typically occurs within the troposphere. Due to negligible presence of aerosols within the troposphere, the addition of BC emissions into this zone was previously thought to have a minimal direct effect on radiative forcing. More recent research has suggested that the effect of soot acts as cloud condensation nuclei (CCN), which in turn leads to enhanced cloud formation, which in the troposphere takes the form of cirrus clouds, which have a significant

effect upon radiative forcing. Aviation soot is predominantly composed of particles with a 10-1000nm diameter. As these particles age they coagulate into larger soot agglomerates and at the larger diameters, enhance their efficiency as ice-nucleating particles (INP), and so ice crystals form within the troposphere. These ice particles have a high refractive index and contribute towards the greenhouse effect. Both of these mechanisms are represented in Figure 1.11.3.

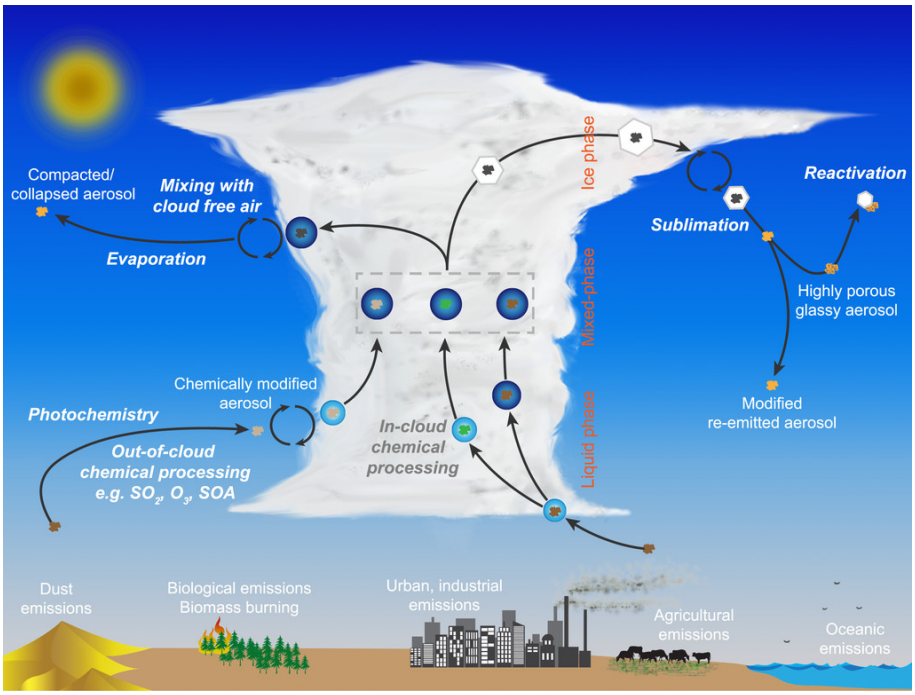

Figure 1.11.3: Nucleating particles and induced cloud formation [9]

Soot has the longest tropospheric lifetime of any aerosol [9], estimated to be around one week, though potentially for much longer [63]. The typical mechanism for the removal of aerosols from the atmosphere occurs through solubility due to precipitation. While aged soot is hydrophilic, freshly emitted soot is thought to be hydrophobic [64], and this behaviour accounts for its long residence time within the atmosphere. BC in other parts of the atmosphere potentially have the time to travel to the troposphere to induce cirrus cloud formation.

1.12 Effects of BC on Health

There is significant interest in reducing the levels of Particulate Matter (PM) in the atmosphere due to its negative effects on human health. Particulate Matter (PM) is

classed as any solid or liquid material suspended in the atmosphere. The term aerosol is erroneously used synonymously with PM, although specifically, aerosol refers to the combination of PM and air. PM can take many forms with its own sizes and specific characteristics depending on its source. The recognised classifications of PM are shown in Table 1.7.

Table 1.7: Summary of Particulate Matter Classification

PM Classification	**PM Type**	**Nominal Diameter**
PM 10	Coarse Particles	$d < 10$ microns
PM2.5	Fine Particles	$d < 2.5$ microns
PM1.0	Ultrafine Particles	$d < 1$ micron

In 2013, the International Agency for Research on Cancer (IARC) designated all PM in outdoor air pollution to be Group I carcinogens [65]. PM is dangerous to animal health due to its inhalability. Due to the relatively small diameters of PM particles they are able to enter the bronchioles of the lungs and be admitted into the bloodstream. Many types of PM are toxic and can cause significant health problems. Areas with elevated levels of PM typically experience more significant adverse health effects than lower ones. PM 10 has been estimated to increase all-cause daily mortality by 0.7% per 10 μgm^{-3} present in the atmosphere [66]. PM 2.5 specifically is thought to increase long-term cardiopulmonary mortality by 6-13% per 10 μgm^{-3} in the atmosphere [67]. PM has previously ranked as the fifth highest cause of premature deaths, accounting for more than 4 million lives annually [68] and a more recent meta-analysis suggests this value may be even higher [69].

As discussed previously, soot diameter is not unimodal and normally is comprised of particles classed as ultrafine, in the range of 10 – 1000 nm. The comparatively small size of soot particles suggest a larger negative effect on inhalability as they are more likely to penetrate deeper into the anatomy of the lung. Soot particulates are also associated with the occurrence of haze, as soot reacts in the atmosphere to form sulphur dioxides and nitrogen oxides, that decrease visibility and degrade air quality. Sulphur dioxide and nitrogen oxides can also mix with water and can cause acidification of precipitation, commonly known as acid rain, which can lead to the acidification of lakes and rivers.

Due to these concerns, many jurisdictions have introduced air quality legislation

targeted at limiting the presence of PM in the atmosphere in an attempt to mitigate the negative health effects encountered. The World Health Organisation (WHO) guidelines as of 2021 [70] recommend that the mean ambient PM 2.5 is no greater than 15 μgm^3 in any 24 hour period and no greater than 5 μgm^3 annually. The PM 10 guidelines are less stringent at 45 μgm^3 and 15 μgm^3 respectively, although it should be noted that the PM 10 measurement includes the PM 2.5 component. Figure 1.12.1 shows the PM 10 and PM 2.5 levels in selected countries classed as medium developed, highly developed, and very highly developed [10].

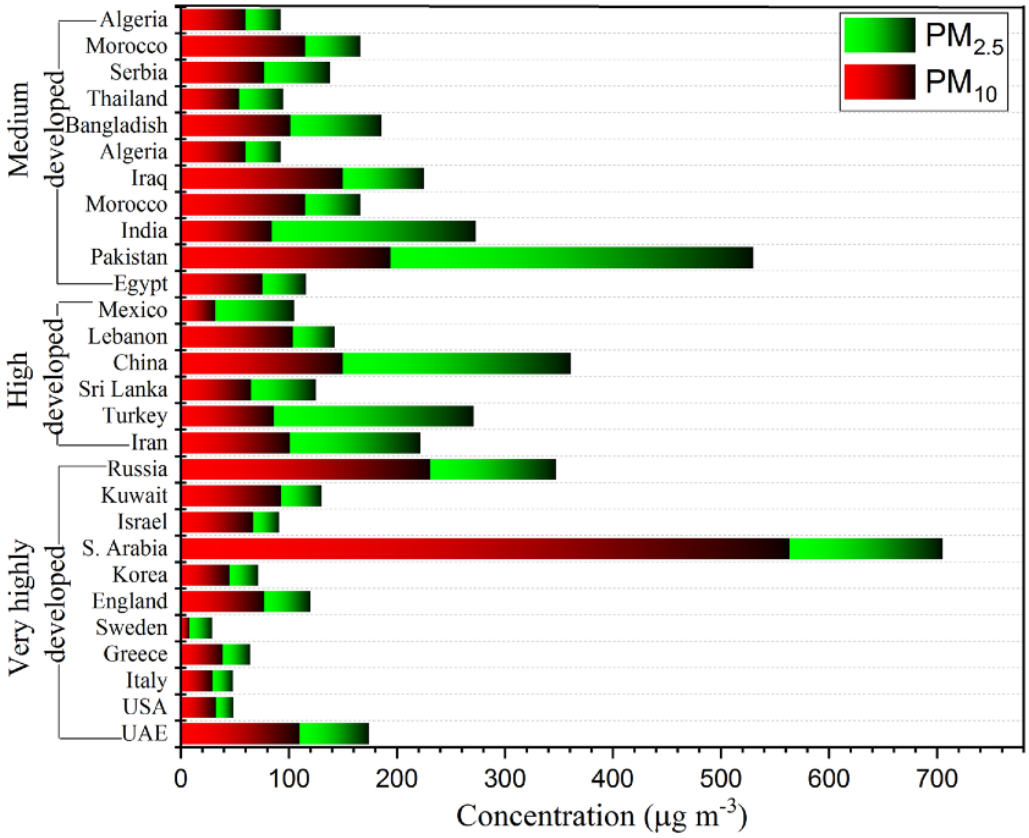

Figure 1.12.1: PM Emissions in Various Countries [10]

Only Sweden, Italy and the USA meet the WHO guidelines for maximum PM 10 as of 2019, while only Sweden meets those for PM 2.5. PM emissions due to aviation are specifically problematic in the areas surrounding commercial airports as they have the potential to cause long term adverse health effects to airport workers, local residents and passengers [71].

1.13 Research Proposal

The research conducted for the purposes of the completion of this thesis will focus on the role of the aromatic component of Jet Fuel on the emissions of nvPM, predominantly in the form of soot. While the volume percentage of aromatic hydrocarbons is associated with an increase in soot production, there is significant interest in analysing the impact of different aromatic molecular structures. This interest is driven by a desire to reduce the environmental and health impact of Jet Fuel by reducing soot emissions. There is also the potential for optimising conventional jet fuel by removing high-sooting components and also in pre-selecting ideal aromatic components that may form part of novel Aromatic Sustainable Alternative Fuels (ASAF).

The literature review pertaining to this work focuses on three main components; the theory underpinning the currently understood mechanisms for soot inception and generation; lab scale testing used to assess the soot forming propensity of individual fuel samples using the smoke point (SP), threshold-sooting index (TSI), and yield-sooting index (YSI); and pilot scale tests using currently approved SAF, NJFCP proposed fuels of interest and conventional fuels, with a specific focus on the proportion and type of aromatics present, to assess which fuel properties are the strongest predictors of a given fuels propensity to produce soot.

In the age of big data, large amounts of specification testing data are becoming available enabling meta-analysis for varying types and configurations of fuel. The current standard for assessing conventional Jet Fuel produced in or supplied to the UK (DEFSTAN 91-91) specifies 34 individual metrics, including the SP for each sample tested and the aromatic volume. Exploratory data analysis is conducted on this data set to assess the impact of aromatic volume on the SP to determine whether aromatic volume is formally a statistically significant predictor of the SP. The other variables of the data set are also analysed to see if any are a stronger predictor of SP. Contemporary machine learning techniques are used to acquire predictive capacity for whether a given fuel sample will fall within one of two categories; high-sooting SP and low-sooting SP.

Experimental campaigns are conducted using a modern range of nvPM classification equipment to measure the mass, size and number emissions of a range of

surrogate fuel blends where aromatic volume is the only direct variable. Aromatics of varying molecular mass and composition, in varying blend proportions are used in the combustion platforms at the LCCC at the University of Sheffield. nVPM Mass, Size and Number concentrations are correlated against available fuel parameters of interest, including the aromatic content (mass and volume), global density, ring carbon content, hydrogen content, blend TSI and YSI to establish which single variable is the strongest predictor of sooting propensity. Regression analysis is then used to obtain multivariate predictions which can then be used to predict soot performance of other potential fuels.

Chapter 2

Literature Review

2.1 BC Formation

Soot formation is a complex subject involving numerous chemical and physical mechanisms and stages. It is a by-product of the combustion process typically, but not exclusively, encountered in fuel rich flames due to incomplete combustion. The occurrence of soot is inextricably linked to the inception, development and growth of Polycyclic Aromatic Hydrocarbons (PAH), which develop into what are essentially carbonaceous particles [72]. While still an ongoing subject of research with uncertainties and unanswered questions, the formation of soot can be sub-categorised into four separate stages. These stages are represented in Figure 2.1.1 [11] and are as follows:

- Homogenous nucleation of soot particles
- Particle coagulation
- Particle surface reactions (growth and oxidation)
- Particle agglomeration

These stages are represented in Figure 2.1.1 [11].

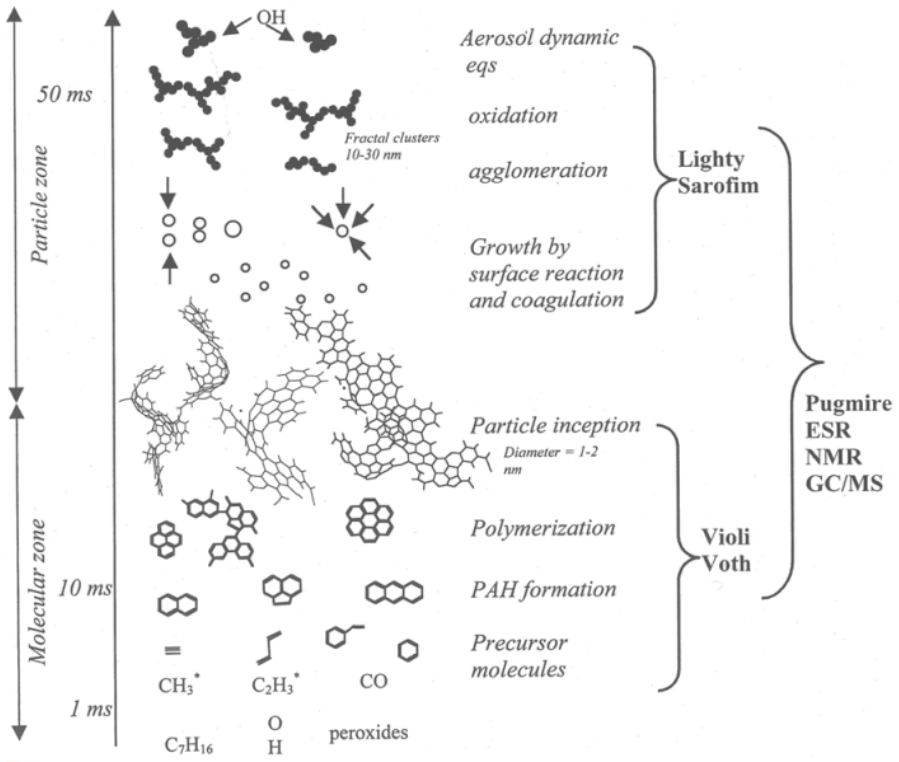

Figure 2.1.1: Soot Formation Process [11]

The route to soot particle nucleation starts with the inception of PAH's, although various reaction pathways have been described. Acetylene is thought to play a key roll in soot inception as shown in Equations 2.1 and 2.2, where acetylene reacts with butatrienyl radicals to form a phenyl group and benzene and a hydrogen atom, respectively.

$$n - C_4H_3 + C_2H_2 \rightarrow phenyl \tag{2.1}$$

$$n - C_4H_5 + C_2H_2 \rightarrow C_6H_6 + H \tag{2.2}$$

It was suggested, however, that both forms of the butatrienyl radicals would rapidly revert to their stable isomers and so would not be present in the quantities necessary to provide sufficient pre-cursors for PAH inception [73]. The authors proposed an alternative model instead whereby propargyl radicals combine to form benzene or a phenyl radical, as shown in Equations 2.3 and 2.4.

$$C_3H_3 + C_3H_3 \rightarrow phenyl \tag{2.3}$$

$$C_3H_3 + C_3H_3 \rightarrow C_6H_6 + H \tag{2.4}$$

Other pathways have been proposed involving cyclopentadiene, one reacting with a methyl radical, and one where two cycopletadiene molecules react to form napthalene and two hydrogen atoms, as shown in Equations 2.5 and 2.6.

$$C_5H_5 + CH_3 \rightarrow C_6H_6 + H + H \tag{2.5}$$

$$C_5H_5 + C_5H_5 \rightarrow napthalene + H + H \tag{2.6}$$

These four routes are thought to be of interest as their presence in combustion dynamics is thought to be ubiquitous, providing sufficient precursors for PAH formation, although it should be noted that only equation 2.4 leads directly to a PAH. Where a certain reaction pathway results in a benzene molecule, PAH formation is thought to occur through the reaction of a benzene radical with a benzene molecule, resulting in bi-phenyl. The subsequent reaction of radical biphenyl with acetylene, again, known to be abundant in combustion chemisty, completes a tricyclic aromatic molecule such as phenanthrene. This conceptual pathway is shown in Equations 2.7 and 2.8.

$$C_6H_5 + C_6H_6 \rightarrow C_6H_5C_6H_5 + H + H \tag{2.7}$$

$$C_5H_5 + C_5H_5 \rightarrow phenanthrene + H \tag{2.8}$$

The generation of a hydrogen atom in the majority of the proposed PAH formation routes is of significance to contemporary understanding of the initial stage soot inception. This is predominantly due to the hydrogen abstraction acetylene addition, or HACA mechanism, proposed by Frenklach and Wang [74]. In this proposed mechanism, a hydrogen atom reacts with a given hydrocarbon to radicalise that hydrocarbon and produce a hydrogen molecule, thas having abstracted a hydrogen atom from the molecule, as shown in Equation 2.9

$$C_nH_m + H \rightarrow C_nH_{m-1} + H_2 \tag{2.9}$$

The second step involves the reaction between the resulting hydrocarbon radical and an acetylene molecule in the location vacated by the previously abstracted hydrogen molecule, as shown in Equation 2.10.

$$C_nH_{m-1} + C_2H_2 \rightarrow C_{n+2}H_{n+1} \tag{2.10}$$

While it is likely that no one pathway exclusively leads to PAH formation, the HACA mechanism is generally thought to dominate due to several reasons. The first is the abundance of hydrogen and acetylene as byproducts of the initial stages of combustion during pyrolysis of most hydrocarbons. Secondly, unlike the acetylene mechanisms described in Equations 2.1 and 2.2, where a specific reagent is required for the acetylene to act upon, the HACA mechanism can occur with any hydrocarbon. This leads to two formation pathways; one where benzene and aromatic structures can be assembled directly from acetylene molecules without an aromatic pre-cursor, and the growth of existing mono or polycyclic aromatics by the addition of sequential acetylene molecules. Two reaction pathways showing the conceptual development of benzene into napthalene via the addition of two acetylene molecules is shown in Figure 2.1.2 [12].

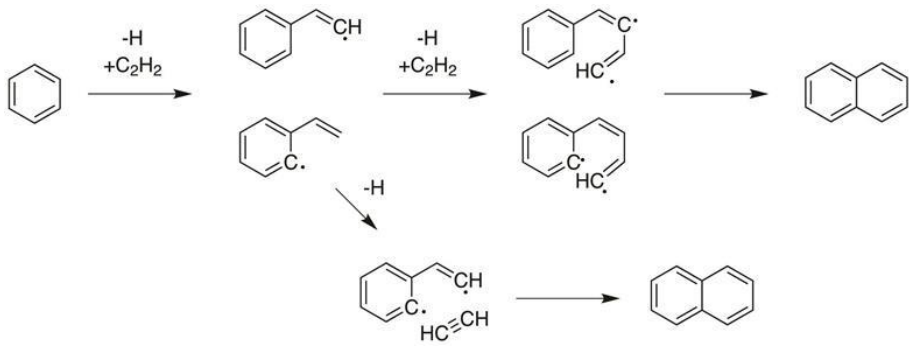

Figure 2.1.2: Benzene to Napthalene reaction pathways via HACA [12]

The significance of the role of Hyrdogen atoms in initiating the HACA mechanism is thought to be most pronounced in the main combustion zone, where soot inception is thought to occur [74]. This is thought to be due to the relative lack of O_2 and the relative abundance of H_2, and as a result, the rate of aromatic growth outpaces

that of aromatic oxidation.

The research pertaining to which pathways dominates PAH chemistry is ongoing. Relating to the topic of this thesis, however, the understanding of contemporary chemical kinetics leading to soot formation is not robust enough yet to comprehensively describe a fuel's propensity to produce soot based on composition alone. In the context of aviation combustion, typical combustion efficiency operates at close to 100%, meaning that the majority of Jet Fuel is decomposed during pyrolysis and reformed into the typical byproducts of hydrocarbon combustion. If a typical Jet Fuel is composed of around 8% to 15% vol of aromatic, then that aromatic component loses it's aromacity during this pyrolysis, and new aromatics, and subsequently PAH, and agglomerates are formed, eventually leading to soot. This soot inception, while most likely determined by the mechanisms discussed in the literature, rely on the relevant precursors being present, whether acetylene, methyl radicals, hydrogen atoms as relevent, which vary is proportion based on the composition of the hydrocarbon in question. There is no comprehensive understanding in chemical kinetics, however, as to how an aromatic will vary PAH formation based on composition alone, as ongoing research focuses on assessing the mechanism of PAH formation of a given aromatic, rather than focus on the aromatic itself. For this reason, empirical methods independent of kinetic studies, have been proposed and adopted to assess sooting propensity of different aromatic molecules and are discussed further here.

2.2 Discussion of Smoke Point

In simple terms, a given fuel's Smoke Point is the height at which a flame can reach without producing visible smoke. Practically, when readings are being taken by an observer, it is the height a flame can reach when it begins to emit visible smoke and ideally with no superfluous mass flow. At this point of transmission, the increase of volumetric fuel rate within a given flame volume increases the residence time of the reagents that are added to the flame. The occurrence of visible smoke that occurs can be attributed to the increased ratio of soot formation to oxidation time within the flame.

The smoke point technique is still widely used, and as discussed previously, is

still the primary method used for specification testing of the jet fuel. It's advantages in a research environment are similar to those as a fit for purpose test; it's relatively inexpensive due the small volume of liquid required, requires rudimentary equipment to operate the test and does not require an exceptional level of skill on behalf of the operator to perform the test. Its disadvantages are poor repeatability and reproducibility, and more importantly in a research context, it is limited in its ability to convey any mechanistic insight into the effects of chemical composition on sooting propensity. The value measured is purely empirical and is useful only as a means of comparison between two given fuels, or against an arbitrary standard, such as a when used for a specification test limit. Another disadvantage of note is the misconception that an increase in smoke point leads to an increase in sooting propensity, as may seem intuitive to legislators and the non-technical, instead of the correct conceptualisation that sooting propensity decreases as smoke point increases.

There has been suggestion [75] that parrafinic fuels with a lower sooting propensity and higher sooting propensity are most prone to experimental error using the SP method. This error can be attributed to the specifics of the apparatus used during the SP test under the ASTM D1322 specification. The scale used to measure flame height covers a range from 0 mm to 50 mm with an optical resolution of 0.1 mm using the manual method, which is reliant on human determination. As pure aromatics tend to be higher sooting fuels, they typically have lower SP's and the proportion of the observer error is larger at lower values. This accounts for the larger error in aromatic samples.

Parrafinic components with a lower sooting propensity typically have smoke points of greater than 50mm, and require the use of larger, non-standard measuring scales, which take them outside the ranges of the specification for which error, repeatability and reproducibility have been quantified. In order to measure the SP's of lower sooting fuels, such as alkanes within the 50 mm range of the ASTM D 1322 equipment, it is necessary to blend with a higher sooting component in order to lower the fuel's SP. The relevant components SP can be calculated using the TSI method which is discussed in the next discussion, but this attempt to back-quantify individual components SP's within the 50 mm range most likely introduces significant experimental uncertainty that is comparable with measurements of the unblended

component and neither method can be claimed to be experimentally robust.

2.3 Discussion of TSI

Several techniques have been proposed to normalise smoke point readings across the literature. These have been made in an attempt to introduce a more intuitive metric that increases with sooting propensity, and also, to mitigate the major weakness of the manual smoke point test; its poor repeatability and reproducibility. Each individual smoke point reading is not only affected by operator subjectivity, but also to the technical specifications of the lamp being used, such as the wick diameter and the ambient conditions under which the test is conducted, such as local temperature and humidity. To address these concerns, Calcote and Manos [45]) proposed the Threshold Sooting Index (TSI), which in its basic form is shown in Equation 1.8.

$$TSI = a\left(\frac{M_w}{h_{SP}}\right) + b \tag{1.8}$$

Where M_w is the molecular weight of the sample, h_{sp} is the smoke point height and a and b are constants specific to the apparatus used for the test. In situations where the smoke point height is unavailable, unobtainable or unreliable, or where mass or volumetric flow rates are found to have greater experimental fidelity, Equations 2.11 and 2.12 are available.

$$TSI_I = a'\left(\frac{M_w}{\dot{V}_{SP}}\right) + b' \tag{2.11}$$

$$TSI_{II} = a''\left(\frac{M_w}{\dot{m}_{SP}}\right) + b'' \tag{2.12}$$

Where V_{sp} is the fuel volumetric flow at the smoke point, m_{sp} is the gravimetric flow rate at the smoke point and a' and b' and a" and b" are constants specific to the experimental apparatus being used, while being distinct from a and b.

The TSI was the first attempt at normalising sooting propensity to be widely adapted and has several advantages over the smoke point. Firstly, it addresses the issue of experimental variability across different experimental platforms through the use of a calibration standard using hexane and 1-methylnapthalene. Individual

apparatus is calibrated to obtain the same TSI for these two substances in order to provide the experimental constants necessary to normalise results across different platforms, and yields a 100 point scale, with hexane at 0 and 1-methylnapthalene at 100. This normalisation reduces experimental variability and allows more accurate comparisons to be made. It also begins to take account of molecular composition by including a term for molecular mass of the fuel being tested. The rational behind this inclusion is an attempt to factor in equivalence ratios and its effects on incomplete combustion. Lower molecular mass fuels in a diffusion flame have a relatively larger molar fraction in the presence of available atmospheric oxygen in the absence of forced counterflow. As molecular mass increases, the number of moles present in a given unit of fuel decreases without an accompanying increase in available oxygen, skewing the stoichiometry of the relation to be fuel rich due to a higher equivalence ratio. This in turn leads to higher soot production due to incomplete combustion.

The advantage of the TSI over the smoke point is the ability to aggregate individual TSI's of a given fuel blend, assuming that the proportion and chemical composition of each component present is known. The equation for a combined TSI is shown in Equation 2.13.

$$TSI_{mix} = \sum_{k=1}^{n} x_k TSI_k \tag{2.13}$$

Where n is the number of components within a given fuel, x_k is the mole fraction of each component and TSI_k is the individual sooting tendency of each component. The ability to quantify the sooting propensity of blends is significant in the context of testing, research and potential optimisation of a fuel for a given purpose.

There are several limitations of the TSI method that have been discussed (Li and Sunderland). Firstly, the inclusion of the molecular mass term can yield results inconsistent with experimental observation. For example, nonane and hexadecane both have SP's of approximately 110mm. This indicates that both of these alkanes burned in a diffusion flame at the same conditions will have the same approximate sooting propensity. The inclusion of their respective molecular masses, however, at 128.3 $gmol^{-1}$ and 226.4 $gmol^{-1}$ yield significant differences in TSI, as shown in Equations 2.14 and 2.15.

$$TSI = a\left(\frac{128.3}{110}\right) + b \tag{2.14}$$

$$TSI = a\left(\frac{226.4}{110}\right) + b \tag{2.15}$$

Accounting for the same constant of a and b, The TSI method for these fuels give that hexadecane has an increase of 77% over nonane, suggesting that hexadecane may produce nearly double the soot of nonane. If the SP is taken as an experimentally valid method of comparing propensity to produce soot, then the TSI method is found to be inconsistent with previously tested SP results in some cases.

The TSI also, like the SP, remains unintuitive to some extent. As an attempt at normalisation, its purpose is to provide a comparative metric between two given fuels. It is not possible however to use the derived TSI quantification to obtain meaningful differences in sooting propensity between two fuels. A given hydrocarbon that has a TSI of 40 might not necessarily produce double the amount of soot under similar conditions as one with a TSI of 20. The TSI scale is essentially non-linear, but without a clearly definable logarithmic base value.

The introduction of a 100-point scale as part of the normalisation is also problematic. The selection of hexane and 1-methylnapthalene as the start and endpoint is arbitrary and without sufficient justification. Since the inception of the TSI method, hydrocarbons have been found to have negative TSI's, which is not only conceptually unintuitive, but introduces complications in the quantification of TSI values in computational models.

Fundamentally, the TSI still relies on the validity of the SP method and its inherent weaknesses as discussed previously. In section 4.1 the method of obtaining individual SP's of a given blend within the 50 mm specification range was considered. Using this method a high sooting fuel is blended with a lower one, with an accompanying high SP. A two component TSI can then be calculated, and given knowledge of the SP higher sooting component, Equation 2.13 can be rearranged to quantify the SP of the low soot component.

These factors mean that the SP and subsequently, the TSI methods not only have inherent flaws for quantifying sooting propensity, but also exhibit their largest

experimental uncertainty with low sooting saturated alkanes and high sooting predominantly unsaturated hydrocarbons, such as aromatics. This is especially problematic for the study of petroleum derived jet fuel and jet fuel surrogates, which are mulit-component and are typically composed of a paraffinic and aromatic component. The accuracy of using component TSI's in predicting surrogate sooting propensity is discussed later in this chapter.

Li and Sunderland [13] suggested an alternative approach and proposed the normalisation of smoke points, NSP, in 2012. They defined the NSP by taking the weighted average of smoke points where found in the literature. This encompassed 12 studies, and omitted any hydrocarbon with just one smoke point measurement in the literature, as an average in unobtainable. The NSP normalisation approach can be seen in Equation 2.16.

$$NSP = mean(AL_{SP}) \tag{2.16}$$

Where A is a fitting constant and L_{sp} is the relevant SP for that hydrocarbon type. To avoid A being under-constrained, they imposed the following condition described by Equation 2.17.

$$\Sigma_{i=1}^{m} \quad \sum_{i=1}^{m} A_i N_i = \Sigma_{i=1}^{m} \quad \sum_{i=1}^{m} N_i \tag{2.17}$$

Where i was the relevant study, Ni the total number of fuels in that study and n the total number of studies. The available data was used to obtain the maximum coefficient of determination of NSP vs SP and was found to have a good agreement with an r^2 of 0.970. The findings are shown in Figure 2.3.1. The authors propose that due to a 3% increase in r^2 over TSI, that the NSP method is statistically comparable to the TSI method and omits the problematic molecular mass term and requires the use of only one fitting constant. Each value is positive and is not arbitrarily scaled, as it is using the TSI method.

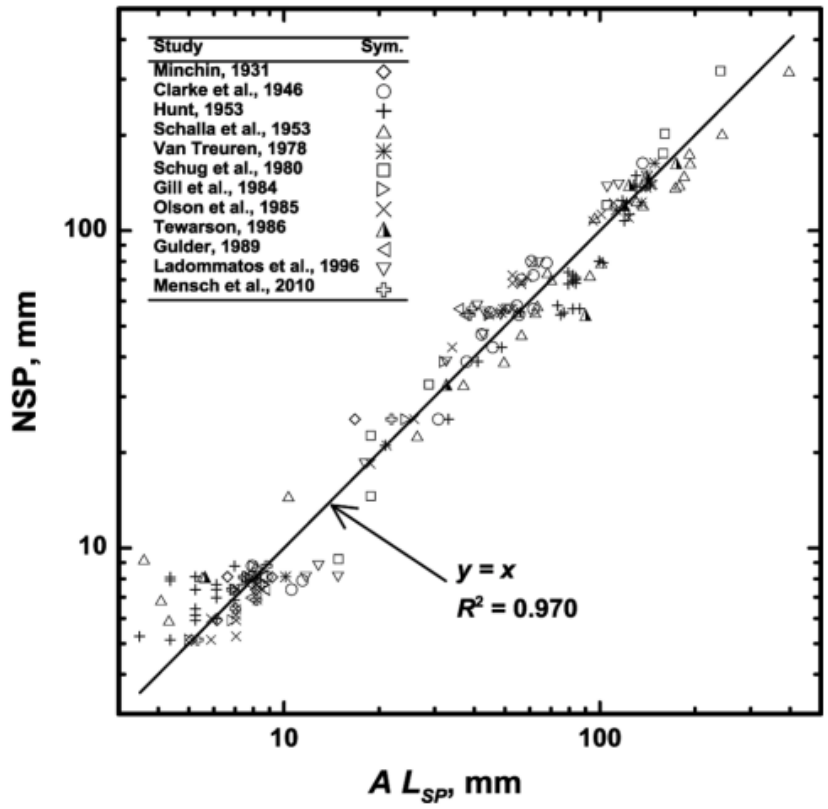

Figure 2.3.1: $AL_{SP} vs NSP$ [13]

There does seem to be significant scatter however, for hydrocarbons with a smoke point of less than 10 mm, which encompasses the aromatics. The authors then assess the NSP against the carbon to hydrogen ratio and find generally good agreement with Equation 2.16.

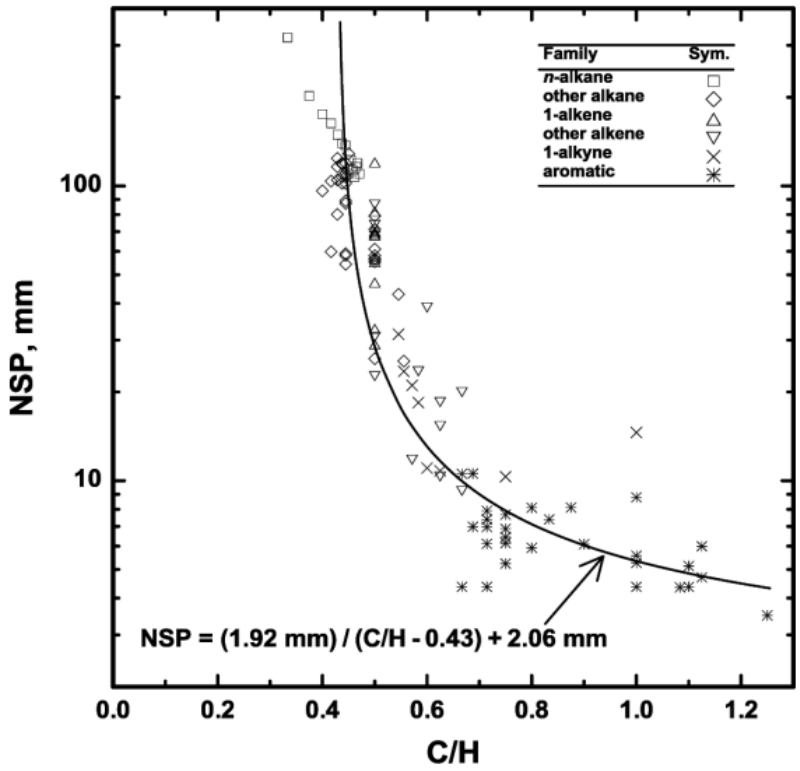

Figure 2.3.2: C:H vs NSP [13]

This is shown in Figure 2.3.2, where again, variability is seen to increase in the aromatic hydrocarbons, suggesting that the commonly suggested C/H ratio is more appropriate for parrafinic compounds, while not fully capturing the sooting behaviour for aromatics. The authors present the aromatic NSP's as shown in Figure 2.3.3, against increasing carbon number. They observe that aromatics with a n-alkane functional group mostly display a lower sooting propensity than other variations in functional group at the same carbon number. This may be somewhat of a spurious observation however, as Benzene and Toluene have no isomers against which to compare and the trend is not observed for Ethylbenzene, leaving only Propylbenzene and Pentylbenzene that potentially demonstrate this behaviour. Polycyclic aromatics are generally observed to have lower NSP's than alkylbenzenes, although this is a very general claim and the authors make no attempt to compare the behaviour to any fuel parameter.

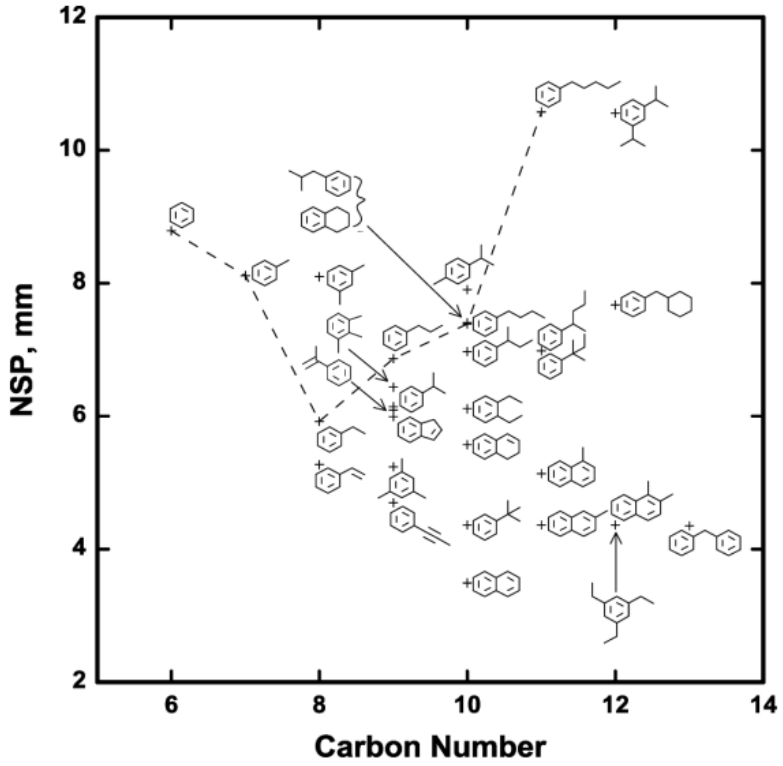

Figure 2.3.3: Carbon Number vs NSP for aromatics[13]

2.4 Discussion of YSI

McNally and Pfefferle [46, 47] proposed the Yield Sooting Index (YSI) in 2007 as an alternative metric for assessing propensity to soot, with a particular emphasis on obtaining more experimentally robust metrics for aromatic soot propensity. They diffused 400 ppm of one isomer of a specific aromatic hydrocarbon at a given molecular mass in a methane/air flame. Laser Induced Incandescence (LII) was then used along the centre-line of the flame to obtain the soot volume fraction. Every dopant was heated to 50^oC before being introduced to the existing flame to obtain a uniform initial temperature for the fuel mixture. As with TSI, an empirical scale was used to compare different fuels using a scale between 30 for benzene and 100 for 1,2-dihydronaphthalene. Benzene was selected due to having the simplest aromatic structure with no functional groups, while leaving values for 0-30 for potentially lower sooting hydrocarbons, without introducing problematic negative values as with TSI's, as discussed. 1,2-dihydronaphthalene was chosen as the upper limit due to it being a liquid at room temperature, as opposed to naphthalene, which is

a solid. The equation used to calculate YSI is show in Equation 1.9.

The authors claim several advantages over the TSI method. As propensity to soot increases, to does the soot volume fraction, fvmax. This avoids the problem of measuring aromatic SP's at low ranges, as discussed previously, as the LII accuracy is consistent over its range of measurements. The method also requires miniscule amounts of fuel; typically less than 100 microlitres, making more expensive fuels testable. 400 ppm typically equates to less than 1% of the fuel blend being comprised of the dopant under question, and so the authors view it as superior in capturing the molecular behaviour of the aromatic contribution to soot as it is not present in sufficient quantities to effect the bulk matter properties of the mixture, such as density and partial pressure. While TSI's are normally obtained by burning pure substances, YSI's are measured using aromatics diffused into an alkane base fuel, which they claim more accurately represents more practical fuel composition where aromatics form a minor component, as they do in Jet Fuel.

The authors initially determined YSI's for 68 individual hydrocarbons. Triplicate measurements were taken for each species, and overall measurement accuracy for each YSI was found to be ± 3%. The authors contrast this with a ± 15% accuracy for the 28 aromatic TSI's initially found by Calcote et al. and claim the YSI model to be at least comparable, if not superior, to the TSI method. Figure 2.4.1 shows the measured YSI's plotted against two groups of literature values for TSI's.

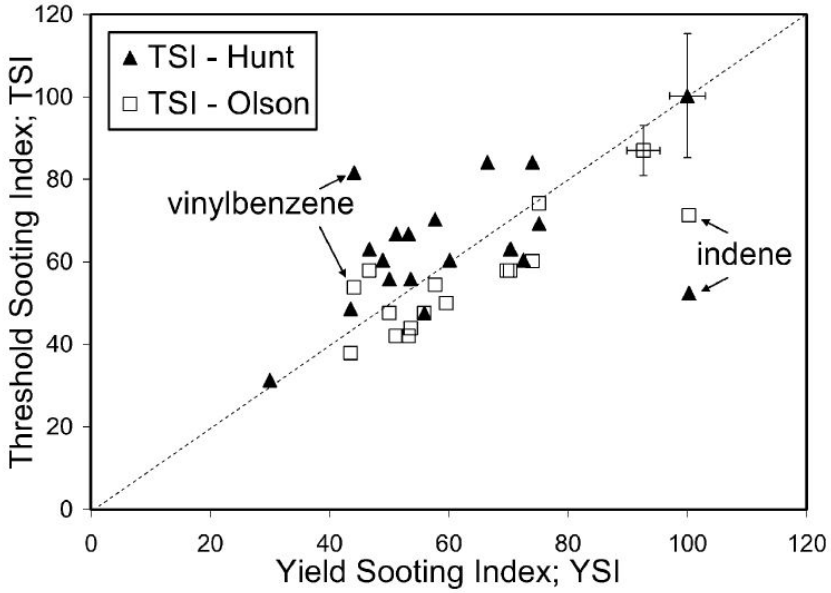

Figure 2.4.1: YSI vs TSI for aromatics[13]

Good agreement is generally seen, with an $r^2 = 0.8$ for the first group of 18 samples, and $r^2 = 0.84$ for the second group of samples. The correlation coefficients between the YSI and TSI groups are observed to be stronger than between the two TSI groups.

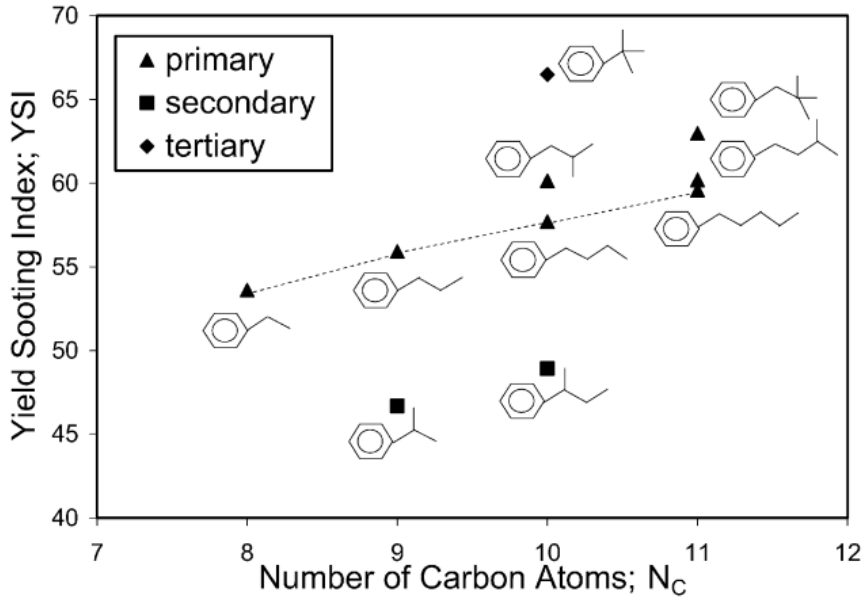

Figure 2.4.2: Carbon Number vs YSI for aromatics[13]

Figure 2.4.2 shows the YSI's found for several alkylbenzenes for ascending carbon number. The authors observed that sooting behaviour can be grouped based on the number of C-C bonds present on the benzylic carbon atom, that being the first carbon atom attached to the phenyl ring, with primary featuring a solitary C-C, secondary two C-C's and tertiary three C-C's. They observed higher YSI's for hydrocarbons in the order show in Equation 2.18.

$$tertiary > primary > secondary \tag{2.18}$$

As with TSI's, monotonic increase in sooting propensity as n-alkylbenzene's increase in carbon number, are observed, though it is claimed, less erratically than TSI values.

The authors use the method to calculate theoretical YSI values for multiply substituted benzenes by aggregating the combined effects of the molecular components present, with the claim that if side-chains do not interact, then the propensity to

soot of a given arrangement of functional groups should be an aggregate of those individual functional groups. This is represented in equation 2.19 for the case of 1-Methyl,3-ethylbenzene.

$$YSI_{1-Methyl,3-ethylbenzene} = YSI_{ethylbenzene} + YSI_{ethylbenzene} - YSI_{benzene} \quad (2.19)$$

It should be noted that it is necessary to remove a YSI value for benzene otherwise the contribution of two phenyl-rings will be aggregated into the final YSI value.

The authors use this technique to compare measured versus calculated YSI's for 26 multiply substituted aromatics as show in Figure 2.4.3.

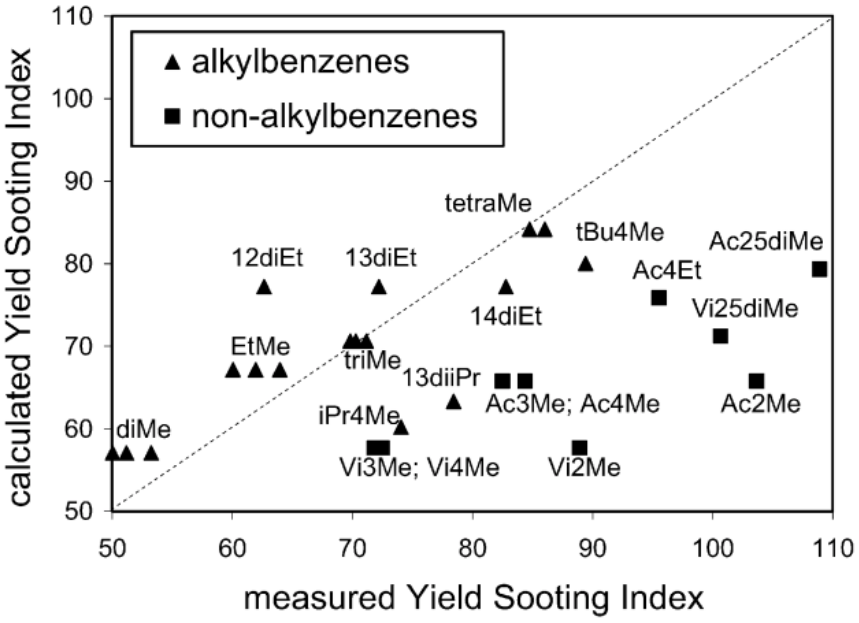

Figure 2.4.3: YSI vs Calculated YSI[13]

Alkylbenzenes are seen to have generally stronger agreement than non-alkylbenzenes, whose calculated YSI's significantly underestimate their observed values. All alkylbenzene isomers are seen to have YSI's within 7% of each other.

The YSI method has the advantage of obtaining more experimentally robust vales that predict the propensity to produce soot for a given hydrocarbon. The YSI values it provides are interpretable, logical and numerically consistent. They are more appropriate in assessing the sooting propensity of aromatic hydrocarbons specifically,

as the methodology was predominantly devised to overcome the disadvantages of previous methods (SP and TSI) of providing accurate values for this sub-category of hydrocarbons.

2.5 NJFCP

The complexity of the AJF approval process means that the introduction of a new drop-in fuel is time-consuming, expensive and with significant uncertainty as to outcomes for the fuel providers and jet engine OEM's. The National Jet Fuel Combustion Program (NJFCP) was created in December 2014 with the goal of aiding the strategic goal Q1 as defined by the FAA's Jet Fuels R & D strategy [76], defined as:

"Facilitate civil and military approval of alternative AJF pathways by enabling efficient evaluation for performance and safety through advancements of certification and qualification processes and collection and analysis of data"

The NJFCP aims to bridge the gap between fundamental lab scale research and applied pilot scale operational applications required by OEM's for certification. As an advisory body, the NJFCP is an organisation that occupies a position of significance in the ongoing discussions regarding the suitability of future AJF's and is influential on regulatory decision making on both the FAA and Subcommittee J of the ASTM International Committee, who in turn take NJFCP findings into consideration when refining the D4054 specification. This in turn means the NJFCP is influential in the process which governs the approval of new AJF pathways. The NJFCP's research collaborations are widespread and include experiments funded at the LCCC at the University of Sheffield.

The NJFCP has defined three areas of focus in their efforts to research the combustion effects of AJF's which they define as Figures of Merit (FOM), which are summarised as follows:

- Lean Blow-Out (LBO)
- Cold Start
- Altitude Relight

The NJFCP, based on the research of its predecessor, the CRATCAF, identifies three fuel properties as having the most significant effect on combustion performance; flash point, viscosity and aromatic content. The focus on aromatic content outside an emissions framework is due to the prevalence of low derived cetane number (DCN) and its adverse effects on Lean Blow-Out performance. While particulate matter emissions are not a specific research focus of the NJFCP, as all Jet Fuel metrics are inter-related, the reduction of aromatic content for combustion performance can positively reduce emission levels and improve combustor longevity but adversely affect energy content and seal swell performance, as discussed previously.

The NJFCP approaches the introduction of alternative fuels as suitable when their performance is comparable to that of petroleum derived kerosene fuel, and has defined three candidate fuels defined as worst-case, nominal and best case, the parameters for which were decided in conjunction with the feedback of OEM's [20].

Given the nomenclature A-1 (best), A-2 (nominal), and A-3 (worst), these three fuels based on JP-8, Jet A and JP-5 respectively, were sourced based on the desired properties described in Figure 2.5.1 and obtained in significant quantities to provide for comprehensive experimentation through various partners. The idealised jet fuel is described as having low density, viscosity, aromatic content and viscosity, while having a high hydrogen content and cetane number.

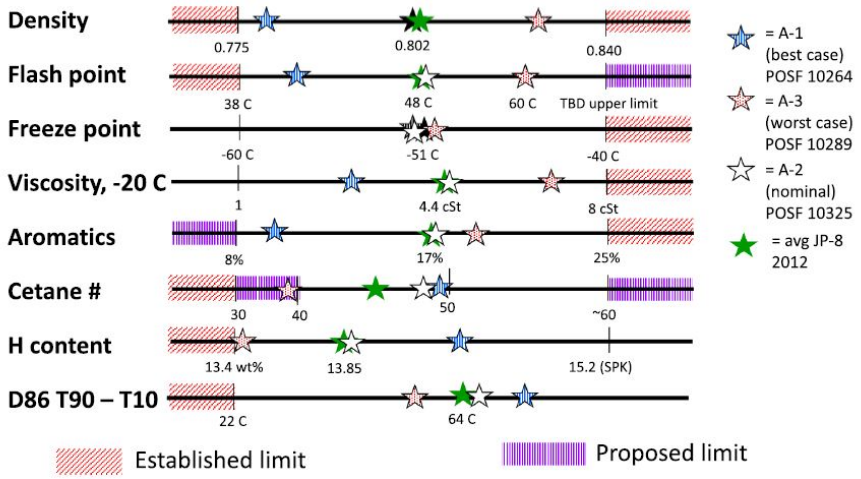

Figure 2.5.1: NJFCP Fuel Classifications[14]

There is research however, that suggests that soot production may correlate with hydrogen content rather than aromatic volume in legacy vehicles [22]. The findings of this paper are discussed later in this chapter.

2.6 Aromatic Specific Work

Table 2.1 summarises the experimental campaigns analysed for the purposes of this literature review whereby the effect of molecular composition, aromatic type or aromatic proportion to particulate matter emissions was a key area of investigation.

Table 2.1: Experiments in which aromatics were varied in order to assess BC emissions

Base Fuel	*Aromatic Additive*	*Research Platform*	*PM Technique*	*Reference*
Jet-A	i)Mixed Xylenes ii) Methyl-Napthalene iii) Anthracene	Phillips "2-inch combustor"	Flame Radiation	[15]
Jet A	i) Solvesso 150 ii) Solvesso 150D	Turbofan - unidentified	BC mass - MSS 483	[77]
JP8 Surrogate	i) 1,3,5-trimethylbenzene ii) n-propylbenzene iii)iso-propylbenzene, iv) m-xylene	Custom Burner Smoke Lamp	LII	[78]
JP8 Surrogate	i) p-xylene ii) sec-butylbenzene iii)benzene, iv) alpha methyl-styrene	Smoke Lamp	LOS Avergae Light Extinction	[79]
n-alkanes	i)Benzene ii) Xylene iii) Toluene iv) 1-methylnapthalene	Phillips "2-inch combustor"	Smoke Lamp	[80]

Naegeli and Moses [15] conducted an experimental campaign in which six test fuels were formed by blending Jet A with various aromatic additives. These test fuels were of equal hydrogen content at 12.8% (by mass) and were burnt at a variety of inlet conditions.

While the overall H/C ratio was maintained, the intent of the experiment was to assess the effect of variations in molecular structure on the propensity of a fuel to produce soot. Measurements of flame radiation were taken in order to indicate the relative levels of soot formation, along with exhaust smoke number (compliant with SAE-ARP1179). Fuel composition was varied in order to include a variety

of aromatic types, including monocyclic (various xylenes), napthalenes (methylnapthalene), dicyclic and tricyclic (anthraciene and tetralin) along with decalin, although no justification is given for the inclusion of this non-aromatic species. It may be presumed that a saturated form of naphthalene may be of interest to fuels that have been hydroprocessed or as a surrogate for pure naphthalene which cannot be blended to the comparable proportions of other aromatic species due to its solubility limits. Diesel Marine Fuel was also included in three blends to vary the final boiling point of the fuel in order to assess as an experimental variable. It should be noted that as with Jet-A, DFM contains various aromatic species. Every add-in is identified as essentially pure, although no purity is quoted and the methylnaphthalene was not identified as a pure substance but a mixture of various polycyclic aromatic molecules. Ambiguities as to the exact composition of each test fuel are compensated somewhat by the inclusion of UV spectroscopy and Flow Injection Analysis (FIA) by type. The results showed a generally good correlation between the smoke number and the relative mean radiation index. The final boiling point of the fuel had no effect on smoke formation, nor did its viscosity. It is of interest that DFM was included in three of six blends for the purpose of raising the boiling point of a given blend. This was not found to be of experimental interest and added additional uncertainty as to the molecular composition of each blend. However, the inclusion of DFM yielded essentially the same radiative index as its comparable fuel without.

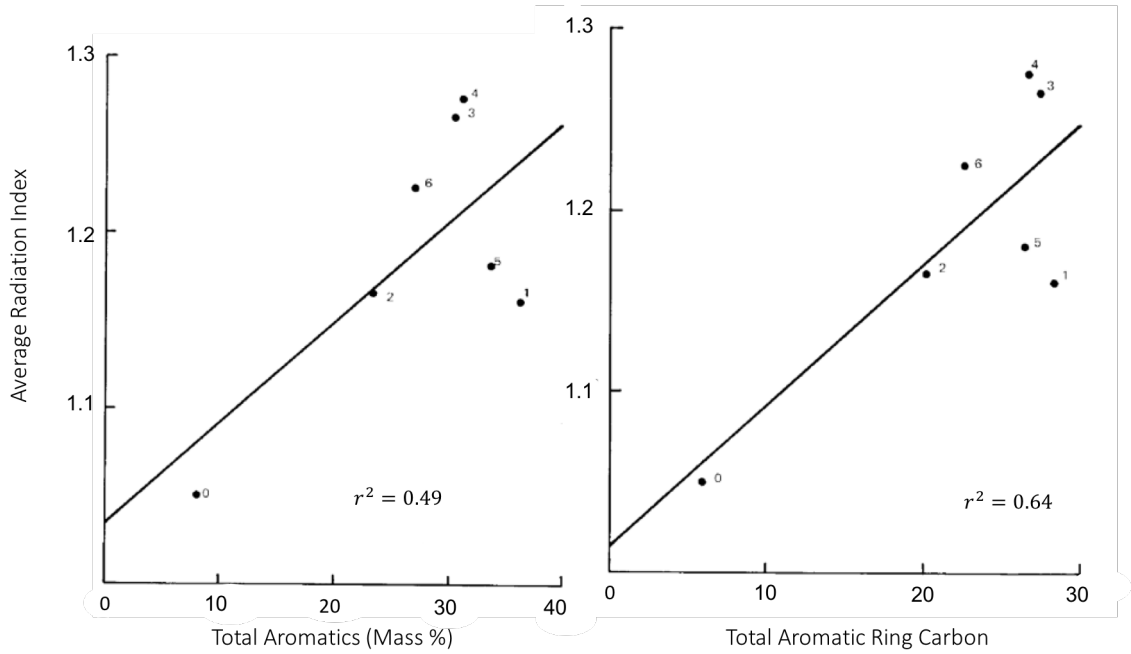

Figure 2.6.1: Flame Radiation correlation with a) Total Aromatic Content and b) Ring Carbon Content. Reproduced from [15]

Figure 2.6.1 show the correlation between total aromatic content (wt%) and ring carbon (wt%) respectively and their effect on the average radiation index. The composition of the fuels labelled 0 to 6 are summarised in Table 2.2.

Table 2.2: Summary of Fuels listed in Figure 2.6.1

Fuel Number	**Fuel Composition**
0	Jet A
1	Jet A with 31.11% mixed xylenes
2	Jet A with 35% decalin and 21.97% mixed xylenes
3	Jet A with 25% methylnapthalene
4	Jet A with 5% DFM and 24.1% methylnapthalene
5	Jet A with 5% DFM, 0.5% anthracene and 21.8% mixed xylenes
6	Jet A with 5% DFM, 23.06% tetralin and 5% mixed xylenes

A positive, but generally weak correlation (r^2=0.49 and r^2=0.64) was found for aromatic ring carbon effect on soot proclivity. This suggests that the proportion of ring carbon present may be more indicative of a fuels propensity to produce soot. The larger proportion of soot generated by fuels 3, 4 and 6 was predominantly attributed to the higher percentage of dicyclic aromatic content, although it should be noted that fuels 3 and 4 used various unidentified polycyclic aromatics in comparison to the pure tetralin used for blend 6. Previous literature had reported strong anti-correlations of hydrogen content with soot formation, although in this study,

only fuels 0 and 1 (Jet A and Jet A with Xylenes) demonstrated this behaviour in a linear fashion. The authors conclude that Jet A supplemented with single ring aromatics, such as Xylene, is representative of the typical composition of Jet A, although a more contemporary assessment of petroleum derived Jet fuel composition shows this assumption to be overly simplistic. Nor do the authors account for the variability of the aromatic fraction of petroleum derived Jet A as demonstrated by metadata analysis contained within this thesis and known at the time of authorship of the paper under discussion. This brings into question the authors decision to confidently infer a linear relationship from only two data points. Despite these points, the data clearly demonstrate a significant variation in flame radiation based purely on a variation of molecular composition as opposed to hydrogen content being the predominant soot determining factor, as established in previous literature. The presence of dicyclic unsaturated and partially unsaturated molecules is shown to significantly increase flame radiation and hence, soot formation.

The authors assessed the deviation from hydrogen content correlation, Δ R, for each fuel with the proportion of polycyclic aromatic ring carbon present. An excellent agreement was found, with a least squares correlation coefficient reported of 0.97. The results for fuel 6 however, containing tetralin (tetrahydronapthalene), does not follow the correlation. The authors attempt to compensate by initially considering tetralin to be the structural equivalent of naphthalene (10 unsaturated ring carbon atoms), which significantly underpredicts the deviation. A compromise was found using a proportioning value created using the ratio of unsaturated ring carbon in naphthalene compared to tetralin. The justification for doing so seems purely empirical and needs further validation, however. While a strong correlation was observed for polycyclic ring carbon, the lack of intermediate blends between the comparatively low and high polycyclic volume (<5% and 18-20%) and the absence of a greater variety of polycyclic molecules leaves further evidence being required as to a definite linear correlation of polycyclic aromatic ring content to soot formation. The effect of anthracene in fuel 5 is not highlighted at all by the authors, whom consider its deviation to be generally in keeping with the linear correlation. The authors do conclude that the presence of decalin as a fully saturated polycyclic has very little effect on soot formation, although no literature or data could be found to

justify this claim.

Brem et al. [77] conducted an experimental campaign on an in-service turbofan to assess the effect of total aromatic content of Jet A on BC and nvPM number. The Jet A was supplemented with two different aromatic solvents, Solvesso 150D and Solvesso 150, with the prior claimed to be predominantly formed of monocyclics and the latter containing an additional 6% v/v of napthalenes. The Jet A and aromatic solvents were not pre-mixed in preparation for this campaign. Instead, the two components were mixed in the fuel line, allowing the aromatic content of the fuel to be increased by 10% v/v. Samples were taken 13.5m upstream of the engine for offline analysis for total aromatic content (ASTMD1319), total napthalenes (ASTMD1840) and hydrogen mass (ASTMD5291). It was found that the bulk matter physical properties of the fuel mixtures varied little dependant on which solvent was used.

BC mass was measured using a Micro Soot Sensor (MSS Model 483, AVL Inc) in parallel to a particle counter (APC, Model 489, AVL inc) to measure nvPM number concentrations and a Scanning Particle Mobility Sizer (SMPS, Model 3983, TSI Inc) to measure nvPM size. Readings were taken at varying thrust levels over the range of operation of the engine, although only results between 7-100% maximum thrust were considered as experimentally valid. The mass and number concentration emission profiles are shown in Figure 2.6.2. Results for nvPM mass dependant on thrust were in keeping with previous performance and expected trends; namely an increase with thrust Particle number, however, peaked around the 65% thrust condition and declined thereafter. This was predominantly attributed to increased coagulation of particles at higher thrust levels. Both fuels, irrespective of composition, followed this trend. However, it was anticipated that the difference in naphthalene content between the two solvents would lead to significant variation in absolute nvPM mass and number concentration, although only slight differences were observed. The normalised results correlated with aromatic concentration and hydrogen content against the performance of unblended Jet-A are shown in Figure 2.6.2.

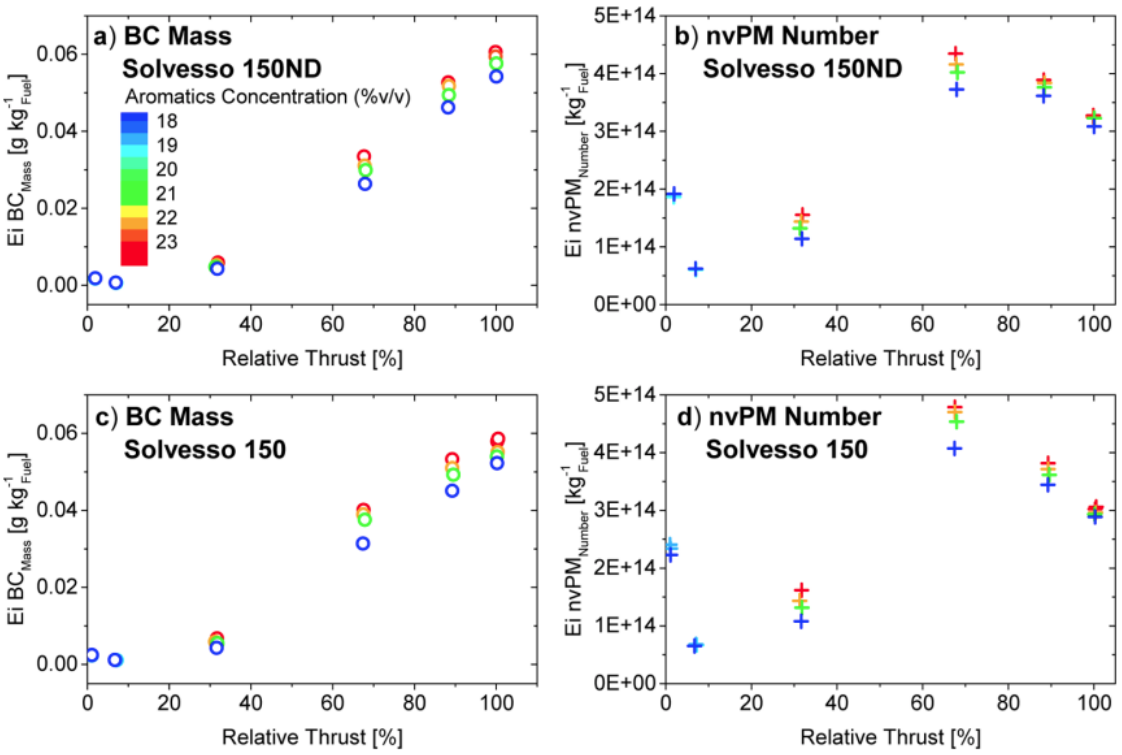

Figure 2.6.2: Black Carbon and NvPM number Emission Indices a) Total AromaticSolvesso ND Content and b) Solvesso 150

The authors proposed that an increase in aromatic proportion is due to condensation of phenyl radicals and addition of smaller hydrocarbons, presumably acetylene and methane radicals. The authors anticipated that the increase in naphthalene content 0.78% v/v to 1.18% v/v would produce significant changes in both emission indices for mass and number, although no significant change in either was observed between the two aromatic solvents before normalised comparison. Both emission indices increased by factors of 1.59 and 1.51 respectively at 30% thrust due to the 5.8% v/v increase in aromatic content. Each increase in thrust however, did not cause as large an increase in either emission indices. It was hypothesised that at lower thrust levels, and accompanying lower temperatures, the 30% thrust condition resulted in a higher proportion of incomplete combustion of the aromatic component, as an RQL combustor configuration was used in this engine. The authors suggest the two oxidation zones in the combustor, featuring rich then lean combustion conditions, had a significant effect on the soot formation in each dependant on their local conditions. The combustion that occurs in the rich zone does so with a relatively high fuel to air ratio, which is more likely to lead to products of incomplete combustion. This

effect is most prominent at 100% thrust and a higher FAR, which diminishes to near stoichiometric conditions near engine idle. The authors also commented that the fuel molecular effects were only relevant in the rich zone as the raw fuel is initially pyrolised and decomposed in comparison to the lean zone, in which potentially only soot is being oxidised.

The increase in emission indices based on aromatic type was compared after being normalised to the performance of unadulterated Jet-A, with 40% higher mass and 30% higher number at the 30% thrust level. It is worth noting that this is with the total aromatic proportion being near identical, such is the significance in the variation in molecular composition. The increased proportion of naphthalene however, was found to be negligible at 100% thrust, which is attributed to the previous argument that fuel chemistry effects being negligible at rich conditions.

When using the fuel hydrogen content as a metric, the effect of the difference in napthalene is negligible, and both fuels seem to correlate well, although no correlation coefficient is quantified. This would suggest that hydrogen content is a more likely indicator of size and mass emissions as opposed to total aromatic or naphthalene content, although the authors acknowledge that their sample size is small, using only one batch of Jet-A which is insufficient given the wide range of aromatic content allowed within the specification. The authors use this work to propose an empirical model for predicting number and mass indices based on Equation 2.20, where ΔEI_x are the emission indices for mass and number, a_0 and a_1 and are coefficients of determination established using a method of least squares, $\hat{F}$ is the percentage of engine thrust and ΔH is the change in hydrogen mass content.

$$\Delta EI_x = (a_0 + a_1 x\hat{F}) \cdot \Delta H \tag{2.20}$$

The model is shown to predict number and mass within 5% except at the 30% thrust condition, where the model underpredicts mass by 12% and number by 8%. The authors acknowledge that the model would be questionable for use in non-RQL combustors, at less than 30% thrust and with hydrogen content deviations of greater than 0.6% m/m.

The primary focus of this work is not on the exact composition of the aromatic component. The authors have not reported any breakdown of the hydrocarbon type

of the base Jet-A blend using a high-resolution test such as GCxGC, and so there is uncertainty as to the proportion of alklybenzenes, napthanlenes and cycloaromatics present. This is also true for the aromatic solvents used, which was selected based on the justification that its boiling point and molecular weight ranges encompass the aromatic component of those found in Jet-A, which is a bold claim to make without the necessary data to support it. The hydrogen correlation corresponds reasonably well however, which may justify this rationalisation. The correlation performs weakly at 30% thrust however, which raises the question as to how the aromatic fuel component is dependent on the fuel-to-air ratio, which ultimately determines temperature, and strongly influences the mechanisms of soot formation. Investigating the particular temperatures at which phenyl groups will not oxidise and subsequently lead to more PAH formation by condensation reaction mechanisms may prove insightful. The work does show that empirical relations based on fuel properties can be appropriate to specific circumstances.

Gu et al. [80] formed surrogates comprised of varying composition whose hydrogen to carbon ratio was maintained at 1.54. The chosen aromatic components were benzene, xylene, toluene and 1-methylnapthalene. Flame radiation was used to indicate BC soot formation. The Smoke Point, aromacity and hydrogen to carbon ratio of each sample was assessed but no single metric could describe the sooting propensity of the fuels. They did, however, propose an empirical model with a correlation coefficient of 0.96 as described in Equation 2.21, where F is the Flame Radiation, a, b and ϕ are constants, S is the Smoke Point and ψ is the hydrogen to carbon ratio.

$$F = aS^b e^{\frac{\phi S}{\psi^2}} \tag{2.21}$$

It should be noted that this study did not use a gas turbine engine or combustor and inferred a relation between flame radiation and actual soot volume fraction, although good experimental agreement is observed between this study and previous experimental data obtained by Olsen et al. [81]

2.7 Surrogate Fuels

As discussed previously, petroleum derived Jet Fuel is comprised of hundreds of hydrocarbon molecular structures in varying proportions. Oxidation mechanisms and reaction pathways, especially for something as complex as soot production, are not fully understood even for single component flames. The complexity of analysing and modelling kerosene fuels beyond bulk matter property relations is not possible at the time of writing. In order to simplify the compositional complexity of Jet Fuel research so that modelling and fundamental fuel property correlations can be made, the use of surrogate jet fuels has been widely adopted in research into Jet Fuel combustion behaviour [82, 83, 84].

A Jet Fuel surrogate can be said to be a selected group of hydrocarbons, whose total number is significantly less than the variety found in kerosene Jet Fuel. As opposed to hundreds of hydrocarbon types, a typical surrogate will feature less than ten. The aim in surrogate component selection is to select hydrocarbons whose aggregate contribution forms a blend whose properties closely resemble that of a petroleum kerosene fuel. It should be noted that in general, the individual hydrocarbons selected are not being assessed specifically and varied to measure their individual contribution, but to achieve specification parameters as close as possible to a kerosene fuel. Such a simplification of composition allows a more practical approach to chemical kinetics modelling. The aim of producing a surrogate fuel is not to explore the effects of vastly varying chemical composition, as with AJF's, but to obtain an optimum composition to explore the behaviour of conventional jet fuel. Nevertheless, as the inclusion of an aromatic component is necessary for the creation of surrogate fuels, their implementation is of relevance to this thesis.

Hydrogen content, ring carbon content, density, TSI, YSI, NSP and aromatic volume are the selected combustion relevant parameters for surrogate fuels found in the literature to date. Despite the wide range of liquid aromatics available for selection in a potential surrogate, only ten individual aromatic molecules are included in the literature, two of which are isomers of trimethylbenzene. Toluene features extensively in the alkylbenzene category and 1-methylnapthalene and tetralin are commonly used as default polycyclics. Toluene, methylnapthane and tetralin are molecules that are widely available, relatively inexpensive, and whose fundamental

chemical kinetics models are the most understood among aromatics.

2.8 Gap Analysis & Contribution to Knowledge

Fuel specification currently controls a given fuels propensity to produce soot by regulating its smoke point and aromatic content by volume. A comprehensive review of the available data concerning Jet-A1 certification for 2014 in the UK shows a weak correlation between these two metrics. As there is sufficient evidence that a fuel's given smoke point will be a generally accurate performance of its smoke number used for engine certification, it can be surmised that aromatic content on its own is not a reliable predictor of soot emission performance. Further analysis shows naphthalenes content alone to have a weaker correlation, while the proportion of naphthalenes in the overall aromatic content is shown to have the strongest correlation concerning aromatic data. The density of a given fuel, which is a strong indicator of its degree of hydrogen saturation, and therefore hydrogen content, shows the strongest correlation of all available metrics, but is not significant enough to be a reliable indicator based on specification data alone. This suggests that there is a significant knowledge gap with regard to the specification and which metric is the main indicator of soot formation, which this proposed work will indicate which is the strongest parameter.

Comprehensive work has been conducted in the literature concerning the total proportion of aromatic content and soot propensity and various properties have been suggested as the most reliable indicator. These properties include hydrogen content (synonymous with hydrogen to carbon ratio), aromatic content, ring carbon content and the presence of polycyclic aromatics in the form of napthalenes. The literature reveals that limited work has been conducted previously on the composition of the aromatic content of jet fuel by assessing the contribution of the presence of individual aromatic species. Where work has been conducted, molecular type has been somewhat of a secondary consideration as typically, low molecular mass aromatic additives such as Toluene and the Xylenes, have been added to conventional Jet-A in order to increase the total proportion of alkylbenzenes. The emission performances of these blends have then been taken as indicative as to the performance of alkylbenzenes or total aromatics generally, an assumption which is not supported

by evidence currently available in the literature. Indeed, available Threshold Sooting Index and Yield Sooting Index data suggests that each aromatic component has a variable contribution to soot formation. This is especially important for isomers of the same molecular mass, as current GCxGC fuel composition techniques only differentiate between molecular weight and not molecular structure. Available GCxGC data suggests that as overall aromatic content is significantly variable, there is also the possibility for significant variation of dominant aromatic types present, which may account for the disparity in smoke point and black carbon indices in the experimental data. TSI and YSI data would suggest that isomers of the same molecular weight present in a given fuel would give the same hydrogen content, aromatic content with slight variations in density and still have significantly varied soot propensity. This thesis will contribute to knowledge by assessing the applicability of the TSI and YSI to individual aromatic performance on an aerospace platform.

There is a desire within the aerospace community to lower the aromatic proportion of petroleum derived jet fuel in order to reduce the soot emissions of the sector due to the correlation between total aromatic content and soot emissions. This can be achieved by various methods such as hydro-processing whereby the saturation of a fuel batch can be increased, whereby aromatic hydrocarbons are converted to cycloparaffins. This process is expensive and has undesirable secondary effects on other fuel parameters. The identification of aromatic species that are more likely to produce soot would allow regulators and refiners the possibility to selectively exclude certain aromatics by omitting certain boiling ranges from final blends or via some other industrial convert high soot to low soot aromatics. This work will contribute to knowledge by identifying these high soot aromatics.

The growing contribution of alternative fuels to the aviation sector also introduces concerns and opportunities with respect to the presence of aromatic hydrocarbons. A significant proportion of alternative fuels have little or no aromatic content and are known as Low Aromatic Content Fuels (LACF). As discussed previously, aromatic hydrocarbons are a necessary fuel component needed to induce seal swell in conjoining fuel lines. Currently, alternative jet fuels are only approved as 'drop-ins' that can be blended with petroleum derived fuel up to 50% by volume, effectively halving the aromatic content already present. In the current situation, this pro-

vides a sufficient aromatic component within experiential limits to induce seal swell. There is significant interest in using independent alternative fuels at 100% blend and potentially, a LACF would need to be augmented by adding an aromatic component. Such an aromatic additive would ideally need to meet an optimum comparative performance in terms of its ability to induce seal swell and provide low soot emissions. This work contributes to knowledge by providing comparative soot performance by aromatic type in order to identify an optimum aromatic additive.

In terms of fundamental combustion and the chemical kinetics of soot formation, significant work has been conducted on individual aromatic species and the various reaction mechanisms that lead to PAH formation and soot particle inception. Limited work has been conducted however on the interaction of various aromatic species and how these reaction pathways may interact and change. Such interactions are of significant interest to applied combustion applications and are required to develop more advanced models which can explain multi species soot formation analytically separately to empirical observations obtained from experimental data.

Chapter 3

Specification Data Analysis

3.1 Context of 2014 Data

Meta-data analysis used for the purpose of measuring fuel performance presents certain challenges. Experimental campaigns of the type discussed in Chapter 2 and conducted for the purpose of this thesis in Chapters 5 and 6 are usually inconsistent in their application. They feature a wide range of fuels burnt at variable conditions across a multitude of different engine types and experimental configurations. As a standardised test, the advantages and limitations of the Smoke Point and its derivatives are discussed extensively in Chapter 2. It remains however, a uniformly applied test that provides comparable results for different fuels using the same apparatus. With the implementation of the automated method and its associated improvements to repeatability and reproducibility, the SP standard may be retained for the foreseeable future. As all commercial Jet Fuel worldwide is subject to the SP test, there is a vast quantity of specification data that can be analysed to attempt to establish relationships between certain metrics. For the purposes of this work, the aim of analysing specification data is to look for reliable predictors of a fuels SP using the other available variables of the specification. In the context of aromatic content and its optimisation given a certain goal, this approach has significant merit. As higher aromatic content is theoretically, experimentally, and even anecdotally associated with higher sooting propensity, it is important to subject a formal hypothesis to robust statistical testing to see if such a relationship can be empirically proven. As the specification data represents a comprehensive list of variables, there is signifi-

cant research value in examining whether other variables are stronger indicators of sooting propensity.

The Energy Institute reports of the quality of Jet Fuel in a given year and collects specification test results for every fuel certified within or imported to the United Kingdom and has done so since 1986. The most recent year reported is the data-set used for the meta-analysis contained in this chapter. While specification data has always been collected and summarised in the UK, it has never previously been made available for statistical analysis in the form of specific entries for a given fuel. In the era of Big Data and increased computational power, data sets such as the one used for meta-data analysis in this chapter are increasingly available, yielding the ability to obtain fresh insights. It should be noted that the specification data used in this chapter is anonymised. The country and refinery of origin, the test location, the final destination and the end user is not reported. As there is no current market for directly purchasing a given fuel based on its performance, anonymised data protects certain refineries should their fuel be regularly found to be deficient for some purpose, even within the specification, such as low specific energy or higher particulates.

The data analysed in this chapter represents all of the Jet fuel submitted for specification testing in 2014 in the UK. A summary of the data was published in 2017 [85] and the full data was made available to the Low Carbon Combustion Centre research group in the same year. This data-set represents 17,131,263 m^3 of fuel approved for purpose as Jet-A1. No further years have been made available at the time of writing, although additional data may hypothetically be obtained by liaising directly with the Energy Institute.

This data-set is comprised of 1,488 entries, each representing a given sample of fuel submitted for testing. There are 34 variables for each entry representing each test required by the specification. A comprehensive list of each variable is shown in Table 3.1. It should be noted however that dependant on the criteria for each specific test, that a variable may be missing if it is not required by the specification. For example, as discussed previously, naphthalene volumetric content does not need to be reported if the smoke point is greater than 25 mm.

A list of every variable described by this data-set is shown in Table 3.1. Many of these variables are strongly suggested to be related to sooting propensity in the

Table 3.1: List of Variables in Data-Set

Colour	Acidity	Aromatics [IP 156]	Mercaptan
IBP	T at 10% Recovered	T at 50% recovered	T at 90% recovered
FBP	Flash Point	Density	Freezing Point
Viscosity	Smoke Point	Napthalenes	Specific Energy
Existent Gum	MSEP	Gravimetric Millipore	ISO Code 4um
ISO Code 6um	ISO Code 14um	ISO Code 21um	ISO Code 25um
ISO Code 30um	PARTIC > 4	PARTIC > 6	PARTIC > 14
PARTIC > 21	PARTIC > 25	PARTIC > 30	Sulphur %
Distillation T50-T10	Distillation T90-T10		

literature, such as aromatic content, napthalenes, density, and the boiling and distillation range of a given fuel. Many others, such as particulate and sulphur content, are not. While it could be argued that the dimensionality of this data-set could be reduced initially by omitting certain redundant variables, from a statistical data science perspective, there is no valid justification to do so initially based on subjective assessment alone. This chapter later contains an experimental methodology for providing legitimate reason for omitting redundant variables unrelated to sooting propensity when experimentally valid.

3.2 Smoke Point Data Discussion

Every entry for this data-set contains a value for its SP as required by the specification. DEF STAN 91-91 was amended to include the automated SP method in late 2012, more than a year before the initial collection of the data under discussion. It is possible that the SP entries could have been obtained via the automated or manual methods, as the specification does not require the method of determination to be reported. Although it would be conjectural to assume the preponderance of one method over another, it is more likely due to increased cost of the automated

method and a delay in uptake, the manual method may be more commonly used in this data-set. As such, the larger error in repeatability and reproducibility needs to be taken into account when analysing the SP.

SP Histogram

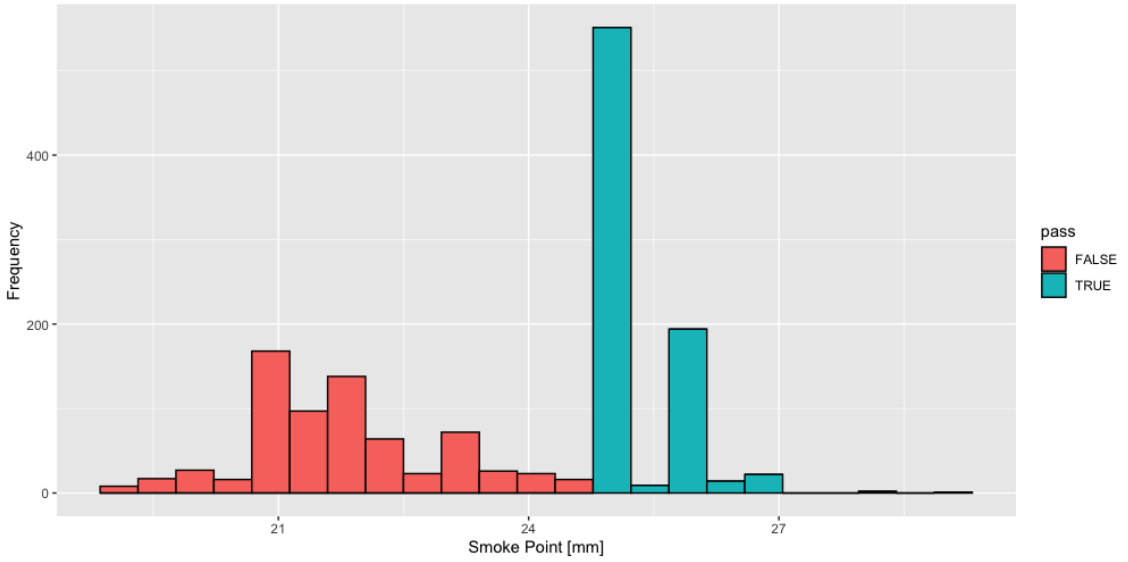

Figure 3.2.1: Histogram of 2014 Smoke Point Data

Figure 3.2.1 shows a histogram of the SP for this data-set. All of the data contained within this set has passed the requirements of the specification. As such, there are no values below 19mm; the bottom limit of the specification. The first specification limit in terms of SP for submitted fuel is that it reach a height of 25mm before emitting visible smoke. Only a slight majority of samples (53.4%) meet this requirement, and a majority of fuel samples (37.9%) have a SP of exactly 25mm. 46.6% of the samples have SP's of lower than 25mm and are subsequently required to meet the lower limit of 19mm and are subject to nathalene volume testing. As there are no entries that fail the specification test, in terms of SP, for this data-set it is useful to consider samples with a SP of at least 25mm as a "pass" and values less than 25mm but greater than 19mm as a "fail". This is of interest for several reasons. Firstly, if SP is to be taken as a reliable indicator of sooting propensity, then a fuel with a 19mm SP may produce 31.6% more smoke/soot if a purely linear relation between SP and BC emissions is inferred. For the goal of reducing particulate matter, all fuels, or a more significant majority, would ideally be able to meet the 25mm threshold. The other reason a "fail" is problematic is

that it places additional constraints upon refineries who subsequently have to meet the requirement that naphthalene volumetric content be no larger than 3%, and may require hydro-processing to saturate polycyclic components within the fuel, and perhaps detrimentally lowering the density as a consequence. Lowering the mass density could potentially reduce the energy density of a given unit of fuel. Imposing a binary "pass/fail" in terms of SP on this data provides valuable insights into the difference variables have on whether a sample passes the initial SP test. It also provides a convenient metric for work such as this that is looking to find key variables than relate to soot production.

It should be noted that the SP data is not Gaussian in its distribution. Values greater than 19mm and less than 25mm do appear to approximate a bell curve with a slight skew towards the higher end. The prominent peak at 25mm however, may suggest that fuel has been specifically processed, or at least only submitted for specification testing, when it has been manipulated to meet the required threshold. Alternatively, the subjectivity of the manual SP test may prejudice an operator to pass a borderline SP reading. As the specific processes that each sample have been subjected to is omitted from the data, explaining the exact cause of this behaviour is conjectural. However, it is not unreasonable to surmise that a combination of hydro-processing, blending and selective elimination is used to ensure a fuel can get to 25mm. All of these processes incur significant cost for refiners and are sub-optimal.

3.3 Variable Correlations

As many of the variables described in Table 3.1 are interrelated, it is appropriate to look at degrees of correlation between each one. This is not only relevant for variables affecting the SP directly, as suggesting changes to a given metric that raises SP may significantly affect a separate variable that may cause it to fail the specification.

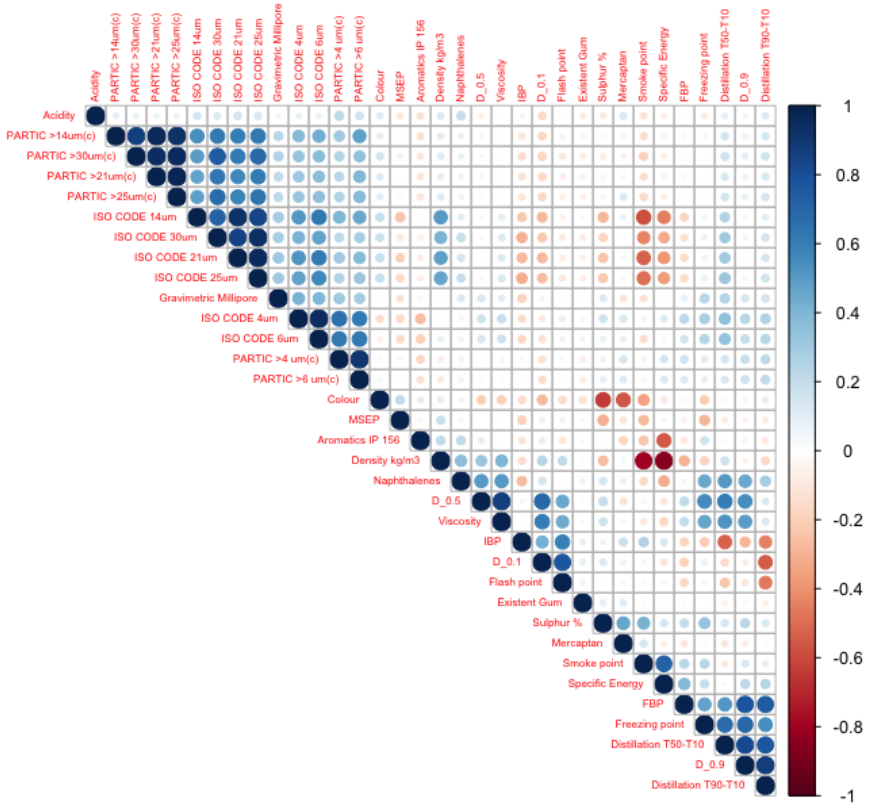

Figure 3.3.1: Correlations of Specification Variables in 2014 Data

Figure 3.3.1 shows a matrix containing all of the correlation coefficients for each variable in this data-set. This Figure was generated from the available date for 2014 using the *corrplot* [86] package in R-Studio. Positive correlations are denoted by blue, with the strongest saturation (darkest colour) having stronger correlations, and red denoting anti-correlations. White suggests no statistical correlation. Correlations with two specific variables are of initial interest to this work; SP and Aromatic volume. While presenting the data in the form of Figure 3.3.1 is useful for a holistic view of every fuel metric, bar-charts for these two variables and their strongest corollaries are shown in Figure 3.3.2 and Figure 3.3.3, for SP and Aromatic Volume, respectively, arranged from largest magnitude negative correlation to strongest positive correlation.

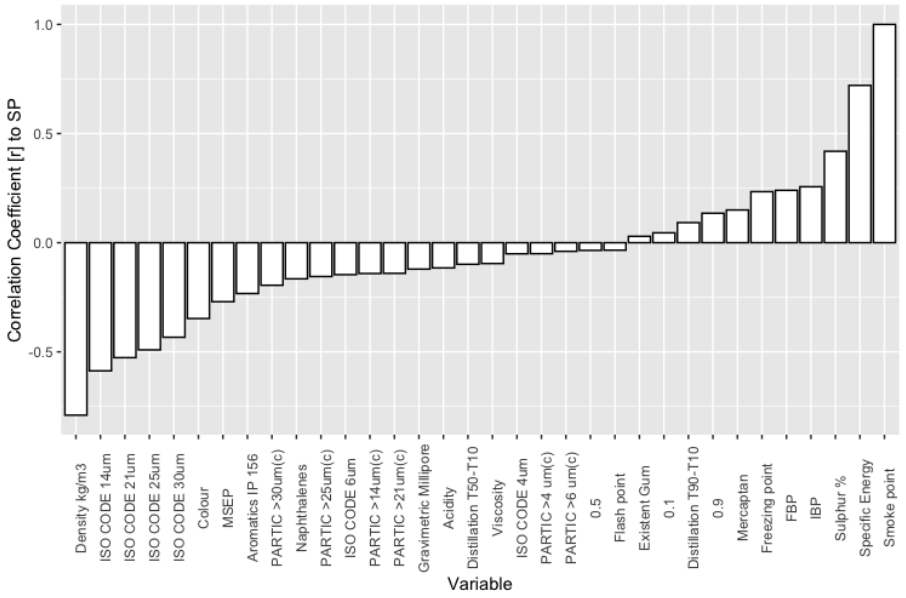

Figure 3.3.2: Correlations of SP with Specification Variables in 2014 Data

There is a strong anti-correlation between density and SP ($r = -0.79$), suggesting that increases in fuel density lower the SP. The only other variables which may be described as having a moderate anti-correlation are ISO CODE 14um and ISO CODE 21um, both measure of a samples cleanliness in terms of particulate size per unit litre. ($r = -0.59$ and $r = -0.54$ respectively). In terms of positive correlations, only the specific energy of the fuel correlates strongly ($r = 0.72$).

As a metric of interest, it should be pointed out that Aromatic Volume anti-correlates weakly with SP ($r = -0.23$). While the correlation coefficient alone is not enough to exclude a link between SP and Aromatic Volume, this initial statistic suggests a weak direct relation with volume itself, with density having a stronger influence. It is of interest, however, that global density, in the context of jet fuel composition, may be most strongly influenced by the aromatic component. If, very broadly, one considers jet fuel as bi-modal; containing an aromatic and non-aromatic fraction, the influence of aromatics on global density can be observed. The non-aromatic as mentioned previously, can be sub-categorised into alkanes, alkenes and cycloparaffins in various configurations. As these groups form the major proportion of the fuels composition (75% to 90% by volume), specifics of the global composition affect global density. However, due to the specific structure of aromatic molecules and their unsaturated nature, they typically feature a higher carbon to hydrogen ratio in a smaller volume and have a higher density than other hydrocarbon con-

figurations. This is especially true for poly-cyclic hydrocarbons. It is illustrative to consider the differences in density for the structural isomers of C_{10} to illustrate the variation of densities for each configuration. Decane, $C_{10}H_{22}$ and 1-Decene, $C_{10}H_{20}$ have densities of 0.730 gcm^{-3} and 0.741 gcm^{-3} respectively. If the non-aromatic proportion of a given jet fuel were composed of 1-Decene and opposed to Decane, this would represent an increase in density of only 1.37%. An aromatic isomer of C_{10}, such as 1,4-Di-ethyl-benzene, however, has a density of 0.871 gcm^{-3}. Proportional increases in alkene volume versus aromatic volume produce larger changes to the overall global density. While it may be appropriate to say that Aromatic Volume alone, is a poor indicator of sooting propensity, but when one considers the effect of aromatic compositon has on density, the strongest corollary, its effects are significant. This statistic reveals nothing however, as to whether density itself is the causal or mechanistic driver of higher soot or smoke, of it is merely a confounder for some other metric or behaviour.

It should also be pointed out that Cycloparaffins, which are not accounted for in the aromatic component of jet fuel, also feature higher densities. The cycloalkane form of C_{10}, Cyclodecane, also has a density of 0.871 gcm^{-3}. If density is found to be deterministic of soot production, the Cycloalkane composition of fuel merits further analysis.

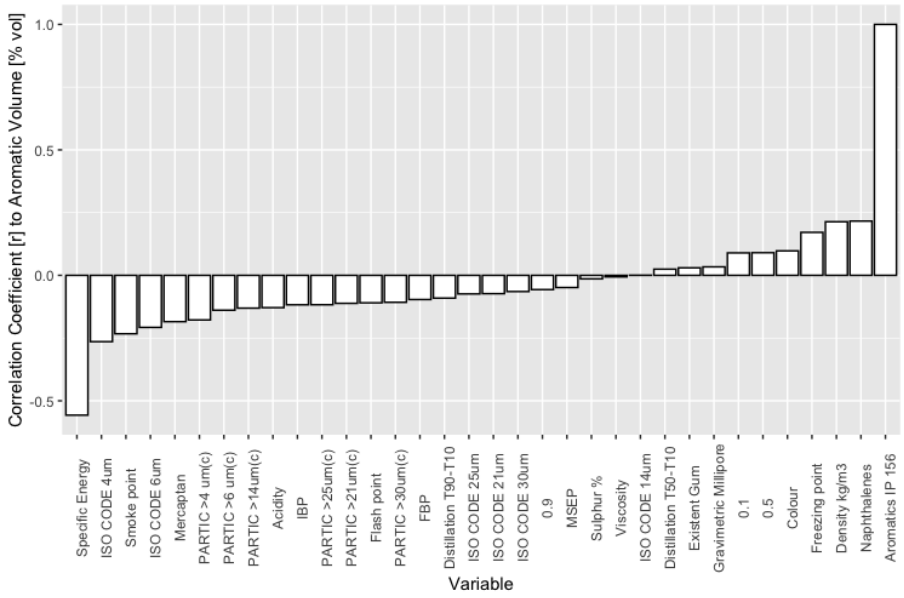

Figure 3.3.3: Correlations of Aromatic Volume with Specification Variables in 2014 Data

Figure 3.3.3 shows the correlation coefficients between Aromatic Volume and all other variables for this data-set. Only Specific Energy is of statistical significance, showing a moderate anti correlation ($r = -0.56$). This is somewhat intuitive and expected behaviour, however. As denser molecules compared to their saturated, non-aromatic counterparts, aromatic molecules contain a higher proportion of C-C bonds as opposed to C-H bonds. While the enthalpy contained in these bond types are comparable (348 $kJmol^{-1}$ and 413 $kJmol^{-1}$ respectively), this higher proportion of carbon means that a similar amount of energy is contained within a "heavier" molecule, which adversely affects the Specific Energy as the numerator of kJm^{-1} is increased. The same behaviour may be inferred in the Smoke Point correlations for Specific Energy, which both correlate positively and strongly. As the density declines, perhaps dictated by changes in the aromatic component, the SP increases. As there is a lower proportion of aromatics that negatively affect Specific Energy, it also increases.

Specific discussion of napthalenes has been limited in this section due an increased focus later in this chapter.

3.4 Aromatic Volume Discussion

The focus of this thesis is on the role of the aromatic component of jet fuel. From a strictly statistical perspective however, the weak correlation between this data sets' specification smoke point data and the proportion of its aromatic volume would suggest that a potential link between these two metrics would not merit further investigation. There is still value however, in exploring the effect of aromatic volume of this data set to determine if any useful insights can be obtained that illustrate the effect, if any, of aromatic volume on smoke point.

Without compartmentalising the data in to pass/fail or any other such classification, the histogram for the entire Aromatic Volume of the data-set is shown in Figure 3.4.1. The y-axis of this histogram measure the distribution density of the data, where the cumulative volume of each bar totals 1. This approach allows for statistical comparison with a normal distribution as shown.

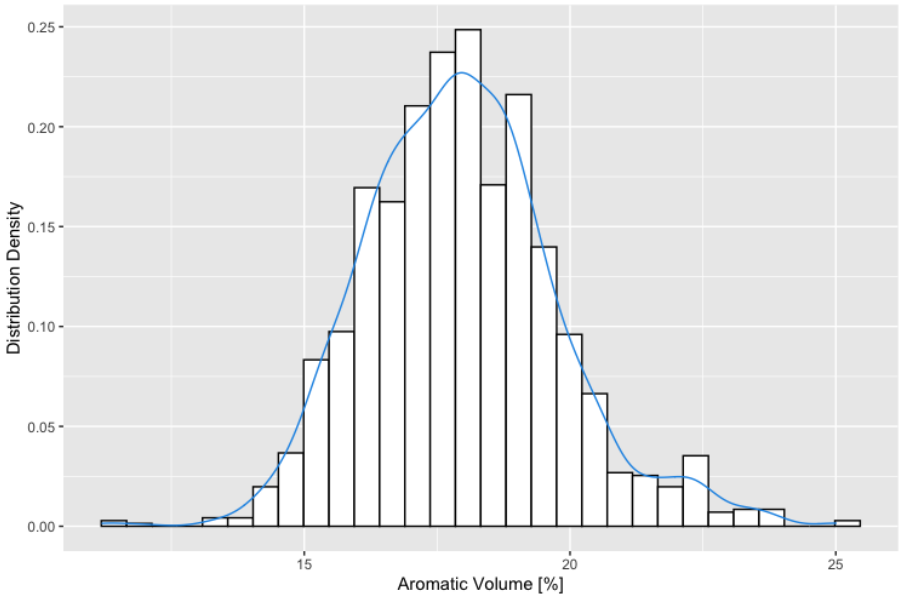

Figure 3.4.1: Histogram of Aromatic Volume in 2014 Specification Data

The mean aromatic volume is 17.95% with a standard deviation of 1.82%. The data can generally be described as Gaussian and follows a normal distribution with skew of 0.405 suggesting a fairly symmetrical distribution. Assuming normality, 95% of the aromatic content for this data can be said to fall between 14.32% and 21.59%. Obtaining this range is useful in suggesting potential ranges for experimental formulated test blends. It does not, however, provide useful insights into the role, if any that aromatic volume plays in smoke production.

Compartmentalising the data using the pass/fail metric defined earlier shows some difference in SP when considering aromatic volume. Figure 3.4.2 shows a box plot and scatter diagrams for the two data sets.

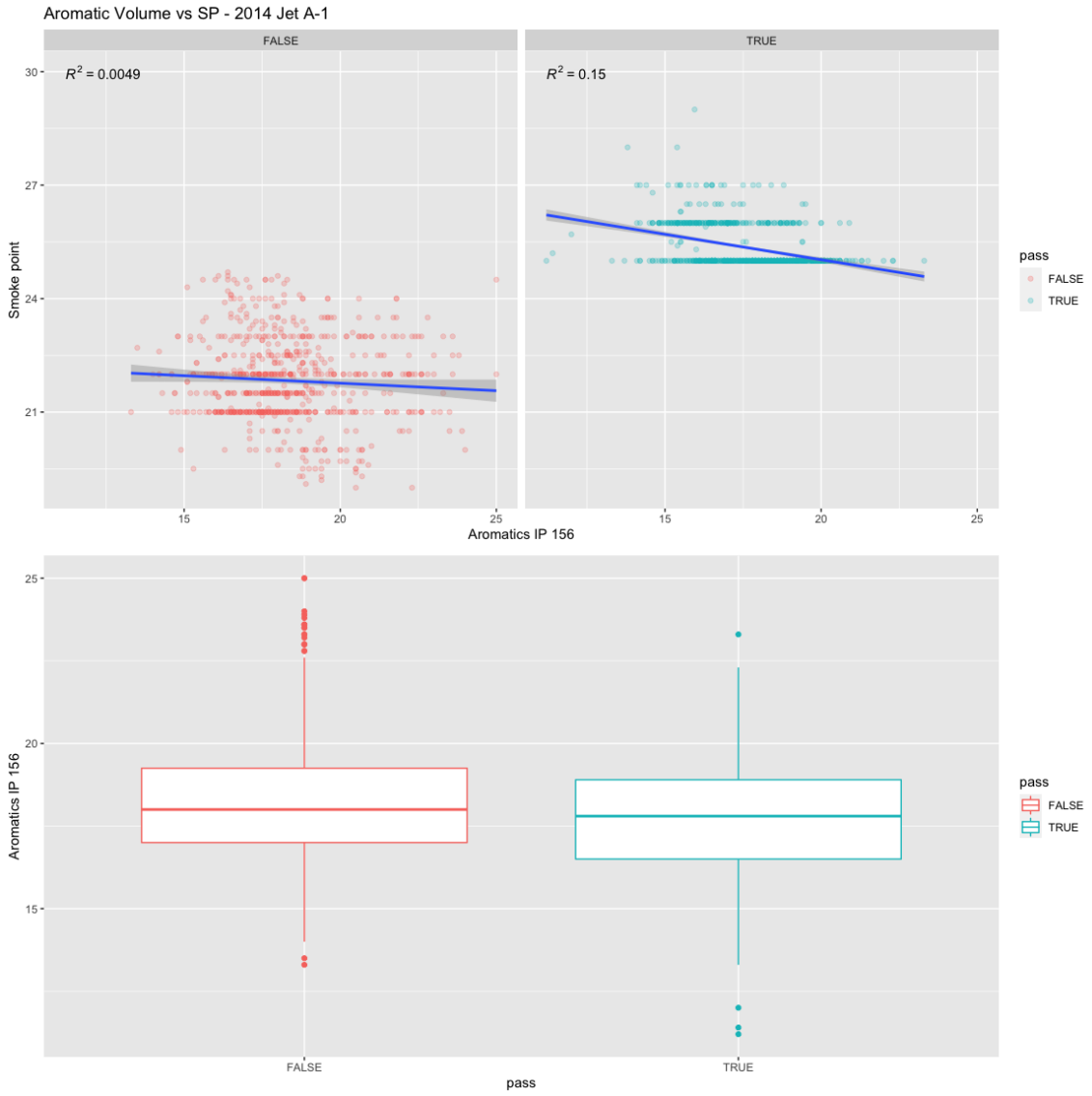

Figure 3.4.2: Aromatic Volume vs SP for Pass/Fail Condition

The mean aromatic content for a pass condition is 17.65%, while a fail is slightly higher at 18.30%. Similarly, the medians are barely distinguishable, with a pass having 17.8% aromatics and a fail having 18%. The box plot in Figure 3.4.2 shows the fail condition having a larger number of outliers with higher aromatic volume than the pass condition, but is not descriptive in general of the overall trend of the data. The inter-quartile range of values for the fail condition do seem to be higher, however. The correlation coefficient between aromatic volume and SP is weak for both pass ($r^2 = 0.15$) and fail ($r^2 = 0.0049$), suggesting that the majority of the variance in this data is not explained by this metric.

Without relying on subjectivity, the strictest way of measuring the statistical

significance of the effect of aromatic volume on the pass/fail condition is to subject the two sub-sets of data to a z-test. The z-test is preferred over the t-test as the variance of both populations is known, and that the sample size is significantly larger than 30. The probability distributions for these two sets can be seen in Figure 3.4.3, assuming a normal distribution of the following form for a pass N(17.66, 1.632) and a fail N(18.30, 1.952).

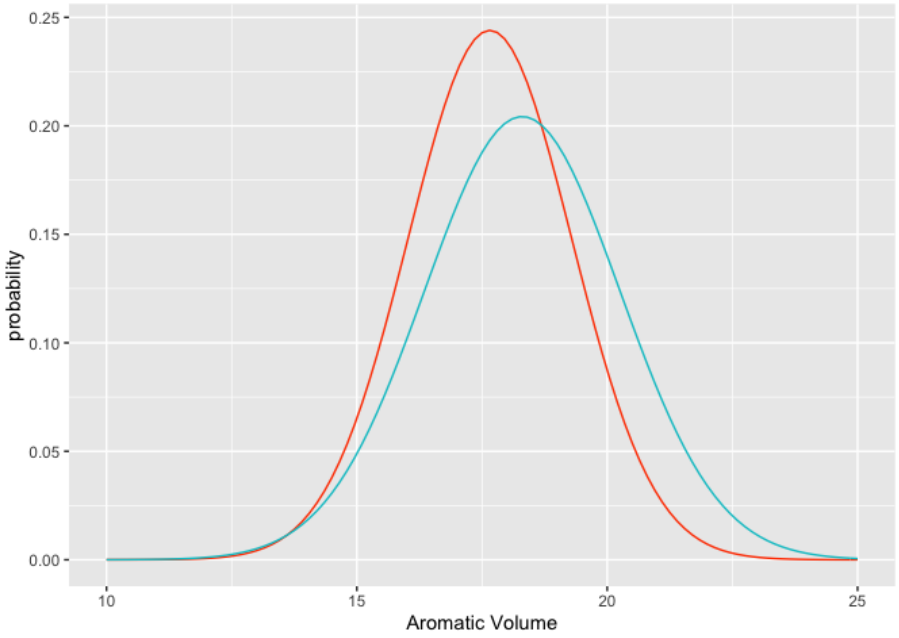

Figure 3.4.3: Normal Distribution of Aromatic Volume for Pass/Fail

The null hypothesis for this z-test is that the difference between the means of these groups is zero. The alternative hypothesis is that specimens that "fail" the initial SP test have higher aromatic volume on average. These hypotheses are formally defined in Equations 3.1 and 3.2 for null (H_o) and alternate (H_a), respectively.

$$H_o : \bar{V}_{aromatic,pass} = \bar{V}_{aromatic,fail} \tag{3.1}$$

$$H_a : \bar{V}_{aromatic,fail} > \bar{V}_{aromatic,pass} \tag{3.2}$$

A right tailed z-test was performed with a confidence level of 99%. Using z-tables at this level of significance, the corresponding critical z-value is 2.58. A z-test statistic greater than this is sufficient to reject the null hypothesis. The z-test statistic for the two populations is calculated using Equation 3.3 and numerically in

Equation 3.4.

$$Z = \frac{(\bar{X}_2 - \bar{X}_1) - (\mu_2 - \mu_2)}{\sqrt{\frac{\sigma_1^2}{n_1} + \frac{\sigma_2^2}{n_2}}} \tag{3.3}$$

$$Z = \frac{(18.30 - 17.66) - (0 - 0)}{\sqrt{\frac{1.632^2}{793} + \frac{1.952^2}{695}}} = 6.807 \tag{3.4}$$

A z-test statistic of 6.81 surpasses the 1 threshold of 2.58 and so it can be claimed that the difference in the two means for the fail and pass condition is significant and statistically valid. While the low correlation and coefficient of determination values for aromatic volume alone explain little variability in the nature and provide a poor model, mean aromatic volume does appear to have an effect on the classification of a fuels SP. This effect can be seen further in Figure 3.4.4, which shows the box-plot for the data when the SP is compartmentalised between the integers of the SP for each sample irrespective of the pass/fail condition.

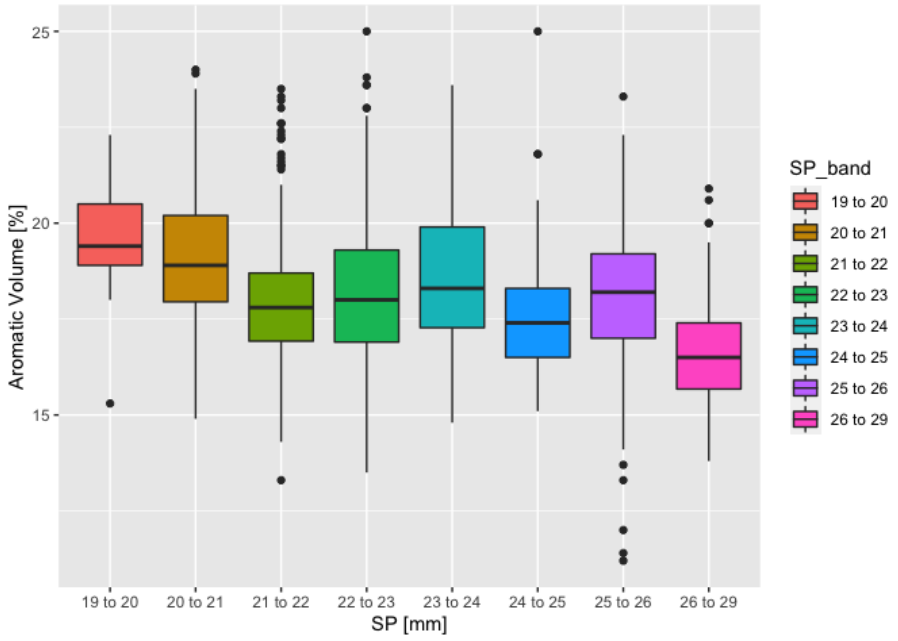

Figure 3.4.4: Box Plots of Aromatic Volume for given ranges of SP

The general trend of the median aromatic volume is shown to generally decrease as the SP increases, whilst retaining significant variability between categories. This trend is also seen when in the values of the mean volume, which are also shown to decrease as SP rises, as shown in Figure 3.4.5. This figure also includes error bars

using plus and minus 2σ, representing 95% of the variance for each band.

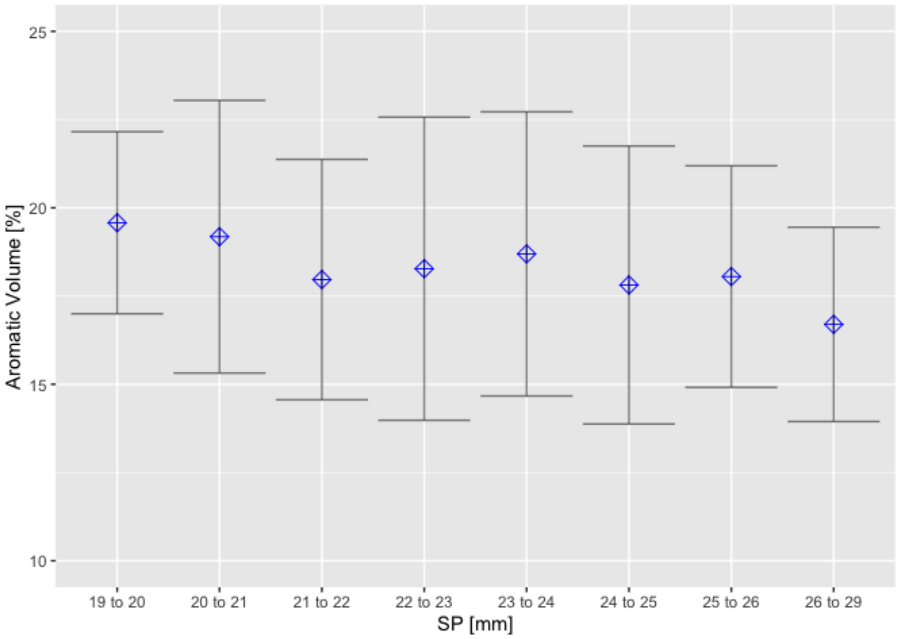

Figure 3.4.5: Mean and SD of Aromatic Volume for given ranges of SP

The repeatability statistics for the two aromatic volume testing methods, ASTM D6379 [87] and ASTM D1319 [34], must be considered as a potential cause for a wide dispersion of values for increasing SP. Both methods, however, have good repeatability statistics, with values of 0.89 and 1.2 at 15% of aromatic volume, and values of 1.26 and 1.4 at 25% volume of aromatic; the maximal amount allowed by the specification. These value do not account for such significant variance in the aromatic volume observed at each SP integer.

From a macro perspective looking at the overall trends in this data-set, aromatic volume does seem to be significant when considering the entire population of the data. It could be claimed, with some statistical validity, that decreasing the aromatic volume of fuel enable more fuels to pass the initial SP test and by raising the mean SP, resulting in lower BC emissions. On a micro scale however, in terms of informing the selection of optimum aromatic content, knowledge of the aromatic volume alone provides no insight as to how individual samples, and therefore potential blends, would perform against each other. Other fuel metrics are needed to provide greater resolution into predicting an individual fuel samples SP.

3.5 Naphthalene Volume Discussion

As discussed previously, fuels that have a SP lower than 25 mm are subject to ASTM D 1840, and must be found to have naphthalenes content of no greater than 3% vol/vol. This is due to the concern that polycyclic aromatic hydrocarbons are more significantly associated with higher soot production, as indicated by their individual SP, TSI and YSI indices. If naphthalenes content is thought to have a profound effect on BC production, it is worth investigating this data-set to see if such concerns are merited. As shown previously, however, there is very weak correlation between SP and naphthalenes content by volume.

As ASTM D1840 is not uniformly applied, only the fuels that fail the initial SP test require measurement, and so naphthalenes content is only reported for fuels with an SP of between 19mm and 25mm. For this data-set, this represents 695 entries, or 46.7 % of the data. A histogram of the naphthalenes percentage volume for the available data is shown in Figure 3.5.1.

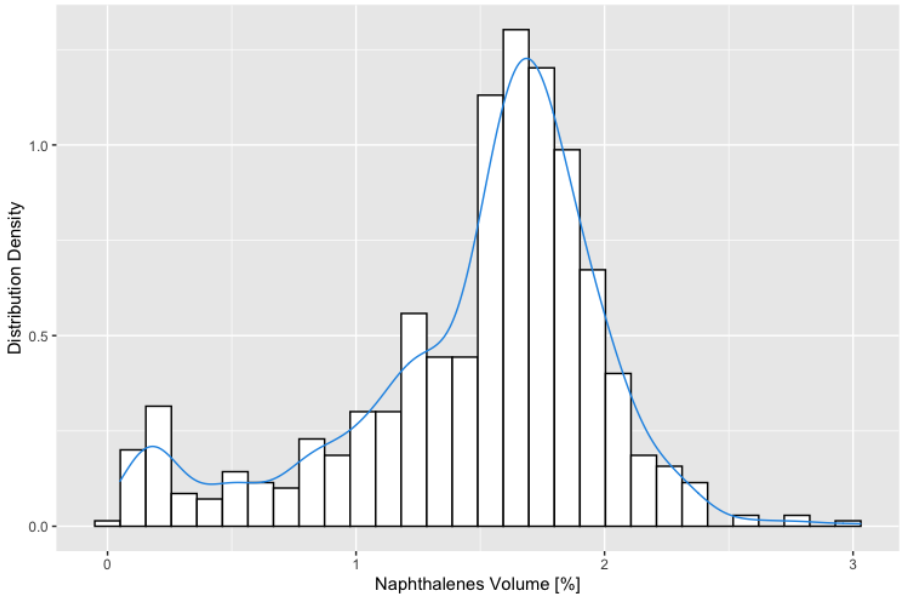

Figure 3.5.1: Histogram of Naphthalenes Volume for 2014 Data Set Fail Condition

The distribution may loosely be described as Gaussian, with a prominent skew towards lower values and a prominent bell-shape between 1.5% and 2%. The mean value of naphthalenes volume is 1.49 % with a standard deviation of 0.52%, suggesting that 95% of this distribution falls between 0.44% and 2.53 %, if a normal distribution were assumed. A count of the actual data, however, reveals that only

65 entries have a napthalenes content of larger than 2%. This may suggest that keeping napthalenes content below 3 % is not a limiting factor in adherence to the specification. If it were necessary to process the fuel to below this limit, a higher proportion of samples would be seen closer to the specification limit of 3%.

As discussed previously, there is a weak correlation between SP and napthalenes content (-0.165). Figure 3.5.2 shows a scatter diagram of SP and naphthalenes percentage for each sample.

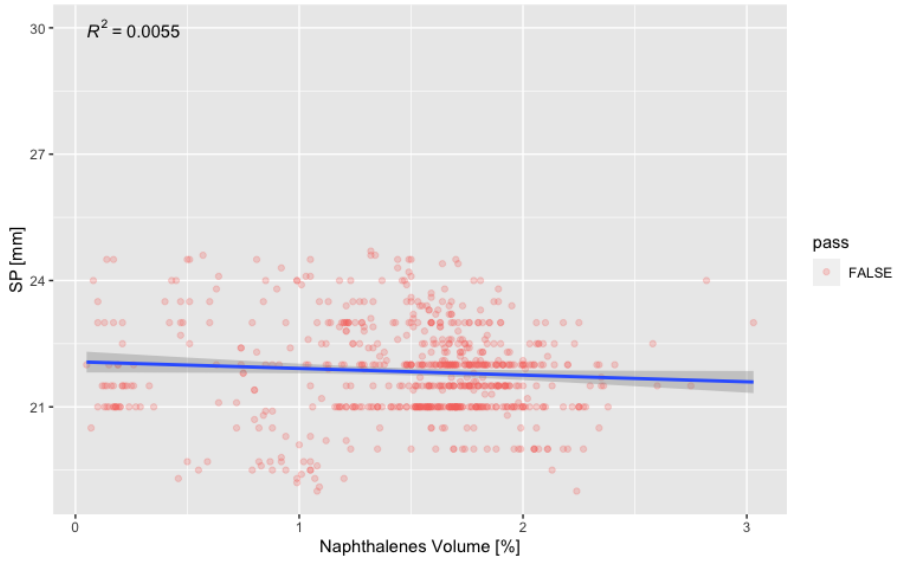

Figure 3.5.2: Scatter Plot of Naphthalenes Volume against SP

The coefficient of determination ($r^2 = 0.0055$) is of no statistical significance and has no value as a potential predictor of SP alone as a metric.

An important point to consider is that the Aromatic volume test, ASTM D 1840, as a measure of overall aromatic content, already accounts for the napthalenes component as napthalenes are a sub-category of aromatics. Using this data-set it is possible to calculate the proportion of aromatic content that is comprised of napthalenes for samples that meet the "fail" condition. Figure 3.5.3 shows a scatter plot of the Napthalenes/Aromatic volume ratio compared to SP values for individual samples.

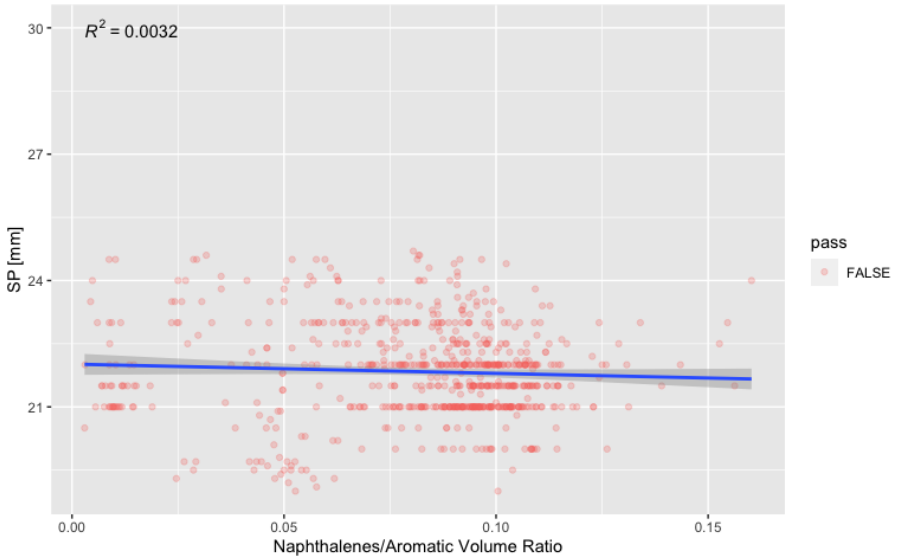

Figure 3.5.3: Scatter Plot of Naphthalenes Volume as Proportion of Aromatic Volume against SP

The coefficient of determination for this metric ($r_2 = 0.0032$) is even lower than the one found for napthalenes alone, and provides no greater insight into the role that napthalenes has on a samples' SP. There are several caveats to highlight here, however. The variation in napthalenes content between each sample is small and considering the normal distribution of values as discussed, mostly fit within a 2% margin. Also as discussed previously, the poor quality of repeatability and reproducibility for the manual SP test can be interpreted as an error of around 10%. Hypothetically, the fluctuations in SP values caused by naphthalenes content could be masked by the noise inherent in the SP test itself. If this were true however, fluctuations in the noise itself would be observed, while the statistical analysis of napthalenes content alone reveals very little indication that there is an underlying relationship.

3.6 Density Discussion

In terms of both correlation and regression analysis, density has been shown to have the strongest relationship with SP so far, and so merits closer investigation in this section. As discussed previously, density is not a variable independent of aromatic consideration, due to the significant differences aromatic proportion and type can have in raising global density. Figure 3.6.1 shows a histogram of density for this

data-set.

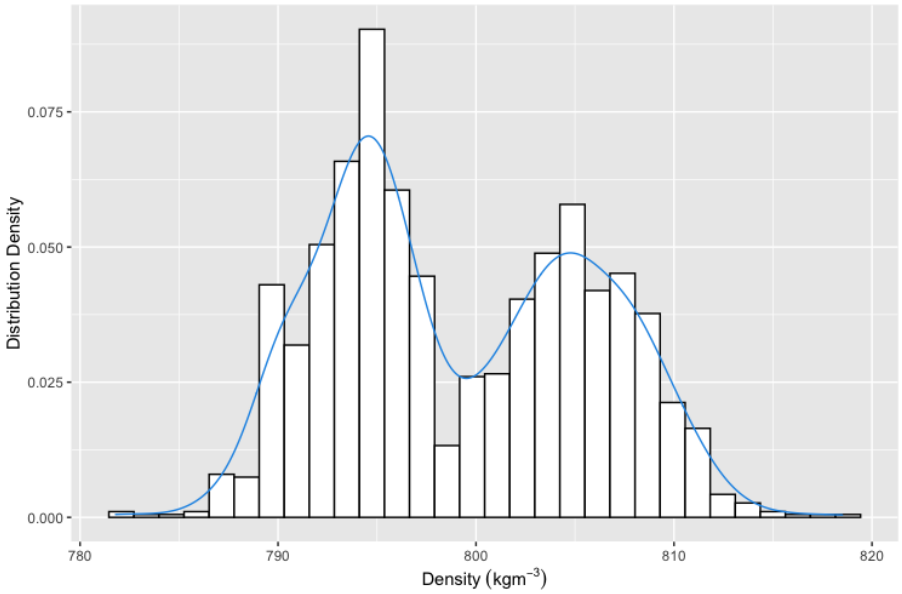

Figure 3.6.1: Histogram of Density for 2014 Data-set

The distribution shows two distinct peaks around 790 kgm^{-3} and 805 kgm^{-3} and appears to contain bi-modal normal distributions. By imposing the SP pass/fail condition as described previously, an interesting trend is observed. As shown in Figure 3.6.2, there appear to be two distinct distributions of densities when separated using a pass/fail metric. Not only are these distributions unique, they are also distinct, with very little overlap. The fail conditions appears to have a skew that slightly tends towards lower densities, while the pass shows the opposite behaviour, with a skew towards lower densities.

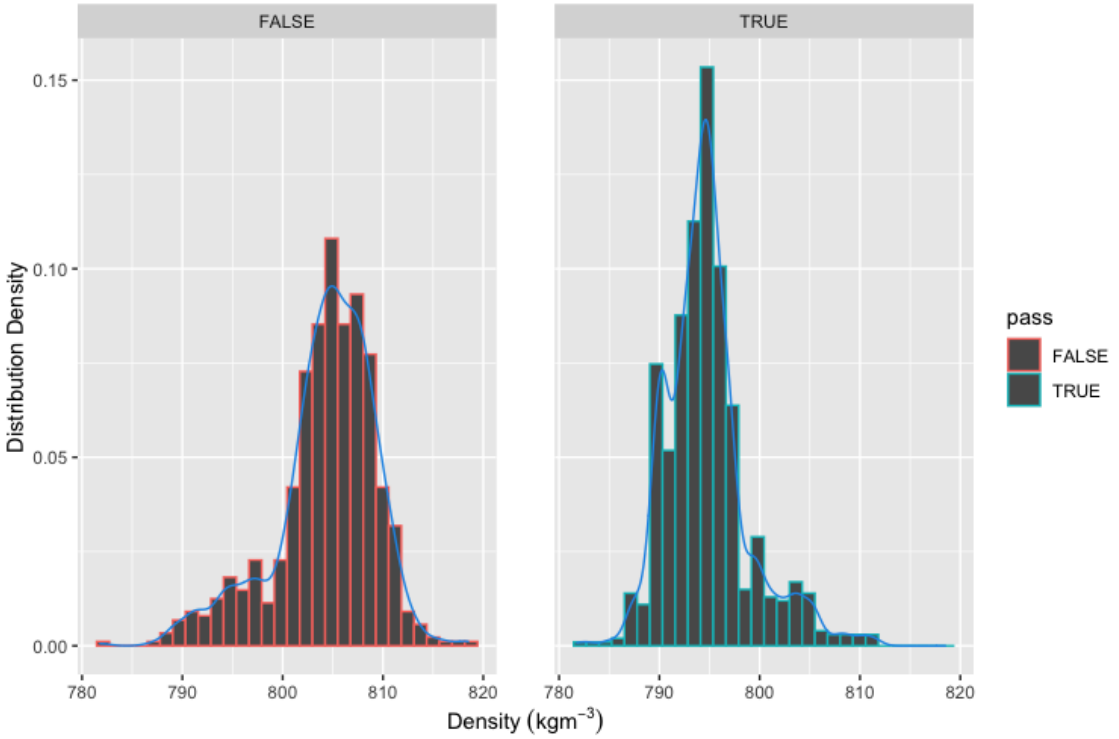

Figure 3.6.2: Histogram of Density at Pass/Fail for 2014 Data-set

The difference is so distinctive that choosing $800kgm^{-3}$ as an arbitrary divide, 90.3% of pass samples fall below this density, while 84.7% of fail samples lie above this density. Density is nearly totally prescriptive when it comes to determining this binary classification based on pass or fail. There are two likely hypothesis for this behaviour. The first, as discussed previously, is that potentially, density itself is deterministic in soot production. Carbonaceous particles in closer proximity due to increased density and shorter inter-molecular distances may produce more significant amounts of soot. The second hypothesis is that these two distinct distributions are an artifact of a process or production, such as hydrogenation, also know as hydro-processing. The hydrogenation industrial process is utilised in refineries whereby molecular hydrogen (H_2) is added to the fuel in the presence of a catalyst such as palladium, nickel or platinum. The usual aim of this process is to remove inorganic atoms or molecules containing sulphur and nitrogen. Extreme hydro-processing, however, can be used to saturate organic compounds such as aromatics and olefins. It's plausible that hydrogenation in order to saturate aromatic rings lowers the global density of the fuel and that this is reflected in this data-set.

It is difficult to say based on this data alone whether a higher or lower density

is causal is affecting soot production. One thing the data does reveal is irrefutable though; that statistically speaking, whether an artifact or not, density is a stronger predictor than aromatic volume of a samples likelihood to pass or fail the initial SP condition. There is much more overlap in the distributions of aromatic volume for SP bands than when using density alone. This raises the question of whether designing potential ASAF blends to have lower density rather than lower aromatic volume may be more effective in lowering soot production. The role of density in discrete SP prediction rather than as a pass/fail categorical variable is explored further later in this chapter.

3.7 PCA and Fuel Properties

One of the challenges of dealing with such a large database with such a substantial variety of variables is finding relationships between the variables that aren't merely correlative. An aim of this chapter, and ultimately, the thesis, is to thoroughly examine a wide range of variables and their dependence upon each other in determining the variable, or group of variables, that have the strongest effect on soot production. Principal Component Analysis (PCA) is an un-supervised machine-learning technique that reduces the dimensionality of a given data-frame and captures the overall pattern of the data in a smaller number of variables, or Principal Components. Each Principal Components is comprised of the eigenvectors for each original variable, and can provide an insight as to how changing one variable affects another. In the context of fuel properties research, this technique has been performed previously on JP-7 and JP-5 to detect classification of jet fuel mixtures based on changes in the volume of each using GCxGC [88] and in a similar way, to a characterise a variety of fuels including aviation, missile and automotive fuel, also using GCxGC data [89]. To date, no examples can be found in the literature of PCA being used to classify Jet Fuel SP's or any other metric using specification test data.

The code used to pre-process and analyse this data using PCA can be found in the Appendices of this thesis. The initial treatment of the data was to examine each variables suitability for analysis using this method. PCA only works with

numerical data and requires a full range of variables with no NA (non-available) or Null values. This presents a challenge as the specification does not require entries to be quantified for every variable, such as Naphthalenes volume. Omitting these variables may mask key factors that determine SP production, even if thought not to be related. The alternative approach was to reduce the number of entries in this data-set to only consider complete cases with a quantitative value supplied for every variable. This approach significantly reduces the amount of data available however, from 1,488 samples down to 166, representing only 11.1% entries of the original data-set. Ultimately, both data sets were analysed independently using PCA for this thesis; using the full data-set with omitted variables and using the reduced data with only complete cases. While both were analysed, only the former method is reported as the reduced groups only include test samples that fail their initial SP test, and hence includes Napthalenes content exclusively as a result. For the sake of clarity and brevity, the latter has been omitted from this chapter. 15 variables were omitted (Napthalenes, Mercaptane and all particulate contamination values). The final database used for PCA analysis was formed of 19 variables.

Each variable was initially scaled and centred, as appropriate when using PCA to analyse variables of differing magnitudes. In total, 19 PC's were quantified using this method; the same number of variables as the original data set. The Proportion of Variance for each PC can be seen in Figure 3.7.1.

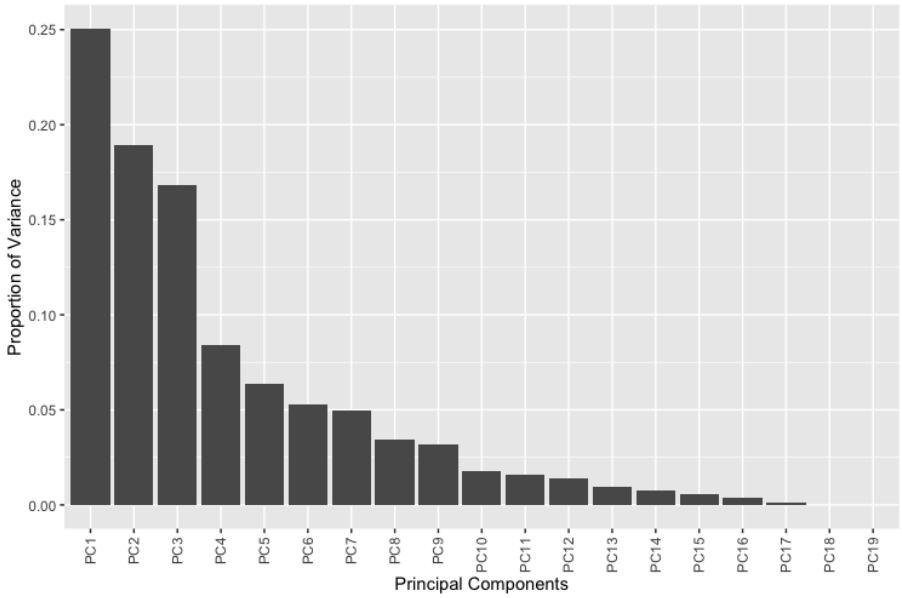

Figure 3.7.1: Principle Components of 2014 Data-set

PC1, PC2 and PC3 capture the largest proportion of variance of all PC's, representing 25.1 %, 18.9 % and 16.81 % respectively. Taking PC1, PC2 and PC3 cumulatively, these three variables alone account for 60.8 % of the total variance of the data, as shown in Figure 3.7.2.

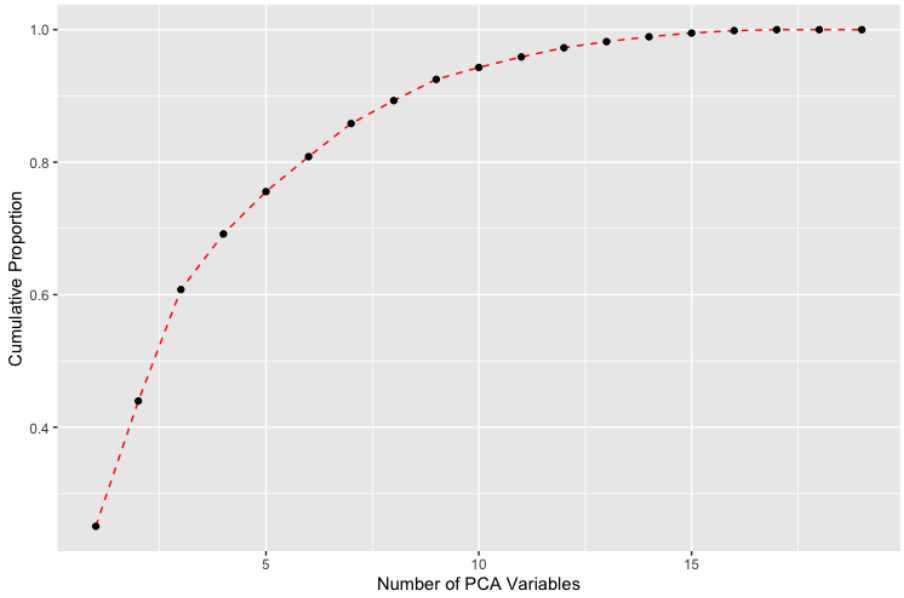

Figure 3.7.2: Cumulative Principle Components of 2014 Data-set

The benefit of using a technique such as PCA is its ability to reduce dimensionality in reducing the total variables required to capture the overall structure of the data. In this case however, the number of PCA variables required to describe 95 % of the data is 10,a moderate reduction from the original 19 variables. A closer inspection of the correlation between each Principal Component and the original variables is shown in Figure 3.7.3.

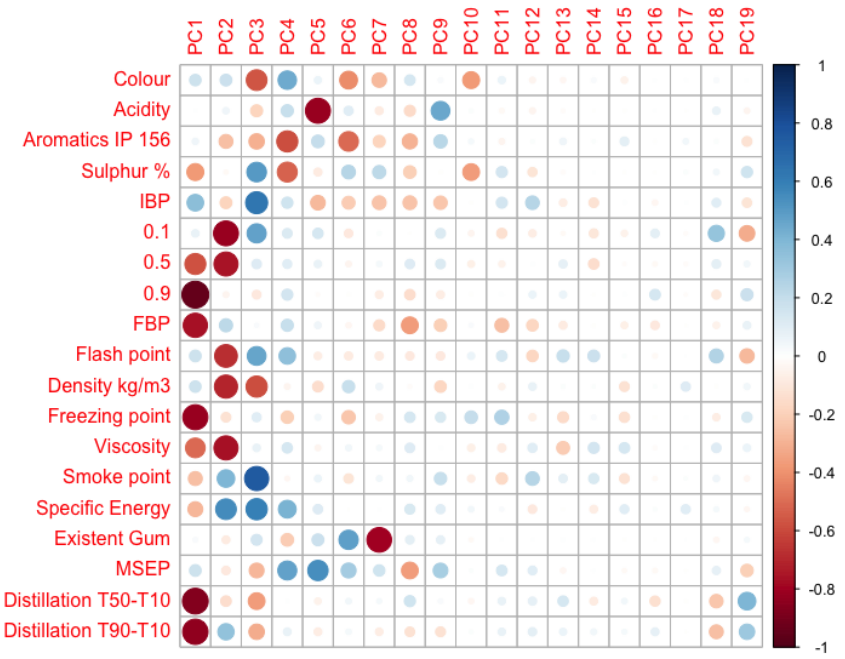

Figure 3.7.3: Correlation of Principle Components with original variables from 2014 Data-set

In terms of the smoke point, only PC1 ($r = -0.253$), PC2 ($r = 0.403$) and PC3 ($r = 0.759$) have a significant correlation. While the first three components only capture 60.8 % of the total variance, they effectively determine the SP of the data. This is significant as it allows an examination of which other variables are affected by increasing or decreasing each principal component and may suggest optimum properties for low sooting blends. A closer examination of the behaviour of each PCA upon the SP illustrates this further.

PC1 weakly anti-correlates with the SP while PC2 moderately correlates with it. Subsequently, one would expect samples failing samples with a low SP to have a higher value for PC1 and a lower value for PC2. This can be seen in Figure 3.7.4, which overlays a 95 % probability distribution across all data points based on the pass/fail condition. Comparing the centroid of each distribution, the fail condition is to the lower right of the pass condition, confirming a higher PC1 and lower PC2 as suggested by the correlations statistics mentioned previously.

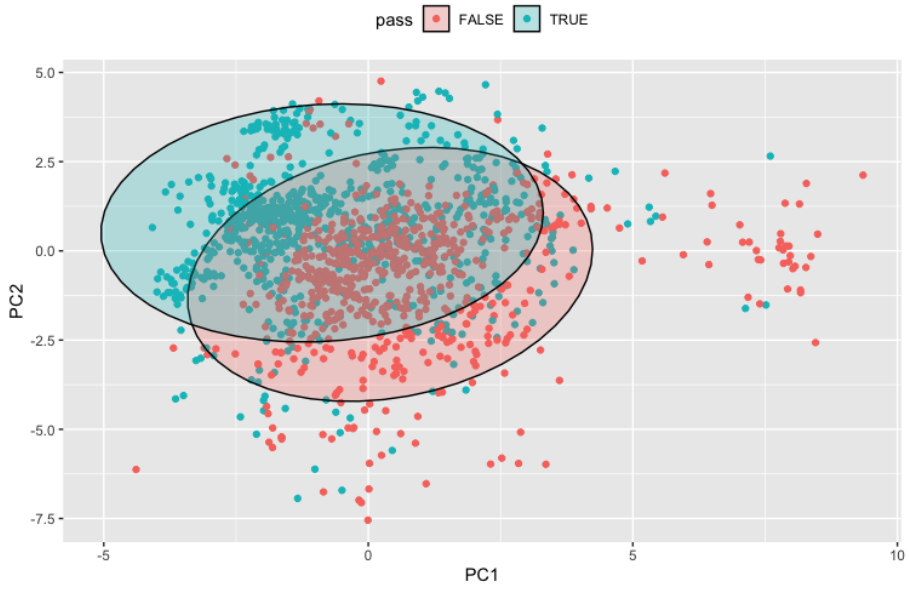

Figure 3.7.4: PC1 vs PC2 and SP pass/fail from 2014 Data-set

When comparing SP bands within the PC1 vs PC2 metric, there is significant overlap and no clear trend can be obtained. It is included here however in Figure 3.7.5 for the sake of completion and in order to compare the clearer trends visible when comparing PC2 and PC3. From the PC1 and PC2 analysis, one might surmise that an optimum fuel with a high SP would ideally have a higher PC2 and lower PC1, although PC1 doesn not seem to have the same significance..

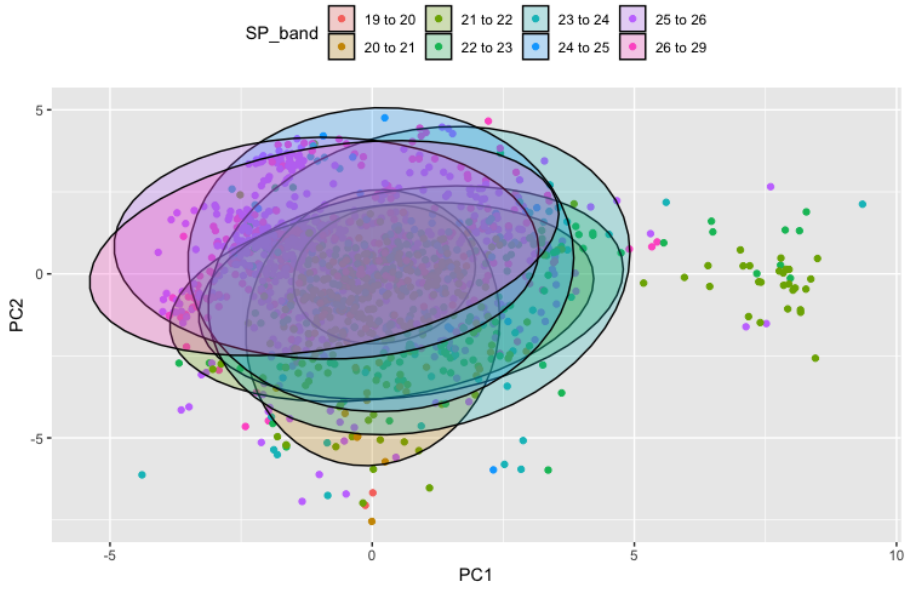

Figure 3.7.5: PC1 vs PC2 and SP bands from 2014 Data-set

As discussed previously, PC2 correlates moderately with SP, while PC3 has the

strongest correlation of any principal component. One would expect a sample with a low SP to have a comparatively lower PC2 and PC3 value as a result. This can be seen in Figure 3.7.6

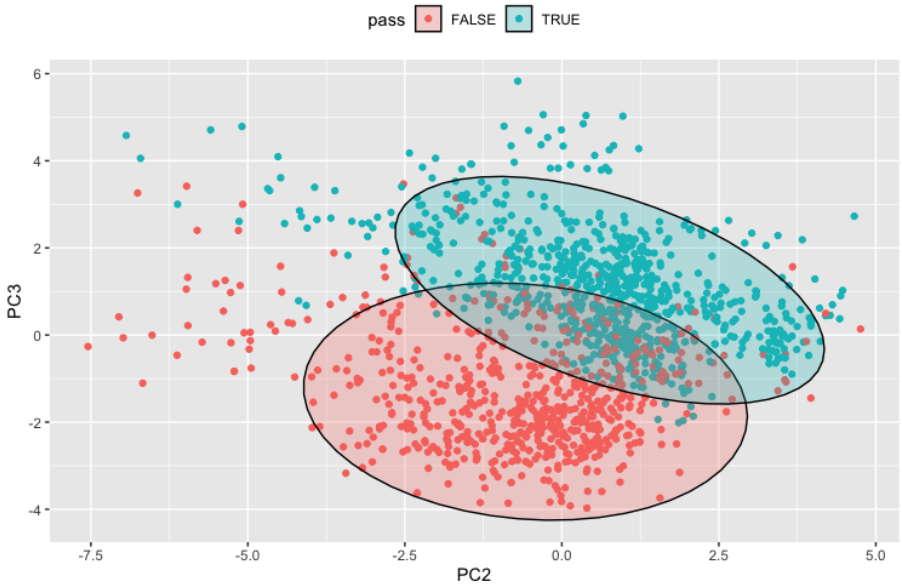

Figure 3.7.6: PC2 vs PC3 and SP pass/fail from 2014 Data-set

Here, the centroid of the probability distribution for the pass condition is clearly higher and to the right than that of the fail condition. Based on passing the SP alone, a sample with a higher PC2 and PC3 is more likely to pass. This effect is pronounced when the data is broken down into SP bands, as before, and can be seen in Figure 3.7.7.

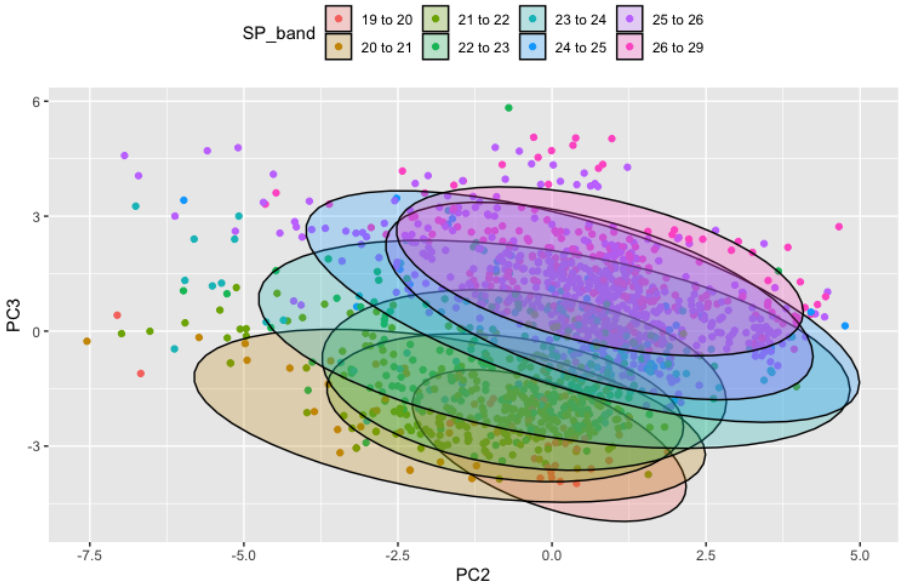

Figure 3.7.7: PC2 vs PC3 and SP bands from 2014 Data-set

A clear progression can be seen through the categories as PC2 and PC3 increase. The probability distribution for the 20 to 21 mm group and 26 to 29 group, for example contain no overlay. It should be noted, however, that the centroid for the 19 to 20 mm group has a higher PC2 than that of the 20 to 21 mm group, so this pattern is not exactly replicated between groups. The pass/fail condition for PC1 and PC3 are shown in Figure 3.7.8. The observed trend agree with the pattern discussed previously; that a given sample is more likely to pass its SP test with a higher PC3 and a lower PC1.

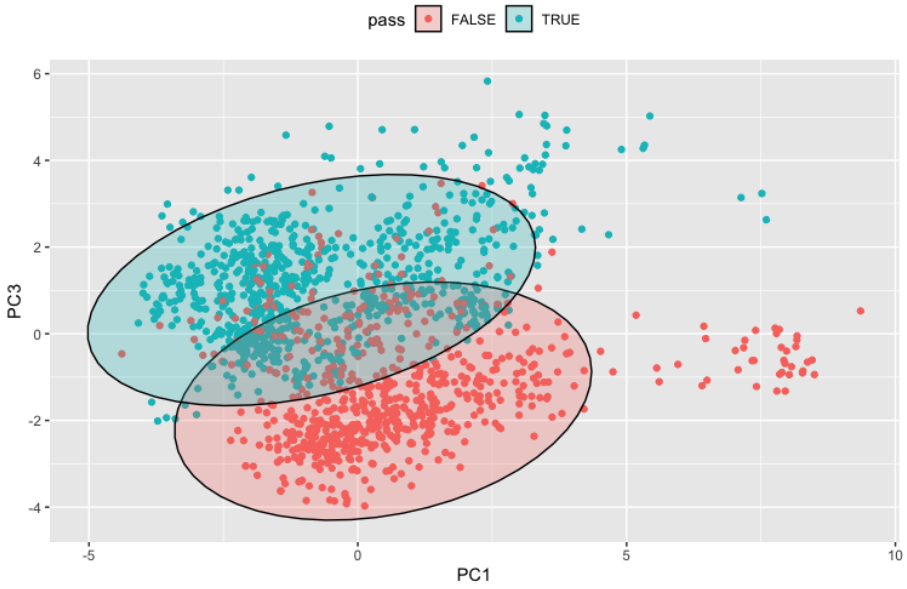

Figure 3.7.8: PC1 vs PC3 and SP pass/fail from 2014 Data-set

The probability of the categorical SP bands is shown in Figure 3.7.9. As previously, there is a clear progression whereby the probability distribution of each group increasing in SP gradually moves up and left, signifying the effect of increasing PC3 and decreasing PC1.

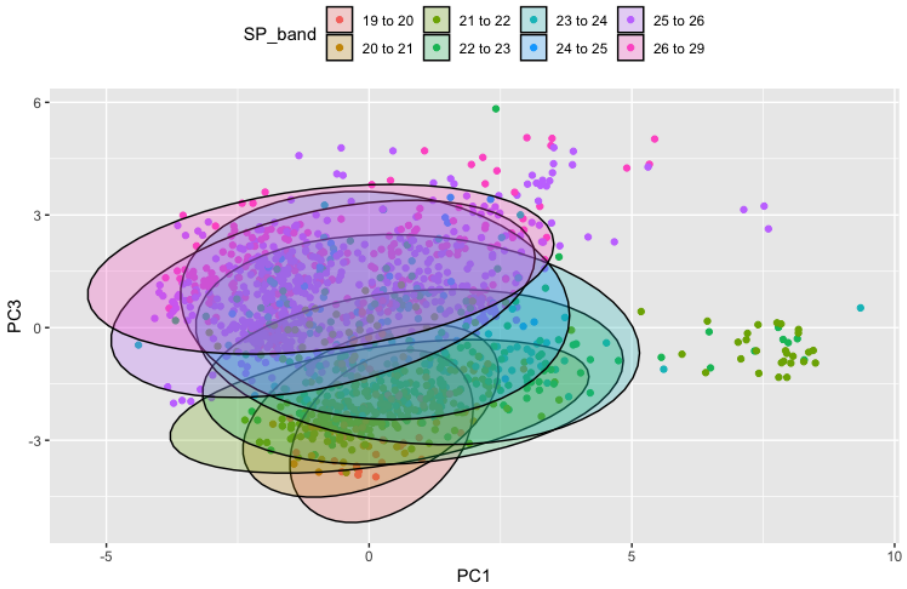

Figure 3.7.9: PC1 vs PC3 and SP bandsl from 2014 Data-set

The advantage of the PCA method is in reducing the complexity of a data set into a few key components that capture the majority of the variability of the data. The downside, however, is that the non-dimensionalised components it produces do

not directly indicate which properties of the original variables are of significance. By comparing the important PC's identified, however, and using a matrix such as that shown in Figure 3.7.3, the degree to which the PC of interest correlates with the original variables can be analysed. The indication of the PCA results indicate that increasing PC2 and PC3 while reducing PC1 results in higher SP's. This same correlation is observed in 3.7.3, where PC1 weakly anti-correlates with SP and PC2 and PC3 correlate strongly with SP. As the effect of PC1 on SP seems minimal, only correlations of interest with PC2 and PC3 are discussed here.

In terms of the other variables, PC2 anti-correlates strongly with five variables; the temperature at which the first 10% of the volume is recovered, the temperature at which the first 50% of the volume is recovered, the flash point, the density, and the viscosity. The distillation results suggest that fuels with a lower SP are composed of molecules in the first 50% vol/vol whose boiling points, and therefore, molecular masses are higher. This may be due to an increase in the respective ratio of carbon to hydrogen as molecular mass increases. Specific energy correlates moderately with PC2, and is the only variable that shows positive correlation of any significance. This effect may be due to an increased prevalence of H-C bonds as opposed to C-C bonds, where a comparable amount of bond energy is contained in the former while using around 50% of the latter's molecular mass, resulting in molecules with comparable energy content and a lower density. This may indicate fuels with a higher hydrogen content result in higher SP's, in agreement with the current understanding of the effects of stoichiometry, as discussed in Section 1.5.

PC3 anti-correlates moderately with colour and density and correlates moderately with sulphur content and temperature of volume where 10% is recovered, while correlating strongly with the initial boiling point and specific energy. The only correlation common to both SP2 and SP3, are that of density (negative correlation) and specific energy (positive correlation).

The use of PCA has shown that it is generally able to capture the shape of the specification data in a reduced number of variables. From a data science perspective, the next step would be to use this reduced dimensionality to produce models that can predict key fuel metrics based on specification parameters [90], although such modelling is outside the scope of this thesis. What PCA has been able to

show, however, is that by non-dimensionalising the variables and measuring their significance, it is possible to see how the actual specification variables interact. It is shown that in the three components that only significantly affect SP (PC1, PC2 and PC3), aromatic volume is of little significance. Of greater significance, is the Density and Specific Energy of the fuel.

3.8 Regression Tree

A regression tree is described here involving SP prediction with a continuous numerical output. The model was developed using 10-fold cross validation based on diving the data into a 70% training set and 30% test set. The results for a sample of predicted versus actual SP values are shown in Figure 3.8.1. The complexity parameter table for the same model is shown in Figure 3.8.2, indicating that ten branches are sufficient to achieve the desired accuracy after which an asymptote is quickly reached and model accuracy does not improve with an increase of branches.

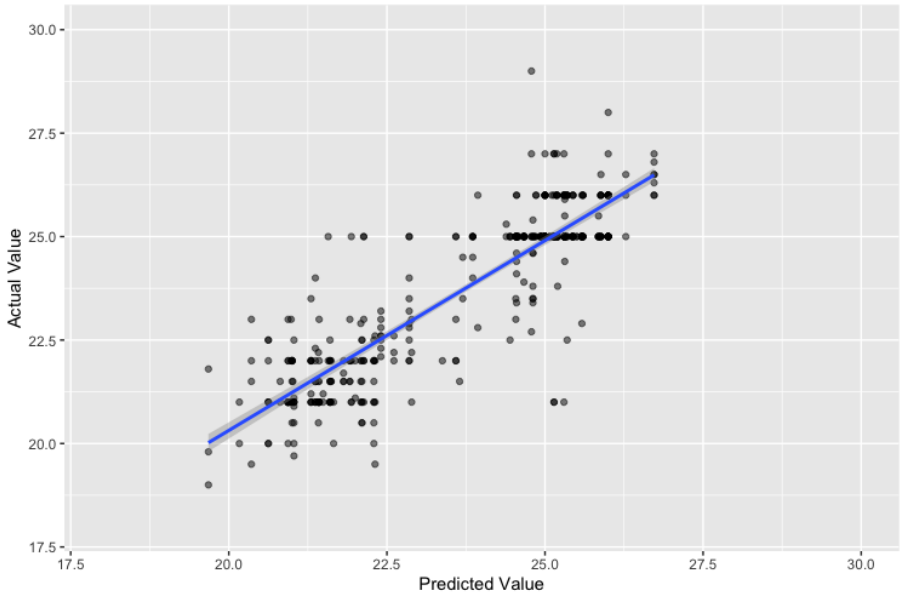

Figure 3.8.1: Predicted vs Actual SP Values for Regression Tree

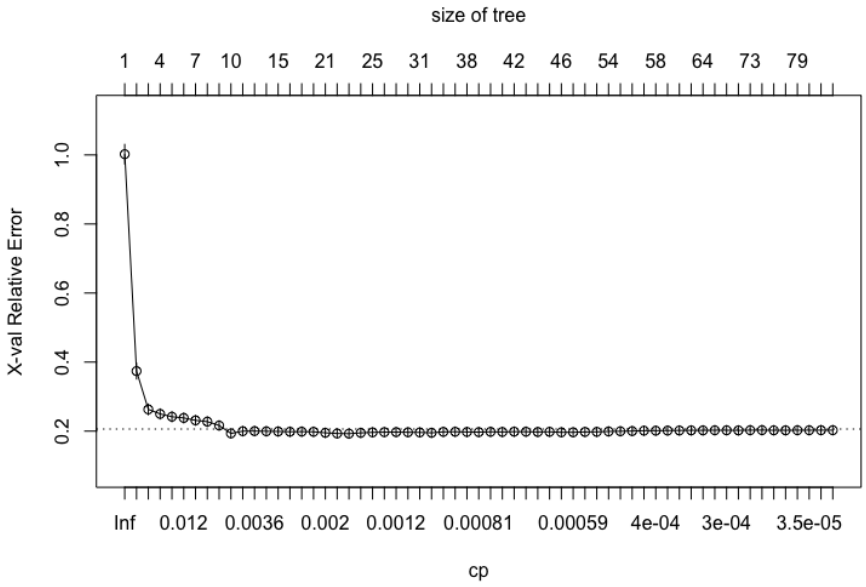

Figure 3.8.2: Complexity Parameter Table for Regression Tree

The model reports good, but not excellent accuracy, with a coefficient of determination of 0.769 and a residual standard error of 0.9416. Using this technique it is generally possible to predict the SP plus or minus 1mm than the actual value.

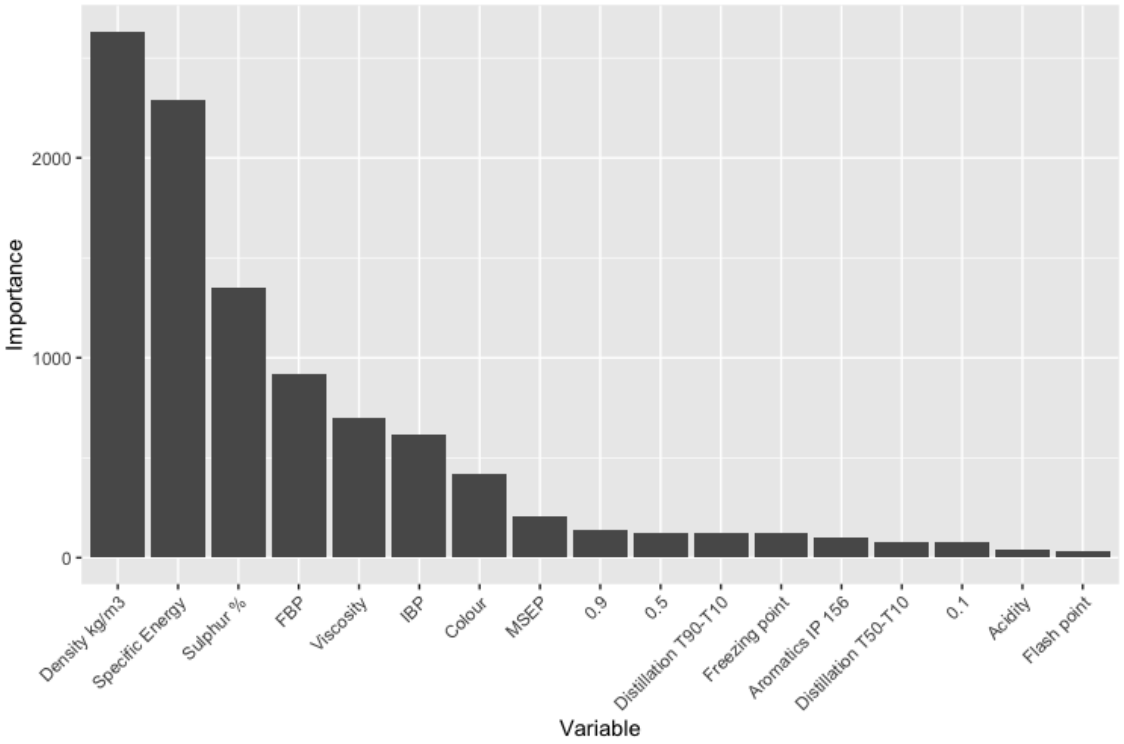

Figure 3.8.3: Importance of Variables for Regression Tree

The importance of the respective variables of this model are shown in Figure

3.8.3. Density and specific energy are the most important variables. The following group have less than 50% of the importance of these two, and includes sulphur content, final boiling point, viscosity and initial boiling point. It should be noted that aromatic content is of no importance to this model.

The significance of Sulphur content as a significant metric, does merit further consideration, however. Hydrodesulfurisation is the main method for the removal of sulphur from refined petroleum products such as jet fuel [91]. This process involves combining the product with molecular hydrogen, and is similar in practice to hydrogenation, where the express purpose of adding the hydrogen is to saturate any hydrocarbons present, such as aromatics. It is plausible that fuel that has undergone hydrodesulfurisation may have become more saturated and a proportion of alkenes will have converted to alkanes and potentially aromatics convert to olefins. An increase in the hydrogen to carbon ratio as a result may result in cleaner burning fuels and higher SP's in the specification data, as suggested by the importance of Sulphur content. As a 10 depth regression tree has been generated from the model, it is not possible to simply measure whether sulphur positively or negatively correlates with SP, as one could do with linear regression, although it's significance here is of interest, nonetheless.

3.9 Discussion of Strongest Predictor

This chapter has comprehensively analysed the effect of all variables included and reported in the UK Jet fuel specification for all fuel in a given year. The only result of statistical significance between aromatic volume and SP found is that the mean value of fuels that pass the SP test have a slightly lower aromatic volume value than those that fail the SP test. Aromatic volume alone, or in conjunction with other variables, has no predictive capability. It would be erroneous however, to conclude that the presence of aromatics has no significance on SP values, as discussed previously, the properties of the aromatic content may have significant effects on the variables that do appear to be deterministic, or closely related to, the factors that drive BC production. Using several techniques, it's been demonstrated here that fuel density appears to have a significant effect on SP values, as does specific energy,

which is heavily influenced by the aromatic proportion of a given fuel.

Chapter 4

Experimental Setup

4.1 Aromatic Selection Criteria

The criteria for the selection of aromatic hydrocarbons for the purposes of this thesis are determined by several factors specific to the research aim. One of the targets of this thesis in to investigate the aromatic contribution to soot propensity in aviation independently of the aromatic volume of the fuel. As discussed in Chapter 3, aromatic volume alone is a poor predictor of a given fuels propensity to produce soot, according to its SP, and other macroscopic fuel parameters, such as density, can be stronger predictors, if not wholly deterministic. In the case of the fuels discussed in the previous chapter, presuming the fuel data set represents petroleum derived kerosene, each sample will likely contain a significant number of different aromatic types with no particular type being present at anything larger than a few percent by volume. As such, the individual sooting behaviour of each contributor, such as its SP, TSI or YSI, may be overridden by the bulk matter properties of the fuel, such as viscosity or density, which could be more deterministic for the sooting propensity of the total blend. The aim of the experimental work of this thesis is to study Jet Fuel surrogates whose aromatic component is a single, uniform aromatic isomer as opposed to multiple components, as in a kerosene fuel. Single aromatic component analysis provides data that can be used to clarify whether those individual aromatic properties, or bulk matter properties, are more deterministic when the variability introduced by multiple aromatics is removed.

The criteria for the selection of appropriate aromatic components for experimen-

tation varies based on consideration of their application to petroleum kerosene or alternative fuels. For petroleum kerosene, aromatics should be included that are thought to be naturally occurring within a significant proportion of different fuels. Identifying these common aromatics is problematic to determine, however, as techniques used to identify individual components, such as NMR, GCMS and GCGC are not available for a significant number of different fuels. It is not, for example, a condition of the specification tests discussed previously to independently identify different aromatic molecules and their proportion within the fuel. Commonly occurring molecules may be suggested by independent studies analysing individual fuel samples [92], but there is insufficient evidence within the literature to suggest whether particular aromatic hydrocarbons occur more commonly in a wide range of fuels than others. For this reason, no consideration has been given when selecting aromatic types naturally occur within petroleum kerosene fuel. For alternative fuels and prospective ASAF's, the consideration of natural occurrence and prevalence is considered moot. As SAF's are produced by a wide range of industrial processes, it is possible that future ASAF's may use a production method that provides aromatic components, whether unitary or multiple, that are not typically prevalent in kerosene petroleum, if it all. It is totally possible, for the purposes of optimisation or necessity, to identify an aromatic component that fills the requirements for a given fuel while not even a typical naturally occurring component of kerosene petroleum.

The main reason that an aromatic component must be present in jet fuel is to ensure sufficient seal swell of o-rings connecting fuel lines. The degree to which certain aromatics induce more seal swell than others was beyond the scope of this thesis and was also not taken into account when selecting potential aromatics for inclusion in experimental campaigns. There is a substantial body of literature, however, into the mechanisms of seal swell and the effects of varying aromatic molecules [93, 94, 95, 96, 97]

The rational and process of selecting aromatics for experimentation took several stages. As much of fuel production is determined by the boiling point of individual components, it was logical to start with aromatic at the lowest boiling point and the simplest molecular structure; benzene. It is impossible to obtain an aromatic hydrocarbon lighter or simpler than benzene, as it has no functional groups and just

one phenyl ring. It was not considered for inclusion for several reasons. Firstly, it is not thought to be a significant component of liquid fuel and is typically only found in trace amounts [98]. This justification alone, however, would be contradictory to the selection criteria discussed previously; that appropriate aromatic components could be found in certain aromatic hydrocarbons that are not thought to be ubiquitous in petroleum kerosene. While this is potentially true for a significant proportion of other aromatics, it is not relevant in the case of benzene due to its deleterious effects on health [99]. The toxicity and carcinogenic nature of benzene provides sufficient justification for its experimental exclusion. Even purely from an objective research interest, it would be unethical to subject fuel technicians, lab services and investigators to fuel blends comprised of a substantial proportion of benzene. In practical terms, legislators and manufacturers of prospective ASAF's would never approve of the inclusion of benzene as a fuel component and it was therefore omitted from consideration. As a result, Toluene was selected as the first appropriate component for consideration.

An initial list of fifty-eight candidate fuels was generated and can be seen in Appendix A, along with a nomenclature signifying reasons for final unconditional exclusion, consideration and final experimental inclusion. This initial selection was formed of aromatics using the following criteria:

- Liquid at room temperature and pressure
- Boiling range greater than that of Toluene and less than 300 $_oC$
- No atomic nitrogen, sulphur or oxygen present
- No differentiation in terms of classification between mono-cyclic and polycyclic hydrocarbons

The decision to limit aromatics to non-solid is due to the practicality of obtaining the necessary blends. For example, the isomer of tetramethylbenzene, durene, has been observed as a component within petroleum kerosene [100] and would be a candidate of interest for a single aromatic component surrogate for experimentation. Pure durene, however, is only available as in crystalline form at room temperature [101] and would need to be blended into an alkane base at any range between zero

and twenty-five percent by volume for potential experimental campaigns. Each crystalline aromatic under consideration would need solubility requirements necessary to blend at such a high proportion. While it is hypothetically possible to obtain a range of soluble solid aromatics that could be blended in significant proportions, their inclusion was considered impractical for the purposes of this work due to the wide availability of liquid candidates, and the potential limitation of aromatic volume introduced by the inclusion of certain solid aromatics. There are contributions to knowledge in the use of the novel liquid aromatics found in this literature without the additional burden of the inclusion of solid-components, and so are considered beyond the scope of this thesis. Their inclusion in subsequent campaigns is discussed further in the future work discussion in Section 7.3.

Pure hydrocarbons were also only considered for initial consideration. The presence of nitrogen and oxygen not only changes the combustion chemistry of the reactions significantly, but also introduces significant ambiguity as to bulk properties of interest to this thesis, such as hydrogen content, as a proportion of mass, as the molar mass of oxygen and nitrogen will affect these values significantly. The inclusion of nitrogen atoms could also potentially contribute to significant fuel NOx and prejudice PM emissions induced by NOx formation [102].

The initial 58 candidates were chosen with no regard to availability or price. Many of the compounds listed in Appendix A are prohibitively expensive for experimentation of the type proposed in this thesis, as their use is predominantly in biochemical applications such as pharmaceutical research. As a result, the initial list of 58 was further refined to 29 affordable candidates and have been marked as such in Appendix A. It should be noted for anyone considering future work that these are the candidates of interest for future work. A final selection of 16 aromatic compounds were selected as shown in Figure 4.1.1. There are twelve alkyl-benzenes, three cyclo-aromatics, and one polycyclic aromatic. One PAH is included predominantly as a point of comparison between the emissions performance of alkylbenzenes and multi-ring compounds. It could be argued that PAH's are of greater research interest due to their higher soot propensity, and merit the inclusion of a wider range of candidates, if not the majority. While not impossible, it is unlikely however, that PAH's will ever be approved for inclusion in prospective ASAF's in the proportions

used in this thesis, and so focus will instead be placed on alkylbenzene components. The inclusion of cyclo-aromatics and polycyclic aromatics also prove useful in statistical regression analysis of key fuel metrics when considering the performance of blends including multiple aromatic categories to see if model accuracy can be achieved without regard for the aromatic category of the fuel.

The structural bonding arrangement for the 16 aromatics selected for inclusion in this thesis are show in Figure 4.1.1 and their correspond relevant bulk-matter properties are summarised in Table 4.1

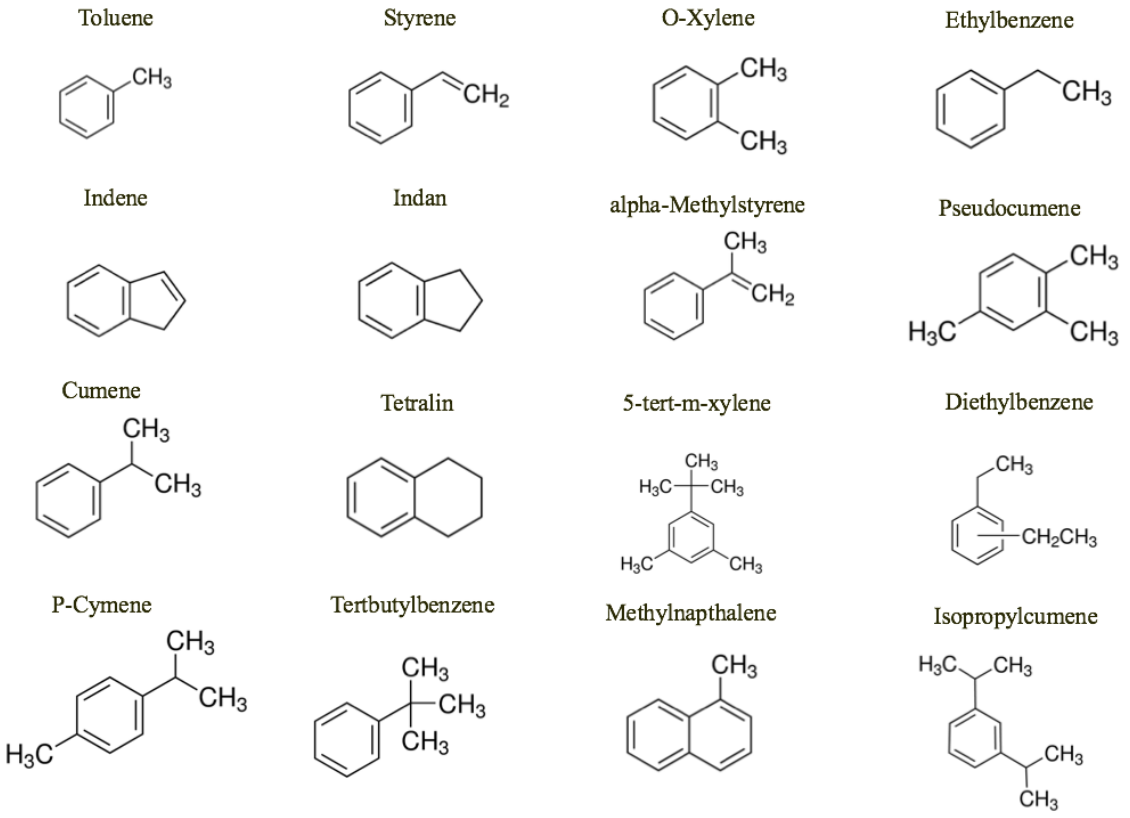

Figure 4.1.1: Structural arrangement of selected aromatics

Table 4.1: Summary of aromatic properties

Name	*CAS*	*Density* $[kgm^{-3}]$	*H:C*	*Specific Energy* $[MJkg^{-1}]$	*Boiling Point* $[^oC]$	*Molecular Mass* $[gmol^{-1}]$
Toluene	108-88-3	865	1.143	40.589	110-111	92.14
Styrene	100-42-5	906	1	42.205	145-146	104.15
o-Xylene	96-47-6	879	1.25	40.961	143-145	106.17
Ethylbenzene	100-41-4	867	1.25	40.938	136	106.17
Indene	95-13-6	996	0.889	41.300	181-182	116.16
Indane	496-11-7	965	1.111	42.162	175-177	118.18
α-Methylstyrene	98-63-6	909	1.111	40.81	165-169	118.18
Pseudocumene	95-63-6	876	1.333	40.984	169-171	120.19
Cumene	98-82-8	864	1.333	41.217	152-154	120.19
Tetralin	119-64-2	973	1.2	42.523	206-208	132.2
Ditheylbenzene	25340-17-4	870	1.4	43.683	180-182	134.22
Tertbutylbenzene	98-06-6	867	1.400	41.422*	169	134.22
p-Cymene	99-87-6	860	1.4	43.644	177	134.22
Methylnapthalene	90-12-0	1001	0.909	40.668	240-243	142.2
Isopropylcumene	99-27-7	856	1.5	41.952*	203	162.27
Tertbutylmxylene	98-19-1	867	1.500	41.952*	205-206	162.27

4.2 Energy Contents

The aromatics selected for this work were tested for their specific energy content using a BombCalorimeter at Intertek UK under ASTM D 4809 [103] with the results presented in Table 4.1. 3-Isopropylcumene, Tert-Butyl-m-Xylene and Tert-Butylbenzene were too volatile to obtain repeatable results and so values could not be obtained using this method. Instead, the net heat of combustion values from the literature were used to estimate the specific energy for tert-Butylbenzene [104]. As to date, there are no literature values for 3-Isopropylcumene or Tert-Butyl-m-Xylene. The specific energy for ter-Buylbenzene was calculated using Equation 4.1, where $\Delta_{c,net}H$ is the net heat of combustion for the relevant aromatic, M is its respective molar mass ($kgmol^{-1}$) and kg the mass of one kilogram.

$$SE[kJkg^{-1}] = \frac{kg}{M} \times \Delta_{c,net}H \tag{4.1}$$

Equations 4.2 shows the calculated value for Tert-Butylbenzene.

$$SE_{3-Isopropylcume}[kJkg^{-1}] = \frac{1}{0.0013422} \times 5559.7 = 41,422.29kJkg^{-1} \tag{4.2}$$

Due to the absense of net heat of combustion values for 3-Isopropylcumene and Tert-Butyl-m-Xylene, the specific energy content of each was estimated using their calculated net heat of combustion using their respective bond enthalpies, the equations for which are found in the Appendix B.1.

4.3 GC-MS Results

The selected aromatics are available at various grades, and therefore vary in purity. For the purposes of combustion research of the type required for this thesis, reagent grade components are unnecessary and relatively small proportions of secondary components would not be likely to significantly affect the fuel behaviour that determines soot production. As a result, anhydrous compounds with a relatively high purity, as close to 100% as possible, were selected. It is important, however, to identify the nature of the impurities in the selected fuels in order to quantify the

appropriate error bounds for each blend based on the know components and for the identification of any particular aromatic compounds that may influence reaction pathways. For his reason, GCMS was performed on each of the 16 purchased samples of selected aromatics. Samples were tested at the Department of Chemical Engineering at the University of Sheffield using a Perkin and Elmer Autosystem XL Gas Chromatograph coupled with a Turbomass Mass Spectrometer. GC-MS results for each sample are included in the Appendix C.1.15 and are summarised in Table 4.2.

There is generally a strong agreement between the quoted and experimental purity. Six of the compounds have no detectable levels of impurity. All compounds are found to have a purity of greater than ninety percent. The lowest, however, 1-methylnapthalene, has an impurity of 6.06% comprised of 2-methylnapthalene, a structural isomer very similar to the required compound. Only indene features a detectible impurity that is not purely formed from pure hydrocarbons, as benzonitrile contains nitrogen. While this impurity is relatively small (2.01%), it needs to be factored into subsequent analysis. Many compounds' impurities are structural isomers of the pure form, such as the isomers of xylene and pseudocumene. Such impurities will not change metrics of interest such as hydrogen content and ring carbon content, but may subtly change global density values.

Table 4.2: Summary of aromatic purity

Aromatic	Tested Purity	Impurities Identified	Proportion
Toluene	100%	N/A	N/A
Styrene	100%	N/A	N/A
o-Xylene	98.68%	m-Xylene, p-Xylene	1.32% combined
Ethylbenzene	100%	N/A	N/A
Indene	92.94%	2-ethyl-1,4-dimethyl-benzene	3.78%
Indan	94.59%	1,3,5-trimethylbenzene	4.29%
α-Methylstyrene	100%	N/A	N/A
Pseudocumene	97.27%	1,2,4-trimethylbenzene, 1-ethyl-2-mthylbenzene	1.29%, 1.44%
Cumene	100%	N/A	N/A
Tetralin	98.77%	Napthalene	1.33%
5-tert-butyl-m-xylene	100%	N/A	N/A
Ditheylbenzene	98.2%	2-methylpropyl-benzene	0.71%
p-Cymene	96.42	All trace amounts	Unidentified
Tertbutylbenzene	100%	N/A	N/A
Methylnapthalene	89.48%	2-methylnapthalene	6.06%
Isopropylcumene	94.31%	1,3-bis(1-methylethyl)-benzene, 1,2-bis(1-methylethyl)-benzene	1.24%, 1.05%

4.4 Surrogate Discussion and Selection

The formulated Jet fuel blends used for this thesis were essentially formed of two parts; an aromatic component and non-aromatic component. It was desirable to find a paraffinic base with high quality hydrocarbons, wherein quality in this case refers to the preponderance of normal alkanes as opposed to branched. A density close to that of Jet-A was also necessary. A solvent manufactured by Banner Chemicals was chosen for this work, a product sold as Banner NP 1014. GCMS performed for the purposes of this work, as seen in Figure 4.4.1, show the presence of C_9 to C_{14} normal alkanes, although C_9 and C_{14} are only present in small amounts. Table 4.3 shows the relevent compositional data of the components contained in NP1014. This solvent is often referred to as BannerSol in LCCC literature.

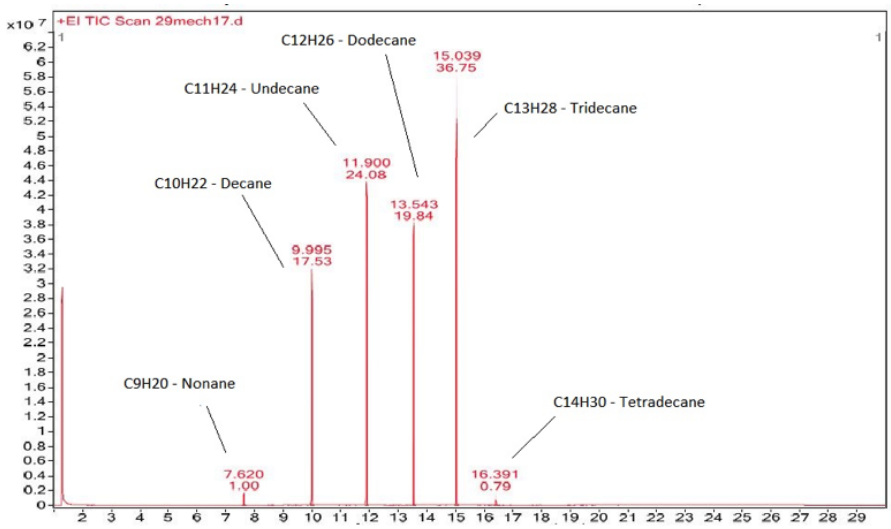

Figure 4.4.1: Components of Banner Chemicals NP 1014

Table 4.3: Table of normal alkane mass percentages present in Banner NP 14 and each respective molar mass

Component	*%˙mass*	*Molar Mass [g.mol^{-1}]*	*Formula*	*Hydrogen:Carbon*
Nonane	1.00	128.20	C_9H_{20}	2.222
Decane	17.53	142.29	$C_{10}H_{22}$	2.200
Undecane	24.08	156.31	$C_{11}H_{24}$	2.182
Dodecane	19.84	170.33	$C_{12}H_{26}$	2.167
Tridecane	36.75	184.37	$C_{13}H_{28}$	2.154
Tetradecane	0.79	198.39	$C_{14}h_{30}$	2.143

4.5 TSI and YSI Values

In order to assess the relevance of the TSI and YSI metrics to the blends used in this work, it is necessary to first obtain the respective values for individual components from the literature, and then calculate the values for each respective blend. Values for TSI, YSI, Unified YSI and Normalised Smoke Point (NSP) are quantified in this section. The YSI and Unified YSI values were taken from the database maintained by McNally et al. through the Harvard dataverse [105]. Unified YSI values were available for all normal-alkanes in the paraffinic base and only tert-butyl-m-xylene was unavailable from the aromatic components selected for this work. To obtain a YSI value, the aggregate method for calculating a YSI using it's component parts was used as suggested by the original methodology [46, 47]. Tert-butyl-m-xylene can be thought of as a Tert-butylbenzene molecule in addition to an m-xylene molecule minus a benzene ring, due to the inclusion of two phenyl groups in the first two components repectively. This is illustrated in Figure 4.5.1.

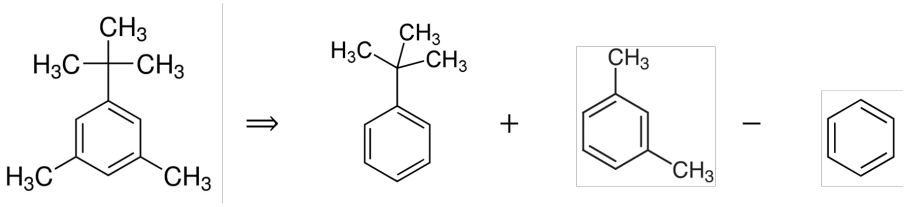

Figure 4.5.1: Component calculation of YSI for tert-butyl-m-xylene

The corresponding calculation for the YSI of tert-butyl-m-xylene is shown in Equations 4.3 and 4.4, using the respective values for each component.

$$YSI_{tert-butyl-m-xylene} = YSI_{tertbutylbenzene} + YSI_{m-xylene} - YSI_{benzene} \tag{4.3}$$

$$YSI_{tert-butyl-m-xylene} = 89.4 + 53.2 - 30 = 112.6 \tag{4.4}$$

The Unified YSI for tert-butyl-m-xylene was calculated using an alternative methodology more appropriate to the unified scale. This methodology was developed by Das et al. [106] and instead of aggregating the whole molecule, the method breaks the molecule down into it's constituent bonds and aggregates their YSI indi-

vidual contributions. This is illustrated in Figure 4.5.2 which shows the calculator used as provided by the National Renewable Energy Research Lab (NREL) [16].

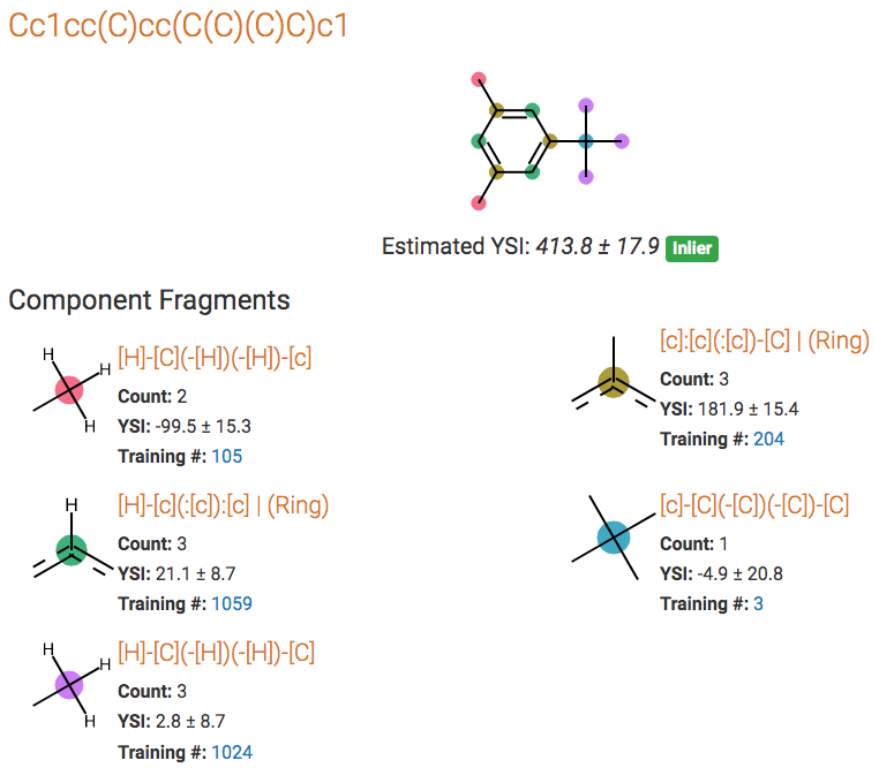

Figure 4.5.2: Component calculation of Unified YSI for tert-butyl-m-xylene using NREL calculator [16]

The Normalised Smoke Point, NSP, first proposed by Li and Sunderland [3], has also been used as a metric for analysis. There is no method in the literature for aggregating NSP's for blended fuels, and so a novel approach is developed for this work using Equation 4.5, where NSP_{agg} is the aggregate Normalised Smoke Point, NSP_n is the Normalised Smoke Point of each component present, and m_n the mass fraction of that component.

$$NSP_{agg} = \Sigma NSP_n m_n \tag{4.5}$$

Table 4.4 shows the YSI, Unified YSI, TSI and NSP for each chemical component used to blend fuels for the purposes of this thesis.

Table 4.4: TSI, NSP, YSI and Unified YSI values

Component	*TSI*	*NSP*	*YSI*	*Unified YSI*
Nonane	3.1	110 ± 27	30.6	50.1
Decane	4.2	122 ± 14	41.7	57.2
Undecane	4.5	113 ± 23	53.3	64.7
Dodecane	5.1	107 ± 24	64.2	71.7
Tridecane	5.2	116 ± unknown	unknown	72.5
Tetradecane	5.4	120 ± unknown	unknown	78.4
Toluene	44	8.12 ± 1.60	43.5	170.9
Styrene	67	5.27 ± 3.49	44.1	174.0
o-Xylene	49	8.10 ± 1.60	50.0	204.8
Ethylbenzene	54	5.92 ± 1.00	53.6	223.7
Indene	62	5.99 ± 0.23	100.3	468.0
Indane	62	5.99 ± 0.23	94.9	439.5
α **-Methylstyrene**	61	6.09	65.6	286.4
Pseudocumene	52	6.43 ± 1.17	69.8	308.2
Cumene	61	6.14 ± 1.78	46.7	187.6
Tetralin	61	7.40 ± 1.21	75.1	336.0
Diethylbenzene	60	6.11		
(1,2-diethylbenzene)			82.8	376.3
(1,3-diethylbenzene)			72.2	320.0
(1,4-diethylbenzene)			62.2	270.6
Tertbutylbenzene	84	4.37	89.4	410.8
p-Cymene	61	7.90 ± 2.84	74.0	330.8
Methylnapthalene	91	5.14 ± 0.48	135.0	649.1
3-Isopropylcumene	51	10.6	78.4	353.3
Tertbutylmxylene	Unknown	Unknown	112.6	413.8

4.6 DMS500 Discussion

As discussed in Chapter 1, the classification of BC emissions in terms of size distribution, geometric mean diameter and number concentration is of significant interest. The Cambustion DMS500 Fast Particle Analyser was used to measure these metrics for the manufactured fuels.

The DMS500 operates using the principle of electrical mobility. First, exhaust samples are passed through a Unipolar Corona Charger, which imparts a positive charge to each particle. The charge received by each particle is approximately proportional to its surface area. The sample is then passed to a cylindrical chamber comprised of a negative high-voltage electrode, which runs along the length of the

central axis, and a combination of twenty-two electrometer detectors, which are arranged in an annular configuration along the inner circumference of the chamber wall. Each positively charged particle that passes through the negative field lines emitted by the electrode is deflected proportionally to the charge of that particle, and moves out in a parabolic radial direction where it is detected as incident on the appropriate detector. The smaller particles, having a proportionally smaller electric charge, also have a smaller surface area and mass and are more easily deflected due to their larger charge to mass ratio. These smaller particles are the first to be detected. As the surface area of particles increases, so does its charge received, which is creates a proportionally smaller charge to mass ratio. Sequentially larger particles are more difficult to deflect and so are detected further along the electometer detectors. This process is shown in Figure 4.6.1 which details the components of the DMS500.

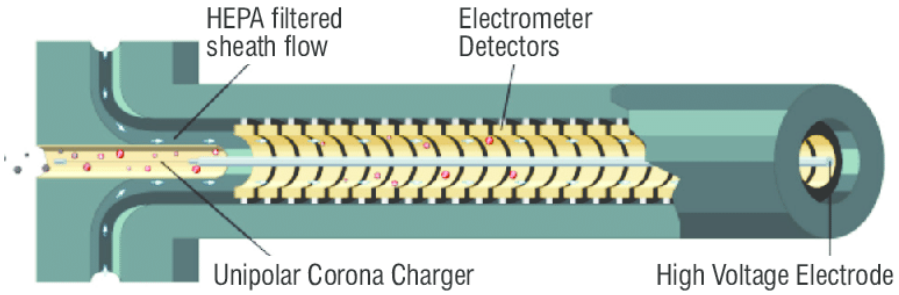

Figure 4.6.1: Internal configuration of DMS500 [17]

This technique allows for the classification of twenty-two bins of particle size, as there are twenty-two detectors and also counts the number of particles detected at each detector.

The DMS500 operates at 10Hz and has a time response of 200ms (T10-90%), allowing it to provide near real time measurements. Alternative configurations such as the Grimm Miniwras [107], the TSI Scanning Particle SizerTM (SMPS) and the Differential Mobility Analyser, Centrifugal Particle Mobility Analyser (DMA-CPMA) allow for increased resolution but at significantly slower response times and scan times. This increased resolution is due to the presence of a Condensation Particle Counter (CPC). The DMA-CPMA-CPC configuration has been used before at the LCCC to measure size distribution concentration and effective particle density, but

due to the significant length of scan times being up to several hours, the technique was considered unsuitable for the work proposed in this thesis.

The DMS500 is capable of two ranges of operation; 5nm – 1000nm (PM 1.0) or 5nm – 2500nm (PM2.5). While the second mode of operation offers a wider range of detection sizes, it does so at the cost of resolution of the smaller sizes, as the number of detectors stays the same for both modes of operation. As discussed previously, soot aggregates are typically around 30nm in range but the larger particles, that contain the majority of the mass concentration, are around 100-250nm. While the second mode loses resolution at the smaller scale, the first loses the ability to capture the presence of particles larger than 1000nm. However, the focus of this work is to characterise the super-fine particles in the 5-1000nm range due to their adverse effects on health and the environment and so that mode has been selected for analysis. The larger proportion, accounting for the majority of the emission mass concentration will instead be accounted for using the mass concentration metric of the LII.

4.7 LII Discussion

Laser Induced Incandescence is an optical technique commonly used in combustion and emissions experiments to determine several metrics of BC emissions in a given exhaust sample in situ in real time (36). For the classification of carbonaceous exhaust emissions due to incomplete combustion, a pulsed laser excitation method is usually utilised. Initially, particles are heated with a high energy or high-power laser which causes their temperatures to rise to around 3500 K. Soot particles are very effective at absorbing radiation as their carbonaceous structure allows them to approximate a black body, and as a consequence, can also emit radiation effectively. These particles emit thermal radiation (incandescence) which is then detected and the absolute strength of which determines the soot volume fraction.

There are multiple options available for measuring BC emissions [108], although LII is considered the most appropriate for the experimental work described in this thesis. Firstly, due to the principles of its operation, the LII method uniquely measures the non-volatile PM component of emissions. This is due to the high temper-

ature to which samples are heated, nominally between 2500K and 4500K. At these temperatures, volatile components within the fuel have sublimed, theoretically leaving only the carbonaceous component intact, which should be purely BC. It should be mentioned that any temperature of operation higher than the recommended range will result in sublimation of carbonaceous particles. The second benefit of using LII for this work is due to the comparatively lower mass concentrations of BC measured of exhaust which has been burnt at atmospheric pressure. The RR Tay emits carbon at approximately 2 orders of magnitude lower than the Honeywell APU at the LCCC, predominantly due to the absence of significant agglomeration found at higher pressure, although this is an ongoing area of research [109]. The LII device used for this thesis is capable of obtaining readings at lower than 1 mgm^3, at which other potential apparatus is unable to obtain readings. APU scale tests such as the Smoke Number produce no discernible difference on virgin versus collected samples, and is considered unsuitable for this work. Gravimetric methods • such as NIOSH 5040 [110] and Method 5I [111] would require several hours of continuous operation to collect the requisite exhaust to provide one reading alone, which makes their use uneconomical due to the prohibitive cost of aromatic fuel components.

The LCCC uses an Artium LII 300, which is kindly on-loan from Rolls-Royce Canada. The calibration against Method 5I was performed by the instrument manufacturer on the 16th May 2016 and was due for re-calibration in May 2018. All experimental results obtained using this apparatus were obtained during this window. The Artium LII 300 features a pulsed ND:YAG laser, with a magnitude of 100mJ, which heats exhaust samples within 20 ns. The laser produces light at a wavelength of 1064 nm, which is above the incandescence signal range of 400 to 800 nm, and so does not influence incident readings at the detector. Conceptualisation of the principles of operation are shown in Figure 4.7.1.

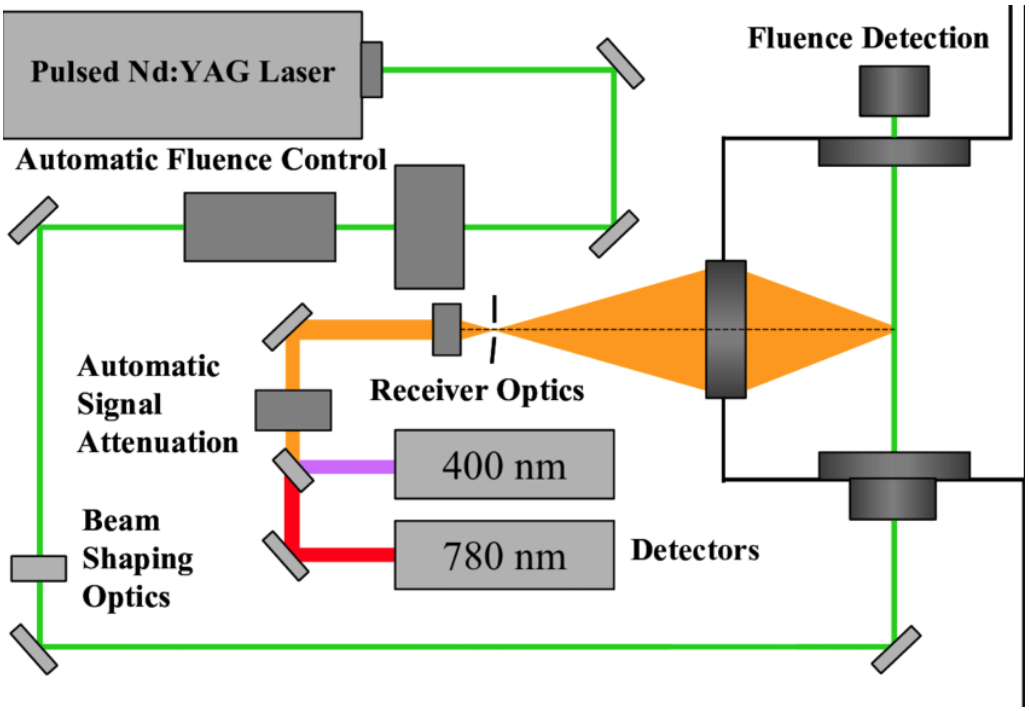

Figure 4.7.1: LII principles of operation

The Artium LII 300 offers a +/− 2% level of precision over its range of operation for measuring gravimetric concentration of BC emissions, even at the low end of its operation ($< 0.2 mgm^{-3}$). This is suited for the typical exhaust concentration found using the RR Tay. While the LII 300 is capable of obtaining the primary particle size of BC, the function has not been used for this work. This is due to the range of particle size than can be detected, and the relative error of this measurement. For the LII 300, the primary particle size is analogous to the Geomeric Mean Diameter obtained using other devices. The range of detectable particle size is 10-100 nm, which encompasses the typical distribution of particle sizes of soot particles, as discussed previously. The majority of a given exhaust's mass, however, is in a proportionally smaller number larger of particles, which the LII 300 is incapable of detecting. The LII 300's particle size also has a +/−2% full scale error, and when this error scales down to the exhaust levels encountered with the RR Tay at atmospheric pressure, the magnitude of the error is larger than the reading itself. For these reasons, the LII 300 primary particle size has neither been quantified or considered for this work, and size and number distributions have instead been quantified using a DMS 500, which overcomes many of the shortcomings described of the LII when quantifying size distributions.

Despite the wide availabilty of various PM measuring equipment, the selection of the DMS 500 and LII ensures measurement of the parameters that are most relevant to the currently regulated ICAO values; nVPM mass and number. Any other metric is essentially superfluous to this work as one of the aims of this thesis is to understand the impact of different aromatics on regulated values.

4.8 Experimental Configuration

The experimental component of this thesis involved two experimental campaigns conducted separately. While it would've been ideal to conduct the campaigns concurrently, the DMS 500 was unavailable for the LII campaign, and the LII was unavaialable for the DMS campaign. The main component of the jet fuel combustion platform at the Low Carbon Combustion Centre is a Rolls-Royce Tay gas turbine engine combustor kindly donated by Rolls-Royce. This combustor is from a ring of annular combustor cans, first designed in 1964, and this has been substituted by new generation engines, which predominantly use a single annular combustor. The Rolls Royce Tay combustor test rig can be seen in Figure 4.8.1.

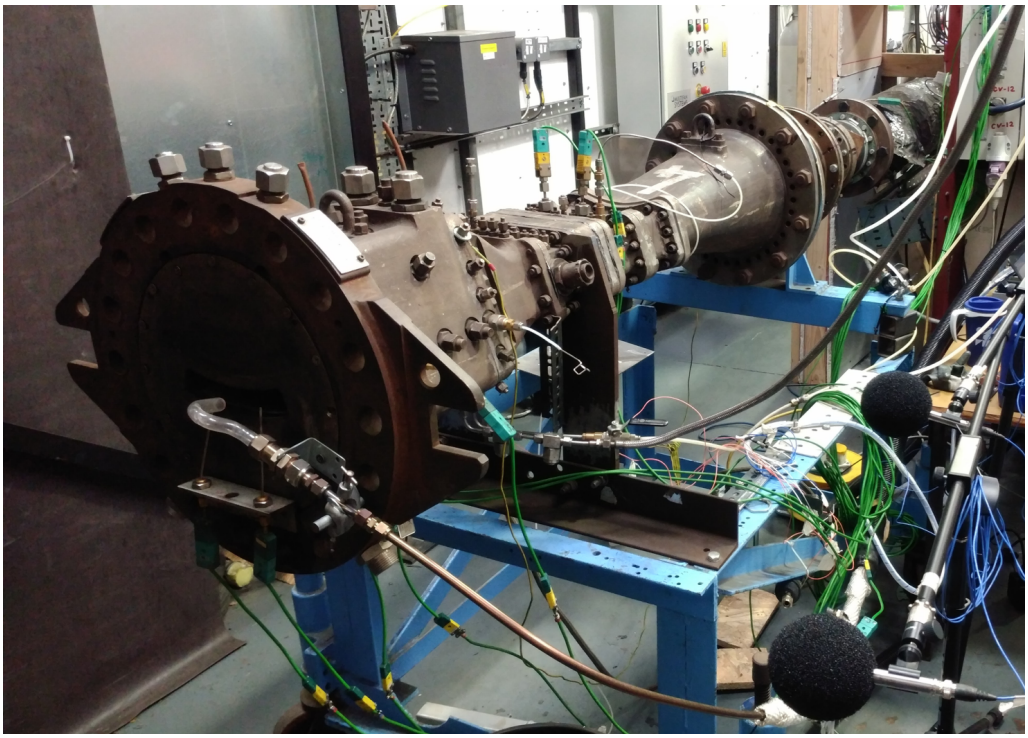

Figure 4.8.1: RR Tay Combustor at the LCCC

The combustor is connected to an upstream air supply capable of providing

up to 320 gs^{-1} and a pre-heat of up to 500^oC. Air is delivered to the combustor from an atmospheric fan through a 6" process line which has been designed and manufactured according to BS 5167. Fuel is supplied to the combustor through an air-blast atomiser supplied by a fuel bomb. The fuel bomb is pressurised using Nitrogen and the flow is regulated using a PID system downstream of a coriolis meter which monitors and reports fuel mass flow rates. The respective air and mass flow rates for the two respective campaigns are detailed subsequently. The uncertainty of the controllable properties for the atmospheric line are summarised in Table 4.5.

Property	**Range**	**Reading Uncertainty**
Air Mass Flow	$0 - 320gs^{-1}$	$\mp 2\%$
Fuel Mass Flow	$0 - 5gs^{-1}$	$\mp 3\%$
Air Supply Temperature	$0 - 500^oC$	$\mp 1\%$

Table 4.5: Uncertainty of controllable properties for atmospheric line

4.9 LII Configuration

A diagram showing the configuration of atmospheric line for the LII campaign can be seen in Figure 4.9.1.

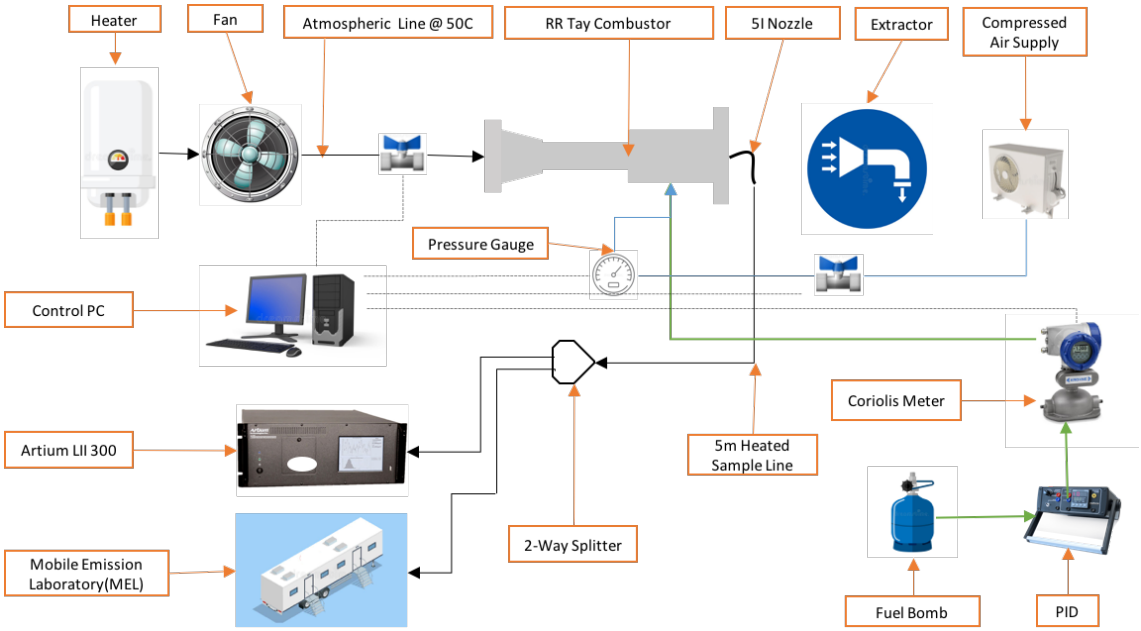

Figure 4.9.1: LII campaign configuration

Air was supplied to the combustor at a rate of 100 gs^{-1} with a pre-heat of 323.15^oK (50^oC). Fuel was supplied at a rate of $1gs^{-1}$ and was maintained throughout. Fuel injection was aided by an air blast atomister set at 0.5 bar. Of the sixteen selected aromatics, three were unavailable at the time of this campaign and so this data set is comprised of thirteen aromatics at four blend proportions for each.

The sample probe was placed at the exhaust plane exit. The probe used was quartz glass in compliance with techniques specified by Method 5I [111]. This probe nozzle has a 14.1 mm outer diameter and an internal diameter of 8mm, with a total lenth of 10cm. The exhaust gas then passed through a 5m heated sample line with an nominal bore of 1/4", inner diameter 8mm, outer diameter 13.72mm. The temperature of the heated line was maintained at $160^oC \mp 15^oC$. The exhaust gas then passed through a two way flow splitter in order to analyse separate streams according to gaseous and particulate emissions. One pathway lead to the LCCC Mobile Emissions Laboratory in order to measure $C0$, CO_2, NO, NO_2 and UHC emissions, although these results are not reported here. The second pathway lead to the Artium LII 300 for the measurement of mass concentration of BC. The LII configuration uses a pump downstream of the device used to draw flow through the device.

To ensure high combustion efficiency during the experiments, exhaust gas temperatures were taken at nine probe positions within and around the combustor. These temperatures were consistent with those expected based on existing adiabatic flame temperature calculations for a campaign such as this. As a further QC check, gaseous emissions were post-processed and analysed after the campaign and a combustion efficiency greater than 99% was obtained.

Once the air was preheated to the required temperature, fuel was supplied to the combustor and was ignited. Once air flow and mass flow had reached stable conditions ($100 gramspersecondair \pm 1 grampersecond$ and $1 grampersecondfuel \pm 0.01 gram$), the LII was initiated to collect data for five minutes of stable operation. This was performed for every aromatic and blend for a total of 52 blends. This was repeated two more times totalling 15 minutes of LII data for each blend.

Post processing the data involved taking the mean LII reading of three thirty second windows within each five minute period for each blend.

4.10 DMS Configuration

A diagram showing the configuration of atmospheric line for the DMS campaign can be seen in Figure 4.10.1.

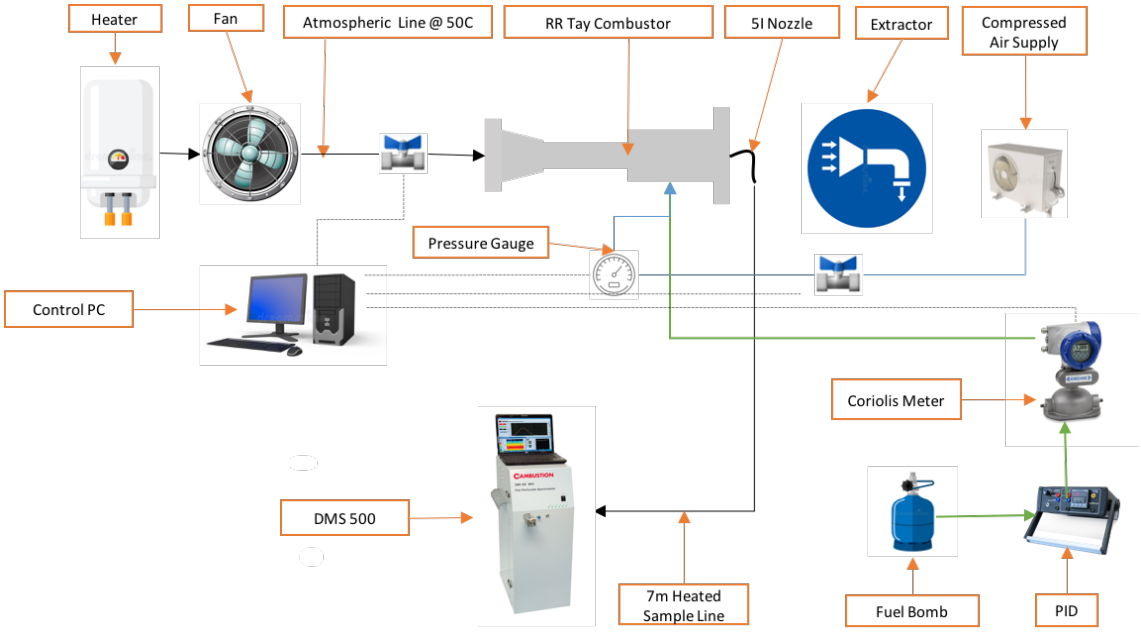

Figure 4.10.1: DMS campaign configuration

Air was supplied to the combustor at a rate of 200 gs^{-1} with a pre-heat of 323.15^oK (50^oC). Fuel was supplied at a rate of 1.5gs^{-1} and was maintained throughout. Fuel injection was aided by an air blast atomister set of 0.5 bar. This campaign ran concurrently with a Lean Blow-Out campaign which meant the air and mass flow rates could not be exactly replicated between the two campaigns.

The sample probe was placed at the exhaust plane exit. The probe used was quartz glass in compliance with techniques specified by Method 5I [111]. This probe nozzle has a 14.1 mm outer diameter and an internal diameter of 8mm, with a total lenth of 10cm. The exhaust gas then passed through a 5m heated sample line with an nominal bore of 1/4", inner diameter 8mm, outer diameter 13.72mm. The temperature of the heated line was maintained at 160$^oC \mp 15^oC$. In order to prevent particles larger than 1 micron from entering and damaging the DMS 500, a cyclone was placed upstream of it. Exhaust gas then entered the DMS 500 for size distribution and number concentration measurement. The DMS 500 was set with a dilution ratio of 5 in order to prevent condensation from occurring within

the sample.

To ensure high combustion efficiency during the experiments, exhaust gas temperatures were taken at nine probe positions within and around the combustor. These temperatures were consistent with those expected based on existing adiabatic flame temperature calculations for a campaign such as this. Gaseous analysis was not available for this campaign, although the exhaust gas temperatures measured were consistent with those measured for the LII campaign.

Once the air was preheated to the required temperature, fuel was supplied to the combustor and was ignited. Once air flow and mass flow had reached stable conditions ($200 grams per second air \pm 1 gram per second$ and $1 gram per second fuel \pm 0.01 gram$), the DMS was initiated to collect data for ten minutes of stable operation. This was performed for every aromatic and blend for a total of 48 blends.

Post processing the data involved taking the mean DMS reading of five thirty second windows within each ten minute period for each blend.

4.11 Unforeseen Issues Affecting Research

The Low Combustion Combustion Centre at the University of Sheffield was located off campus on an industrial estate outside the city. In October of 2019, during inclement weather, the building suffered severe flood damage. At its worst, the water inside the building reached 1.3 metres. Damage was caused to the building, infrastructure, equipment and fuel supplies. The destruction was so significant that it effectively shut down the LCCC as a research facility. Much of the equipment was bespoke or specialist so that it could not be replaced within a reasonable time-frame, if at all. The onset of the Covid 19 pandemic shortly after and the ensuing lock-downs effectively brought a premature end to the potential for any further experimental work pertaining to this thesis. It should be noted that even had experimental facilities been made available elsewhere, the loss of the aromatic fuels, purchased at significant cost for aromatic work at the LCCC, were financially irreplaceable as the funds provided for the completion of this work had been depleted.

Fortunately, a large proportion of the data required for the completion of this thesis had already been obtained, and is presented here in Chapters 5 and 6. There are,

however, unavoidable omissions that somewhat adversely affect the logical thread of this work. There are two outstanding campaigns that were originally part of the scheme of work. The first was a multi-component campaign where blends would be formed of several aromatic components instead of just one. This campaign would've provided a method of verification for the multivariate regression equations obtained in Chapters 5 and 6. While this data would have been beneficial, it was not integral to the flow of the thesis. The second campaign, however, would have used the Automated Smoke Point method to obtain the SP for all formulated blends used for this work. This data would've brought this work to a logical conclusion. While the LII and DMS 500 data reported in Chapters 5 and 6 is useful, and perhaps provides greater fidelity and resolution than the SP method, their use is not standardised or as ubiquitous as the SP method, despite its shortcomings, as previously discussed. The absence of this data is somewhat mitigated by the comparison of BC emissions against NSP, TSI and YSI values, as each can be considered an extension of the SP research methodology, as discussed in Chapter 2 of this thesis.

The SP's were not obtained during the original experimental campaigns as the LCCC had no SP meters at that time, neither automated nor manual. While a manual SP metre was obtained from Stanhope-Seta before the flood, it was not found to have the ability to effectively contrast the different SP performance due to a high range of values found for each blend. The LCCC was in the process of negotiating the loan of an automated SP meter with greater fidelity leading up to the flood. Again, even had one been obtained, the loss of the aromatic components for new blends, the loss of original blends which had been stored, and lack of access to experimental facilities, made automated SP testing effectively impossible to perform.

Due to the loss of experimental facilities used to obtain the data in this thesis, this chapter is missing the breadth of detail that was intended. Experimental configurations and procedures have been been described and depicted using the surviving documentation, mostly gleaned from publications relating to this work.

Chapter 5

LII Results

5.1 LII Results

Before looking at how bulk matter properties affect BC concentration in the exhaust it is useful to look at the raw LII results as it allows subjective, classification comparisons between two given blends. A bar chart of mean BC concentration emissions are shown in Figure 5.1.1. In this figure, the blends have been ordered by best performing aromatic (Toluene) to worst performing aromatic (Methylbenzene), where worst refers to higher BC concentration levels, when averaged across the four blend proportions. Toluene, for example, generally produces lower concentrations of BC in each group, excepting for the 22.5 % vol/vol group. This does not affect it's positioning within the group however as this affects readability of the graph. The same is true for discrepancies in the order of other species; that incongruities do not change their respective positions. While the 12.5%, 17.5% and 22.5% groups show a generally uniform increase inc BC concentrations for the given order, the 7.5% group does not show this trend, as the results are more variable for their given positions compared to the other groups. A possible explanation for this could be that at lower aromatic concentrations, the combination of blending errors, fluctuations in fuel supplied to the combustor and LII readings are more significantly effected and lead to variable results. There are other explanations for this behaviour, however, that are discussed later in the Aromatic Volume section of this chapter.

The trend of increasing BC emissions for increasing aromatic content can be seen for every aromatic species. The is no aromatic that increases it proportion and

doesn't cause an increase in BC concentrations. While this is useful as a frame of reference for comparison, there is no clear indication as to any underlying feature or property that is determining these results. It does show however, that BC results can vary significantly based on aromatic composition alone, irrespective of volumetric proportion.

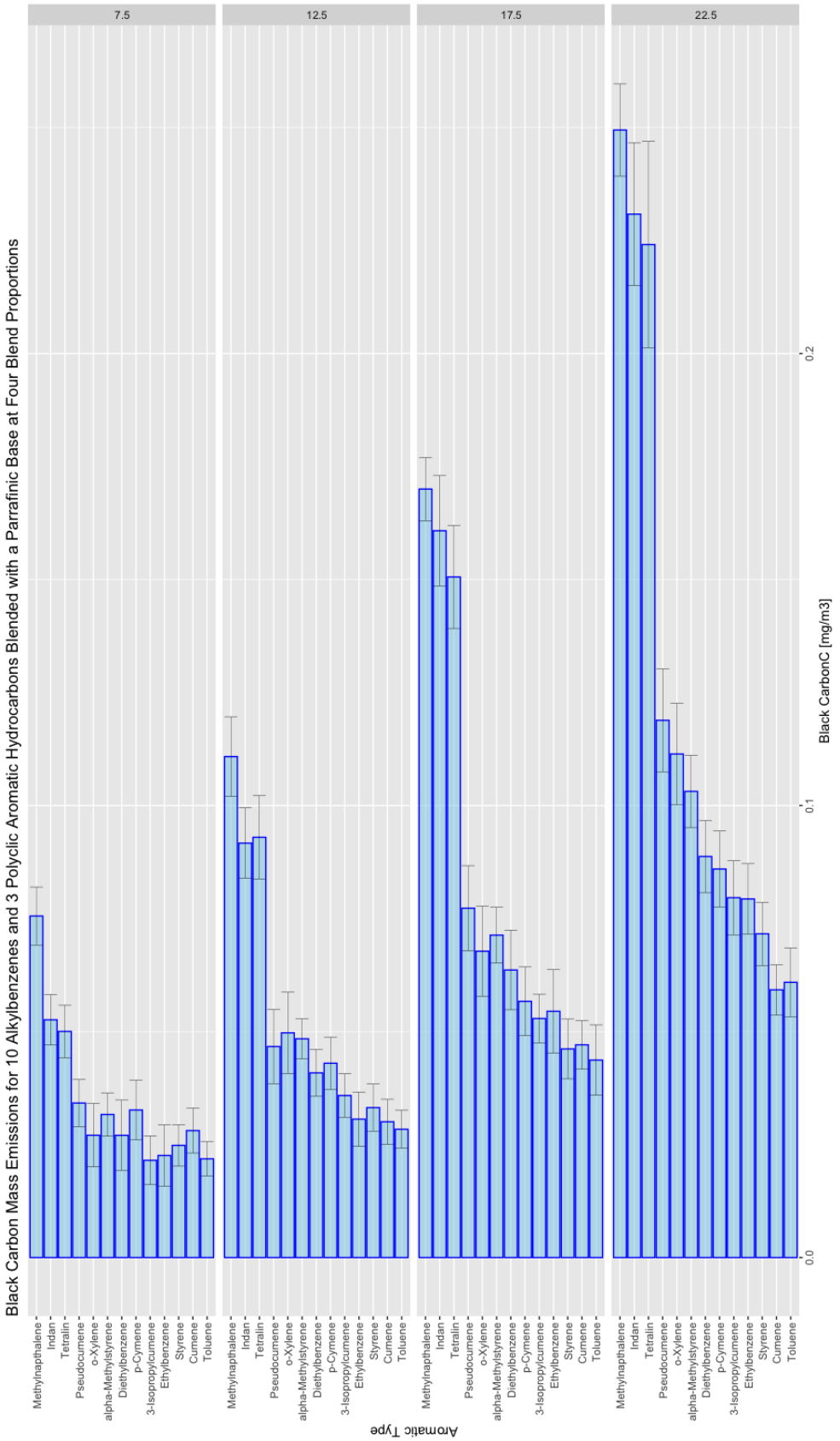

Figure 5.1.1: Black Carbon Concentration Emissions for 10 Alkylbenzenes and 3 Polycyclic Aromatic Hydrocarbons blended with a paraffinic base at four blend proportions

The error bars shown in Figure 5.1.1 are two standard deviations around the mean of the nine readings taken for each fuel. Two standard deviations are shown as this encompassed 95.4% of the data around the mean. Appendix D.1.13 shows the results for blends specific to an aromatic type. The error bars included on these scatter diagrams show two standard deviations of the fluctuation in individual LII readings. D.1.13.

Figure 5.1.1 allows subjective comparisons of aromatic type. For example, in each group, the three polycyclic molecules, Tetralin, Indan and Methylnapthalene, all produce the highest BC concentration emissions for each group. This behaviour is expected based on the previously discussed literature and specification limitations and show that polycyclic structures do produce higher BC levels. It shoudl be noted, however, that Indan and Tetralin are not true PAH's as they do not contain multiple unsaturated carbon rings, but are cycloaromatics, using the NJFCT nomenclature.

Comparing isomers of various aromatic groups, or those with a very similar molecular formula reveal interesting changes in emissions levels and may or may not be suggestive of the effect of molecular structure. For example, cumene (C_9H_{12}) and pseudocumene (C_9H_{12}) are true isomers of each other. Despite this, cumene ranks only 2nd while psuedocumene ranks 10th, and is the alklylbenzene with the highest BC concentrations, on average. These are two molecules that also have identical hydrogen to carbon ratios and ring carbon content but show significantly different performance in terms of emissions. Similarly, ethylbenzene (C_8H_{10}) and o-xylene (C_8H_{10}) are true isomers, but come 4th and 9th respectively. Comapring across alkylbenzenes and cyclcoaromatics types, cumene (C_9H_{12}) and indan (C_9H_{12}) are also isomers, but yet indan produces aproximatly three times the BC concentration of cumene, a relatively good performer. As there are significant differences in emissions despite many of these aromatics having similar or identical hydrogen to carbon ratios, it suggests that hydrogen content is not an appropriate metric by which to assess and aromatics surrogate fuels propensity to produce BC, as discussed further in Section 5.6.

A question of this thesis was whether these varying performance levels are a result of variations in molecular composition at a micro scale where structure affects reaction pathways, or whether changes in aromatic composition affects bulk matter

properties which dictate BC performance. It is impossible to answer this question by comparing types in the manner done so in this section, but serves to point out the discrepancies that require further investigation. It was a design of this thesis to include multiple isomers for this reason. The next sections look at commonly discussed fuel parameters in order to look for statistically significant predictors of BC concentration emissions.

5.2 Regression Equations per Species

Figures D.1.1 to D.1.26 show the BC mass results for each aromatic blend against five key fuel property metrics of interest, along with a plot of each respective linear regression equation and accompanying coefficients of determination for each species. Figure 5.2.1 shows the collated results from all the aromatic surrogate fuels at the four blend proportions for five fuel metrics; Aromatic Mass [% mass/mass], Aromatic Volume [% vol/vol], Ring Carbon Content [% mass/mass], Hydrogen/Carbon Ratio, Blend Density [kgm^{-3}]. Regression statistics are omitted while the regression line remains.

With such a relatively small range of data points for each species, care must be taken when inferring behaviour specifically indicated by statistical analysis. It is also worth noting that as each of these metrics are bulk properties, linear increases in the volume proportion of each blend produces a linear increase in each other property. This is reflected in the similarity of R-squared numbers for each metric for a given aromatic species. There is generally good agreement, however, between the variables and each fuel metric, with R-squared values for Volume Content Percentage ranging between 0.92970 and 0.98626.

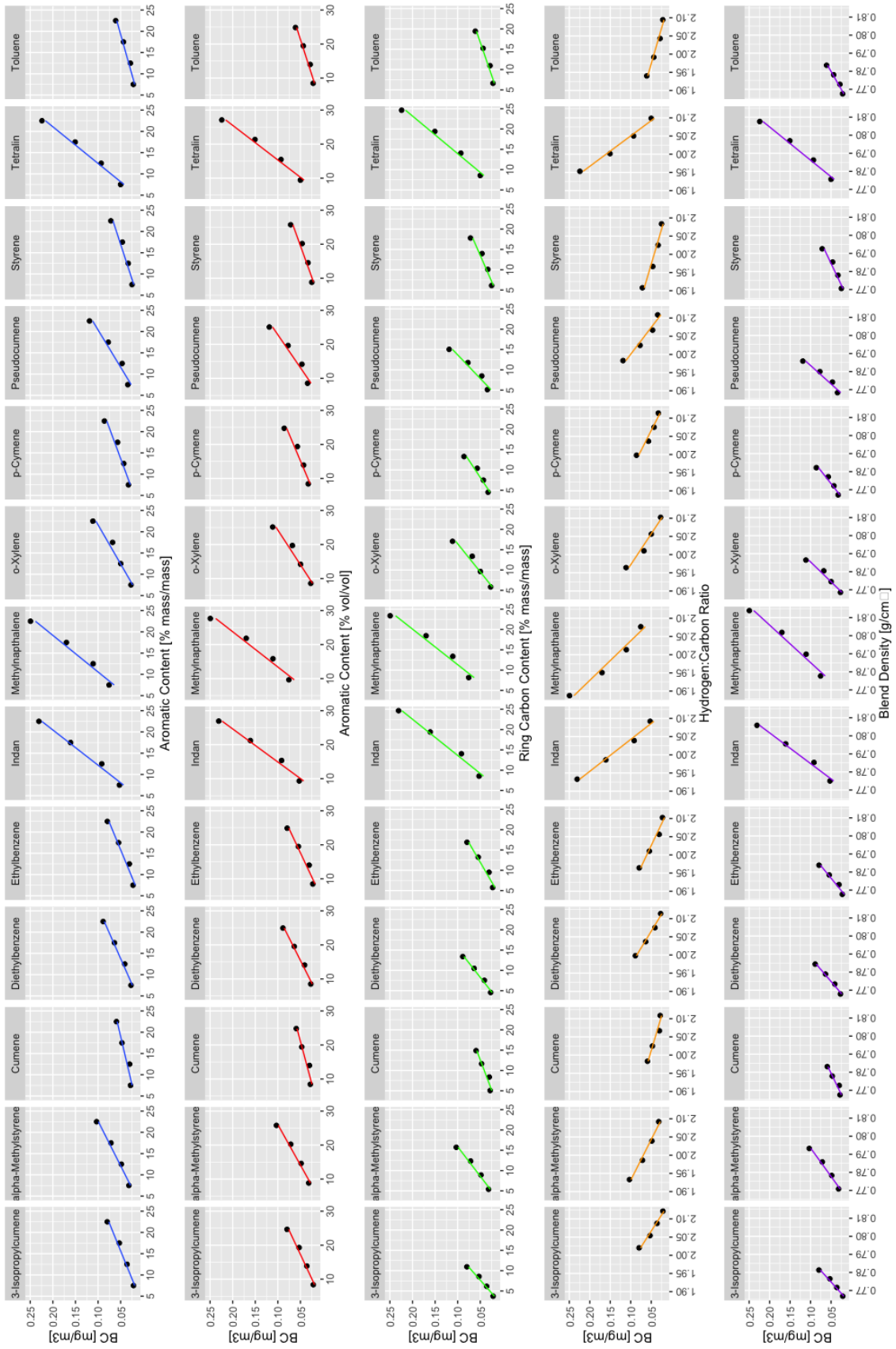

Figure 5.2.1: Individual BC emissions for thirteen aromatics at four blend proportions for five fuel properties

A possible interpretation is that the relationship between aromatic volume percentage and BC emission levels is linear, at least with respect to a specific aromatic species. However, as each of the metrics under consideration is a bulk matter property, volume percentage may only be co-linear and another con-founder for one of the other properties that defines a potential linear relation. A closer examination of the data points suggests that whichever property is the determining factor, that the relation may not be linear. For every aromatic species presented, a derived linear interpolation underestimates BC emissions at the 7.5% and 22.5% aromatic volume points. The interpolation also overestimates BC emissions for the 12.5% and 17.5% data points for every species. The uniformity of this trend across every species may suggest that the relationship with these properties and BC emission levels is not linear, but instead is polynomial, either with respect to volume or some other property. This is also suggested when considering the linear intercept for each volumetric linear regression equation. Every intercept at the 0% volume condition suggests a negative BC emission level, with the exception of Cumene. This is practically and logically inconsistent, primarily because a negative emission level is impossible. But logically, gradually removing the aromatic content of a blend to zero would not reduce its BC emission levels to zero but would eventually approach the asymptote of the remaining base fuel; in this case, pure Banner NP14. This should also be true at the higher end of the scale as a majority of aromatic content is approached; logically, an asymptote would be arrived at for the emission levels of a purely aromatic fuel. While these are tenuous assumptions outside the range of these results, it provides a logical framework to suggest why the mechanistic factors that cause these results may not appear linear.

Despite these arguments against linearity, linear trends have been used to produce models for each fuel metric in the subsequent sections. The rational for this approach is that without a mechanistic understanding or justification why that specific fuel property in question should infer a non-linear relationship, a linear relationship will be used.

5.3 Analytical Methodology

The aim of the remainder of this chapter is to compare the BC mass levels obtained via LII to key metrics of interest. The aim is to find a metric which is statistically significant in accounting for the variance within the data while also being mechanistically logical and attributable. As many of these metrics are co-variants and increase and aromatic proportion increases, there is a danger of attributing significance erroneously due to correlation alone, without the accompanying evidence of causality. In an attempt to avoid relying on a incomplete correlative conclusion, each metric is assessed across several criteria. This involves breaking down each statistic based on specific characteristics and then comparing accordingly. For each metric, the blends are initially broken down by classification into alkylbenzene and polycyclic structures, and then are broken down into each blend proportion group. This initially comprises eight groups for analysis (alkylbenzene-7.5%, alkylbenzne-13.5%, alkylbenzene-17.5%, alkylbenzene-22.5%, polycyclic-7.5%, polycyclic-12.5%, polycyclic-17.5%, polycyclic-22.5%). The statistics presented and analysed for these groups, following linear correlation, include the coefficient of correlation, coefficient of determination and p-value. The second phase of analysis omits the blend proportion, and following linear regression, presents the statistics for all alkybenzenes, all polycyclic structures, and finally, every blend irrespective of classification in what can be considered as a uniform category.

For a metric to be considered to be significant, there must be statistical significance across all groups. It is not sufficient to obtain a high coefficient of correlation for the unified group for a given metric when such behaviour is not replicated within a given blend group, as the increase of that metric as aromatic volume increases is falsely imposing a correlation that is an artifact of that volume increase.

5.4 Aromatic Volume Discussion

The BC results obtained via LII are shown in Figure 5.4.1 compared to its volumetric percentage content of aromatics. The accompanying statistics for every fuel and blend for this metric is shown in Table 5.1, while the coefficients of the accompanying regression equations are shown in Table 5.2.

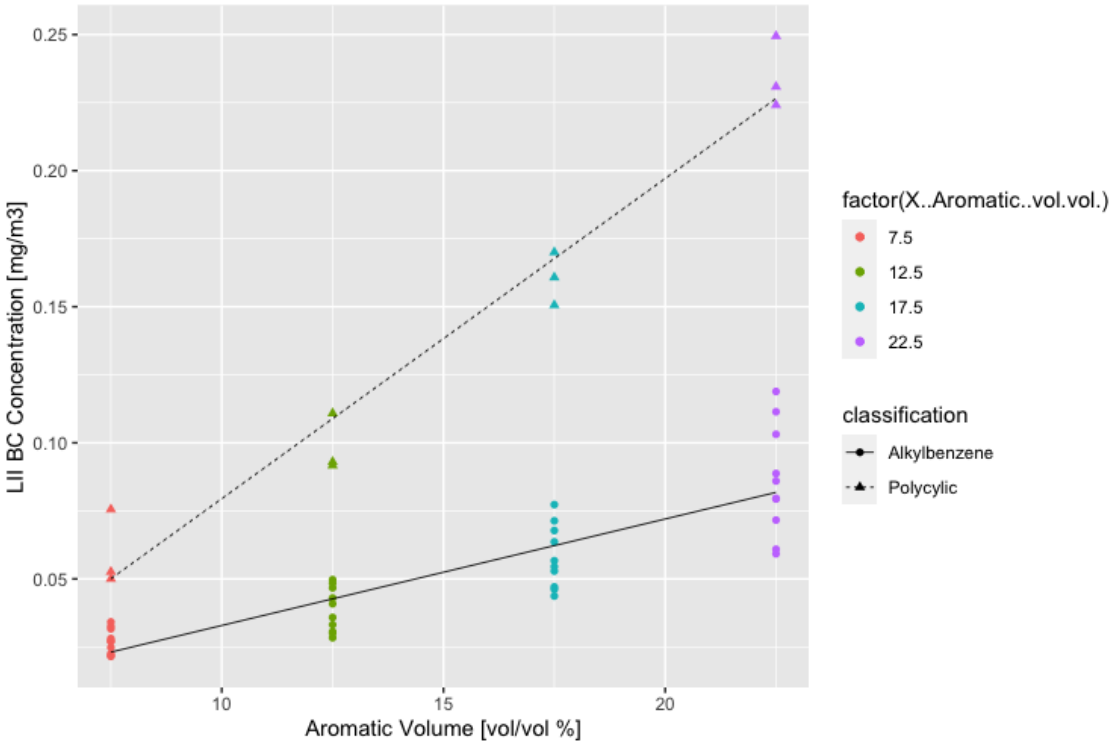

Figure 5.4.1: Scatter Plot showing Aromatic Content by Volume and BC Concentration obtained via LII for all Blends

Table 5.1: Aromatic Volume % BC Statistical Results

	Multiple R	*R-squared*	*Adjusted R-squared*	*RMS Error*
Unified	0.6017	0.3612	0.3484	0.0434
Alkylbenzenes	0.8676	0.7528	0.7463	0.01286
Polycyclics	0.9803	0.961	0.9571	0.01451

Table 5.2: Aromatic Volume % BC Regressions Equations

Classification	$Y = mx + c$	*Linear Regression*	*Standard Error*	*tStat*	*P-Value*
Unified	c	-0.013601	0.017235	-0.789	0.434
	m	0.005731	0.001077	5.317	2.47×10^{-6}
Alkylbenzene	c	0.0062347	0.0058215	-1.071	0.291
	m	0.0039125	0.0003637	10.758	4.31×10^{-13}
Polycyclic	c	-0.0381546	0.0119931	-3.181	0.0098
	m	0.0117632	0.0007492	15.701	2.25×10^{-8}

For every aromatic species, an increase in aromatic content by volume results in an increase in BC emissions. When considering alkylbenzenes and polycyclics separately, the coefficients of determination are 0.753 and 0.961 respectively, suggesting 75.1% and 96.1% of variance can be attributed to volume. The higher result for polycyclics is most likely due to the smaller range of fuels tested. There is clearly a noticeable difference between the two classifications however, and grouping the blends together for analysis reduces the regression statistics significantly.

With an R-squared value of 0.3612, 36.1% of BC emission levels are attributable to volumetric proportion alone. This is a sharp contrast to the results for individual aromatic species at various blends where there was generally agreement of between 92.3% and 98.6%. This suggests that while BC emissions increase with additional aromatic volumetric content overall, there are significant variations between two fuels containing two different aromatic species and volume alone is a poor predictor of a fuels propensity to soot when aromatic composition is the only variable introduced into a surrogate fuel. It is also worth considering that if the hypothesis that sooting propensity is not linear to aromatic content as discussed previously, these errors will compound when considering the data set as a whole. A decrease in causation of more than 50% however is significant and suggests that other con-founders may be more relevant to sooting propensity than volumetric proportion alone. While this is a poor correlation overall, it is significantly higher than the relation obtained using aromatic volumetric content and the smoke point data as discussed in Chapter 3, which yielded an association of 5.4%, which is comparatively lower. This suggests that aromatic content by volume may be more significant than specification fuel testing indicates, although this may be specific to simple, fomulated, surrogate blends. The three polycyclic hydrocarbons can be distinctly seen as being separate to the alkylbenzenes in terms of emission levels.

The BC results obtained via LII are shown in Figure 5.4.2 compared to its mass percentage of aromatic content. The accompanying statistical data for every fuel and blend for this metric is shown in Table 5.3.

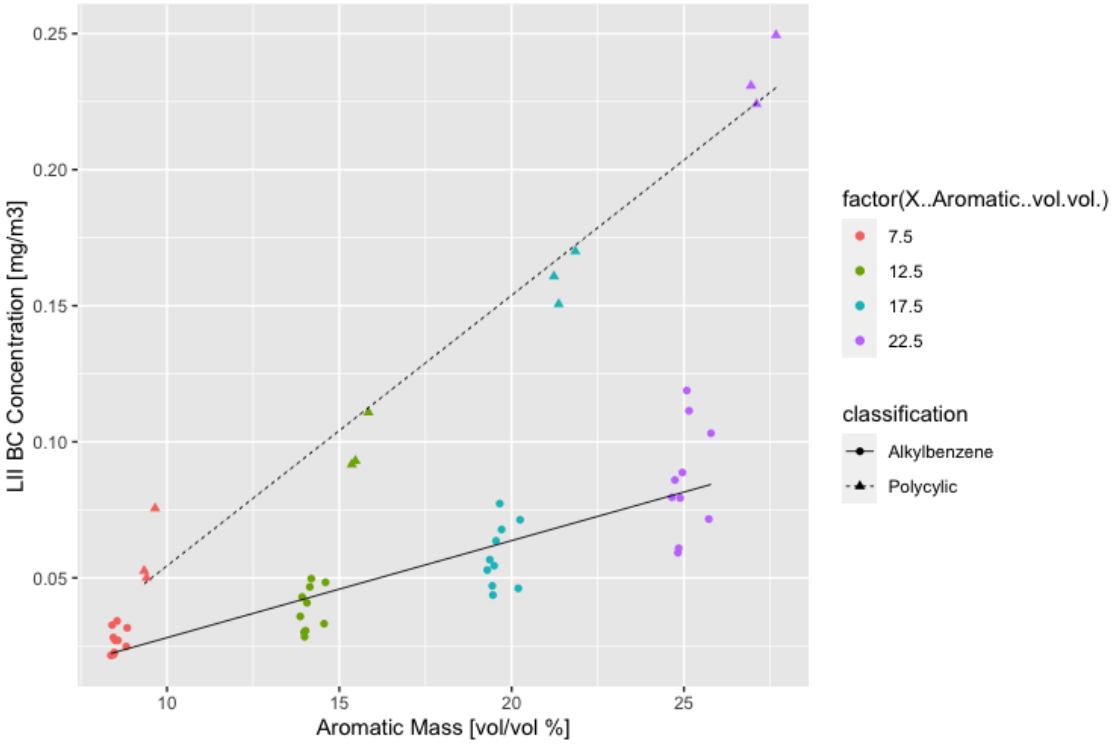

Figure 5.4.2: Scatter Plot showing Aromatic Content by Mass and BC Concentration obtained via LII for all Blends

Table 5.3: Ring Carbon % BC Statistical Results

	Multiple R	*R-squared*	*Adjusted R-squared*	*RMS Error*
Unified	0.6823	0.4656	0.4549	0.0397
Allylbenzenes	0.8718	0.7601	0.7538	0.01267
Polycyclics	0.9823	0.9650	0.9615	0.01375

There is a stronger agreement between the mass metric and the volumetric metric discussed previously, with an increase in potential causality of 10.4% to 46.6%. This increase is perhaps attributable to the fact that these fuels where supplied at a constant mass and FAR rate, and that many of the key fuel properties are mass specific and not volume specific, and so the equivalence ratio may not be consistent as a result. As discussed previously, there are incongruities in the specification as to volumetric and gravimetric testing methods, with aromatic content and naphthalene content using the former (ASTM D 1319 and ASTM D 1840) and net heat of combustion and density using the latter (ASTM D 3338 and ASTM D 1298). While this metric is interesting in comparison, it still provides no indication as to

an underlying bulk matter property that may be attributed to a fuels propensity to produce soot.

5.5 Aromatic Ring Carbon Discussion

The BC results obtained via LII are shown with accompanying regression lines for each blend with respect to its ring carbon percentage per unit mass in Figure 5.5.1 and for all data points in Figure 5.5.2. The accompanying statistical data based on individual blend proportions is shown in Tables 5.4 and 5.5 with regard to alkylbenzenes and polycyclics respectively.

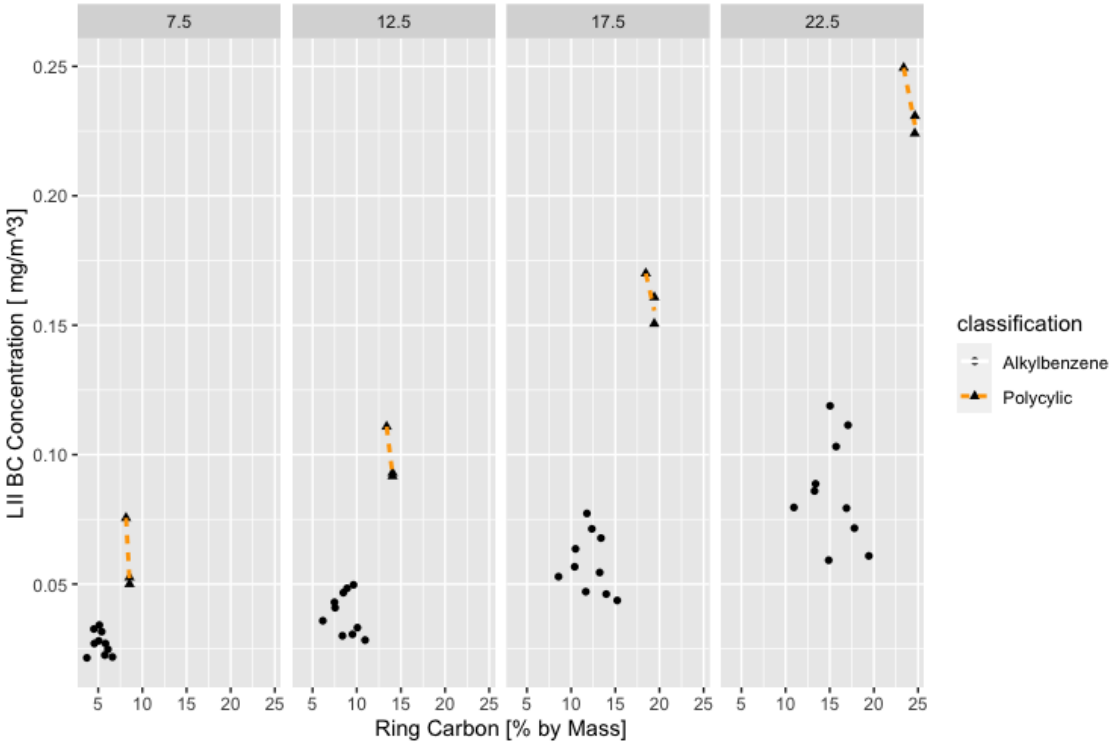

Figure 5.5.1: Scatter Plot showing Ring Carbon Content by Mass and BC Concentration obtained via LII per Blend Volume Group

Table 5.4: Ring Carbon % BC Statistical Results for Alkylbenzenes

Aromatic Content [vol/vol %]	7.5	12.5	17.5	22.5
r	-0.2077	-0.2396	-0.2224	-0.1606
R-squared	0.04312	0.05742	0.04948	0.02580
p-value	0.5648	0.5049	0.5368	0.6576

Table 5.5: Ring Carbon % BC Statistical Results for Polycyclics

Aromatic Content [vol/vol %]	7.5	12.5	17.5	22.5
r	-0.9969	-0.9980	-0.8482	-0.9632
R-squared	0.9938	0.996	0.7195	0.9277
p-value	0.0503	0.0404	0.355	0.1733

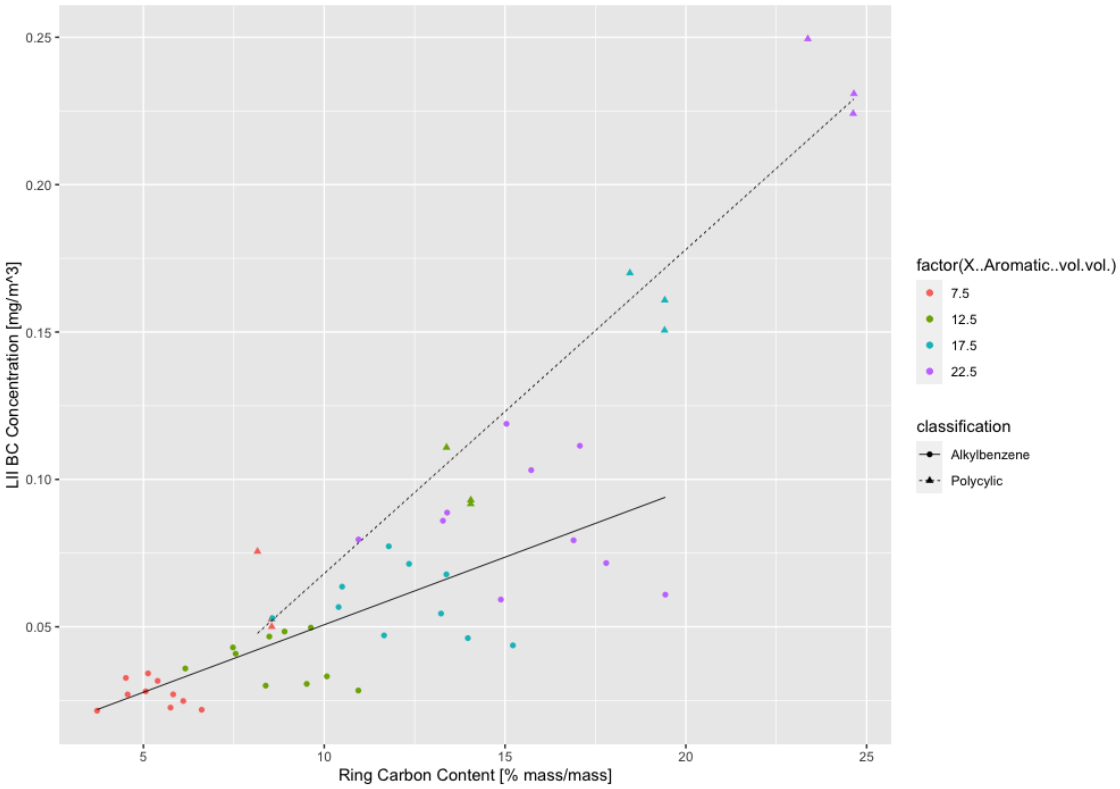

Figure 5.5.2: Scatter Plot showing Ring Carbon Content by Mass and BC Concentration obtained via LII for all Blends

Table 5.6: Ring Carbon % BC Statistical Results

	Multiple R	*R-squared*	*Adjusted R-squared*	*RMS Error*
Unified	0.8588	0.7376	0.7323	0.02782
Allylbenzenes	0.7556	0.5710	0.5597	0.01694
Polycyclics	0.9673	0.9357	0.9292	0.01864

Table 5.7: Ring Carbon % BC Regression Equations

Classification	$Y = mx + c$	*Linear Regression*	*Standard Error*	*tStat*	*P-Value*
Unified	c	-0.0299382	0.0094446	-3.17	0.0026
	m	0.0086845	0.0007326	11.86	3.87×10^{-16}
Alkylbenzene	c	0.0048610	0.0072086	0.674	0.504
	m	0.0045840	0.0006446	7.111	1.74×10^{-8}
Polycyclic	c	-0.0418218	0.0158766	-2.634	0.025
	m	0.0109906	0.0009115	12.058	2.79×10^{-7}

The inclusion and comparison with this metric is based on the concept that carbon available in the non-aromatic base fuel and in the substituted groups attached to the phenyl ring potentially behaves differently in regard to soot generation than the carbon bound to the phenyl ring itself. Potentially, non-cyclic carbon would follow a HACA kinetic route mechanism to PAH inception compared to phenyl ring polymerisation of cyclically bound carbon. Following this rational, one would expect to see an increase in BC emissions with an increase in the proportion of ring-bound carbon. These results, howeverThese results, however, show the opposite trend; a negative correlation between ring carbon content and LII emissions. This correlation is weak for alkylbenzenes (r = -0.21. r= -0.24, r = -0.22, r = -0.16), and much stronger for polycyclics (r = -0.999, r = -0.998, r = -0.848, r = -0.963) for the 7.5%, 12.5%, 17.5% and 22.5% groups, respectively.

Regression statistics for all data points vary significantly based on classification, with alkylbenzenes having an R-squared of 0.571 and polycyclics having 0.936, suggesting that the presence of ring carbon may be of more significance to cyclic structures. This raises problems however, as there is ambiguity, as discussed previously in Chapter 2, as to whether to consider the unsaturated carbon in the secondary ring of tetralin and indan as the same as saturated carbon included in a phenyl ring. Previous authors used scaling factors derived empirically to fit their results to apportion a significance for unsaturated carbon as a fraction of saturated carbon. For the purposes of this work however, unsaturated cyclic carbon has been treated as unsaturated cyclic carbon.

The concept as ring carbon as a determining factor of soot propensity also remains somewhat inconsistent with a closer examination of the results. Toluene, the lowest molecular mass aromatic that can be formed, has only a methyl group, and in so has a higher proportion of molecular weight bound in unsaturated ring carbon. If a higher proportion of ring carbon led to increased polymerization of phenyl rings due to a larger presence per unit mass of fuel, one would expect to see Toluene as potentially forming higher levels of BC. This is not seen in this dataset however, as can be seen in Figure 5.5.3 which shows all the alkyl-benzene results for the 17.5% vol/vol group, in which toluene has the lowest emission levels.

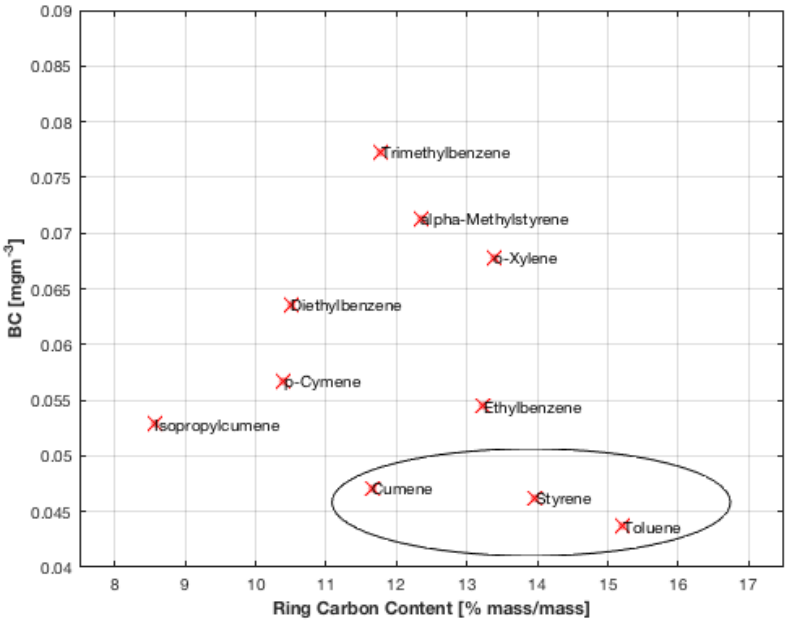

Figure 5.5.3: Scatter Plot showing Ring Carbon Content by Mass and BC Concentration obtained via LII for 17.5% group

Conversely, Isopropylcumene contains a comparatively smaller proportion of its carbon bound cyclically, and yet has relatively lower BC emission levels, comparible with Toluene. A potential point of interest arises from these results when considering the number of substituted groups attached to each aromatic ring. Cumene, Styrene, Toluene all feature one substituted group each being a methyl, acetylene and propyl-group, respectively, along with the lowest BC levels of all ten alkylbenzene aromatic species. The following five species; Ethylbenzene, Isopropylcumene, p-Cymene, Diethylbenzene and o-Xylene have two substitutes groups each, being d-ethyl, di-propyl, methyl and propyl and d-methyl respectively. The highest emission levels are for Trimethylbenzene, which has three methyl substituted groups. The result that doesn't meet this trend is alpha-Methylstyrene, which has only one functional group and yet has the second highest emission levels.

Irrespective of classification, ring carbon mass proportion for all blends yields a coefficient of determination of 0.7376, which is higher than that of aromatic volume proportion. However, due to the reasons discussed, it is not thought that ring carbon proportion is an appropriate metric, whether statistically or conceptually, in determining BC emission levels of aromatic content.

5.6 Hydrogen Content Discussion

The BC results obtained via LII with accompanying regression lines for each blend with respect to its hydrogen content are shown in Figure 5.6.1 and for all data points in Figure 5.6.2. The accompanying statistical data based on individual blend proportions is shown in Tables 5.8 and 5.9 with regard to alkylbenzenes and polycyclics respectively.

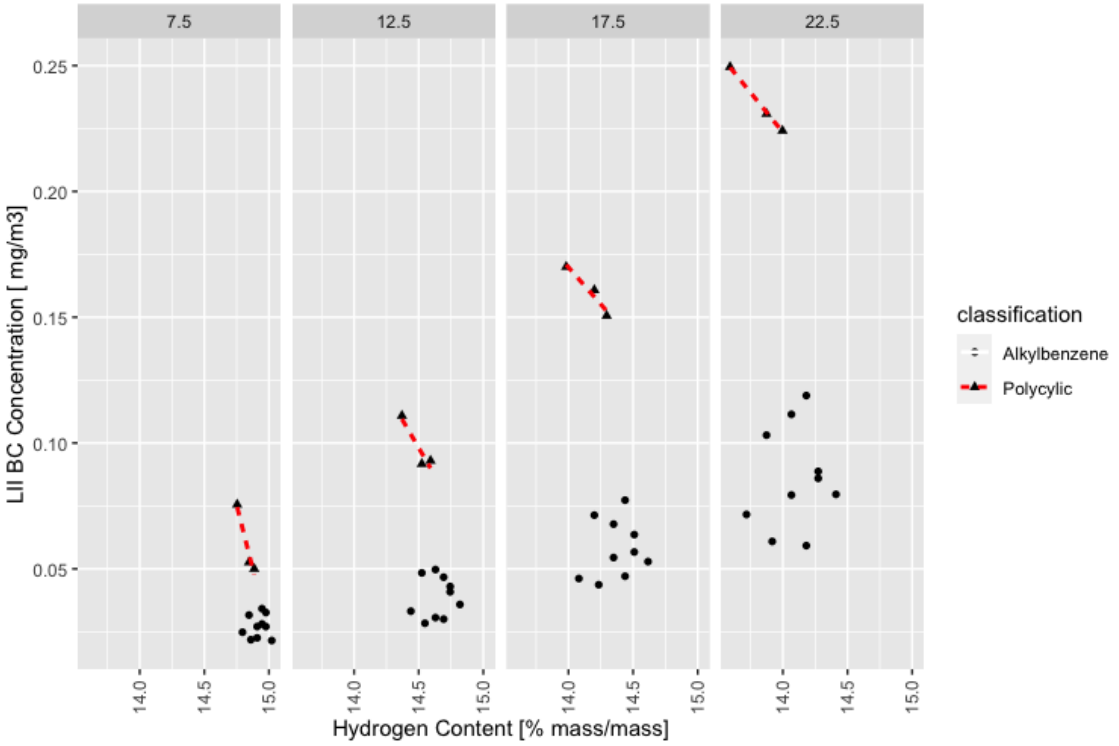

Figure 5.6.1: Scatter plot showing hydrogen content and BC concentration obtained via LII per blend volume group

Table 5.8: Hydrogen/Carbon BC Statistical Results for Alkylbenzenes

Aromatic Content [vol/vol %]	7.5	12.5	17.5	22.5
r	0.0951	0.1211	0.1703	0.1171
R-squared	0.00904	0.0146	0.0290	0.01371
p-value	0.7939	0.7390	0.6381	0.747

Table 5.9: Hydrogen Content BC Statistical Results for Poylcyclics

Aromatic Content [vol/vol %]	7.5	12.5	17.5	22.5
r	-0.9779	-0.9345	-0.9689	-0.9990
R-squared	0.9562	0.8740	0.9387	0.9981
p-value	0.1342	0.231	0.1592	0.02771

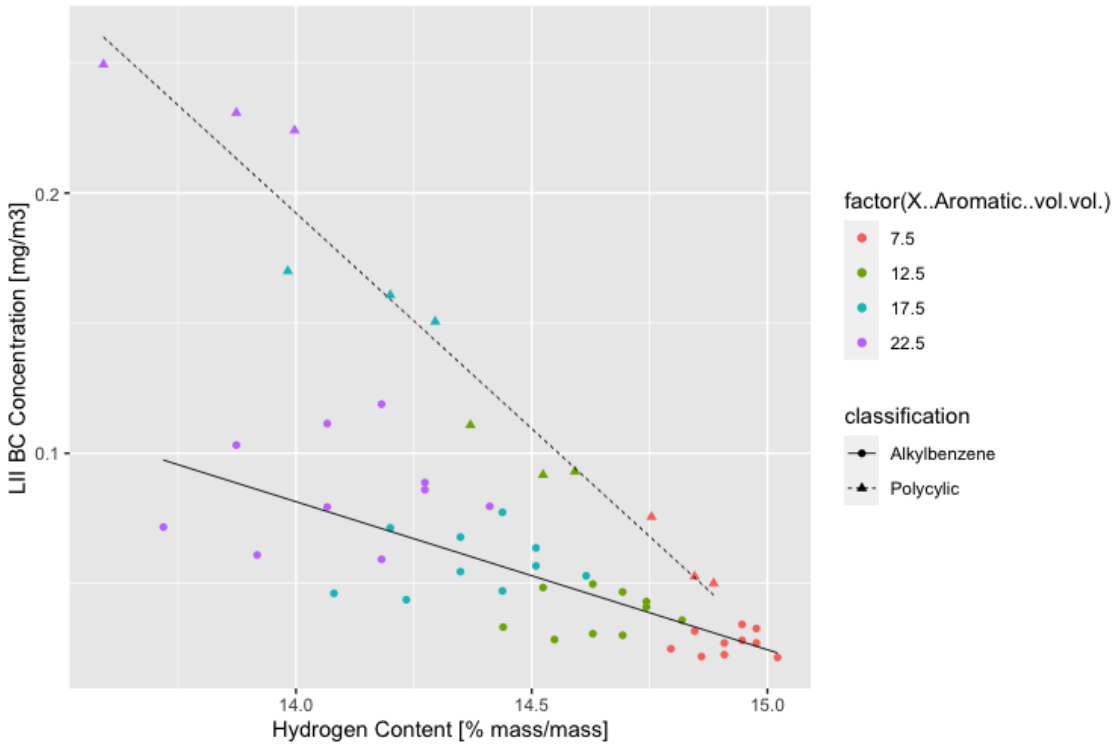

Figure 5.6.2: Scatter plot showing Hydrogen Content and BC concentration obtained via LII for all data points

Tables 5.10 and 5.11 show statistics for all data points with and without classification.

Table 5.10: Hydrogen Content BC Statistical Results

	Multiple R	*R-squared*	*Adjusted R-squared*	*RMS Error*
Unified	0.7150	0.5113	0.5015	0.0278
Allylbenzenes	0.7626	0.5816	0.5706	0.01673
Polycyclics	0.9740	0.9486	0.9434	0.01667

Table 5.11: Hydrogen Content BC Regression Equations Results

Classification	$Y = mx + c$	*Linear Regression*	*Standard Error*	*tStat*	*P-Value*
Unified	c	1.38352	0.18137	7.628	6.28×10^{-10}
	m	-0.64601	0.08932	-7.233	2.60×10^{-9}
Alkylbenzene	c	0.75952	0.09732	7.804	2.06×10^{-9}
	m	-0.34717	0.04777	-7.268	1.07×10^{-8}
Polycyclic	c	2.1739	0.1500	14.49	4.86×10^{-8}
	m	-1.0143	0.0747	-13.58	9.06×10^{-8}

Within each alkylbenzene blend, there is a slight positive correlation between BC and Hydrogen Content(r = 0.0951, r = 0.1211, r = 0.1703, r = 0.1171) in the 7.5%, 12.5%, 17.5% and 22.5% groups, respectively. This is not in agreement with the reasoning behind the importance of Hydrogen Content in combustion. A higher Hydrogen Content fuel has a lower proportion of carbonaceous precursors available to form BC. As such, an increase in the Hydrogen Content should lead to a decline in BC emissions. This effect is not observed for the alkylbenzenes in this data. However, The correlation is very weak and does not suggest that a higher Hydrogen Content leads to higher BC emissions overall. The expected trend is observed for the polycyclic group (r = -0.9779, r = -0.9345, r = -0.9689, r = -0.990), as BC emissions negatively correlates with Hydrogen Content.

Omitting blend proportion, Hydrogen Content has coefficients of determination of 0.5113, 0.9486 and 0.5816 for alkylbenzenes, polycyclics and all data points, respectively. Figure 5.6.2 shows what could be described as heteroskedasticity in the data, in that the variance seems to gradually increase as the Hydrogen Content is reduced. This may be due to the contribution of a separate confounder that weakly correlates with Hydrogen Content.

5.7 Global Density Discussion

The BC results obtained via LII with accompanying regression lines for each blend with respect to its global density are shown in Figure 5.7.1 and for all data points in Figure 5.7.2. The accompanying statistical data based on individual blend proportions is shown in Tables 5.12 and 5.13 with regard to alkylbenzenes and polycyclics respectively.

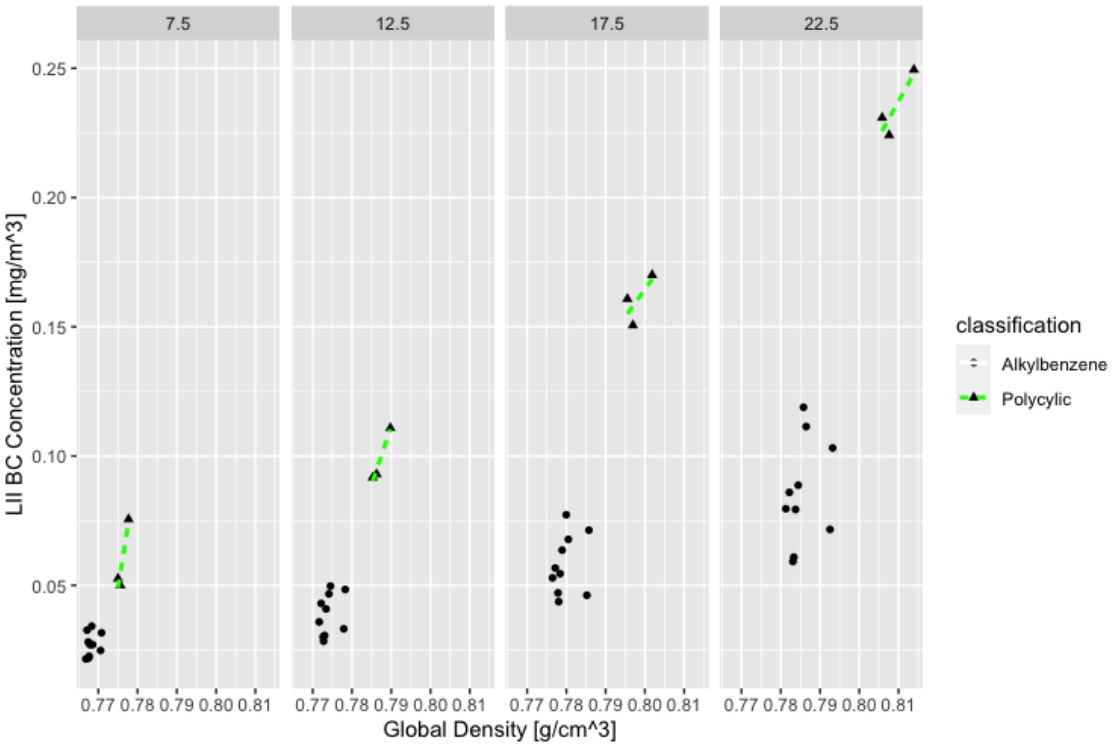

Figure 5.7.1: Scatter plot showing global density and BC concentration obtained via LII per blend volume group

Table 5.12: Global Density BC Statistical Results for Alkylbenzenes

Aromatic Content [vol/vol %]	7.5	12.5	17.5	22.5
r	0.2542	0.3393	0.2773	0.2936
R-squared	0.0646	0.1151	0.07692	0.08622
p-value	0.4784	0.3376	0.4378	0.4102

Table 5.13: Global Density BC Statistical Results for Poylcyclics

Aromatic Content [vol/vol %]	7.5	12.5	17.5	22.5
r	0.9538	0.9883	0.7206	0.8904
R-squared	0.9098	0.9767	0.5193	0.7929
p-value	0.1942	0.09747	0.4877	0.3008

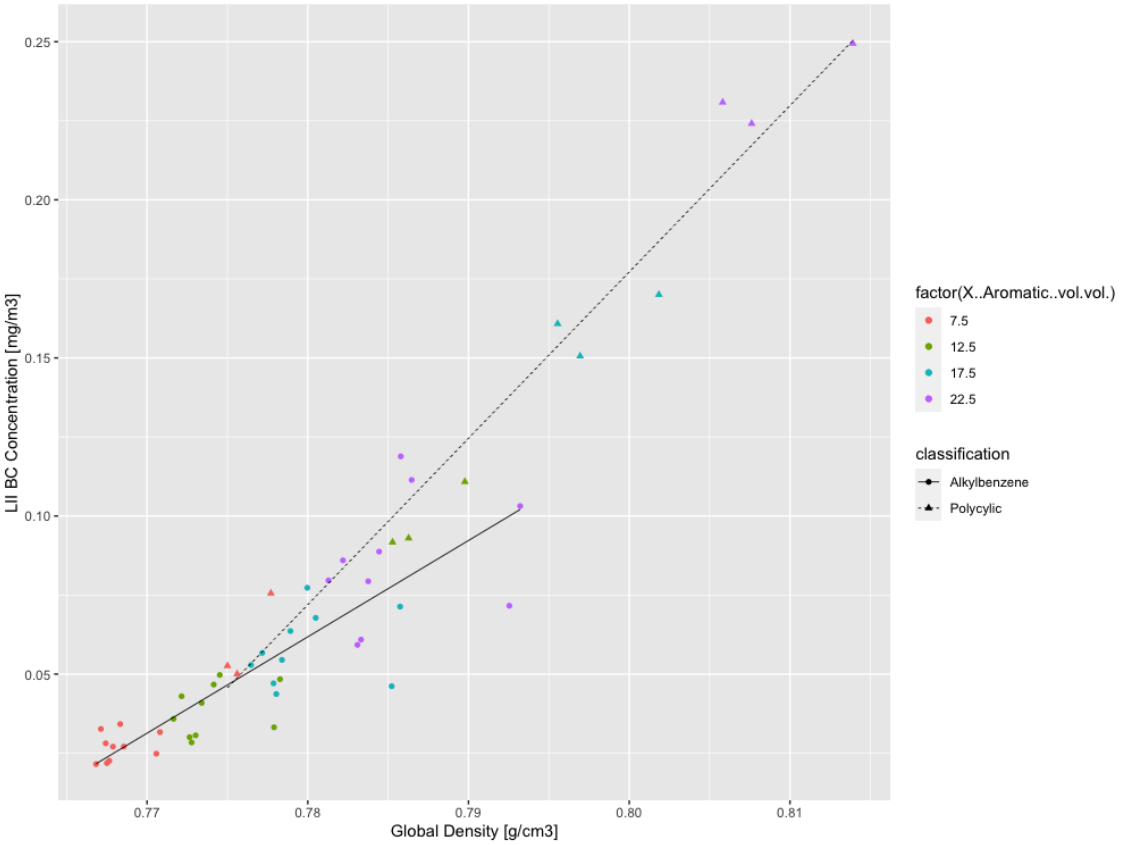

Figure 5.7.2: Scatter plot showing global density and BC concentration obtained via LII for all data points

Tables 5.10 and 5.11 show statistics for all data points with and without classification.

Table 5.14: GLobal Density BC Statistical Results

	Multiple R	*R-squared*	*Adjusted R-squared*	*RMS Error*
Unified	0.9439	0.8911	0.8889	0.01792
Allylbenzenes	0.8507	0.7237	0.7165	0.01359
Polycyclics	0.9843	0.9688	0.9657	0.01298

Table 5.15: Global Density BC Regression Equations

Classification	$Y = mx + c$	*Linear Regression*	*Standard Error*	*tStat*	*P-Value*
Unified	c	-3.5392	0.1786	-19.82	2.0×10^{-16}
	m	4.6268	0.2287	20.23	2.0×10^{-16}
Alkylbenzene	c	-2.3151	0.2373	-9.756	6.76×10^{-12}
	m	3.0473	0.3054	9.977	3.64×10^{-12}
Polycyclic	c	-4.0322	0.2368	-17.03	1.03×10^{-8}
	m	5.2618	0.2987	17.61	7.40×10^{-9}

Within each blend group, global density weakly correlates with BC emissions for alkylbenzenes (r = 0.2542, r = 0.3393, r = 0.2773, r = 0.2936) and strongly for polycyclics (r = 0.9538, r = 0.9883, r = 0.7206, r = 0.8904). The p-values for both alkylbenzene and polycyclic groups do not meet a level of statistical significance.

However, the global density of the fuel irrespective of blend proportion provides strongest statistics, with a coefficient of determination of 0.7237 for alkylbenzenes, 0.9688 for polycyclics and 0.8911 for all data points. A higher global density for a pure hydrocarbon indicates a higher proportion of carbon per unit volume of fuel. A higher proportion of carbon suggests reduced proximity between aromatic bound carbon atoms with in the fuel. This closer proximity may lead to an increase in the rate of chemical kinetic mechanisms leading to increased PAH formation and hence, increased BC emissions.

There are indications in the data however, that suggest that there are properties unrelated to the global density that cause variations in the emissions of BC. This can be observed in the alklybenzene results for the 17.5% vol/vol group in Figure 5.7.3. The trend decscribed here is common to other groups.

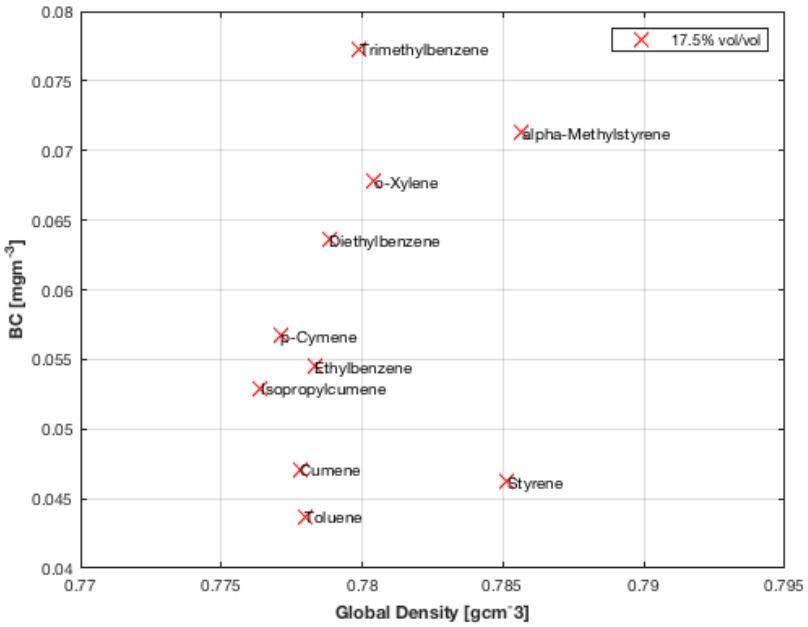

Figure 5.7.3: Scatter plot showing global density and BC concentration obtained via LII for 17.5% group

Styrene and alpha-Methylstyrene both feature a substituted group that contains

a double carbon-carbon bond. As a result, both molecules have a slightly higher density than the other alkylbenzenes under consideration. This does not, however, result in significantly higher emission levels when compared to the global density metric in line, as would be expected if the strong correlation these results indicate that higher densities produce higher BC emission levels. It should be noted that the specification test analysis performed in Chapter 3 also indicated that a fuels density was the strongest indication of sooting propensity, albeit using a smoke lamp method and in the absence of ring carbon and hydrogen content data.

5.8 Aromatic TSI Discussion

The BC results obtained via LII with accompanying regression lines for each blend with respect to its aggregated TSI are shown in Figure 5.8.1 and for all data points in Figure 5.8.2. The accompanying statistical data based on individual blend proportions is shown in Tables 5.16 and 5.17 with regard to alkylbenzenes and polycyclics respectively.

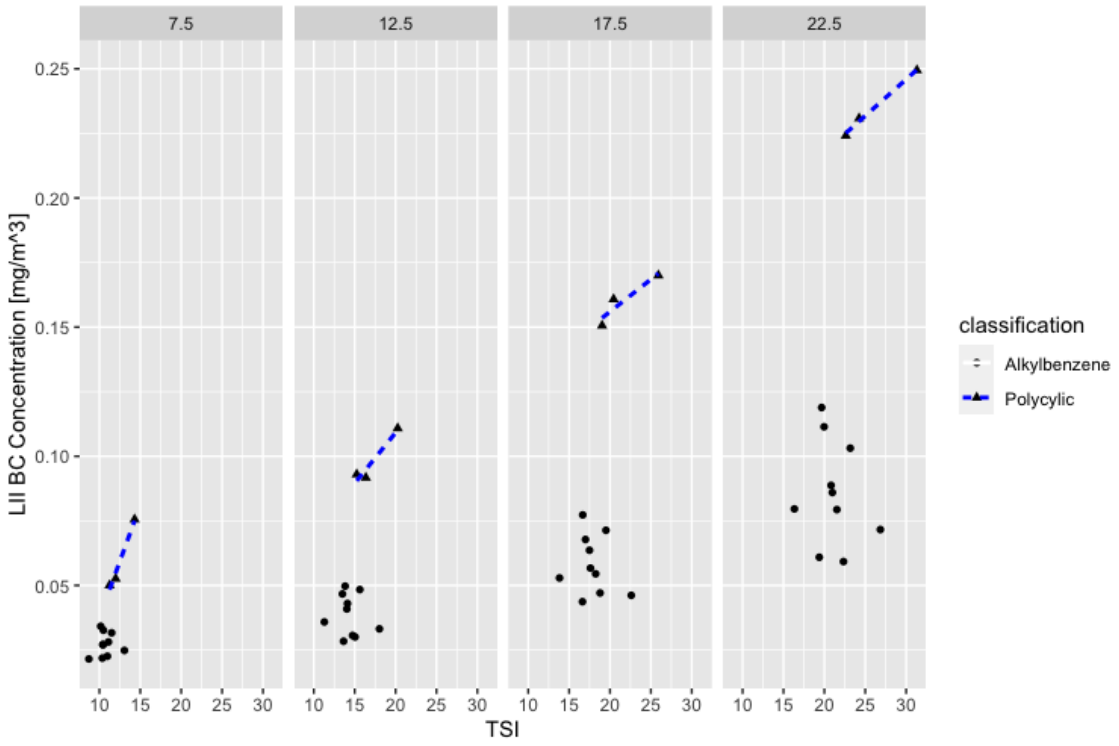

Figure 5.8.1: Scatter plot showing aggregate TSI and BC concentration obtained via LII per blend volume group

Table 5.16: TSI BC Statistical Results for Alkylbenzenes

Aromatic Content [vol/vol %]	7.5	12.5	17.5	22.5
r	0.1173	0.1214	0.1737	0.1727
R-squared	0.01376	0.01474	0.03016	0.02984
p-value	0.7469	0.7383	0.6313	0.6332

Table 5.17: TSI BC Statistical Results for Poylcyclics

Aromatic Content [vol/vol %]	7.5	12.5	17.5	22.5
r	0.9897	0.9627	0.9365	0.9966
R-squared	0.9796	0.9268	0.8770	0.9933
p-value	0.09113	0.1744	0.2281	0.05226

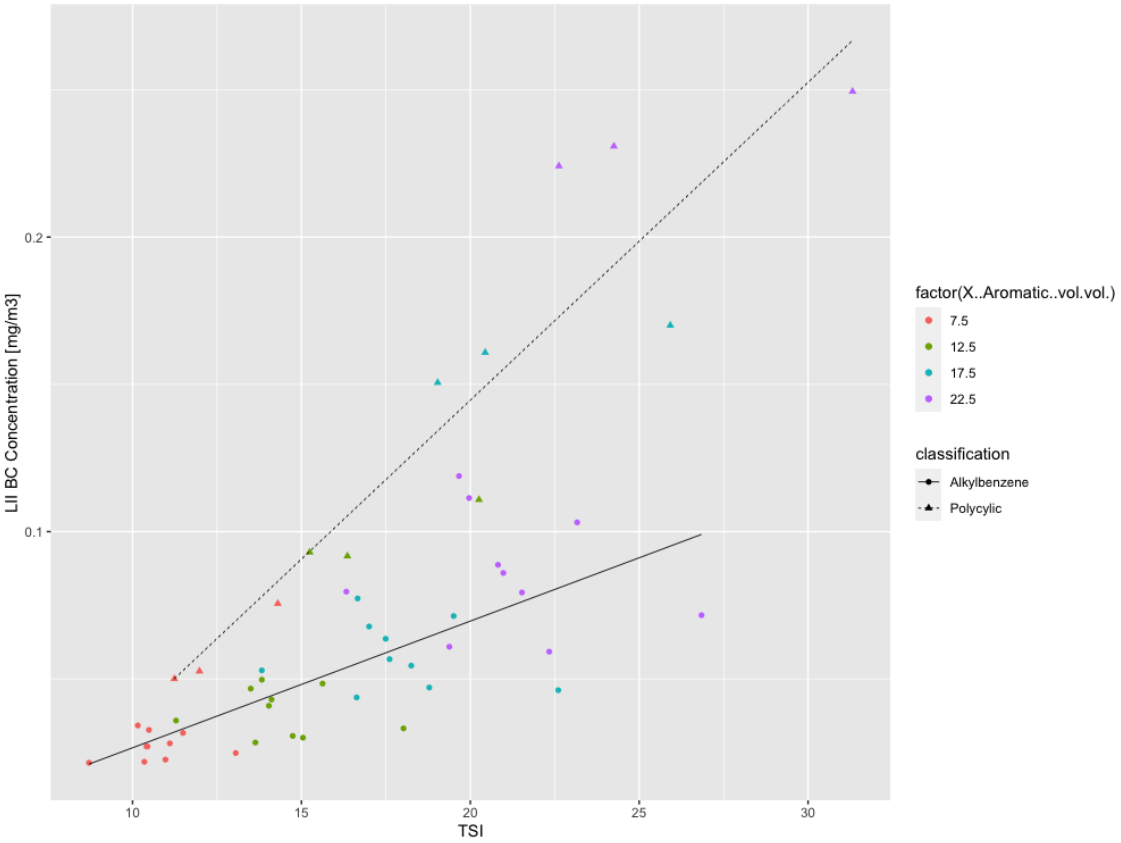

Figure 5.8.2: Scatter plot showing aggregate TSI and BC concentration obtained via LII for all data points

Tables 5.18 and 5.19 show statistics for all data points with and without classification.

Table 5.18: TSI BC Statistical Results

	Multiple R	*R-squared*	*Adjusted R-squared*	*RMS Error*
Unified	0.7495	0.5618	0.5530	0.03595
Allylbenzenes	0.7395	0.5468	0.5349	0.01741
Polycyclics	0.9226	0.8511	0.8362	0.02835

Table 5.19: TSI BC Regression Equations

Classification	$Y = mx + c$	*Linear Regression*	*Standard Error*	*tStat*	*P-Value*
Unified	c	-0.064293	0.017769	-3.618	0.00069
	m	0.008130	0.001015	8.006	1.63×10^{-10}
Alkylbenzene	c	-0.0164013	0.0105348	-1.557	0.128
	m	0.0043007	0.0006352	6.771	5.03×10^{-8}
Polycyclic	c	-0.071212	0.028892	-2.465	0.0334
	m	0.010792	0.001427	7.561	1.92×10^{-5}

TSI is seen to weakly anti-correlate with BC emissions in each blend group (r=0.117,-0.1214,-0.1737,-0.1727), while strongly positively correlating with polycyclics (r=0.9867, r=0.9627, r=0.9365, r=0.9966). The coefficients of determination for alklylbenzenes are weak (0.01376, 0.01474, 0.03016, 0.02984) but strong for polycyclics (0.9796, 0.9268, 0.8770, 0.9933)

When comparing all data points in Figure 5.8.2, the effect of increased volume imposes a positive correlation onto alkylbenzenes (r=0.7395) and is maintained for polycyclics (r=0.9226). Weak coefficients of determination are found for alkylbenzens (0.5468) while strong for polycyclics (0.8511).

TSI does not meet the criteria as a metric of interest due to its lack of ability to differentiate between alkylbenzenes within a blend to any degree of statistical merit.

The BC results obtained via LII for each blend with respect to its aggregated NSP are shown in Figure 5.8.3 and for all data points in Figure 5.8.4. The accompanying statistical data based on individual blend proportions is shown in Tables 5.20 and 5.21 with regard to alkylbenzenes and polycyclics respectively.

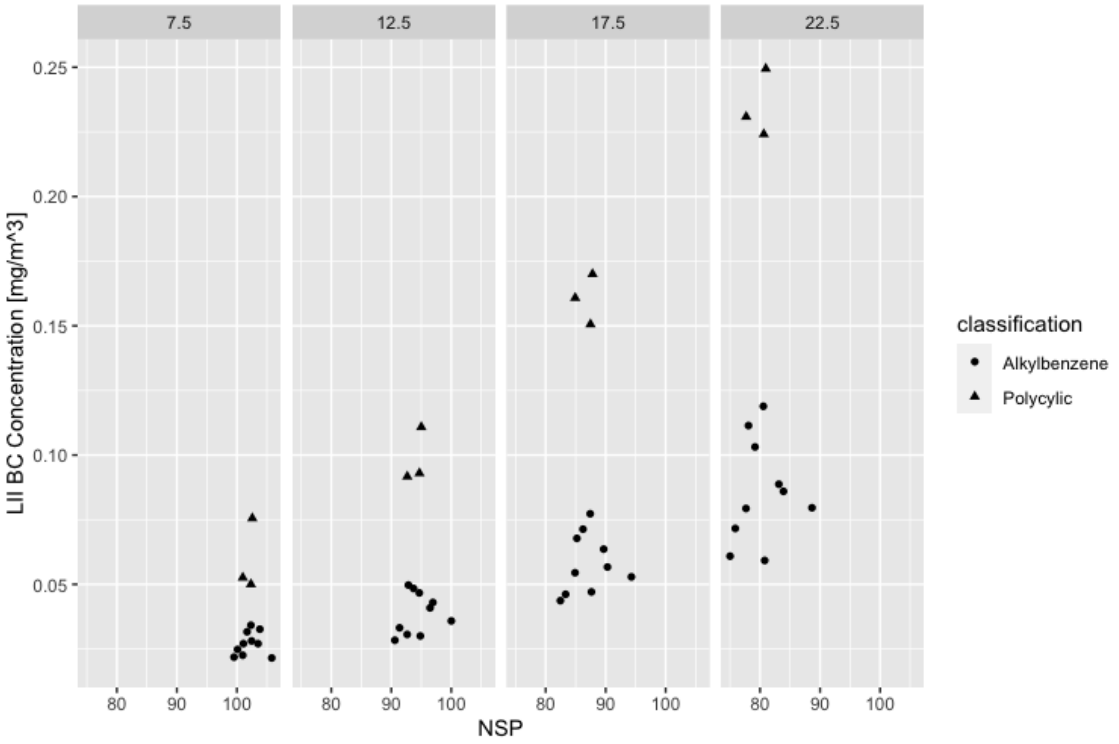

Figure 5.8.3: Scatter plot showing aggregate NSP and BC concentration obtained via LII per blend volume group

Table 5.20: NSP BC Statistical Results for Alkylbenzenes

Aromatic Content [vol/vol %]	7.5	12.5	17.5	22.5
r	0.1572	0.2143	0.1699	0.1174
R-squared	0.02471	0.04593	0.02888	0.01379
p-value	0.6645	0.5521	0.6388	0.7466

Table 5.21: NSP BC Statistical Results for Poylcyclics

Aromatic Content [vol/vol %]	7.5	12.5	17.5	22.5
r	0.5363	0.6490	0.07952	0.3499
R-squared	0.2876	0.4212	0.006323	0.1224
p-value	0.6397	0.5504	0.9493	0.7725

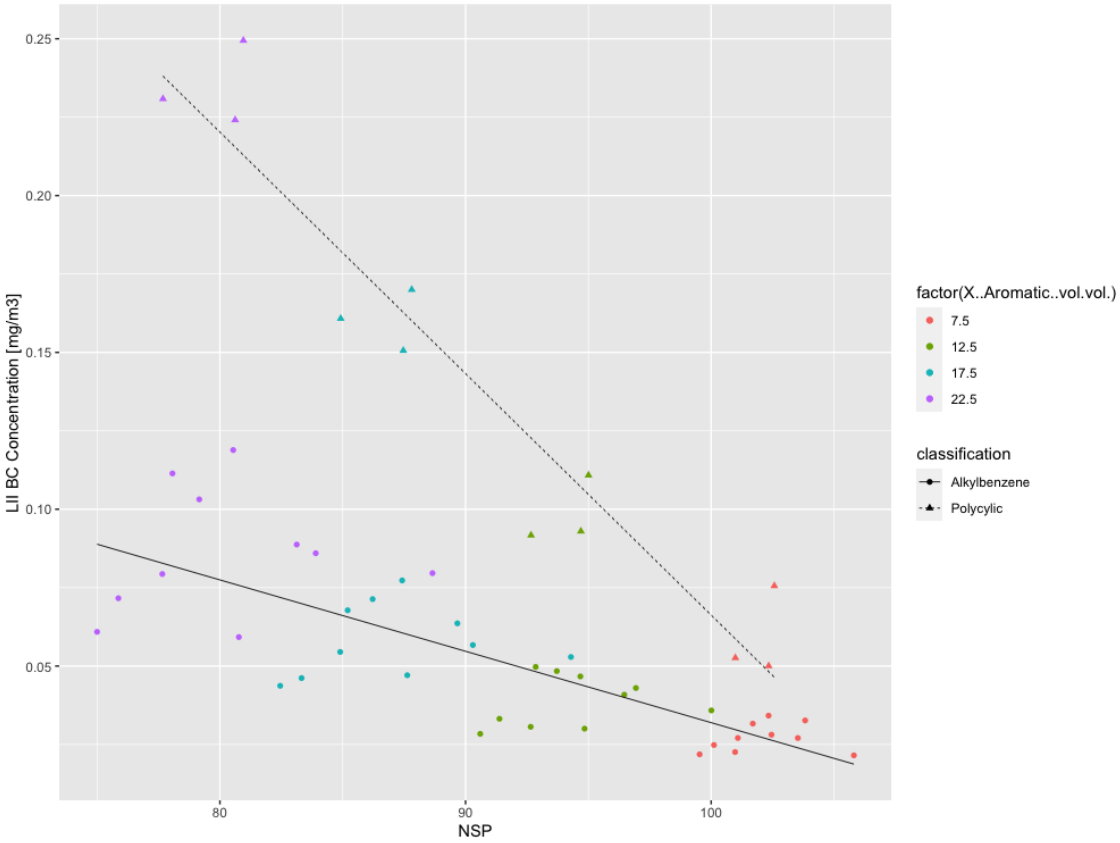

Figure 5.8.4: Scatter plot showing aggregate NSP and BC concentration obtained via LII for all data points

Tables 5.22 and 5.23 show statistics for all data points with and without classification.

Table 5.22: NSP BC Statistical Results

	Multiple R	*R-squared*	*Adjusted R-squared*	*RMS Error*
Unified	-0.5705	0.3255	0.3120	0.0446
Allylbenzenes	-0.7851	0.6164	0.6063	0.01602
Polycyclics	-0.9597	0.9211	0.9132	0.02064

Table 5.23: NSP BC Statistical Results

Classification	$Y = mx + c$	*Linear Regression*	*Standard Error*	*tStat*	*P-Value*
Unified	c	0.3925589	0.0655006	5.993	2.24×10^{-7}
	m	-0.0035232	0.0007173	-4.912	1.01×10^{-5}
Alkylbenzene	c	0.2595028	0.0266162	9.750	6.87×10^{-12}
	m	-0.0022755	0.0002912	-7.815	2.00×10^{-9}
Polycyclic	c	0.8362165	0.0648817	12.89	1.49×10^{-7}
	m	-0.0076997	0.0007128	-10.80	7.8×10^{-7}

NSP is seen to weakly correlate with BC emissions in each alkylbenzene blend group (r=0.1572,0.2143,0.1699,0.1174), and also correlate weakly to moderate with polycyclics (r=0.5363, r=0.0.6490, r=0.07952, r=0.3499). The coefficients of determination for alklylbenzenes are weak (0.02471, 0.04593, 0.02888, 0.01379) and weakly for polycyclics (0.2876, 0.4212, 0.006323, 0.1224)

When comparing all data points in Figure 5.8.4, the effect of aggregated NSP shows a strong negative correlation with BC alkylbenzenes (r=-0.7851) and is maintained for polycyclics (r=0.9597). Weak coefficients of determination are found for alkylbenzens (0.6164) while strong for polycyclics (0.9211).

The aggregated NSP is interesting in that it shows moderate performance in capturing the shape of the data when all date points are considered, and also shows the expected trend of increased NSP. As discussed in Chapter 2, an increased NSP should result in lower BC emissions. As shown in Figure5.8.4, the lowest emisions are seen in the 7.5% group which also has the highest NSP values. This trend is true for both alkylbenzene and polycyclic classifications. Within each blend proportion however, the expected trend is not observed. For both classifications, BC emissions increase as NSP increases, albeit by varying degrees. This trend is not expected and may suggest that the increase in volume and consequently some other metric is actually determining the increase in BC emissions; that the rise in aggregated NSP not causative due to the effect of some other confounder. There is also a significant discrepancy between the regressions statistics both classifications at similar aggregated NSP's, suggesting that this metric itself is not deterministic to BC emissions.

5.9 Fuel YSI Discussion

The BC results obtained via LII with accompanying regression lines for each blend with respect to its Unififed YSI are shown in Figure 5.9.1 and for all data points in Figure 5.9.2. The accompanying statistical data based on individual blend proportions is shown in Tables 5.24 and 5.25 with regard to alkylbenzenes and polycyclics respectively.

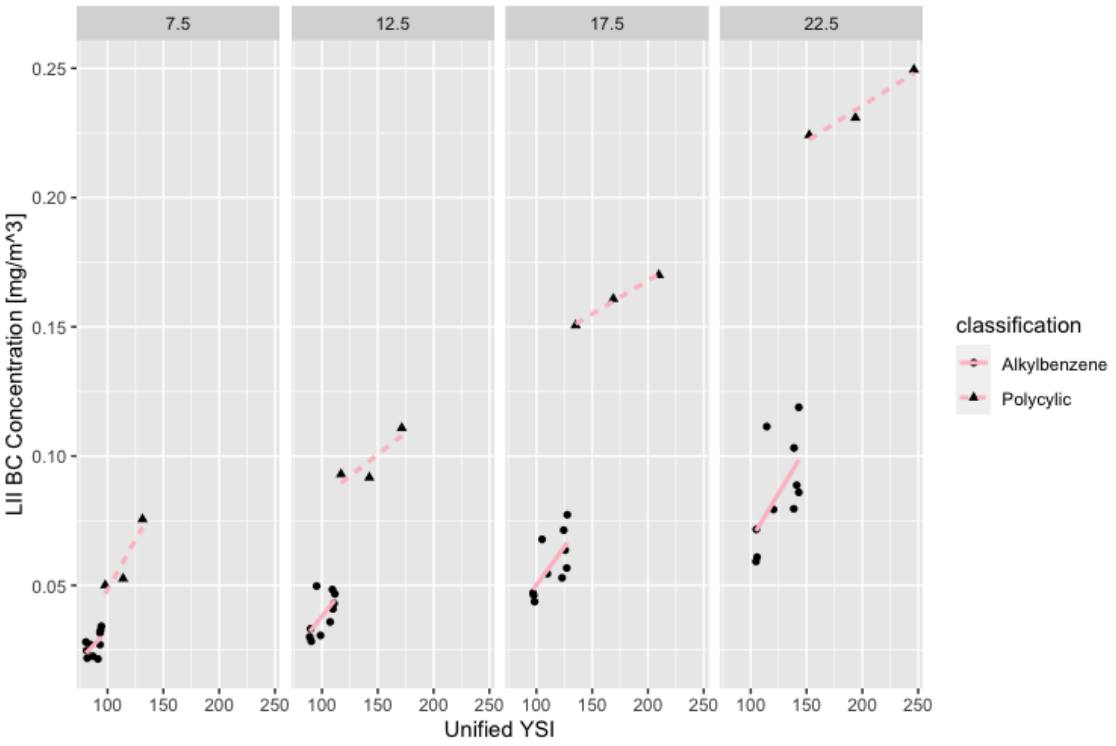

Figure 5.9.1: Scatter plot showing Unified YSI and BC concentration obtained via LII per blend volume group

Table 5.24: YSI BC Statistical Results for Alkylbenzenes

Aromatic Content [vol/vol %]	7.5	12.5	17.5	22.5
r	0.5507	0.6322	0.6818	0.6029
R-squared	0.3033	0.3997	0.4681	0.3635
p-value	0.09897	0.04985	0.02911	0.06506

Table 5.25: YSI BC Statistical Results for Poylcyclics

Aromatic Content [vol/vol %]	7.5	12.5	17.5	22.5
r	0.9182	0.8575	0.9965	0.9807
R-squared	0.8430	0.7323	0.9930	0.9618
p-value	0.2594	0.3462	0.05321	0.1252

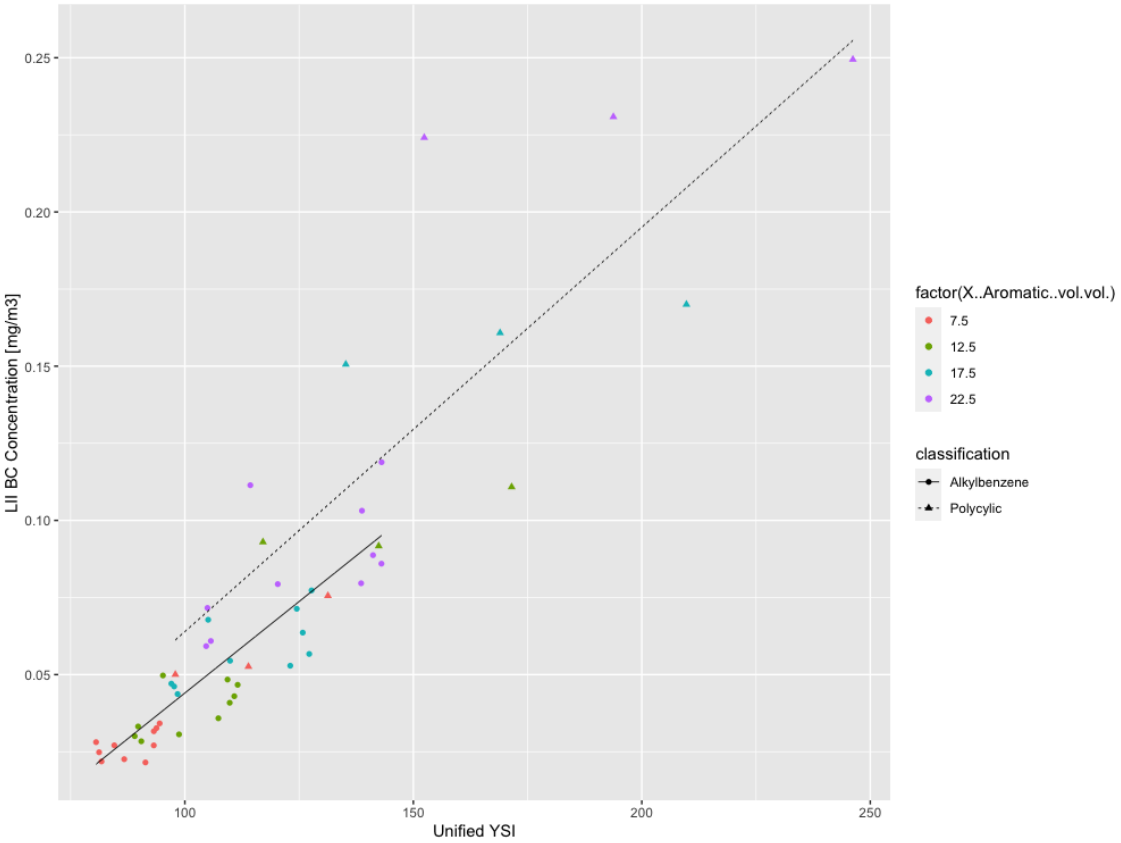

Figure 5.9.2: Scatter plot showing Unified YSI and BC concentration obtained via LII for all data points

Tables 5.26 and 5.27 show statistics for all data points with and without classification.

Table 5.26: YSI BC Statistical Results

	Multiple R	*R-squared*	*Adjusted R-squared*	*RMS Error*
Unified	0.8983	0.8069	0.8031	0.02386
Allylbenzenes	0.8504	0.7232	0.7159	0.01361
Polycyclics	0.8127	0.6605	0.6265	0.04282

Table 5.27: YSI BC Statistical Results

Classification	$Y = mx + c$	*Linear Regression*	*Standard Error*	*tStat*	*P-Value*
Unified	c	-0.0997143	0.0123475	-8.076	1.27×10^{-10}
	m	0.0014507	0.0001003	14.457	2.00×10^{-16}
Alkylbenzene	c	-0.0746054	0.0129320	-5.769	$1.18 * 10^{-6}$
	m	0.0011864	0.0001191	9.964	3.77×10^{-12}
Polycyclic	c	-0.0671344	0.0481861	-1.393	0.19374
	m	0.0013109	0.0002972	4.411	0.00131

Unified YSI is seen to moderately correlate with BC emissions in each alkylbenzene blend group (r=0.5507, 0.6322, 0.6818, 0.6029), and also correlate strongly to moderate with polycyclics (r=0.9182, r=0.8575, r=0.9965, r=0.0.9807). The coefficients of determination for alklylbenzenes are weak (0.3033, 0.3997, 0.4681, 0.3635) and strong for polycyclics (0.8430, 0.7323, 0.9930, 0.9618)

When comparing all data points in 5.8.4, the effect of Unified YSI shows a strong correlation with BC for alkylbenzenes (r=0.8504) and is maintained for polycyclics (r=0.8127). Strong coefficients of determination are found for alkylbenzens (0.7232) and moderate strong for polycyclics (0.6605).

The effect of increasing Unified YSI shows the expected performance as discussed previously in Chapter 2; that increasing this metric increases the emissions of BC. This is true both within blend groups and also when all the data is analysed irrespective of blend proportion. Unified YSI is one of the few metrics analysed for this thesis that demonstrates this consistency within classification blend proportion groups, and maintains that consistency for all data points. It is unusual, however, in that its statistics are generally weaker than other metrics for polycyclics than they are for alkylbenzenes. However, if the objective of this thesis is to find a metric that is predictive and statistically coherent for both classifications, consistency between the two is of interest and the similarity of polycyclic statistics to those of alkylbenzes may suggest that this is a more appropriate statistic.

5.10 Multi-variate Modelling

The selection of variables to include in a multi-variate model used to predict gravimetric BC emissions for this data-set requires careful consideration. An objective of this thesis is to not erroneously attribute significance to or include variables erroneously rather than identify confounders that are actually deterministic in describing and predicting gravimetric BC emissions. Including every variable previously discussed is not statistically robust as it will lead to an over-fitted model, and without a subsequent campaign to validate the findings of such a model on novel data, the findings would be spurious. It would also be inappropriate to include variables that have been found to be logically or categorically inconsistent, as discussed in Section 5.3. It is appropriate however, to construct the multi-variate model initially using every variable and then selectively exclude each based on its contribution or lack thereof. The model is trained on every data point without categorising by classification. The suitability of each model to each classification is refined and separated however at the end of this section.

The initial model includes the eight variables discussed and analysed earlier in this chapter, namely Aromatic Volume Percentage, Aromatic Mass Percentage, Global Density, Ring Carbon Percentage, Hydrogen Content, Aggregate TSI, Aggregate NSP, and Aggregate Unified YSI. For this initial model, two variables, Ring Carbon Percentage and Aggregate TSI are found to be of no statistical significance due to high p-values (p=0.4277 and p=0.06161) which are above the p=0.05 threshold. It should be noted that this initial model shows a high adjusted coefficient of determination (0.9860), which shows, despite the inclusion of a large number of variables, that when accounted for, this model is generally accurate in predicting the data that it's based on. It is however, considered to be over-fitted at this point.

The second model omits these two variables; Ring Carbon Percentage and Aggregate TSI. The six remaining variables all meet the threshold of statistical significance with every all of them having a p-value significantly less than p=0.05. The adjusted coefficient of determination remains strong at 0.9847, suggesting the omission of these two variables is appropriate due to their lack of significance. At this point, variables are selectively excluded based on their suitability according to the analytical methodology described previously in this chapter. YSI is included as it

shows strong correlation, coefficient of determination and consistency within blend groups and classification. Aggregate NSP is omitted as within it each blend group it suggests both classifications increase BC emissions with increased NSP, contrary to its conceptualisation. Global Density is included as it shows strong correlation, coefficient of determination and consistency within blend groups and classification. Aromatic Mass Percentage is chosen over Aromatic Volume Percentage as they are both a simple metric of compositional proportionality, and the inclusion of both is redundant to modelling. Mass is chosen over volume due to slightly stronger coefficient of determination. Hydrogen Content is omitted as in preliminary models, it has a positive coefficient. This would suggest that higher Hydrogen Content values incur higher values for BC emissions, which is opposite to the conceptual role of increased hydrogen content in combustion fundamentals and BC formation. This refined model is comprised of three variables; Aromatic Mass Percentage, Global Density and Unified YSI. This model has an adjusted coefficient of determination of 0.9261.

The final model omits Aromatic Mass Percentage leaving two variables; Global Density and Unified YSI. Aromatic Mass Percentage has a p-value of 0.0381, slightly below the threshold of significance. Its omission, however, does not significantly adversely affect the model, which retains a similar coefficient of determination of 0.9208. The omission of Aromatic Mass Percentage accounts for a reduction of 0.53% in variability, and is therefore considered redundant.

The predicted versus actual response for the final model is shown in Figure 5.10.1 and the standardised residuals with respect to every data point is shown in Figure 5.10.2.

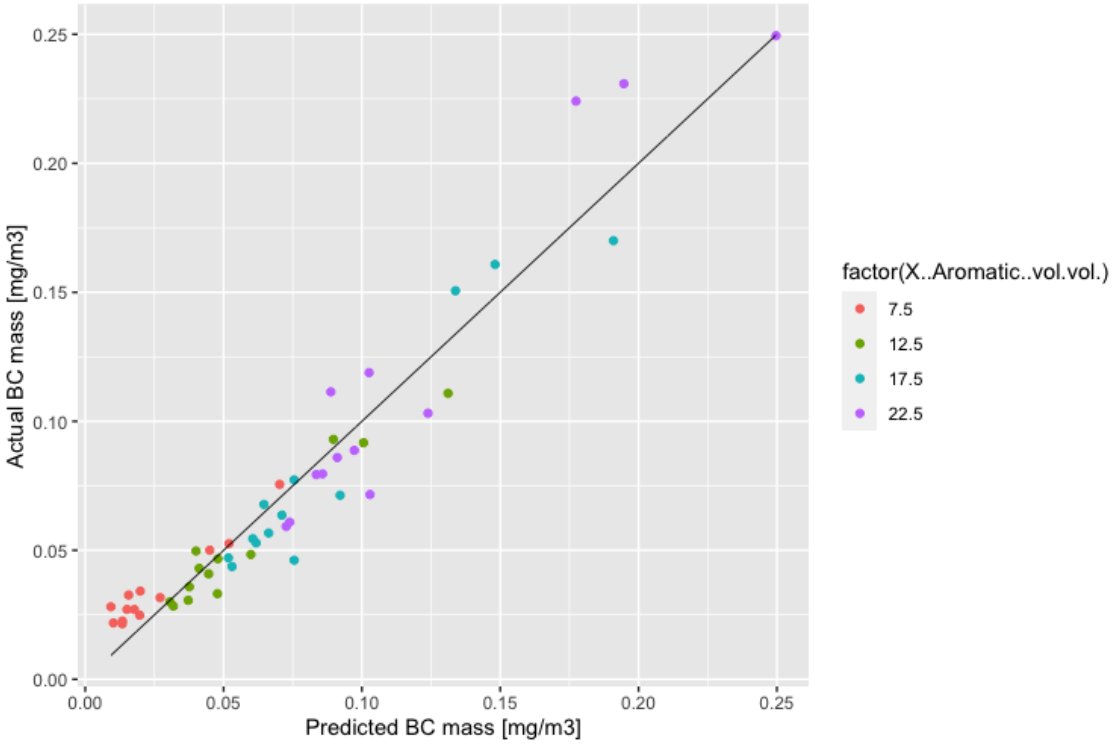

Figure 5.10.1: Scatter plot showing predicted BC and actual BC for all blends

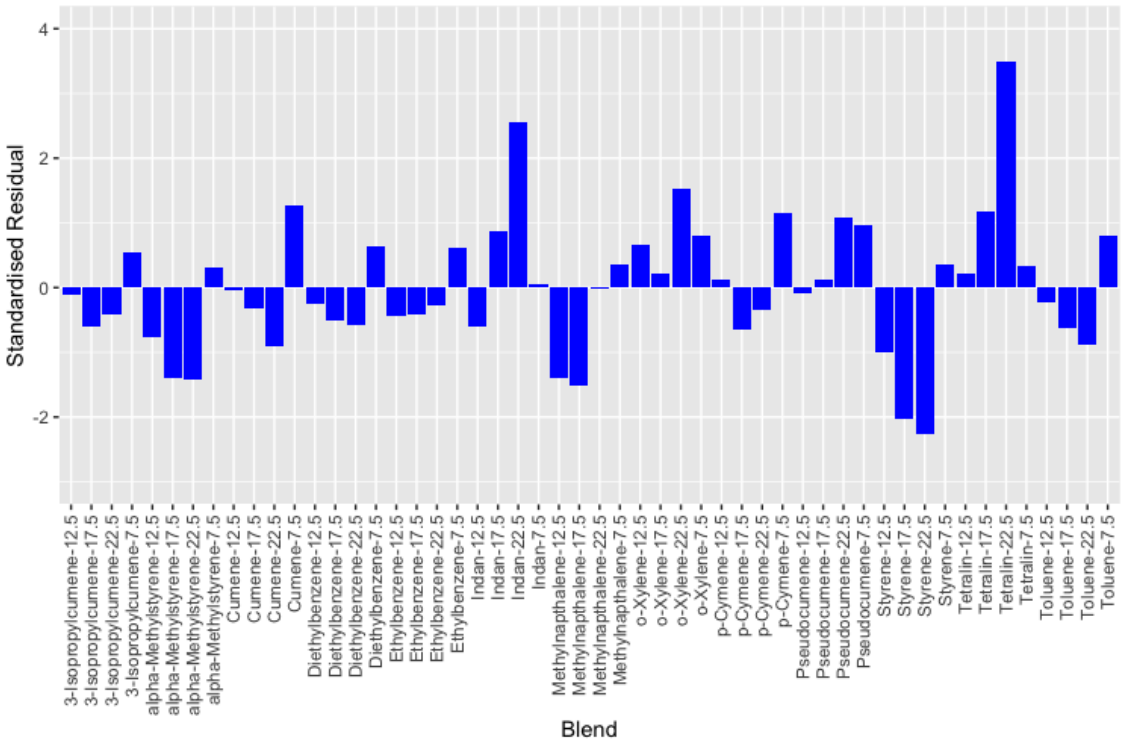

Figure 5.10.2: Scatter plot showing standardised residuals for each blend for all blends

The general form of the final model is shown in Equation 5.2 including variables for global density, Unified YSI and an intercept value.

$$BC_{conc} = a.\rho_g + b.YSI + c \tag{5.1}$$

The coefficients from the final model are included in Equation 5.3

$$BC_{conc,unified} = 3.190\rho_g + 5.564 \times 10^{-4}.YSI - 2.484 \tag{5.2}$$

The model shows good agreement between predicted and actual values as the model accounts for between 92.4% and 92.1% of the variability in the data. The positive coefficients of each variable are logically consistent with observations, as an increase in either should cause an increase in BC emissions conceptually, as demonstrated. In terms of residuals, if an outlier is considered to have a standardised residual of 3 or higher, then o-Xylene at 22.5% is the only fuel content data point to exceed this criteria.

In terms of dividing the data by classification into alkylbenzenes and polycyclics, two further models are proposed for each. The first for alkylbenzenes takes the same general form as Equation 6.4 and the coefficients for which are shown in Equation 5.3.

$$BC_{conc,alkylbenzenes} = 1.814\rho_g + 7.053 \times 10^{-4}.YSI - 1.433 \tag{5.3}$$

The model for polycyclics omits the Unified YSI term due to statistical insignificance for the general form shown in Equation 5.4 with coefficients being shown in Equation 5.5.

$$BC_{conc} = a.\rho_g + c \tag{5.4}$$

$$BC_{conc,polycyclics} = 5.262\rho_g - 4.0322 \tag{5.5}$$

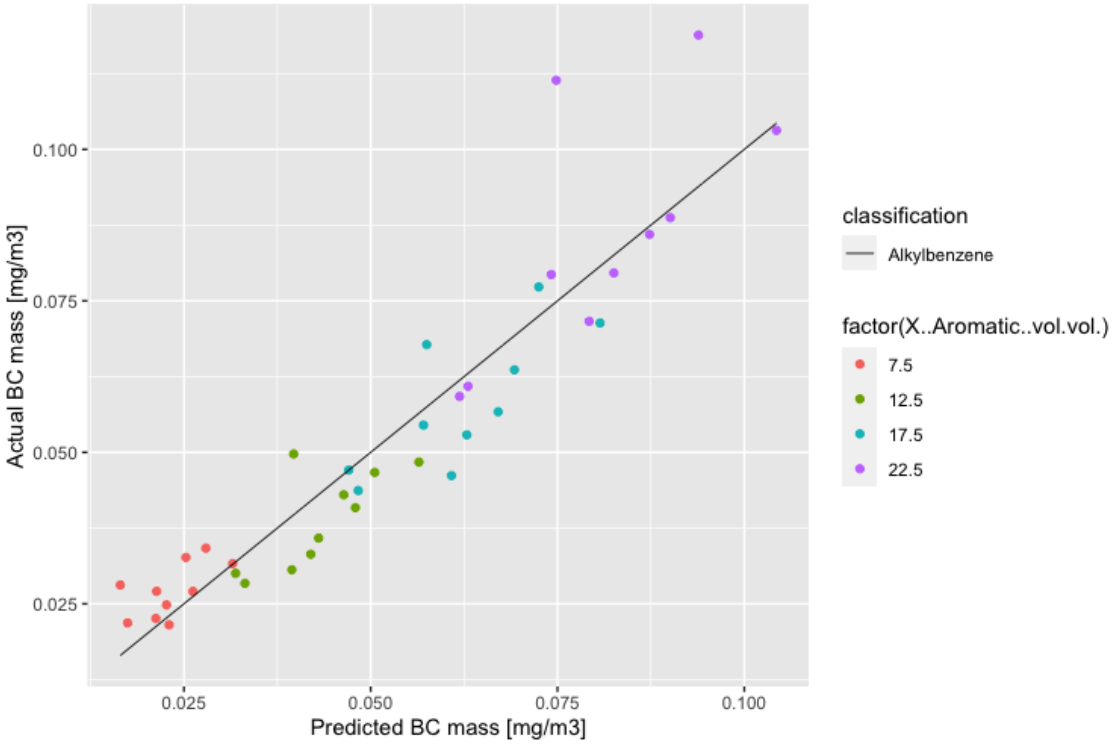

Figure 5.10.3: Scatter plot showing predicted BC and actual BC for alkylbenzenes

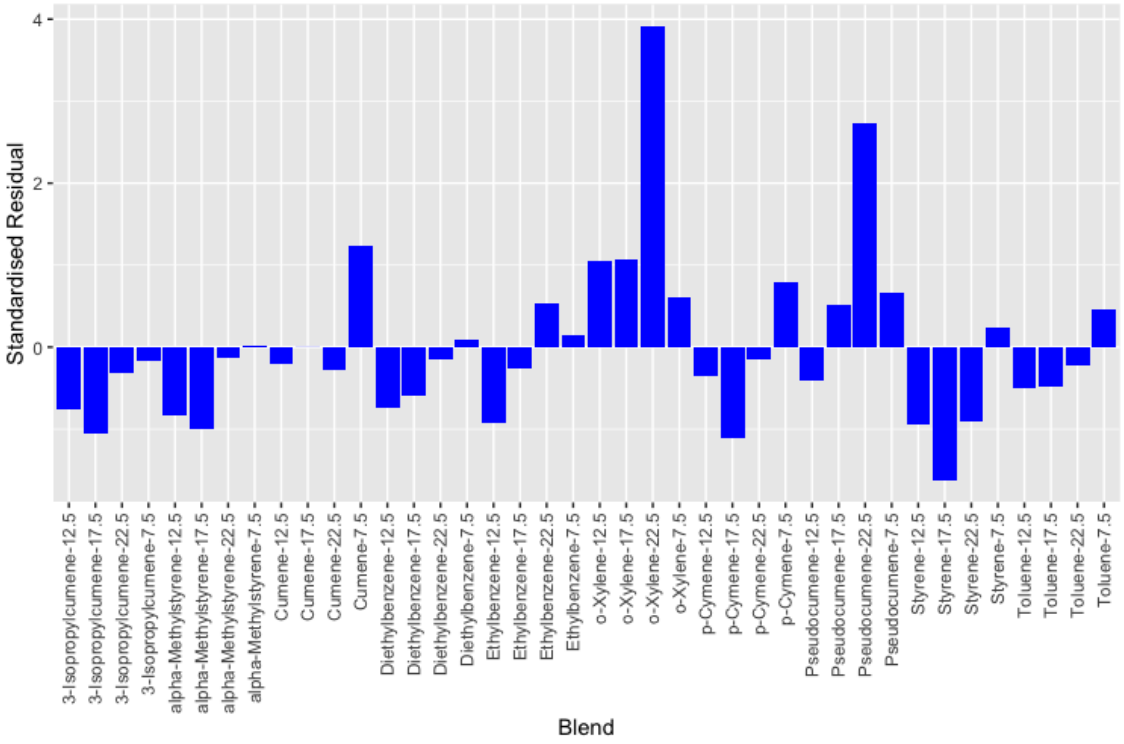

Figure 5.10.4: Scatter plot showing standardised residuals for each blend for alkylbenzenes

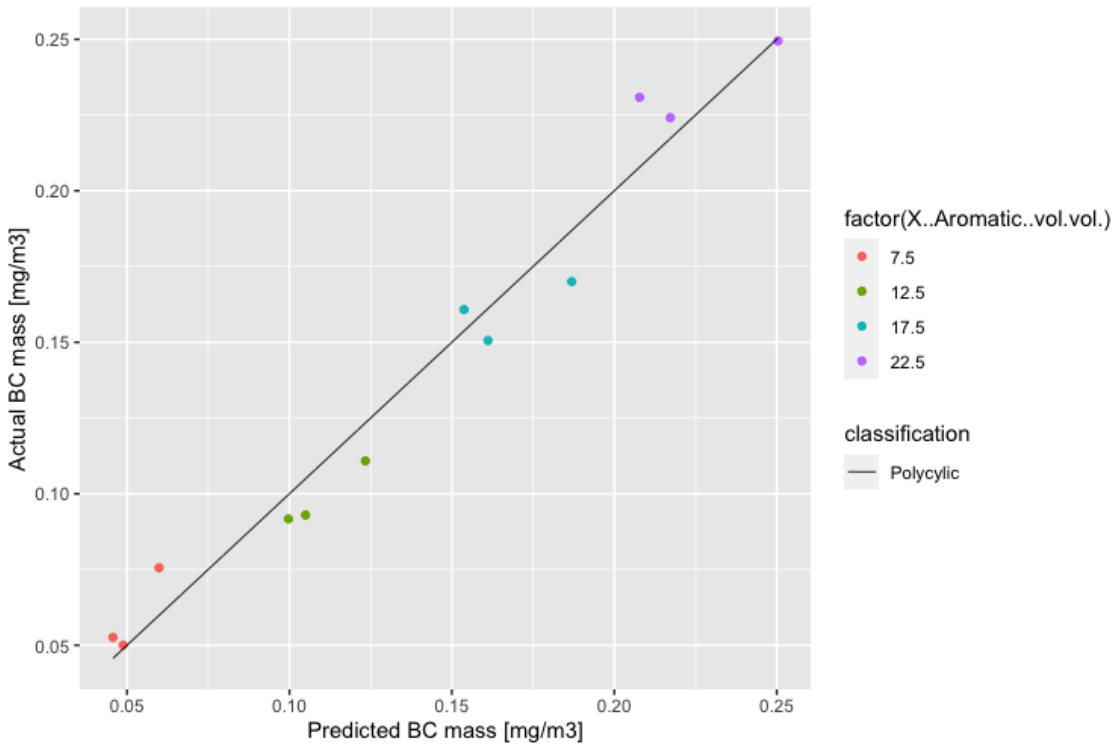

Figure 5.10.5: Scatter plot showing predicted BC and actual BC for polycyclics

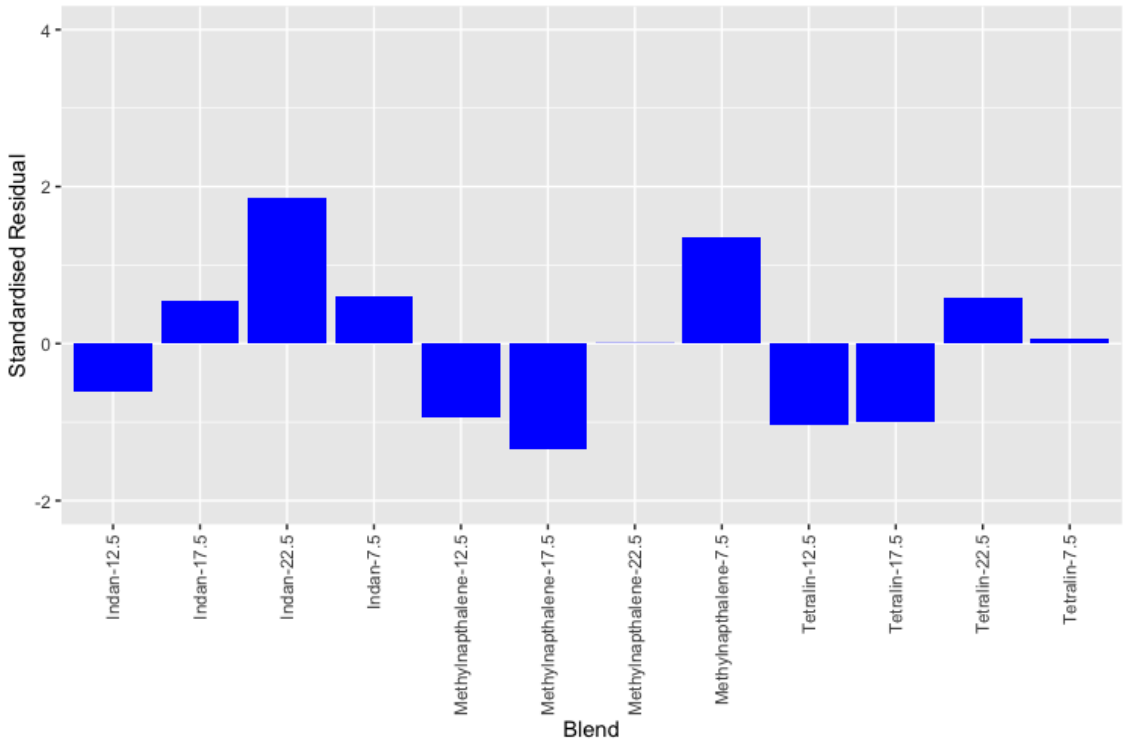

Figure 5.10.6: Scatter plot showing standardised resiudals for each blend for polycyclics

The predicted versus actual response for the final model for alkylbenzenes is shown in Figure 5.10.3 and the standardised residuals with respect to every data point is shown in Figure 5.10.4.

The predicted versus actual response for the final model for polycyclics is shown in Figure 5.10.5 and the standardised residuals with respect to every data point is shown in Figure 5.10.6.

A statistical summary for the three models generated are shown in Table 5.28.

Table 5.28: Multivariate BC Statistical Results

	p-value	*R-squared*	*Adjusted R-squared*	*RMS Error*
Unified	2.200×10^{-16}	0.9239	0.9208	0.015130
Alkylbenzenes	2.200×10^{-16}	0.8609	0.8534	0.009775
Polycyclics	7.404×10^{-9}	0.9688	0.9657	0.012980

There is strong agreement between predicted and actual values for the alkylbenzene category (0.8534), albeit with a lower coefficient of determination than the unified model by around 7%. As with the unified model, the only true outlier with a standardised residual above three is o-Xylene at 22.5% volume, although it should be noted that Pseudocumene at 22.5% is close to this threshold.

There is strong agreement between predicted and actual values for the polycyclic category (0.9657), with a higher coefficient of determination than the unified model by around 4%. There are no outliers in the polycyclic model.

While both polycyclic and alkylbenzene models have lower coefficients of determination than the unified model, their RMS errors are both lower, at 0.009775 and 0.012980 respectively, than the unified RMS (0.015130). This would suggest that the use of these models to predict the performance of novel blends would achieve more accurate results by choosing a model specific to the classification of the aromatic being used. The similarity of performance of all three models, however, suggests that the majority of variance of the data is being accounted for irrespective of which model is chosen.

The inclusion of the YSI component in two of the final models merits further discussion. The only two variables that met the criteria for inclusion are global density and Unified YSI. A univariate model using only global density accounts for a significant proportion of the variance in the data for unified, alkylbenzene and

polycyclic classifications (0.8911, 0.7237, 0.9688). In the case of polycyclics, density alone is almost totally prescriptive in predictive BC emissions, albeit with a smaller range of fuels and subsequently, a smaller data set. Nevertheless, global density is sufficient on its own. With alkylbenzenes, however, the YSI term raised the coefficient of determination from 0.7237 to 0.8534, reflecting an increase in the proportion of variance accounted for by 12.97%, making Unified YSI a true confounder in modelling terms. Global density alone correlates very well with these results but the finding is purely correlative and can't be claimed to be totally prescriptive. There is a conceptual framework however as to why density may drive BC production due to decreased inter-molecular distances. YSI however, is a descriptive measure based on observation of performance. Its inclusion provides little insight as to the mechanisms that determines BC production, but as a modelling coefficient is able to provide predictive capability to reduce variance in the data for a given density. While YSI cannot be measured directly for a petroluem derived fuel, a SAF produced via alternative methods can be measured to determine its composition and proportion of each component to a good degree of accuracy, and so the Unified YSI technique is appropriate as a predictive metric.

Chapter 6

DMS Results

6.1 PM Number Results

The total number concentration of PM for 16 aromatics in three blend proportions (8%, 13%, 18% vol/vol) are reported here. The reduction in the number of blends from four to three was made in order to reduce the fuel expense by excluding the blend highest proportion of aromatic (22.5%). Each blend was raised by half a percent each to bring the lower limit in line with the specification limits of 8%.The size distribution and geometric mean diameter of PM for each fuel blend is also reported. The results contained in Chapters 5 and 6 were conducted separately. They share a common analytical methodology, however, which was already laid out in Chapter 5, and is omitted here for the sake of brevity. Comparisons between the data from this Chapter and Chapter 5 are presented and discussed in Chapter 7.

Figure 6.1.1 shows the total number concentration of PM found measured in the exhaust of each blend. With respect to every aromatic species, increasing its respective proportion increases the number concentration of PM emissions. The blends containing the four polycyclic aromatics have the highest concentrations compared to the alkylbenzene blends, except for tetralin at 18% vol/vol. 3-isopropylbenzene has the lowest concentration of emissions in all three blend proportions.

The error bars shown in Figure 6.1.1 are two standard deviations around the mean of the five readings taken for each fuel. Two standard deviations are shown as this encompassed 95.4% of the data around the mean.

Figure 6.2.1 shows the size distributions for each aromatic with respect to its

three blend proportions. Irrespective of magnitude, the pattern for each shows the expected distribution with a peak of soot particles of around 25-35nm. There is a notable increase in the peak of the distribution for every aromatic species as the blend proportion increases.

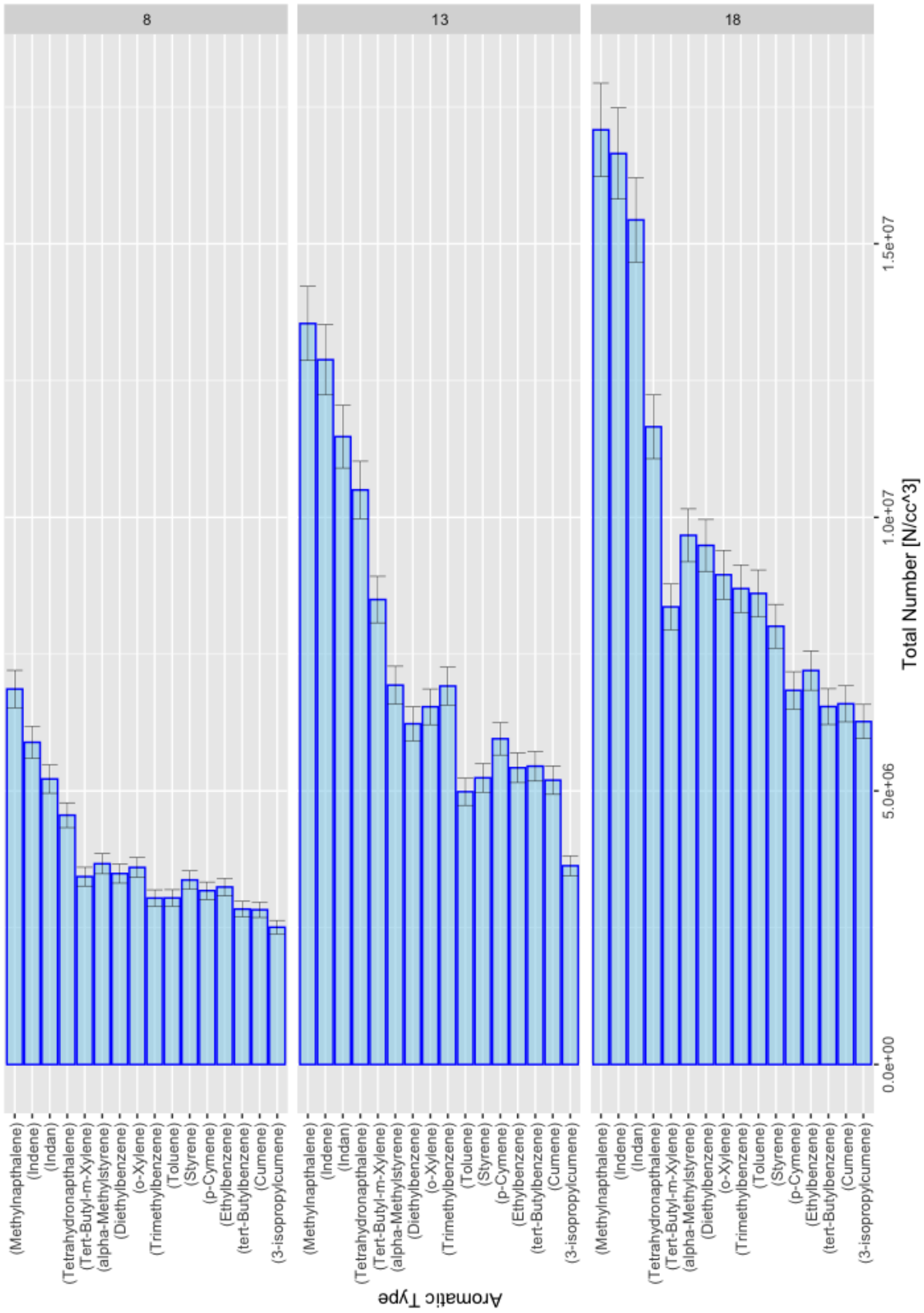

Figure 6.1.1: Particle Number Concentration Emissions for 14 Alkylbenzenes and 4 Polycyclic Aromatic Hydrocarbons blended with a paraffinic base at three blend proportions

6.2 DMS500 Size Results

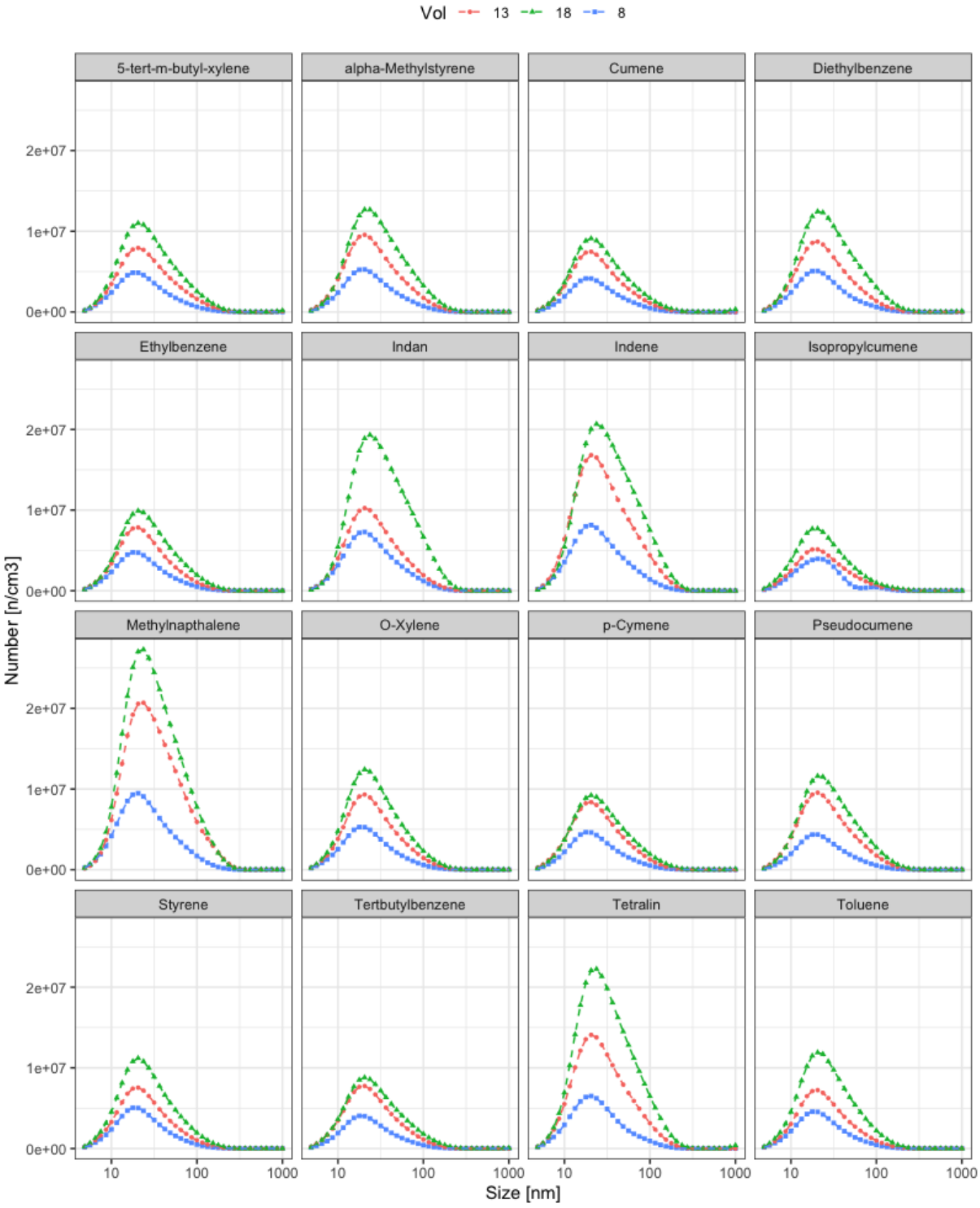

Figure 6.2.1: Size distributions for each aromatic blend at 8%, 13% and 18% vol/vol

6.3 GMD

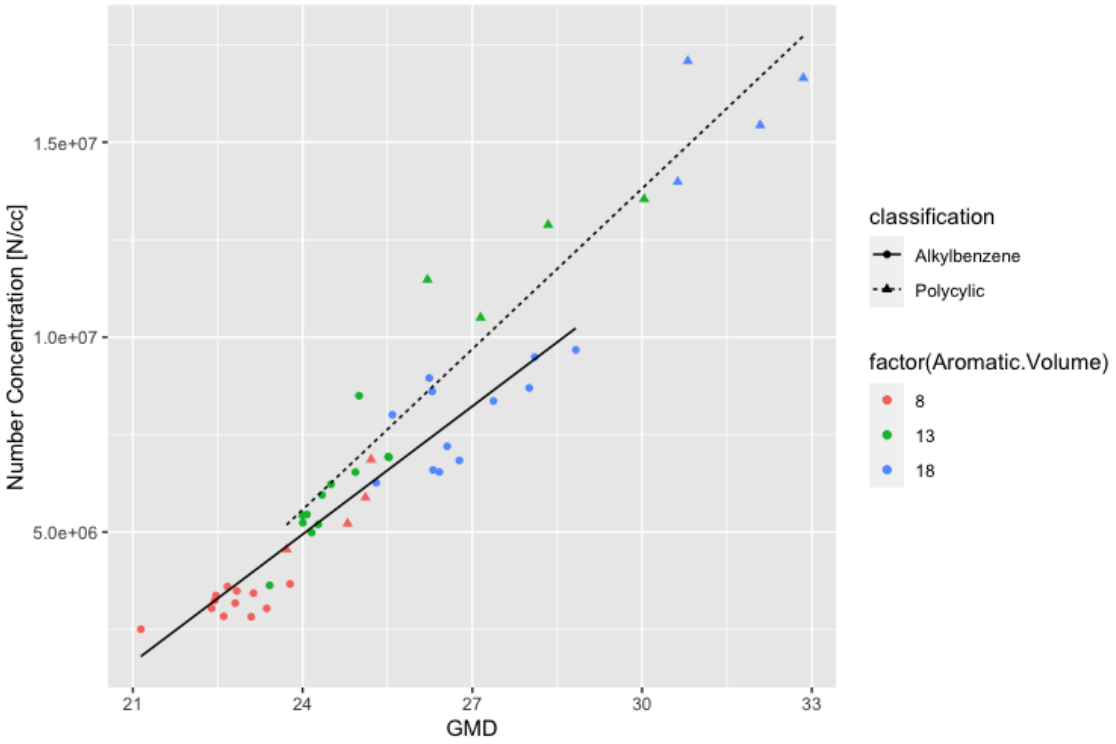

Figure 6.3.1: Geometric Mean Diameter vs PM Number Concentration

Table 6.1: Geometric Mean Diameter PM Number Statistical Results

	r	*R-squared*	*Adjusted R-squared*	*RMS Error*	*p-value*
Unified	0.9531	0.9084	0.9064	1.153×10^{6}	2.2×10^{-16}
Alkylbenzenes	0.9285	0.8621	0.8581	0.831×10^{6}	3.4×10^{-16}
Polycyclics	0.9489	0.9005	0.0.8905	1.499×10^{6}	2.5×10^{-6}

Figure 6.3.1 shows the relationship between the geometric mean diameter of the soot particles for each blend and the number concentration of PM, where a strong positive correlation is observed. Table 6.1 shows the accompanying statistics, with strong coefficients of determination for alkylbenzenes (0.8621), polycyclics (0.9005) and irrespective of classification (0.9531).

On the basis of these results it can be claimed that a general increase in aromatic content irrespective of aromatic species produces a larger number of larger soot particles.

6.4 Aromatic Volume Discussion

The PM results obtained via DMS are shown with accompanying regression lines for each blend with respect to its volume in Figure 6.4.1 for all data points. The accompanying statistical data based on is shown in Tables 6.2 and 6.3 with regard to alkylbenzenes and polycyclics respectively.

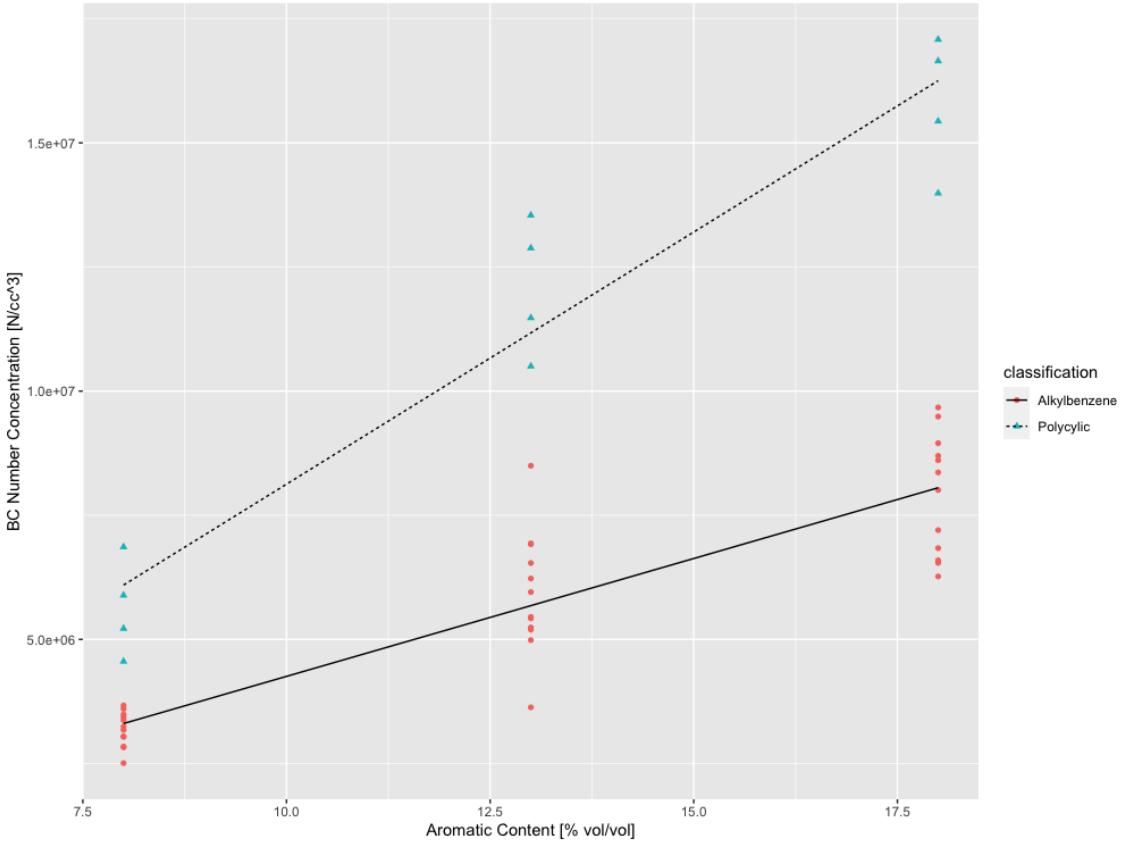

Figure 6.4.1: Scatter chart of aromatic content against number concentration at 8%, 13% and 18% vol/vol

Table 6.2: Aromatic Volume % PM Number Statistical Results

	Multiple R	*R-squared*	*Adjusted R-squared*	*RMS Error*
Unified	0.6678	0.4459	0.4339	2.836×10^6
Alkylbenzenes	0.8913	0.7944	0.7884	1.015×10^6
Polycyclics	0.9559	0.9137	0.9051	1.396×10^6

Table 6.3: Aromatic Volume % PM Number Regressions Equations

Classification	$Y = mx + c$	*Linear Regression*	*Standard Error*	*tStat*	*P-Value*
Unified	c	-877914	1366184	-0.643	0.524
	m	610064	100263	6.085	2.16×10^{-7}
Alkylbenzene	c	-493511	564467	-0.874	0.388
	m	474856	41426	11.463	3.16×10^{-13}
Polycyclic	c	-2031122	1344898	-1.51	0.162
	m	1015686	98701	10.29	1.22×10^{-6}

An increase in aromatic volume is positively correlated with PM Number Concentration strongly for alkybenzes (r=0.8013) and polycyclics (r=0.9559) and moderately irrespective of classification (r=0.6678). The coefficients of determination are strong for alkylbenzenes (0.7944) and polycyclics (0.9137) and moderate for all data points irrespective of classification (0.4459).

Due to the discrepancy between regression statistics between the two classifications, aromatic volume is not thought to be deterministic and that an other variable is a confounder for this correlation.

6.5 Aromatic Ring Carbon Discussion

The PM Number Concentration results obtained via DMS are shown for each blend with respect to its ring carbon percentage per unit mass in Figure 6.5.1 and for all data points in Figure 6.5.2. The accompanying statistical data based on individual blend proportions is shown in Tables 6.4 and 6.5 with regard to alkylbenzenes and polycyclics respectively.

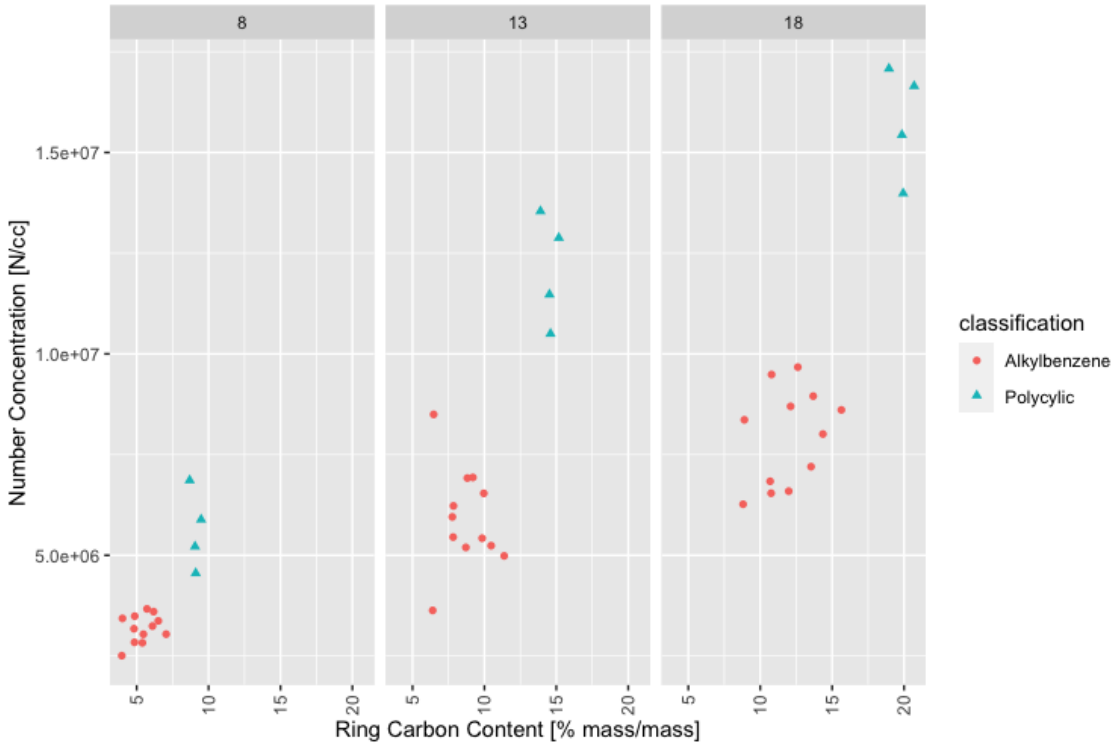

Figure 6.5.1: Scatter chart of ring carbon content against number concentration at 8%, 13% and 18% vol/vol

Table 6.4: Ring Carbon % PM Number Statistical Results for Alkylbenzenes

Aromatic Content [vol/vol %]	8	13	18
r	0.3092	-0.1558	0.3463
R-squared	0.09563	0.02426	0.1199
p-value	0.328	0.6289	0.2701

Table 6.5: Ring Carbon % PM Number Statistical Results for Polycyclics

Aromatic Content [vol/vol %]	8	13	18
r	-0.4188	-0.2392	-0.1985
R-squared	0.1754	0.05723	0.0394
p-value	0.5812	0.7608	0.8015

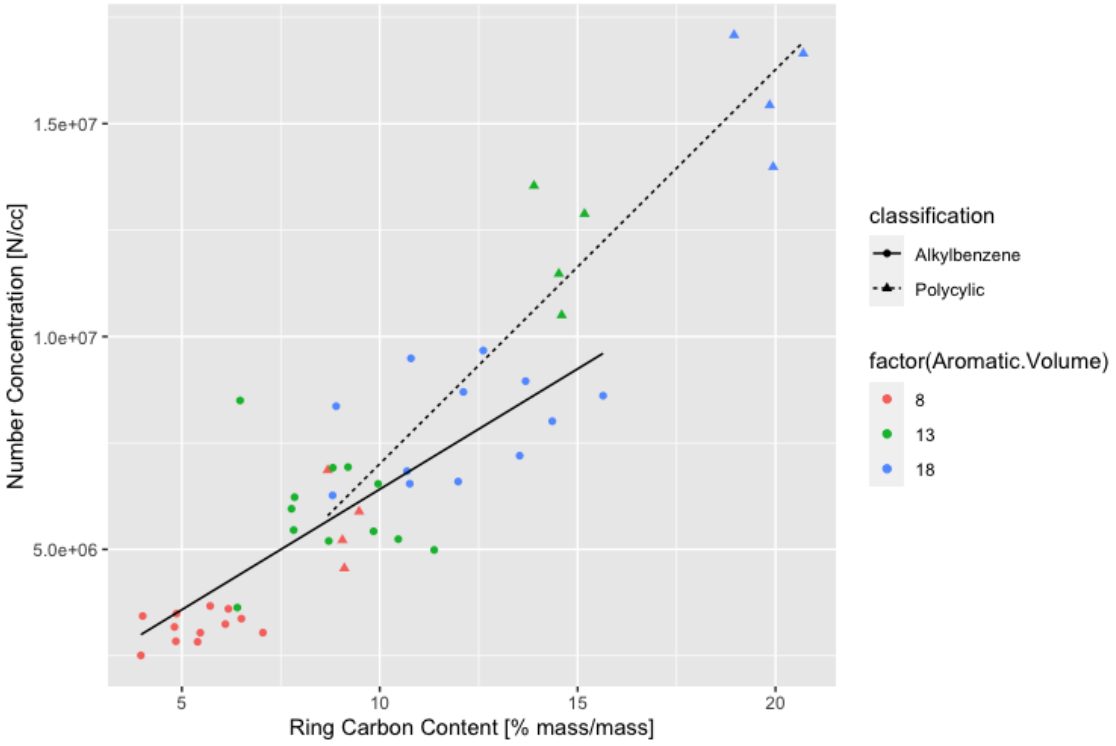

Figure 6.5.2: Scatter chart of ring carbon content against number concentration for all data points

A table including regressions statistics for all three models is shown in Table 6.6 and coefficients of the accompanying regression equations is shown in Table 6.7.

Table 6.6: Ring Carbon % PM Number Statistical Results

	Multiple R	*R-squared*	*Adjusted R-squared*	*RMS Error*
Unified	0.9221	0.8503	0.8266	1.569×10^6
Alkylbenzenes	0.8052	0.6483	0.6379	1.327×10^6
Polycyclics	0.9451	0.8932	0.8825	1.553×10^6

Table 6.7: Ring Carbon % PM Regressions Equations

Classification	$Y = mx + c$	*Linear Regression*	*Standard Error*	*tStat*	*P-Value*
Unified	c	-998682	582563	-1.714	0.0932
	m	792898	52854	15.002	2.00×10^{-16}
Alkylbenzene	c	753499	660449	1.141	0.262
	m	565760	71470	7.916	3.21×10^{-9}
Polycyclic	c	-2253873	1535161	-1.468	0.173
	m	926147	101277	9.145	3.58×10^{-6}

For alkylbenzes, an increase in ring carbon content correlates weakly for the 8% and 18% group (r=0.3092 and r=0.3468) and shows no correlation for the 13% group (r=-0.1558). The trend of increased ring carbon and PM in conceptually coherent but inconsistent and weak across the three groups. For Polycyclics, all three blend proportions anti-correlate weakly for all three blend proportions (r=-0.4188, r=0.2392, r=0.1985). This trend is not conceptually coherent with the idea of increased ring carbon content. Polycyclics are predominantly composed of cyclical carbon and if the expected trend were observed, an increase in ring carbon should elicit higher PM emissions. It should be noted, however that all four polycyclics have relatively similar proportions of ring carbon at each blend proportion. Low coefficients of determination are observed within the alkylbenzene (0.09563, 0.02326, 0.1199) and polycyclic 0.1754, 0.05723, 0.0394) classifications.

Irrespective of blend proportion, increased ring carbon correlates with PM Number Concentration for alklybenzenes (0.8052), polycyclics (0.9451) and all data points (0.9921), with moderate to strong coefficients of determination (0.8503, 0.6483, 0.8932). No classification or blend proportion has a p-value below 0.05 suggestive of statistical significance.

The predictive ability of Ring Carbon is mixed. Strong regression performance for all data points suggests that Ring Carbon is an potentially significant metric. It's weak and inconsistent performance within blend proportions however, may suggest that this metric is not descriptive.

6.6 Hydrogen Content Discussion

The PM Number Concentration results obtained via DMS are shown with accompanying regression lines for each blend with respect to its hydrogen content per unit mass in Figure 6.6.1 and for all data points in Figure 6.6.2. The accompanying statistical data based on individual blend proportions is shown in Tables 6.8 and 6.9 with regard to alkylbenzenes and polycyclics respectively.

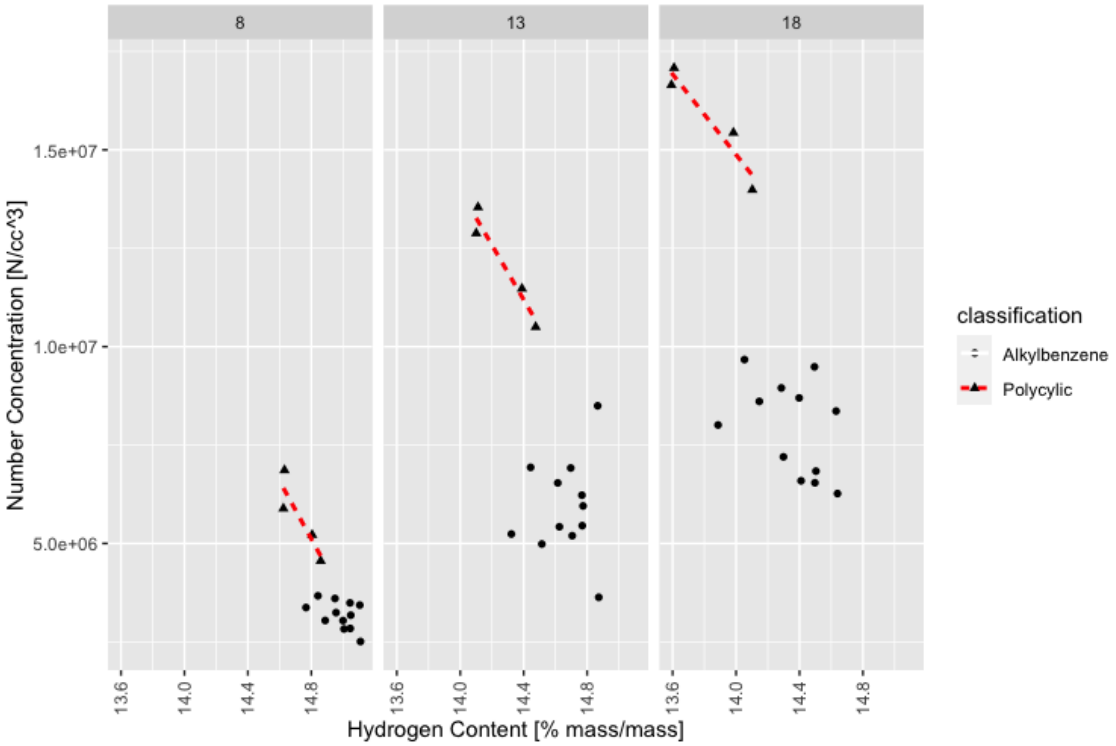

Figure 6.6.1: Scatter chart of hydrogen content against number concentration at 8%, 13% and 18% vol/vol

Table 6.8: Hydrogen Mass% PM Number Statistical Results for Alkylbenzenes

Aromatic Content [vol/vol %]	8	13	18
r	-0.4463	0.07389	-0.4161
R-squared	0.1992	0.005459	0.1731
p-value	0.1458	0.8195	0.1786

Table 6.9: Hydrogen Mass % PM Number Statistical Results for Polycyclics

Aromatic Content [vol/vol %]	8	13	18
r	-0.8934	-0.9688	-0.9559
R-squared	0.8071	0.9386	0.9137
p-value	0.1016	0.03117	0.04412

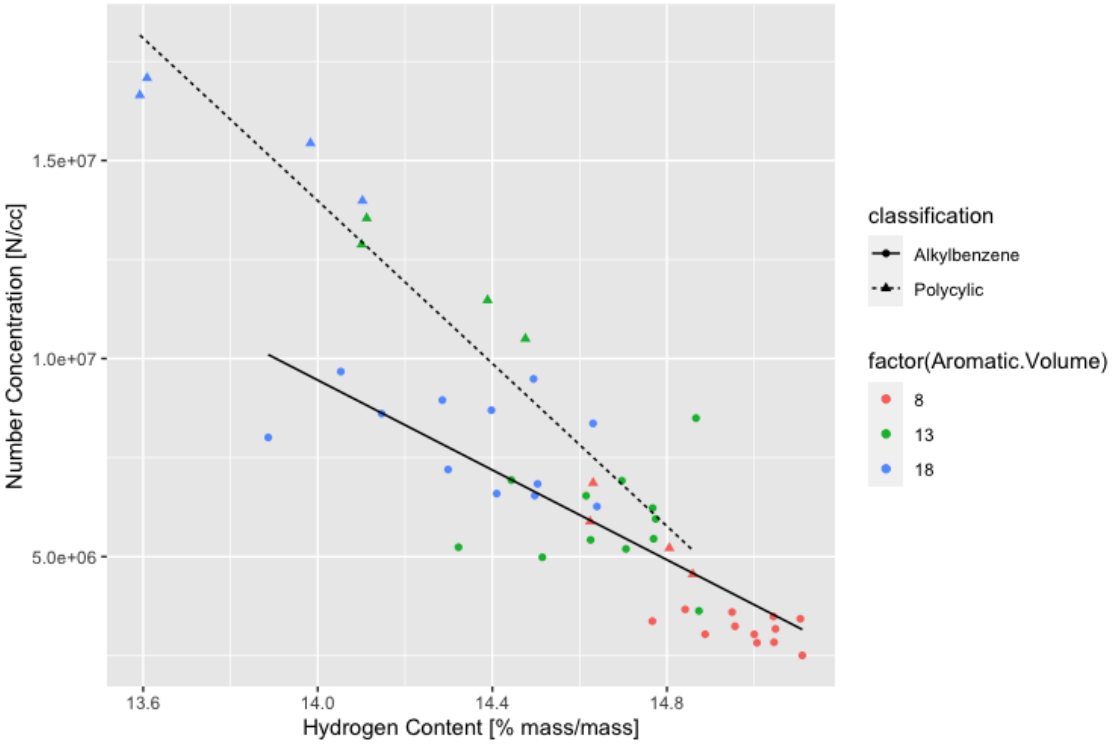

Figure 6.6.2: Scatter chart of hydrogen content against number concentration for all data points

A table including regressions statistics for all three models is shown in Table 6.10 and coefficients of the accompanying regression equations is shown in Table 6.11.

Table 6.10: Aromatic Volume % PM Statistical Results

	Multiple R	*R-squared*	*Adjusted R-squared*	*RMS Error*
Unified	-0.8797	0.7738	0.7689	1.812×10^6
Alkylbenzenes	-0.7982	0.6372	0.6266	1.348×10^6
Polycyclics	-0.9675	0.9360	0.9296	1.203×10^6

Table 6.11: Aromatic Volume % PM Regressions Equations

Classification	$Y = mx + c$	*Linear Regression*	*Standard Error*	*tStat*	*P-Value*
Unified	c	134335683	10150330	13.23	2×10^{-16}
	m	-8737135	696523	-12.54	2×10^{-16}
Alkylbenzene	c	88833020	10762050	8.254	1.24×10^{-9}
	m	-5669757	733643	-7.728	5.47×10^{9}
Polycyclic	c	157686456	12123946	13.01	1.37×10^{-7}
	m	-10264595	849043	-120.9	2.72×10^{-8}

Hydrogen Content anti-correlates with PM Number Concentraion weakly for alkylbenznes for the 8% and 18% groups (r=-0.4463 and r=-0.4161) and no correlation is observed for the 13% group (r=0.07389) Hydrogen Content anti-correlates strongly with PM Number Concentration for all blend proportions with respect to polycyclics (r=0.8934, r=-0.9688, r=-0.9559). Weak coefficients of determination are observed for alkylbenzenes (0.1992, 0.0055, 0.1731) and strong for polycyclics (0.8071, 0.9386, 0.9137). The only p-values of significance below 0.05 are for the polycyclic classification at 13% and 18%.

Irrespective of blend proportion, an increase in hydrogen content anti-correlates strongly with PM Number Concentration for all data points across alkylbenzene, polycyclic and without classification (r=-0.7982, r=-0.9675, r=-0.8797). Moderate to strong coefficients of determination are observed for alkylbenzenes, polycyclics and without classification (0.6372, 0.9360, 0.7738).

The observed trends demonstrate the expected relationship between increased hydrogen content and PM emissions; as the proportion of carbon present decreases, so do PM emissions. This is observed across every classification and blend proportion excepting for the alkylbenzene group at 13%. The correlation and accompanying regression statistics are poor for alklybenzenes, however, and it is likely that this metric is not reflecting the mechanistic properties determining PM formation using this metric alone.

6.7 Global Density Discussion

The PM Number Concentration results obtained via DMS are shown with accompanying regression lines for each blend group with respect to its global density in Figure 6.7.1 and for all data points in Figure 6.7.2. The accompanying statistical data based on individual blend proportions is shown in Tables 6.12 and 6.13 with regard to alkylbenzenes and polycyclics respectively.

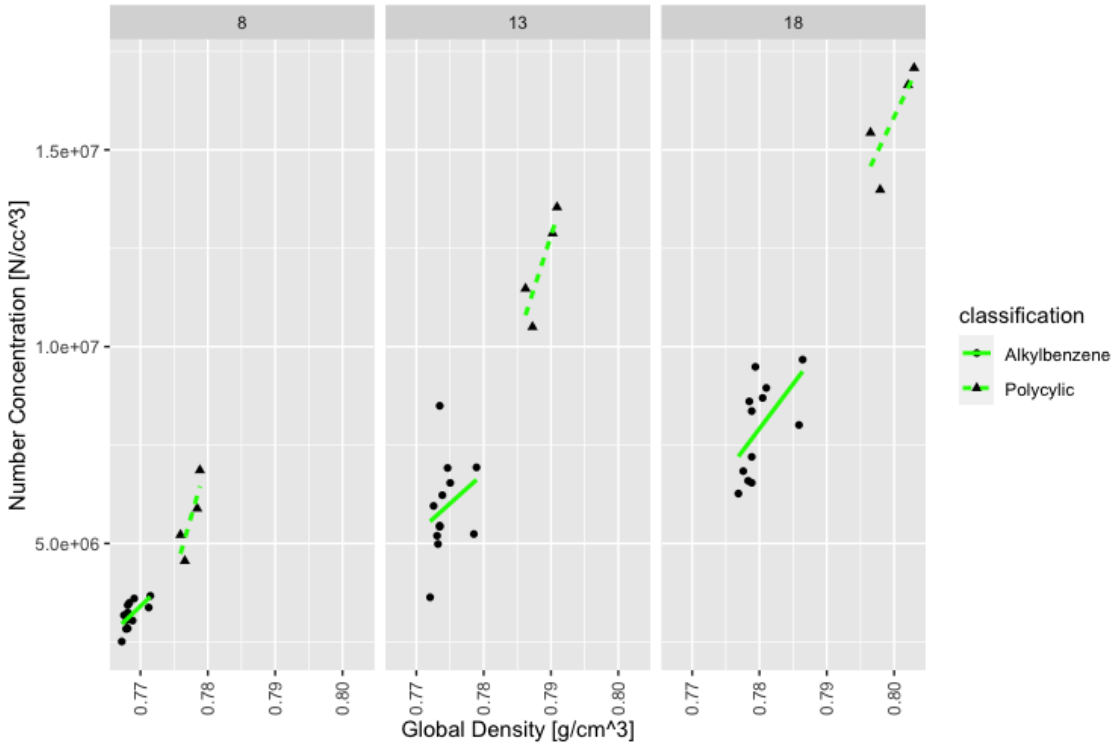

Figure 6.7.1: Scatter chart of global density against number concentration at 8%, 13% and 18% vol/vol

Table 6.12: Global Density % PM Statistical Results for Alkylbenzenes

Aromatic Content [vol/vol %]	8	13	18
r	0.6290	0.2733	0.5727
R-squared	0.3957	0.07471	0.3280
p-value	0.02842	0.3900	0.05163

Table 6.13: Global Density % PM Statistical Results for Polycyclics

Aromatic Content [vol/vol %]	8	13	18
r	0.8471	0.8822	0.8086
R-squared	0.7175	0.7783	0.6539
p-value	0.1529	0.1178	0.1914

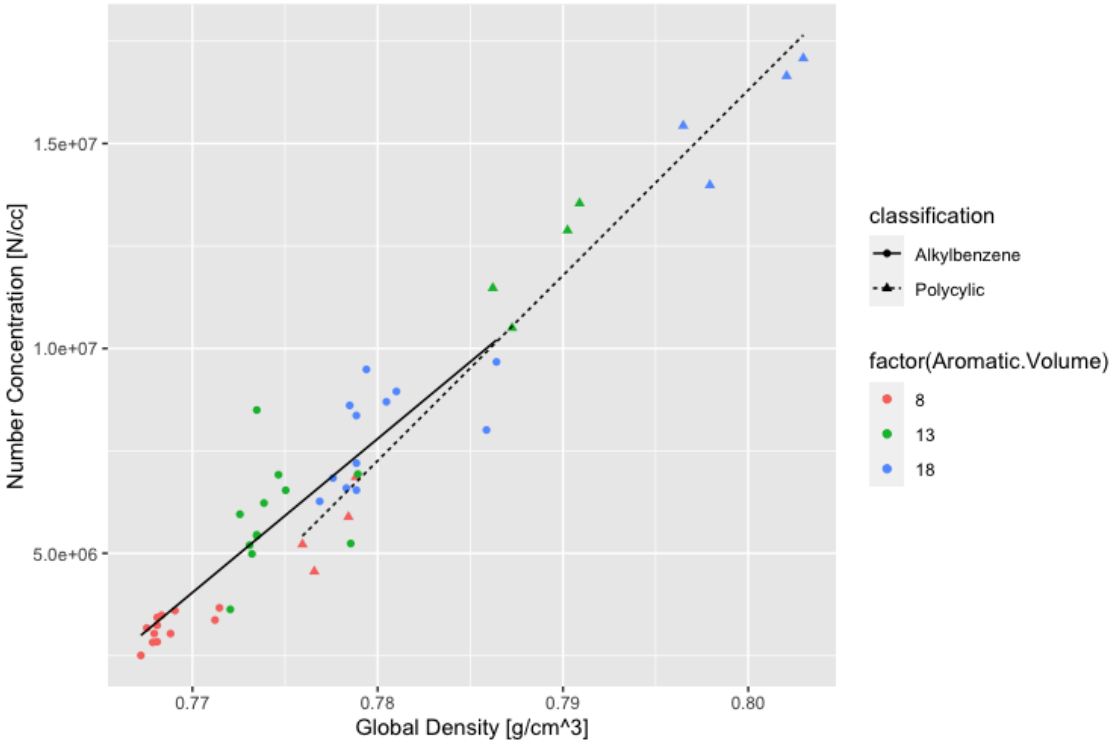

Figure 6.7.2: Scatter chart of global density against number concentration for all data points

A table including regressions statistics for all three models is shown in Table 6.14 and coefficients of the accompanying regression equations is shown in Table 6.15.

Table 6.14: Global Density PM Number Statistical Results

	Multiple R	*R-squared*	*Adjusted R-squared*	*RMS Error*
Unified	0.9629	0.9272	0.9256	1.028×10^6
Alkylbenzenes	0.8912	0.7943	0.7883	1.015×10^6
Polycyclics	0.9783	0.9570	0.9527	0.9860×10^6

Table 6.15: Global Density PM Number Regressions Equations

Classification	$Y = mx + c$	*Linear Regression*	*Standard Error*	*tStat*	*P-Value*
Unified	c	-304741874	12886652	-23.65	2×10^{-16}
	m	400797674	16564092	24.20	2×10^{-16}
Alkylbenzene	c	-285109624	25375244	-11.24	5.11×10^{-13}
	m	375520424	32768442		3.19×10^{-13}
Polycyclic	c	-345464224	23914883	-14.45	5.02×10^{-8}
	m	452210592	30321580	14.91	3.70×10^{-8}

Global Density correlates moderately with PM Number Concentration for alkylbenzenes and 8% and 18% (r=0.6920 and r=0.5727) and weakly at 13% (r=0.2733). Global Density correlates strongly with PM Number Concentration for polycyclics and for all blend proportions (r=0.8471, r=0.8822, r=0.8086). Weak coefficients of determination are observed for alkylbenzenes (0.3957, 0.0747, 0.3280) and strong coefficients of determination are observed for polycyclics (0.7175, 0.7783, 0.6539). P-values are only of significance for the 8% alkylbenzene group.

Irrespective of blend proportion, global density correlates stronly with alkylbenzenes (r=0.8912), polycyclics (r=0.9783) and irrespective of classification (r=0.9629). Strong coefficients of determination are observed for alkylbenzenes (0.7943), polycyclics (0.9570) and irrespective of classification (0.9629).

Global density shows several features of interest as a metric to predict PM Number Concentration Emissions. The expected behaviour as discussed in Chapter 3 is observed, that an increase in global density correlates well with increased emissions. Unlike other metrics of interest, the regression lines for the two classifications are almost coincident, suggesting that global density is capturing some of the variability that is deterministic of the variance of both alkylbenzene and polycyclic classifications. However, the regression statistics are poor when predicting PM Number Concentration within blend proportions when considering the coefficients of determination for both alkylbenzenes and polycyclics. The observed RMS Error is the lowest for any metric used in this chapter, suggetsing that if not totally deterministic, global density is an effective predictor for PM Number Concentration emissions.

6.8 Fuel TSI Discussion

The PM Number Concentration results obtained via DMS are shown with accompanying regression lines for each blend group with respect to its agreggated TSI in Figure 6.8.1 and for all data points in Figure 6.8.2. The accompanying statistical data based on individual blend proportions is shown in Tables 6.16 and 6.17 with regard to alkylbenzenes and polycyclics respectively.

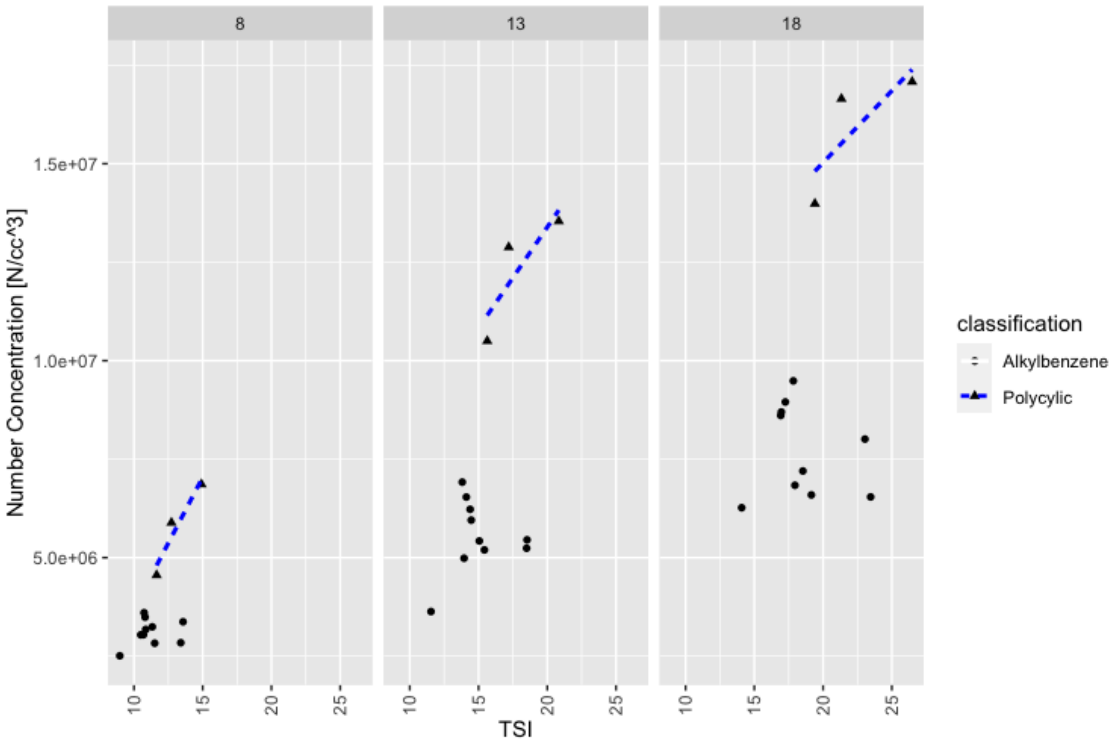

Figure 6.8.1: Scatter chart of TSI against number concentration at 8%, 13% and 18% vol/vol

Table 6.16: TSI PM Number Statistical Results for Alkylbenzenes

Aromatic Content [vol/vol %]	8	13	18
r	0.2392	0.1418	-0.1337
R-squared	0.05722	0.02012	0.01788
p-value	0.5057	0.6959	0.7126

Table 6.17: TSI PM Number Statistical Results for Polycyclics

Aromatic Content [vol/vol %]	8	13	18
r	0.9603	0.8567	0.7958
R-squared	0.9222	0.7339	0.6333
p-value	0.1800	0.3451	0.4141

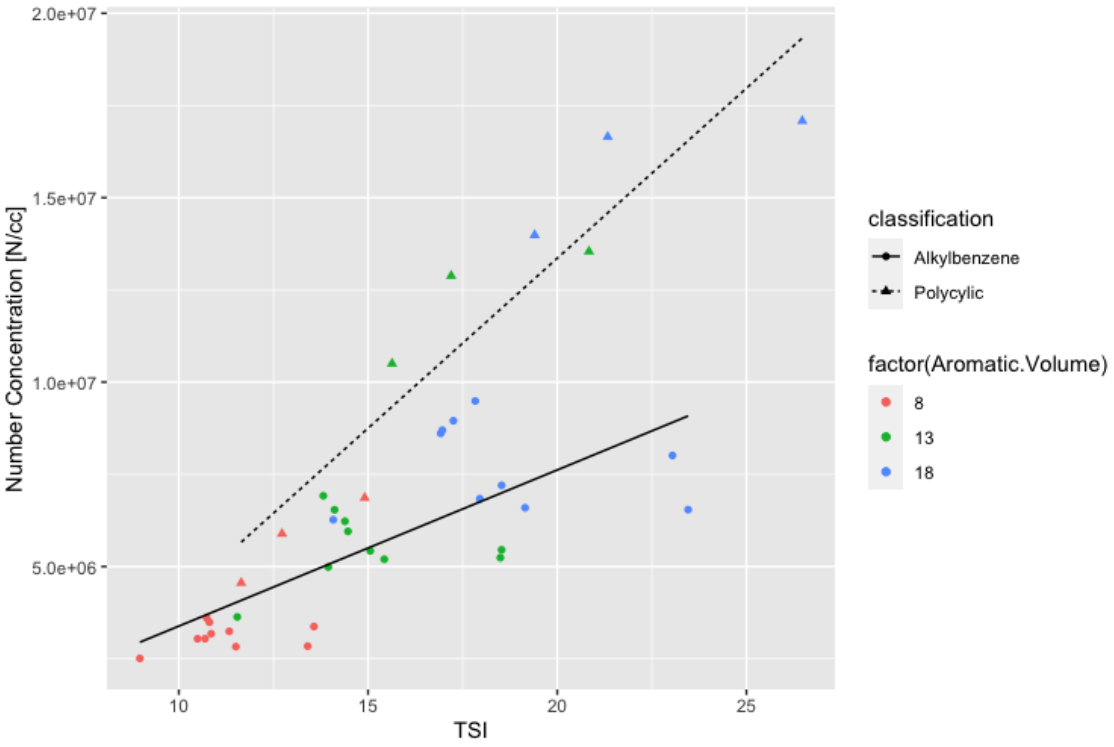

Figure 6.8.2: Scatter chart of TSI against number concentration for all data points

A table including regressions statistics for all three models is shown in Table 6.18 and coefficients of the accompanying regression equations is shown in Table 6.19.

Table 6.18: TSI PM Number Statistical Results

	Multiple R	*R-squared*	*Adjusted R-squared*	*RMS Error*
Unified	0.7691	0.5915	0.5804	2.435×10^6
Alkylbenzenes	0.7463	0.5569	0.5410	1.419×10^6
Polycyclics	0.9341	0.8726	0.8544	1.769×10^6

Table 6.19: TSI PM Number Regressions Equations

Classification	$Y = mx + c$	*Linear Regression*	*Standard Error*	*tStat*	*P-Value*
Unified	c	-4251666	1561752	-2.722	0.00983
	m	710512	97080	7.319	1.07×10^{-8}
Alkylbenzene	c	-849872	1095362	-0.776	0.444
	m	423359	71372	5.932	2.2×10^{-6}
Polycyclic	c	-5075097	2440915	-2.079	0.076177
	m	921654	133096	6.925	0.000226

The aggregate TSI shows no statistical correlation with PM Number Concentration for aklylbenzenes (r=0.2392, r=0.1418, r=-0.1337) and strong correlation with polycyclics (r=0.9603, r=0.8567, r=0.7958). Weak coefficients of determination are observed for alkylbenzenes (0.0572, 0.0201, 0.0178) and strong coefficients of determination are found for polycyclics at 8% vol (0.9222) and moderate at 13% and 18% (0.7339, 0.6333). No p-value for any classification or blend proportion meets the threshold for significance.

Irrespective of blend proportion, the aggregate TSI shows a strong positive correlation with PM Number Concentration for alkylbenzenes (r=0.7463), polycyclics (r=0.9341) and irrespective of classification (r=0.7691). Coefficients of determination are moderate for alkylbenzenes (0.5569), strong for polycyclics (0.8726) and moderate irrespective of classification (0.5915).

Aggregate TSI shows relatively poor performance as a predictor of PM Number Concentration emissions. Within each blend group, the expected trend of increased TSI resulting in higher emissions is observed for all but one group; alkylbenzenes at 18%. However, the statistics are so weak for alkylbenzenes that they do not reach the threshold for any degree of correlation. Irrespective of blend proportion, the regression statistics for aggregate TSI are worse than other metrics of interest. It is no thought that aggregate TSI is of predictive merit and any degree of correlation found is due to the increase of some other confounder that increases as TSI does.

6.9 Fuel Aggregate NSP Discussion

The PM Number Concentration results obtained via DMS are shown for each blend group with respect to its aggregated NSP in Figure 6.9.1 and for all data points in Figure 6.9.2. The accompanying statistical data based on individual blend proportions is shown in Tables 6.20 and 6.21 with regard to alkylbenzenes and polycyclics respectively.

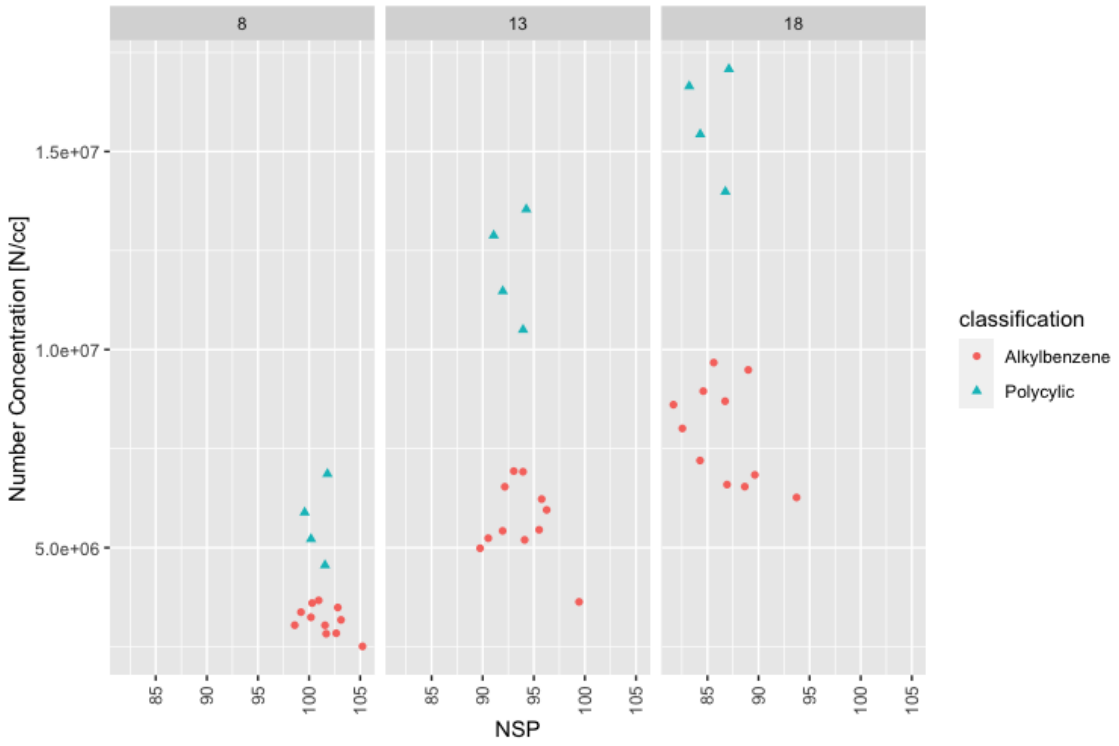

Figure 6.9.1: Scatter chart of aggregate NSP against number concentration at 8%, 13% and 18% vol/vol

Table 6.20: NSP PM Number Statistical Results for Alkylbenzenes

Aromatic Content [vol/vol %]	8	13	18
r	-0.5061	-0.2861	-0.4653
R-squared	0.2561	0.08185	0.2165
p-value	0.1122	0.3937	0.1492

Table 6.21: NSP PM Number Statistical Results for Polycyclics

Aromatic Content [vol/vol %]	8	13	18
r	0.1094	-0.0874	-0.2212
R-squared	0.01196	0.007645	0.04891
p-value	0.8907	0.9126	0.7789

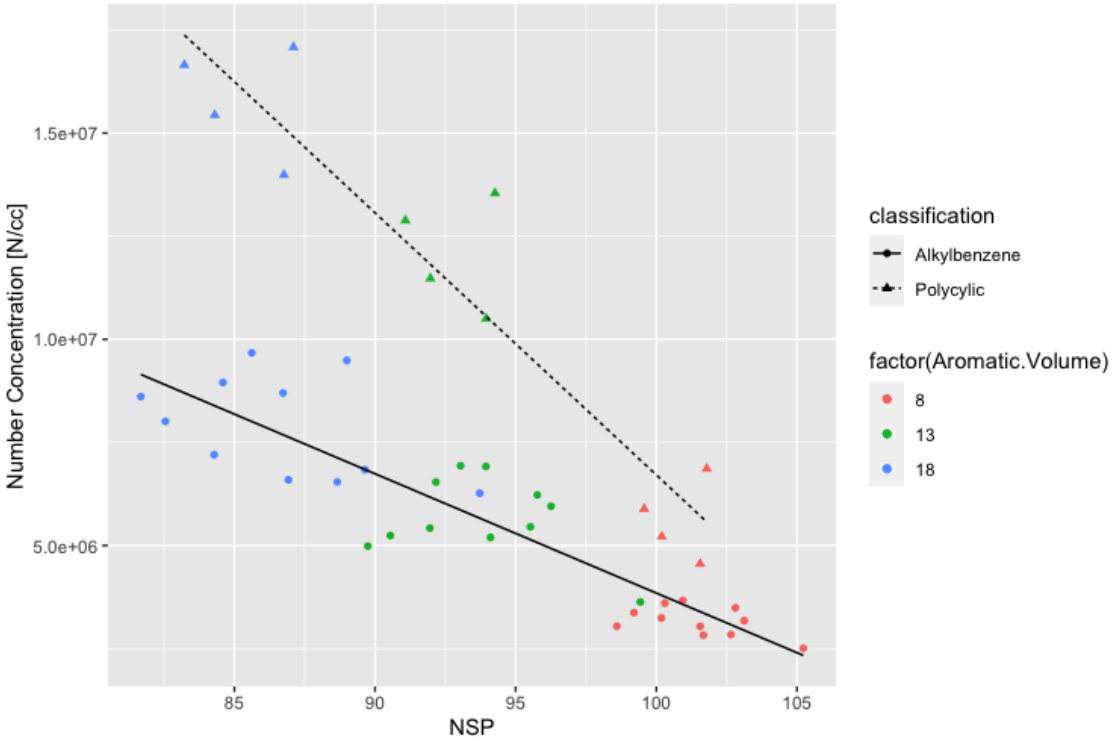

Figure 6.9.2: Scatter chart of aggregate NSP against number concentration for all data points

A table including regressions statistics for all three models is shown in Table 6.22 and coefficients of the accompanying regression equations is shown in Table 6.23.

Table 6.22: NSP PM Number Statistical Results

	Multiple R	*R-squared*	*Adjusted R-squared*	*RMS Error*
Unified	-0.6960	0.4844	0.4724	2.293×10^6
Alkylbenzenes	-0.8975	0.8055	0.7993	0.9694×10^6
Polycyclics	-0.9436	0.8904	0.8794	1.573×10^6

Table 6.23: NSP PM Number Regressions Equations

Classification	$Y = mx + c$	*Linear Regression*	*Standard Error*	*tStat*	*P-Value*
Unified	c	44767738	5944974	7.530	2.21×10^{-9}
	m	-402166	63270	-6.356	1.11×10^{-7}
Alkylbenzene	c	32771293	2405427	13.62	1.25×10^{-14}
	m	-289244	25525	-11.33	1.49×10^{-12}
Polycyclic	c	70273429	6573258	10.691	8.59×10^{-7}
	m	-635625	70526	-9.013	4.09×10^{-6}

Aggregate NSP anti-correlates weakly with PM Number Concentration for every alkylbenzene group (r=-0.5061, r=-0.2861, r=-0.4653). Aggregate NSP shows no statistical correlation with PM Number Concentration for polycyclics (r=-0.1094, r=-0.0874, r= 0.2212). Coefficients of determination are weak for alkylbenzenes (0.2561, 0.0819, 0.2165) and are also weak for polycyclics (0.01196, 0.0076, 0.0489). No p-value for any classification or blend proportion meets the threshold of statistical significance.

Irrespective of blend proportion, aggregate NSP anti-correlates with PM Number Concentration for alkylbenzenes (r=-0.8975), polycyclics (r=-0.9436) and irrespective of classification (r=-0.6960). Coefficients of determination are strong for alkylbenzenes (0.8055) and polycyclics (0.8904) and moderate irrespective of classification (0.4844).

The overall trend of NSP performance is consistent with its conceptual framework in the literature; that as NSP decreases, PM emissions increase. Aggregate NSP as a predictor of PM Number Concentration performs relatively strongly for each classification, but drops significantly as a holistic metric irrespective of classification. The polycyclic blends have similar values for aggregate NSP as the alkylbenzenes, but with significantly higher PM emissions. This would suggest this metric is not deterministic and the correlation for all data points is due to some other confounder than increases with NSP.

6.10 Unified Fuel YSI Discussion

The PM Number Concentration results obtained via DMS are shown with accompanying regression lines for each blend group with respect to its Unified YSI in Figure 6.10.1 and for all data points in Figure 6.10.2. The accompanying statistical data based on individual blend proportions is shown in Tables 6.24 and 6.25 with regard to alkylbenzenes and polycyclics respectively.

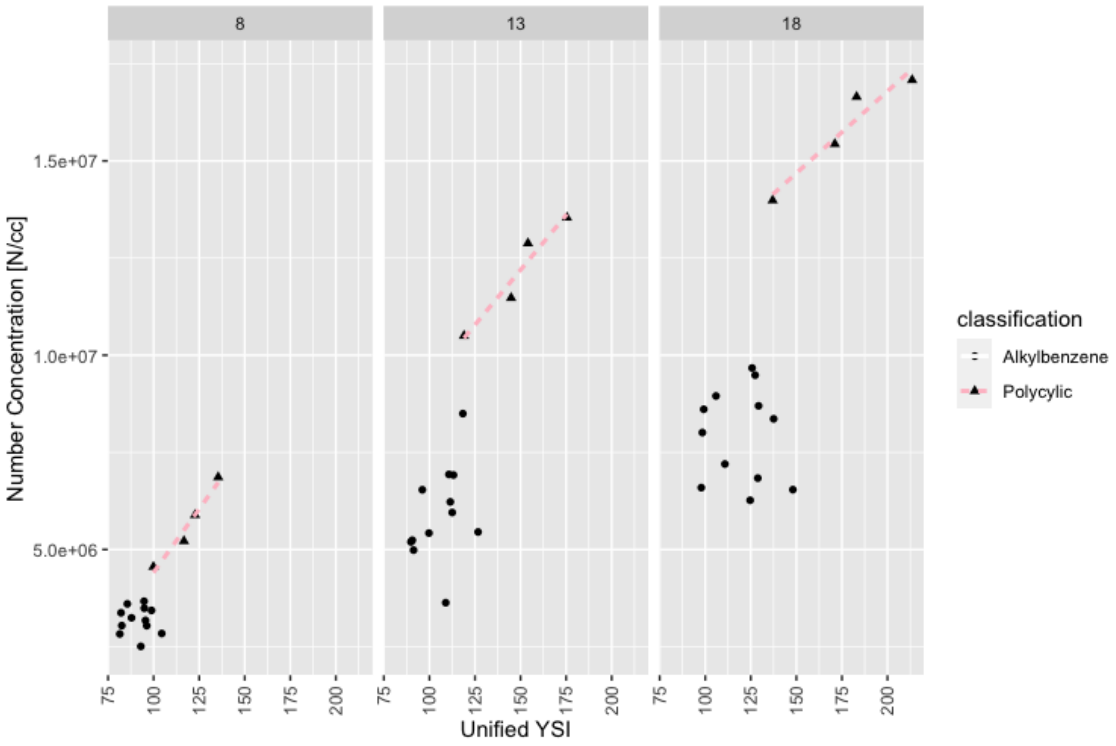

Figure 6.10.1: Scatter chart of YSI against number concentration at 8%, 13% and 18% vol/vol

Table 6.24: Unified YSI PM Statistical Results for Alkylbenzenes

Aromatic Content [vol/vol %]	8	13	18
r	-0.04621	0.3818	-0.06409
R-squared	0.002135	0.1458	0.004108
p-value	0.8866	0.2206	0.8431

Table 6.25: Unified YSI PM Statistical Results for Polycyclics

Aromatic Content [vol/vol %]	8	13	18
r	0.9792	0.9636	0.9607
R-squared	0.9588	0.9285	0.9229
p-value	0.02084	0.03643	0.03935

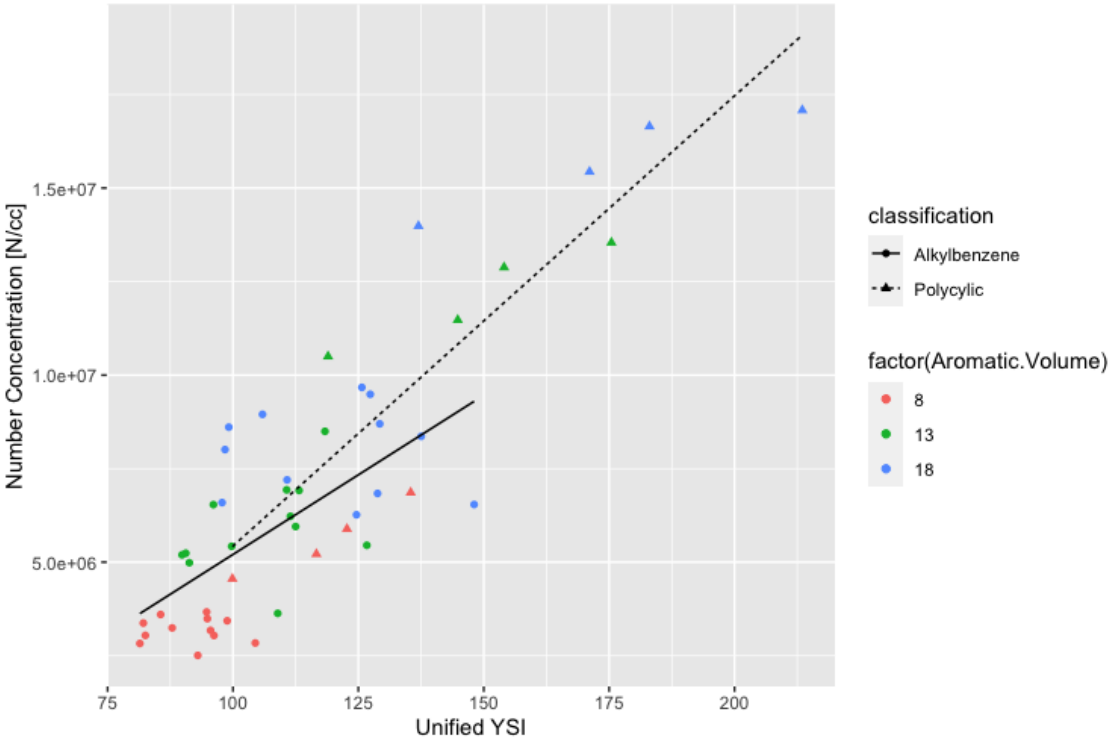

Figure 6.10.2: Scatter chart of YSI against number concentration for all data points

A table including regressions statistics for all three models is shown in Table 6.26 and coefficients of the accompanying regression equations is shown in Table 6.27.

Table 6.26: Unified YSI PM Number Statistical Results

	Multiple R	*R-squared*	*Adjusted R-squared*	*RMS Error*
Unified	0.8680	0.7535	0.7481	1.892×10^6
Alkylbenzenes	0.6503	0.4229	0.4059	1.700×10^6
Polycyclics	0.8738	0.7636	0.7400	2.310×10^6

Table 6.27: Unified YSI PM Number Regressions Equations

Classification	$Y = mx + c$	*Linear Regression*	*Standard Error*	*tStat*	*P-Value*
Unified	c	-6331859	1161439	-5.452	1.90×10^{-6}
	m	115290	9724	11.857	1.38×10^{-15}
Alkylbenzene	c	-3305082	1822291	-1.814	0.0786
	m	85117	17054	4.991	1.76×10^{-5}
Polycyclic	c	-6599029	3196971	-2.064	0.065927
	m	120311	21167	5.684	0.000203

Unified YSI correlates weakly with PM Number Concentration strongly for alkylbenzenes at 13% (r=0.3818) and shows no degree of statistical correlation at 8% and 18% (r=-0.04621, r=-0.06409). Unified YSI correlates strongly with PM Number Concentration for polycyclics at all blend proportions (r=0.9792, 0.9636, 0.9607). Coefficients of determination are week for alkylbenzenes (0.0021, 0.1458, 0.004) and strong for polycyclics (0.9588, 0.9285, 0.9229). No p-value for any classification or blend proportion meets the threshold of statistical significance for this metric.

Irrespective of blend proportion, Unified YSI correlates with PM Number Concentration moderatly for alkylbenzenes (r=0.6503), strongly for polycyclics (0.8738) and strongly irrespective of classification (0.8680). Coefficients of determination are moderate for alkylbenzenes (0.4229), strong for polycyclics (0.8738) and strong irrespective of classification (0.8680).

Unified YSI shows mixed performance as a predictor of PM Number Concentration. It shows strong regression performance when volume proportion is not taken into account but performs poorly in predicting the performance of alkylbenzenes at a given blend proportion. Similar to global density, however, the regression equations, while not being coincident, are similar, suggesting that this metric may be reflecting deterministic qualities common to both classifications.

6.11 Multivariate Modelling

The selection of variables to include in a multi-variate model used to predict PM Number Concentration emissions for this data-set requires careful consideration. An objective of this thesis is to not erroneously attribute significance to or include variables erroneously rather than identify confounders that are actually deterministic in describing and predicting PM emissions. Including every variable discussed is not statistically robust as it will lead to an over-fitted model, and without a subsequent campaign to validate the findings of such a model on novel data, the findings would be spurious. It would also be inappropriate to include variables that have been found to be logically or categorically inconsistent, as discussed in Section 6.1. It is appropriate however, to construct the multi-variate model initially using every variable and then selectively exclude each based on its contribution or lack thereof. The model is trained on every data point without categorising by classification. The suitability of each model to each classification is refined and separated however at the end of this section.

The initial model includes the eight variables discussed and analysed in this chapter; Aromatic Volume Percentage, Aromatic Mass Percentage, Global Density, Ring Carbon Percentage, Hydrogen Content, Aggregate TSI, Aggregate NSP, and Aggregate Unified YSI. For this initial model, three variables; Aromatic Volume Percentage, Aromatic Mass Percentage and Ring Carbon Percentage are found to be of no statistical significance due to high p-values (p=0.7691, p=0.8198, p=0.8749) which are above the p=0.05 threshold. It should be noted that this initial model shows a high adjusted adjusted coefficient of determination (0.9593), which shows, despite the inclusion of a large number of variables, that when accounted for, this model is generally accurate at predicting the data it's based on. It is however, considered to be over-fitted at this point.

The second model omits one variable; Hydrogen Content as it's p-value does not meet the threshold for significance and is also excluded due to its weak coefficients of determination for alkylbenzenes as shown in Table 6.8. The four remaining variables all meet the threshold of statistical significance with every all of them having a p-value less than p=0.05. The adjusted coefficient of determination remains strong at 0.9606, suggesting the omission of this variable is appropriate due to its lack of

significance.

The third model uses global density, blend TSI, blend NSP and Unified YSI as variables. This creates a regression model with three empirical coefficients. Each empirical coefficient is modelled exclusively with global density in a bi-variate model and the performance is assessed. A model using global density and aggregate TSI returns a p-value for TSI above the threshold of significiance (0.91). A model using global density and aggregate NSP also returns a p-value above the threshold of significance (0.294). In a model using global density and Unified YSI, however, both variables feature p-values significantly that meet the threshold of significance (p¡0.05) and form the coefficients of the final model.

The predicted versus actual response for the final model is shown in Figure 6.11.1 and the standardised residuals with respect to every data point is shown in Figure 6.11.2.

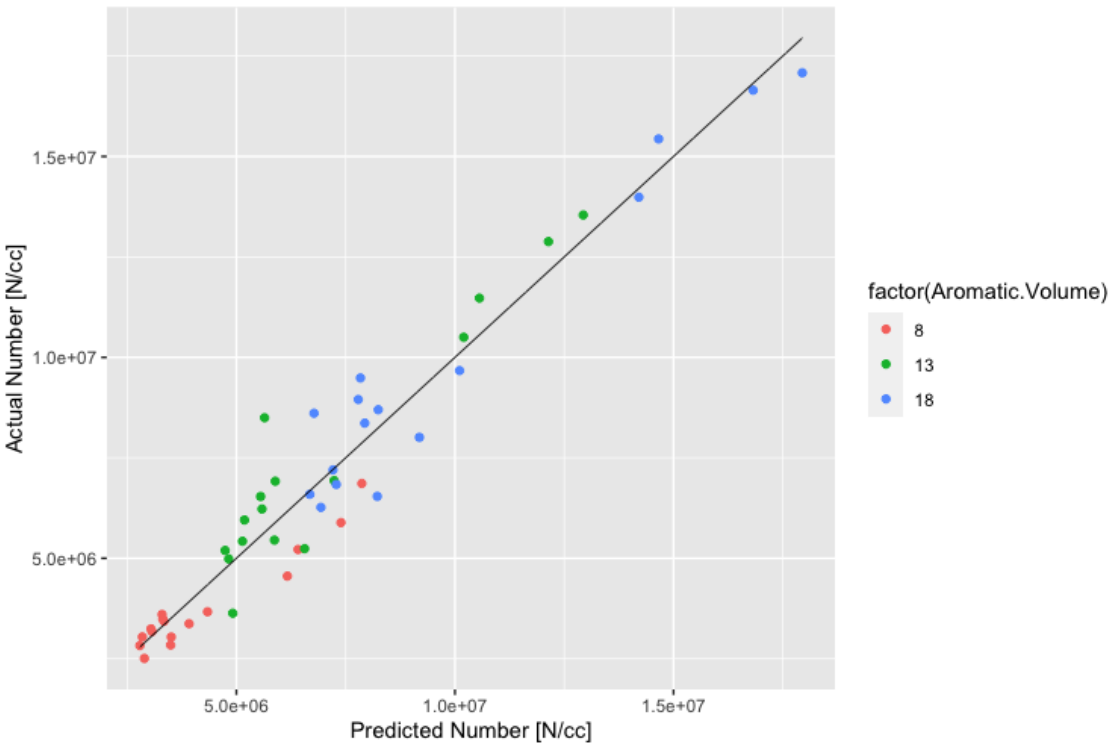

Figure 6.11.1: Scatter plot showing predicted PM and actual PM for all blends

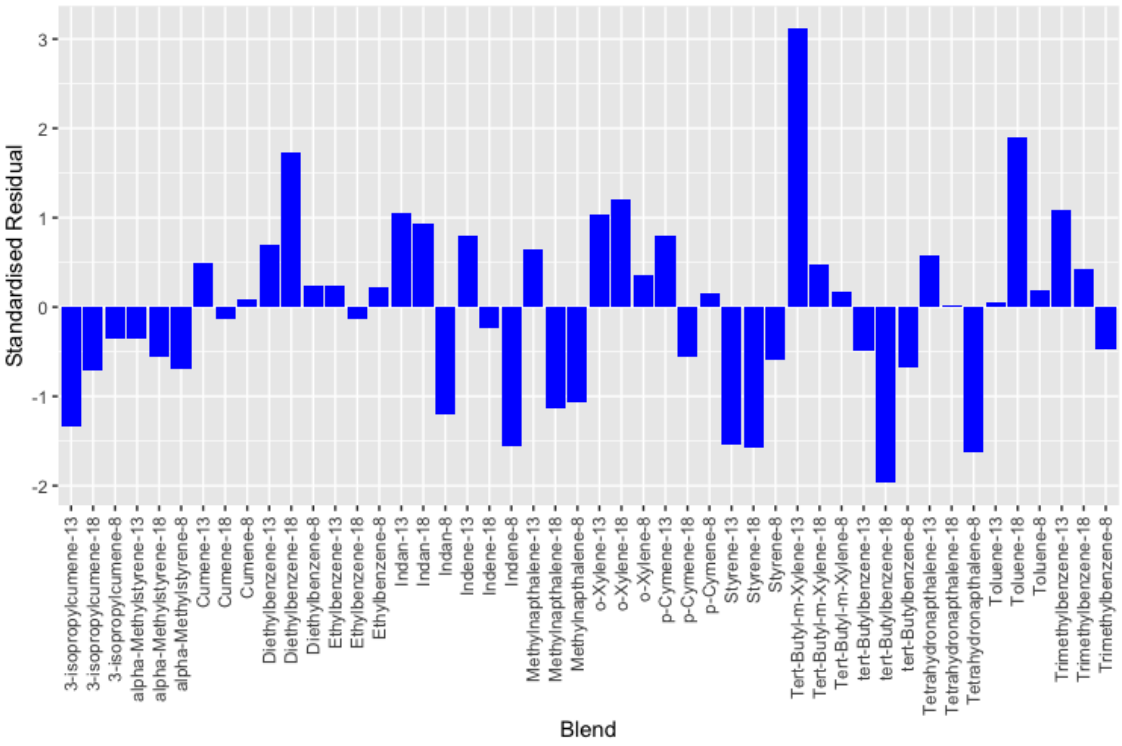

Figure 6.11.2: Scatter plot showing standardised resiudals for each blend for all blends

The general form of the final model is shown in Equation 6.1 including variables for global density, Unified YSI and an intercept value.

$$PM_{conc} = a.\rho_g + b.YSI + c \tag{6.1}$$

The coefficients from the final model are included in Equation 6.4.

$$PM_{conc,unified} = 3.295 \times 10^8 \rho_g + 2.7153 \times 10^8 .YSI - 2.524 \times 10^8 \tag{6.2}$$

The model shows good agreement between predicted and actual values as the model accounts for between 94.0% and 93.7% of the variability in the data. The positive coefficients of each variable are logically consistent with observations, as an increase in either should cause an increase in PM emissions conceptually, as demonstrated. In terms of residuals, if an outlier is considered to have a standardised residual of 3 or higher, Tert-Butyl-m-Xylene at 13% is the only one.

In terms of dividing the data by classification into alkylbenzenes and polycyclics, two further models are proposed for each. The first for alkylbenzenes takes the same general form as Equation 6.1 and the coefficients for which are shown in Equation 6.4.

$$PM_{conc,alkylbenzene} = 3.238 \times 10^8 \rho_g + 2.8580 \times 10^8 .YSI - 2.481 \times 10^8 \tag{6.3}$$

The model for polycyclics retains the Unified YSI term for the general form shown in Equation 6.1 with coefficients being shown in Equation 5.5.

$$PM_{conc,polycyclic} = 3.295 \times 10^8 \rho_g + 2.7153 \times 10^8 .YSI - 2.524 \times 10^8 \tag{6.4}$$

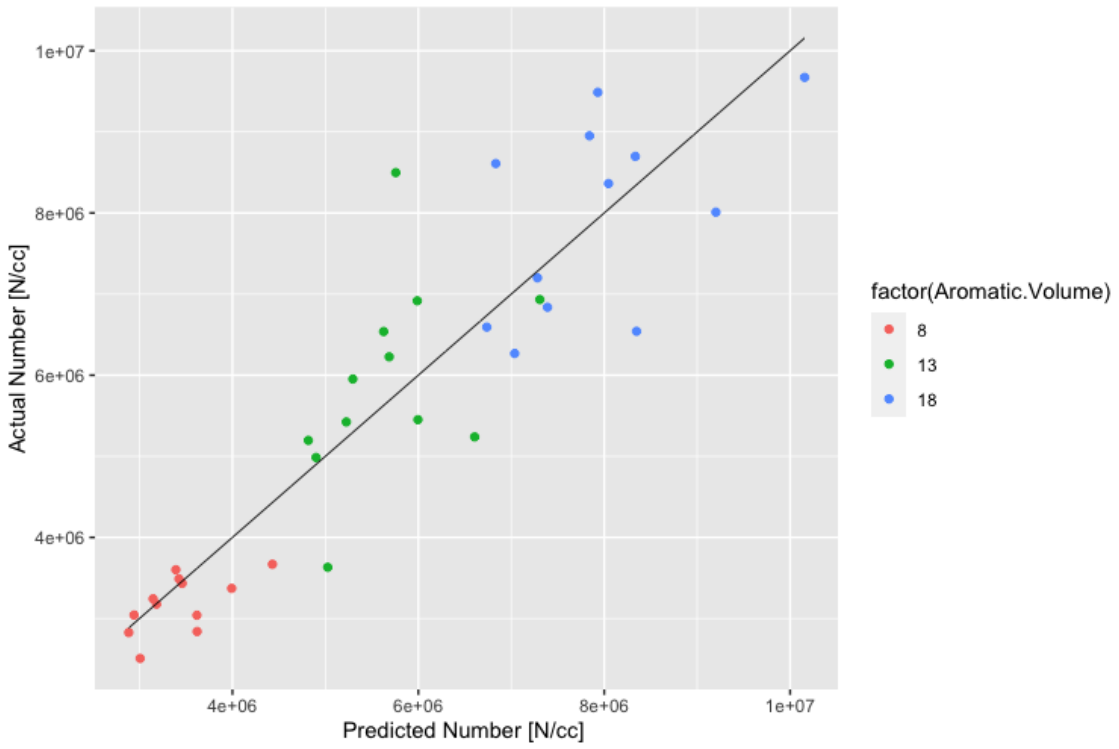

Figure 6.11.3: Scatter plot showing predicted PM and actual PM for alkylbenzenes

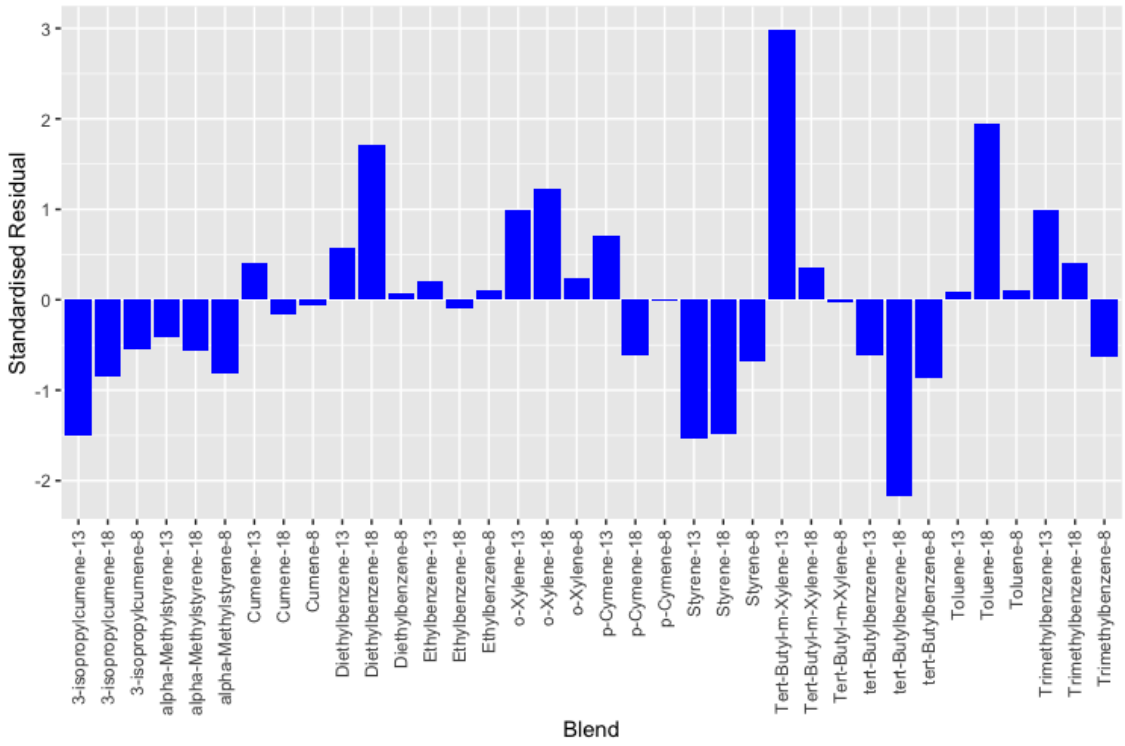

Figure 6.11.4: Scatter plot showing standardised resiudals for each blend for alkylbenzenes

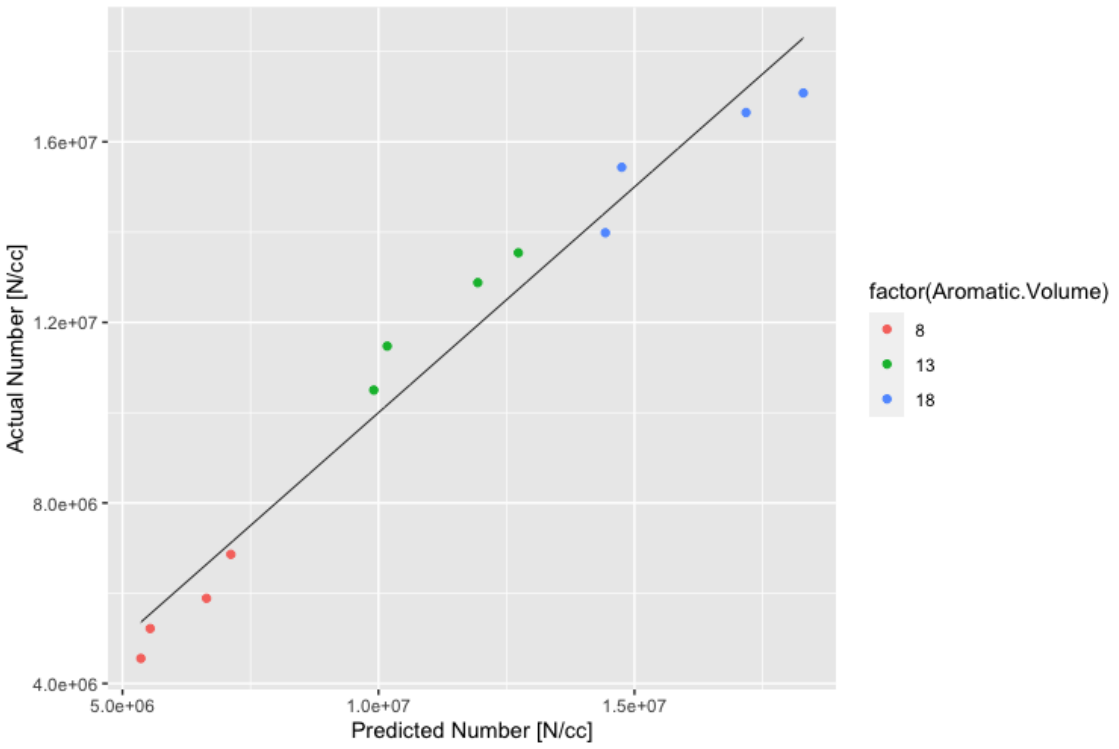

Figure 6.11.5: Scatter plot showing predicted PM and actual PM for polycyclics

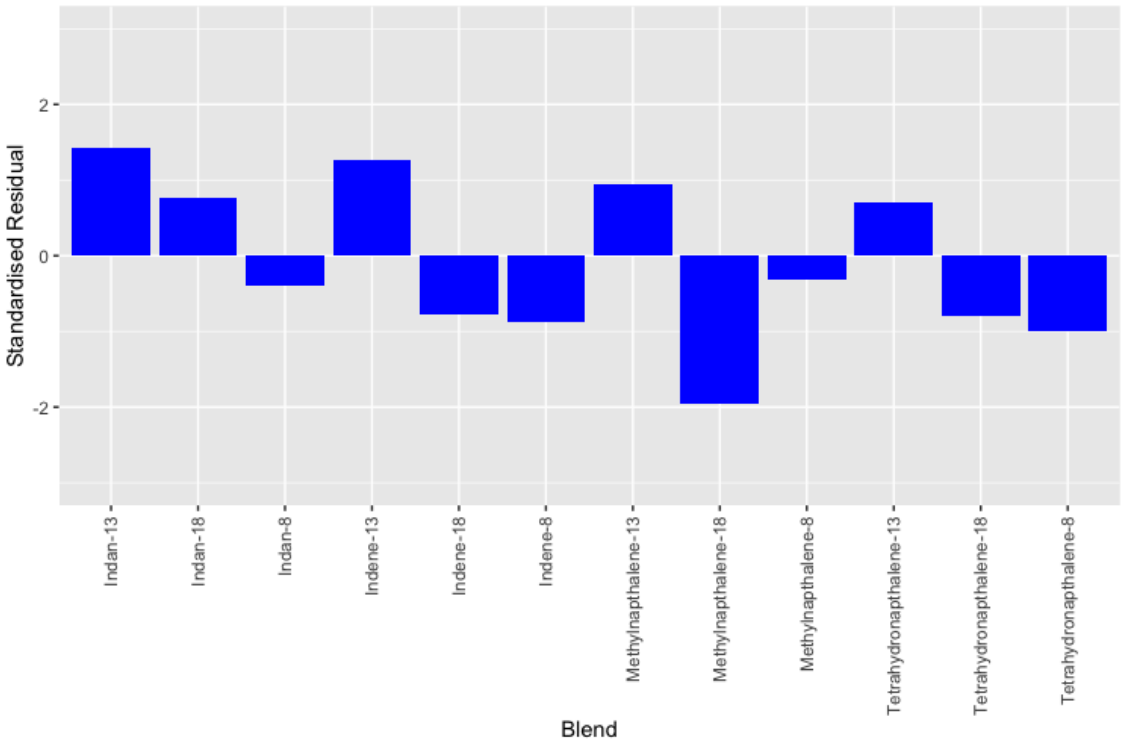

Figure 6.11.6: Scatter plot showing standardised resiudals for each blend for polycyclics

The predicted versus actual response for the final model for alkylbenzenes is shown in Figure 6.11.3 and the standardised residuals with respect to every data point is shown in Figure 6.11.4.

The predicted versus actual response for the final model for polycyclics is shown in Figure 6.11.5 and the standardised residuals with respect to every data point is shown in Figure 6.11.6.

A statistical summary for the three models generated are shown in Table 6.28.

Table 6.28: Multivariate PM Statistical Results

	p-value	*R-squared*	*Adjusted R-squared*	*RMS Error*
Unified	2.687×10^{-13}	0.9396	0.9369	946900
Allylbenzenes	2.089×10^{-7}	0.9672	0.9599	906800
Polycyclics	2.200×10^{-16}	0.9396	0.9369	946900

There is strong agreement between predicted and actual values for the alkylbenzene category ($r^2 = 0.9672$). As with the unified model, the only true outlier with a standardised residual above three is Tert-Butyl-m-Xylene at 13% volume. There is strong agreement between predicted and actual values for the polycyclic category ($r^2 = 0.9396$). All three models show similar performance and similar RMS errors for alkylbenzenes (906,800), polycyclics (946,900) and without dividing by classification (945,000).

Chapter 7

Conclusion

7.1 BC Mass vs PM number Concentration

This Section compares the experimental results shown in Chapters 5 and 6. The BC mass concentration and PM number concentration campaigns were conducted separately using different blend proportions of aromatic. The highest proportion aromatic blend group (22.5% vol/vol) has been omiited as there is not a DMS group with as high a proportion of aromatic. This leaves the 7.5%, 12.5% and 17.5% aromatic blend group for the LII campaign and the 8%, 13% and 18% aromatic blend group for the DMS campaign. As Indene, tert-Butylbenzene and tert-Butyl-m-Xylene were unavailable for the LII campaign, their mass concentration data has been approximated using Equation 5.1 from Chapter 5.

The resulting data was first normalised using Equation 7.1 for the mass concentration data and Equation 7.2 for the DMS data, where $m_{c,norm}$ and $n_{c,norm}$ are the normalised mass and number concentrations, $m_{c,i}$ and $n_{c,i}$ are the mass and number concentrations of individual data points, and $\overline{m}_c$ and $\overline{m}_c$ are the mean mass and number concentrations of all the data, respective to each campaign.

$$m_{c,norm} = \frac{m_{c,i} - \overline{m}_c}{\overline{m}_c} \tag{7.1}$$

$$n_{c,norm} = \frac{n_{c,i} - \overline{n}_c}{\overline{n}_c} \tag{7.2}$$

The resulting normalised data for both campaigns is shown in Figure 7.1.1. The

7.5% LII and 8% DMS blend groups are now labelled as Low Aromatic Proportion, the 12.5% LII and 13% DMS blend groups are now labelled as Medium Aromatic Proportion and the 17.5% LII and 18% DMS blend groups are now labelled as High Aromatic Proportion.

There is a strong positive correlation between mass and number concentrations of BC and PM, respectively, with an coefficient of determination of 0.8874. The relationship appears to be linear, although not directly proportional, with a gradient of 1.241, suggesting that am increase in the mass concentration of BC is accompanied by a proportionally larger increase in PM number concentration.

In terms of individual data points, it appears that the PM number concentration values are high for tert-Butyl-m-Xylene at the Medium Aromatic Proportion (13% DMS blend group) and Toluene at the High Aromatic Proportion (17.5% LII blend group). Tert-Butylbenzene and tert-Butyl-m-Xylene appear to have low mass concentrations according to the trend, although it should be noted that moth of these values were generated by Equation 5.1 and may be underestimated. The general trend, however, suggest that an increase in mass concentration of BC is accompanied by an increase in number concentration of PM, along with an increase in the GMD of PM particles, according to Figure 6.3.1

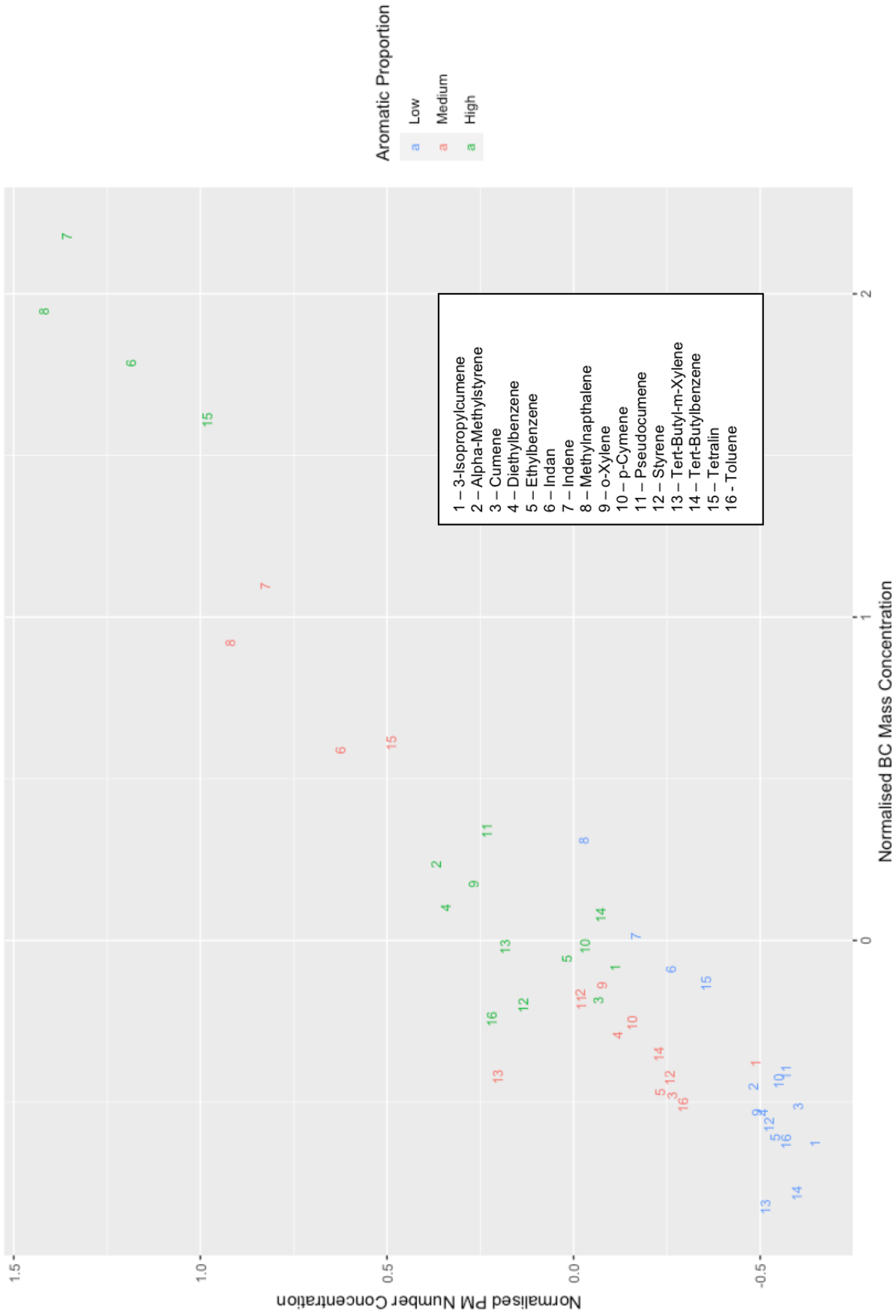

Figure 7.1.1: Normalised BC Mass Concentration vs PM Number Concentration Scatter Plot

7.2 Summary

The aim of this thesis was to investigate the role that the aromatic content of jet fuels play in the formation of carbonaceous particulate matter emissions. Aromatics are a necessary component of Jet-fuel, and may be for the foreseeable future. As such, it is important to develop a greater understand of their composition on the formation of black carbon and soot.

The novelty of the completed research is based on its analysis of a comprehensive range of aromatic surrogate fuels tested in an aerospace context and the impact of the presence of different species on soot formation and characterisation in terms of PM mass, size and number. While in the literature, individual aromatic species have been assessed individually to determine their YSI and TSI, limited work has been conducted in the context of aviation fuel surrogates on a comprehensive range of fuels. The current literature and specification are ambiguous as to which fuel parameter is the strongest indicator of a fuels propensity to produce soot, with hydrogenmass percentage, smoke point and aromatic or naphthalene content all suggested as significant contributors. This thesis will provide further clarification by comprehensively investigating the contribution of the aromatic component. As aromatic content is required in order to induce seal swell in fuel lines, it is also of interest to provide suggestions for the optimal aromatic species to dope Low-Aromatic-Content-Fuel for optimisation.

The findings of this thesis can be summarised as follows:

- The introduction comprehensively looked at the practical and regulatory issues concerning the aromatic component of Jet Fuel. It was established that this component is the only type of hydrocarbon that is limited by the specifications governing the production of Jet Fuel, with that limit currently being 25%. The role of kerosene in Gas Turbine Engines for aviation propulsion was discussed, and the conceptual framework governing the production of incomplete combustion, leading to PAH, and ultimately, soot and black carbon production. The use of Smoke Point to measure a given fuel's propensity to produce visible soot was introduced. The context of aromatics on the production of alternative fuels was discussed, as currently there are no approved production

pathways that lead to fuel where aromatics are a significant component of the final product. As aromatics are required in order to improve the energy density of Jet Fuel and as a promoter of seal swell moving forwards, their inclusion, either via production or addition to Sustainable Alternative Fuel, as Aromatic Sustainable Alternative Fuel, is a possibility. It was concluded as necessary then, to propose experimental campaigns to ascertain which individual aromatic molecules lead to low levels of particulate matter emissions in terms of mass, size and number concentration, and which are worthy of consideration as potential compoents of inclusion. The importance of minimising particulate emissions and its deleterious effects on health and the environment, was briefly outlined.

- A literature review was undertaken with a specific emphasis on researching three components; the contemporary understanding of the mechanisms leading to soot formation, the current experimental methodology used to characterise and compare a given fuel blend, or individual components propensity to produce soot, and a look at several experimental campaigns conducted at pilot or industrial scale where varying the aromatic component or volume of the fuel was a point of interest. Soot production was found to be fundamentally related to the production of Polycyclic Aromatic Hydrocarbons in the initial stages of product formation following pyrolysis. Contemporary understanding of PAH inception is related to a few specific mechanisms namely, the Hydrogen Ablation Acetylene Addition mechanism, related to the rate of acetylene free radical as a kinetic route to form phenyl-rings, and pheynyl poymeristaion, where intact phenyl-rings that stay intact during pyrolysis effectively polymerise to form larger, multi-ring PAH strutures. Four contemporary lab scale tests are currently used to characterise soot production of fuels and components; the Smoke Point, Threshold Sooting Index, Normalised Smoke Point and Yield Sooting Index. The advantages and disadvataged of each are discussed and it was found that Unified YSI's were of significant interest and perhaps produced the most robust results, although there was increased variability of predictive models for aromatics. Pilot and industral scoipe campaigns typically tested a small range of aromatics on various combustion platforms, with various metrics

of interest suggested, such as ring carbon and hydrogen content. A knowledge gap was established as to which metric is most appropriate to categorise the black carbon production propensity when aromatic components of aviation fuel was a concern.

- Access to specification testing data from 2014 was made available to the LCCC in 2018. This data contained the test results for every variable in the DEF STAN 91 specification requirements for Jet A-1. This encompased all fuel produced in and imported to the UK in 2014. In the absence of comprehensive literature concerning aromatics, analysis of this data set provided key insights into the role of aromatic volume in specification tetsing, in the hopes of providing insight into optimum composition and vairables of interest in minimising black carbon emissions from potnential ASAF's. Very weak correlations were found between SP's and aromatic content in terms of volume. Weak correlations were also found when the type of aromatic was limited to napthalenes. Density, however, was found to have the strongest correlation of any variable in predicting smoke points. Density was found to be nearly perfectly prescriptive in predicting whether a given sample would pass or fail its initial SP test ($SP < 25$). This was potentially attributed to the presence of a aromatics of a comparatively higher density, an increased proportion of cycloaromatics, or even a higher proportion of cycloparaffins, which have a high component density but would not be reflected in aromatic volume testing. Novel Principal Component Analysis was conducted in order to minimise and non-dimensionalise the variables determining the overall variance of the dataset. Three principal components were found to account for the variance of 60% of the data, and after correlating these three components with the original variables, were found to be nearly totally prescriptive of a fuels SP. Again, aromatic volume did not correlate well, although density did. It was concluded that density would be a metric of interest moving forwards without being attributed causality spuriously without further testing.

- An experimental campaign was conducted at the LCCC, university of Sheffield where 13 aromatics were blended at 4 proportions representing the typical composition of Jet Fuel (7.5%, 12.5%, 17.5% and 22.5%). These 10 alkylbenznes,

2 cyclo-aromatics and one naphthalene were burnt in a Rolls Royce Tay single can combustor rig at atmospheric pressure and constant AFR of 100:1. The black carbon mass emissions were measured using Laser Induced Incandescence at the engine exhaust. In every case, it was found that multi-ring aromatics produced more BC mass in a given blend proportion than alkylbenzenes within the same group. For Alkylbenzenes, it was generally observed that singly substituted aromatics produced the lowest BC, the doubly substitute and finally triply substituted, in agreement with prior literature. The exception to this was Styrene. In terms of metrics of interest, only global density, hydrogen to carbon ratio and Unified YSI were of statistical significance. H/C was omitted as a strong potential candidate however, due to the suggestion in the data that alkylbenzenes had higher BC production as HC increased. Multi-variate regression analysis including global density and Unified YSI as variables found excellent agreement between predicted and actual values of BC mass concentration.

- An experimental campaign was conducted at the LCCC, university of Sheffield where 16 aromatics were blended at 3 proportions representing the typical composition of Jet Fuel (8%, 13% and 18%). These 13 alkylbenznes, 3 cyclo-aromatics and one naphthalene were burnt in a Rolls Royce Tay sing can combustor at atmospheric pressure and constant AFR of 200:1.5. The PM emissions were measured using a Differential Mobility Spectrometer in order to obtain the number concentration and size distribution of PM emissions. In every case, it was found that multi-ring aromatics produced a higher PM number concentration at given blend proportion that their alkylbenzene counterparts. In terms of metrics of interest, only global density, hydrogen to carbon rataio and Unified YSI were of statistical significance. Hydrogen Content was omitted as a strong potential candidate however, due to the suggestion in the data that alkylbenzenes had higher BC production as HC increased. Multi-variate regression analysis including global density and Unified YSI as variables found excellent agreement between predicted and actual values of BC. There was strong correlation between the Geometric Mean Diameter and total number concentration of each sample. This was then shown to be consistent with mass

concentration results; PM size and number concentration correlate strongly to BC mass concentration.

7.3 Future Work

While this thesis represents a substantial piece of work, the potential for future work became apparent at several points during its development. Suggestions for future researchers are as follows:

- The aromatics selected for experimentation for this thesis were limited in scope by affordability and practicality. Aromatic components are expensive in isolation and the prospective researcher is limited to certain aromatics as they need to be burnt in such amounts that the price becomes prohibitive. It may be possible to obtain a wider range of aromatics that would be otherwise affordable through lab chemistry. Should smaller amounts become available in may be beneficial to use a pilot scale combustion platform that is more applied to an aerospace context without requiring as much fuel as a RR Tay Combustor or APU. The aromatics selected for this work were also limited to species that are liquid at room temperature. This was a necessity to ensure that each could be blended to the volumetric proportion required to be homogeneous across the blends. Aromatic species that are solid at room temperature have a higher molecular mass, and so the selection of liquid aromatics essentially biased this thesis toward aromatics at the lower end of the boiling range distribution of kerosene. It is possible, however, to dissolve solid aromatics in a parrafinic solvent such as the BannerSol used in this thesis. Doing so, however, requires substantial work to be done on solubility limits.

- The experimental campaigns conducted for this thesis took place at atmospheric pressure. This approach is sub-optimal, however, as it does not account for the substantial influence of pressure on PM formation. A complementary campaign could be conducted using the fuels used in this thesis at typical pressured found in Jet Engines. While colleagues at the LCCC have conducted complementary work to this at pressure on Compression Ignition Engines [112, 113, 114], this is a fundamentally different mode of combustion compared to gas turbine usage.

- The experimental campaigns conducted for this thesis took place using a uniform non-aromatic component, essentially comprised of straight chain alkanes.

It would be of interest to vary the composition of the paraffinic component to include more diverse components in order to assess the impact on BC and performance when using aromatics in the manner used in this theis. Of particular interest would be the effect and roll of cyclo-paraffins. If the suggestions of the thesis have merit; that global density of fuel is an important factor in the generation of BC, then cyclo-paraffins may have a substantial impact of PM formation and emissions. It would also be of interest to blend aromatics with existing SAF's, particularly LACJF with low or no aromatic content.

- No consideration has been given to economical production pathways to any of the aromatics contained in this thesis. The practicalities of obtaining substantial quantities of aromatics of interest would be of significant interest to researchers and OEM's.

Bibliography

[1] I. C. A. Authority, "Trends and scenarios on alternative fuels," *CONFERENCE ON AVIATION AND ALTERNATIVE FUELS*, vol. Agenda Item 4: Defining the ICAO vision on aviation alternative fuels and future objectives, 2017.

[2] R. Striebich, S. LM, W. ZJ, and Z. S, "A comparison of thermal and flow modulation gcxgc with dual fid-ms for aviation fuels," *Gulf Coast Conference*, 2018.

[3] A. Liati, B. T. Brem, L. Durdina, M. Vögtli, Y. Arroyo Rojas Dasilva, P. Dimopoulos Eggenschwiler, and J. Wang, "Electron microscopic study of soot particulate matter emissions from aircraft turbine engines," *Environmental Science & Technology*, vol. 48, no. 18, pp. 10 975–10 983, 2014, pMID: 25180674. [Online]. Available: https://doi.org/10.1021/es501809b

[4] A. International, "Standard test method for smoke point of kerosene and aviation turbine fuel," *ASTM*, vol. ASTM D 1322, 2018.

[5] C. Lieuwen and V. Yang, *Gas Turbine Emissions*. Cambridge University Press, 2013.

[6] "Icao annex 16 volume ii - 5th edition," ICAO, Tech. Rep., 2023.

[7] A. International, "Life-cycle analysis of alternative aviation fuels in greet," *ASTM*, no. ANL/ESD/12-8, 2012.

[8] I. P. on Climate Change, *Anthropogenic and Natural Radiative Forcing*. Cambridge University Press, 2014, p. 659–740.

[9] Z. A. Kanji, L. A. Ladino, H. Wex, Y. Boose, M. Burkert-Kohn, D. J. Cziczo, and M. Krämer, "Overview of ice nucleating particles," *Meteorological Monographs*, vol. 58, pp. 1.1 – 1.33, 2017. [Online]. Available: https://journals.ametsoc.org/view/journals/amsm/58/1/amsmonographs-d-16-0006.1.xml

[10] M. Ali, G. Liu, B. Yousaf, H. Ullah, Q. Abbas, and M. A. M. Munir, "A systematic review on global pollution status of particulate matter-associated potential toxic elements and health perspectives in urban environment," *Environmental geochemistry and health*, vol. 41, no. 3, p. 1131–1162, 2019.

[11] R. Pugmire, Shihong, and R. Gill, "The effects of molecular structure on soot formation ii. diffusion flames," *Combustion and Flame*, vol. 62, no. 1, pp. 43–60, 1985. [Online]. Available: https://www.sciencedirect.com/science/article/pii/0010218085900926

[12] S. G. Davis, A. V. Joshi, H. Wang, and F. Egolfopoulos, "An optimized kinetic model of h2/co combustion," *Proceedings of the Combustion Institute*, vol. 30, no. 1, pp. 1283–1292, 2005. [Online]. Available: https://www.sciencedirect.com/science/article/pii/S0082078404003054

[13] L. Li and P. B. Sunderland, "An improved method of smoke point normalization," *Combustion Science and Technology*, vol. 184, no. 6, pp. 829–841, 2012. [Online]. Available: https://doi.org/10.1080/00102202.2012.670333

[14] M. Colket, J. Heyne, M. Rumizen, M. Gupta, T. Edwards, W. M. Roquemore, G. Andac, R. Boehm, J. Lovett, R. Williams, J. Condevaux, D. Turner, N. Rizk, J. Tishkoff, C. Li, J. Moder, D. Friend, and V. Sankaran, "Overview of the national jet fuels combustion program," *AIAA journal*, vol. 55, no. 4, pp. 1087–1104, 2017.

[15] D. Naegeli and C. Moses, "Effect of fuel molecular structure on soot formation in gas turbine engines," *Gas Turbine Conference and Products Show*, vol. American Society of Mechaical Engineers, 1979.

[16] "MS Windows NT kernel description," https://ysi.ml.nrel.gov/, accessed: 2022-10-30.

[17] "Cambustion dms 500 animation," https://www.cambustion.com/products/knowledgebase/dms-animation, accessed: 2023-12-5.

[18] C. Corporation, "Aviation fuels technical review," 2007.

[19] "Alternative fuels data center," in *U.S. Department of Energy*. Energy Efficiency Renewable Energy. [Online]. Available: https://afdc.energy.gov/fuels/sustainable˙aviation˙fuel.html

[20] S. Blakey, C. W. Wilson, M. Farmery, and R. Midgley, "Fuel effects on range versus payload for modern jet aircraft," *The Aeronautical Journal*, vol. 115, no. 1172, p. 627–634, 2011.

[21] S. G. C. Insights, "Global jet fuel recovery lags air travel as flights return to pre-pandemic levels," 2023.

[22] I. A. of Air Transport, "Economic performance of the airline industry - international forecast," *IATA*, 2018.

[23] BOEING, "Current market outlook 2015-2034," 2015.

[24] Airbus, "Global market forecast - flying by numbers 2015-2034," 2015.

[25] I. P. on Climate Change, "Ipcc special report - aviation and the global atmosphere," 1999.

[26] I. C. A. Organisation, "Aviation and climate: An update," *ICAO Global Aviation Partnerships on Emission Reductions (E-GAP) Seminar*.

[27] "Alternative aviation fuels: Overview of challenges, opportunitiesand next steps," *Office of Energy Efficiency and Renewable Energy (EERE)*, 2017.

[28] A. International, "Astm d7566-18 standard specification for aviation turbine fuel containing synthesised hydrocarbons," *West Conshohocken, PA*, 2018.

[29] A. T. A. Group, "Beginner's guide to sustainable aviation fuel," 2017.

[30] A. Prüss-Üstün, J. Wolf, C. F. Corvalán, R. Bos, and M. P. Neira, *Preventing disease through healthy environments: a global assessment of the burden of disease from environmental risks*. World Health Organization, 2016.

[31] T. Bond, S. Doherty, D. Fahey, P. Forster, T. Bernsten, B. DeAngelo, M. Flanner, K. B. Ghan, S, D. Koch, S. Kinne, and Y. Kondo, "Bounding the role of black carbon in the climate system: A scientific assessment," *Journal of Geophysical Research*, vol. 118, 2013.

[32] P. Lobo, B. Christie, B. Khandelwal, S. Blakey, and D. Raper, "Evaluation of non-volatile particulate matter emission characteristics of an aircraft auxiliary power unit with varying alternative jet fuel blend ratios," *Energy and Fuels*, vol. 29, 2015.

[33] R. WA, "Multidimensional high resolution gas chromatography investigation of hydrocarbon fuels and various turbine engine fuel precursors," *Air Force Wright Aeronautical LAboratories*, vol. AFWAL-85-TR-2033, 1985.

[34] A. International, "Standard test method for hydrocarbon types in liquid petroleum products by fluorescent indicator adsorption," *ASTM*, vol. ASTM D1319-02, 2021.

[35] U. M. of Defence, "Turbine fuel, kerosine type, jet a-1, nato code f-35; joint service designation: Avtur 2019," *Def Stan*, vol. 91-091, no. 10, 2019.

[36] G. Liu, L. Wang, H. Qu, H. Shen, X. Zhang, S. Zhang, and Z. Mi, "Artificial neural network approaches on composition–property relationships of jet fuels based on gc–ms," *Fuel*, vol. 86, no. 16, pp. 2551–2559, 2007. [Online]. Available: https://www.sciencedirect.com/science/article/pii/S001623610700097X

[37] A. International, "Standard specification for aviation turbine fuels," *ASTM International*, vol. D1655-18b, 2019.

[38] J. Ströhle and T. Myhrvold, "An evaluation of detailed reaction mechanisms for hydrogen combustion under gas turbine conditions," *International Journal of Hydrogen Energy*, vol. 32, no. 1, pp. 125–135, 2007. [Online]. Available: https://www.sciencedirect.com/science/article/pii/S0360319906001716

[39] J. Olfert and S. Rogak, "Universal relations between soot effective density and primary particle size for common combustion sources," *Aerosol Science*

and Technology, vol. 53, no. 5, pp. 485–492, 2019. [Online]. Available: https://doi.org/10.1080/02786826.2019.1577949

[40] M. Schenk, N. Hansen, H. Vieker, A. Beyer, A. Gölzhäuser, and K. Kohse-Höinghaus, "Pah formation and soot morphology in flames of c4 fuels," *Proceedings of the Combustion Institute*, vol. 35, no. 2, pp. 1761–1769, 2015. [Online]. Available: https://www.sciencedirect.com/science/article/pii/S1540748914002971

[41] H. Shahad, "An experimental investigation of soot particle size inside the combustion chamber of a diesel engine," *Energy Conversion and Management*, vol. 29, no. 2, pp. 141–149, 1989. [Online]. Available: https://www.sciencedirect.com/science/article/pii/019689048990023X

[42] B. Chemical. Np-1014. [Online]. Available: http://www.bannerchemicals.com/product/banner-np-1014

[43] E. Institute, "Petroleum products - determination of the smoke point of kerosine," vol. IP 57, 2013.

[44] A. International, "Standard test method for napthalene hydrocarbons in aviation turbine fuels by ultraviolet spectrophotometry," *ASTM*, vol. ASTM D 1840, 2017.

[45] C. D. Manos HF, "Effect of molecular structure on incipient soot formation," *Combustion and Flame*, vol. 49, 1983.

[46] M. L. Pfefferle C, "Sooting tendancies of nonvolatile aromatic hydrocarbons," *Proceeding of the combustion institute*, vol. 32, 2009.

[47] M. L. Pfefferle CS, "Improved sooting tendancy measurements for aromatic hydrocarbons and their implications for napthalene formation pathways," *Combustion and Flame*, vol. 148, 2007.

[48] "Introduction to the icao engine emissions databank," *European Union Aviation Safety Agency*, 2020.

[49] "Icao circular 344," *International Civil Aviation Organistation*, 2015.

[50] "Icao annex 16 volume ii - 1st edition," ICAO, Tech. Rep., 2017.

[51] A. de Klerk, "Chapter 10 - aviation turbine fuels through the fischer–tropsch process," in *Biofuels for Aviation*, C. J. Chuck, Ed. Academic Press, 2016, pp. 241–259. [Online]. Available: https://www.sciencedirect.com/science/article/pii/B978012804568800010X

[52] S. Ltd. (2010) Sasol takes to the skies with the world's first fully synthetic jet fuel. [Online]. Available: https://www.sasol.com/media-centre/media-releases/sasol-takes-skies-world-s-first-fully-synthetic-jet-fuel

[53] A. International, "Standard practice for evaluation of new aviation turbine fuels and fuel additives," *ASTM*, vol. ASTM D1319-22, 2022.

[54] ——, "Standard specification for aviation turbine fuel containing synthesized hydrocarbons," *ASTM*, vol. ASTM D7566-21, 2022.

[55] IATA, "Sustainable aviation fuels road-map," *IATA*, 2020.

[56] C. Ltd. (2021) United to become first in aviation history to fly aircraft full of passengers using 100https://www.prnewswire.com/news-releases/united-to-become-first-in-aviation-history-to-fly-aircraft-full-of-passengers-using-100-sustainable-fuel-301435009.html?mkt˙tok=NDkwLUVIWi05OTkAAAGBGq5x6THmdpxZC2rkZp9GrA8YC

[57] A. Anuar, V. Undavalli, B. Khandelwal, and S. Blakey, "Effect of fuels, aromatics and preparation methods on seal swell," *The Aeronautical Journal*, vol. 125, no. 1291, p. 1542–1565, 2021.

[58] M. L. Stone, M. S. Webber, W. P. Mounfield, D. C. Bell, E. Christensen, A. R. Morais, Y. Li, E. M. Anderson, J. S. Heyne, G. T. Beckham, and Y. Román-Leshkov, "Continuous hydrodeoxygenation of lignin to jet-range aromatic hydrocarbons," *Joule*, vol. 6, no. 10, pp. 2324–2337, 2022.

[59] "Uk plans to bring forward ban on fossil fuel vehicles to 2030; announcement expected in autumn to help trigger green economic recovery from covid-19," *The Guardian (London)*, 2020.

[60] R. A. Kerr, "Global warming. soot is warming the world even more than thought," *Science (American Association for the Advancement of Science)*, vol. 339, no. 6118, p. 382, 2013.

[61] B. Kärcher, O. Möhler, P. DeMott, S. Pechtl, and F. Yu, "Insights into the role of soot aerosols in cirrus cloud formation," *Atmospheric chemistry and physics*, vol. 7, no. 16, pp. 4203–4227, 2007.

[62] U. Lohmann, F. Friebel, Z. A. Kanji, F. Mahrt, A. A. Mensah, and D. Neubauer, "Future warming exacerbated by aged-soot effect on cloud formation," *Nature geoscience*, vol. 13, no. 10, pp. 674–680, 2020.

[63] F. Friebel, P. Lobo, D. Neubauer, U. Lohmann, S. Drossaart van Dusseldorp, E. Mühlhofer, and A. A. Mensah, "Impact of isolated atmospheric aging processes on the cloud condensation nuclei activation of soot particles," *Atmospheric Chemistry and Physics*, vol. 19, no. 24, pp. 15 545–15 567, 2019. [Online]. Available: https://acp.copernicus.org/articles/19/15545/2019/

[64] U. Dusek, G. P. Reischl, and R. Hitzenberger, "Ccn activation of pure and coated carbon black particles," *Environmental science technology*, vol. 40, no. 4, pp. 1223–1230, 2006.

[65] IARC, "Air pollution and cancer," *IARD*, vol. IARC Scientific Publication No. 161, 2013.

[66] J. I. Levy, J. K. Hammitt, and J. D. Spengler, "Estimating the mortality impacts of particulate matter: What can be learned from between-study variability?" *Environmental health perspectives*, vol. 108, no. 2, pp. 109–117, 2000.

[67] S. Fatima, A. Ahlawat, S. K. Mishra, V. K. Soni, and R. Guleria, "Respiratory deposition dose of pm2.5 and pm10 before, during and after covid-19 lockdown phases in megacity-delhi, india," *MĀPAN : journal of Metrology Society of India*, vol. 37, no. 4, pp. 891–900, 2022.

[68] D. Cohen, Aaron J, P. Brauer, Michael, P. Burnett, Richard, P. Anderson, H Ross, M. Frostad, Joseph, M. Estep, Kara, P. Balakrishnan, Kalpana, P. Brunekreef, Bert, P. Dandona, Lalit, P. Dandona, Rakhi, P. Feigin, Valery,

M. Freedman, Greg, P. Hubbell, Bryan, P. Jobling, Amelia, P. Kan, Haidong, P. Knibbs, Luke, P. Liu, Yang, P. Martin, Randall, P. Morawska, Lidia, P. Pope, C Arden, P. Shin, Hwashin, P. Straif, Kurt, P. Shaddick, Gavin, P. Thomas, Matthew, P. van Dingenen, Rita, P. van Donkelaar, Aaron, P. Vos, Theo, P. Murray, Christopher J L, and P. Forouzanfar, Mohammad H, "Estimates and 25-year trends of the global burden of disease attributable to ambient air pollution: an analysis of data from the global burden of diseases study 2015," *The Lancet (British edition)*, vol. 389, no. 10082, pp. 1907–1918, 2017.

[69] N. T. Waidyatillake, P. T. Campbell, D. Vicendese, S. C. Dharmage, A. Curto, and M. Stevenson, "Particulate matter and premature mortality: A bayesian meta-analysis," *International journal of environmental research and public health*, vol. 18, no. 14, p. 7655, 2021.

[70] A. Goshua, C. A. Akdis, and K. C. Nadeau, "World health organization global air quality guideline recommendations: Executive summary," *Allergy (Copenhagen)*, vol. 77, no. 7, pp. 1955–1960, 2022.

[71] K. Riley, R. Cook, E. Carr, and B. Manning, "A systematic review of the impact of commercial aircraft activity on air quality near airports," *City and Environment Interactions*, vol. 11, p. 100066, 2021. [Online]. Available: https://www.sciencedirect.com/science/article/pii/S2590252021000118

[72] M. Frenklach, "Reaction mechanism of soot formation in flames," *Phys. Chem. Chem. Phys.*, vol. 4, pp. 2028–2037, 2002. [Online]. Available: http://dx.doi.org/10.1039/B110045A

[73] J. A. Miller and C. F. Melius, "Kinetic and thermodynamic issues in the formation of aromatic compounds in flames of aliphatic fuels," *Combustion and Flame*, vol. 91, no. 1, pp. 21–39, 1992. [Online]. Available: https://www.sciencedirect.com/science/article/pii/0010218092901248

[74] M. Frenklach and H. Wang, "Detailed modeling of soot particle nucleation and growth," *Symposium (International) on Combustion*, vol. 23, no. 1, pp. 1559–1566, 1991, twenty-

Third Symposium (International) on Combustion. [Online]. Available: https://www.sciencedirect.com/science/article/pii/S0082078406804261

[75] B. Graziano, T. Ottenwalder, D. Manderfeld, S. Pischinger, and G. Grunefeld, "Advanced methodology for the detection of smoke point heights in hydrocarbon flames," *Energy fuels*, vol. 32, no. 3, pp. 3908–3919, 2018.

[76] N. Science, T. Council, O. of Science, and T. Policy, *Federal Alternative Jet Fuels Research and Development Strategy*. CreateSpace Independent Publishing Platform, 2017.

[77] B. Brem, S. F. Durdina, L, P. Beyerle, K. Bruderer, T. Rindlisbacher, S. Rocci-Denis, M. Andac, J. Zelina, and O. Penanhoat, "Effects of fuel aromatic content on nonvolatile particulate emmisions of an in-production aircraft gas turbine," *Environmental Science and Technology*, vol. 49, 2015.

[78] V. Iyer, "Effect of aromatic components in surrogate fuels on soot in co-flow flames and a model gas turbine combustor," *Pennyslvania State University*, 2012.

[79] B. M. Gulder OL, Glavincevski B, "Fuel molecular structure and flame temperature effects on soot formationin gas turbine combustors," *Transactions of the ASME*, vol. 112, no. 52.

[80] O. L. Gu¨lder, B. Glavinc˘evski, and S. Das, "Effect of Molecular Structure on Soot Formation Characteristics of Aviation Turbine Fuels," *Journal of Engineering for Gas Turbines and Power*, vol. 111, no. 1, pp. 77–83, 01 1989. [Online]. Available: https://doi.org/10.1115/1.3240230

[81] D. Olson, J. Pickens, and R. Gill, "The effects of molecular structure on soot formation ii. diffusion flames," *Combustion and Flame*, vol. 62, no. 1, pp. 43–60, 1985. [Online]. Available: https://www.sciencedirect.com/science/article/pii/0010218085900926

[82] D. D. Das, C. S. McEnally, T. A. Kwan, J. B. Zimmerman, W. J. Cannella, C. J. Mueller, and L. D. Pfefferle, "Sooting tendencies of diesel fuels, jet fuels,

and their surrogates in diffusion flames," *Fuel (Guildford)*, vol. 197, no. C, pp. 445–458, 2017.

[83] A. Mensch, R. J. Santoro, T. A. Litzinger, and S.-Y. Lee, "Sooting characteristics of surrogates for jet fuels," *Combustion and flame*, vol. 157, no. 6, pp. 1097–1105, 2010.

[84] T. Kathrotia, P. Oßwald, J. Zinsmeister, T. Methling, and M. Köhler, "Combustion kinetics of alternative jet fuels, part-iii: Fuel modeling and surrogate strategy," *Fuel (Guildford)*, vol. 302, p. 120737, 2021.

[85] E. Institute and the Coordinating Research Council, "The quality of fuel available in the united kingddom annual survey 2014," 2018.

[86] T. Wei and V. Simko, *R package 'corrplot': Visualization of a Correlation Matrix*, 2021, (Version 0.92). [Online]. Available: https://github.com/taiyun/corrplot

[87] A. International, "Standard test method for determination of aromatic hydrocarbon types in aviation fuels and petroleum distillates—high performance liquid chromatography method with refractive index detection," *ASTM*, vol. ASTM D6379-21e1, 2021.

[88] K. J. Johnson and R. E. Synovec, "Pattern recognition of jet fuels: comprehensive gc×gc with anova-based feature selection and principal component analysis," *Chemometrics and Intelligent Laboratory Systems*, vol. 60, no. 1, pp. 225–237, 2002, fourth International Conference on Environ metrics and Chemometrics held in Las Vegas, NV, USA, 18-20 September 2000. [Online]. Available: https://www.sciencedirect.com/science/article/pii/S0169743901001988

[89] P. E. Sudol, S. Schöneich, and R. E. Synovec, "Principal component analysis of comprehensive three-dimensional gas chromatography time-of-flight mass spectrometry data," *Journal of Chromatography Open*, vol. 2, p. 100043, 2022. [Online]. Available: https://www.sciencedirect.com/science/article/pii/S2772391722000147

[90] T. Hastie, J. H. J. H. Friedman, and R. Tibshirani, *The elements of statistical learning : data mining, inference, and prediction*, 2nd ed., ser. Springer series in statistics. New York: Springer, 2009.

[91] T. Kabe, A. Ishihara, and W. Qian, *Hydrodesulfurization and hydrodenitrogenation : chemistry and engineering*. Weinheim ; Chichestere: Wiley-VCH, 1999.

[92] J. M. Mehta, P. T. Lynch, E. K. Mayhew, and K. Brezinsky, "Evaluation of chemical functional group composition of jet fuels using two-dimensional gas chromatography," *Energy fuels*, vol. 37, no. 3, pp. 2294–2306, 2023.

[93] M. Romanczyk, J. H. Ramirez Velasco, L. Xu, P. Vozka, P. Dissanayake, K. E. Wehde, N. Roe, E. Keating, G. Kilaz, R. W. Trice, D. J. Luning Prak, and H. Kenttmaa, "The capability of organic compounds to swell acrylonitrile butadiene o-rings and their effects on o-ring mechanical properties," *Fuel (Guildford)*, vol. 238, pp. 483–492, 2019.

[94] A. Anuar, V. Undavalli, B. Khandelwal, and S. Blakey, "Effect of fuels, aromatics and preparation methods on seal swell," *Aeronautical journal*, vol. 125, no. 1291, pp. 1542–1565, 2021.

[95] E. Corporan, T. Edwards, L. Shafer, M. J. DeWitt, C. Klingshirn, S. Zabarnick, Z. West, R. Striebich, J. Graham, and J. Klein, "Chemical, thermal stability, seal swell, and emissions studies of alternative jet fuels," *Energy fuels*, vol. 25, no. 3, pp. 955–966, 2011.

[96] M. J. DeWitt, E. Corporan, J. Graham, and D. Minus, "Effects of aromatic type and concentration in fischertropsch fuel on emissions production and material compatibility," *Energy fuels*, vol. 22, no. 4, pp. 2411–2418, 2008.

[97] D. D. Link, R. J. Gormley, J. P. Baltrus, R. R. Anderson, and P. H. Zandhuis, "Potential additives to promote seal swell in synthetic fuels and their effect on thermal stability," *Energy fuels*, vol. 22, no. 2, pp. 1115–1120, 2008.

[98] "Some industrial chemicals and dyestuffs," *Food and chemical toxicology*, vol. 22, no. 2, p. 172, 1984.

[99] M. T. Smith, "Advances in understanding benzene health effects and susceptibility," *Annual review of public health*, vol. 31, no. 1, pp. 133–148, 2010.

[100] D. Graf, J. Waßmuth, and R. Rauch, "Co-hydroprocessing of fossil middle distillate and bio-derived durene-rich heavy ends under hydrotreating conditions," *Reactions (Basel, Switzerland)*, vol. 4, no. 3, pp. 531–551, 2023.

[101] C. H. Stam, "A refinement of the crystal structure of durene," *Acta Crystallographica Section B*, vol. 28, no. 8, pp. 2630–2632, 1972.

[102] L. Zhang, D. Su, and M. Zhong, "The effect of functional forms of nitrogen on fuel-nox emissions," *Environmental monitoring and assessment*, vol. 187, no. 1, pp. 4195–4195, 2015.

[103] A. International, "Standard test method for heat of combustion of liquid hydrocarbon fuels by bomb calorimeter (precision method)," *ASTM*, vol. ASTM D4809-18, 2018.

[104] "Chemical properties of benzene, tert-butyl- (cas 98-06-6)," https://www.chemeo.com/cid/27-113-6/Benzene-tert-butyl, accessed: 2022-10-30.

[105] C. S. McEnally, D. D. Das, and L. D. Pfefferle, "Yield Sooting Index Database Volume 2: Sooting Tendencies of a Wide Range of Fuel Compounds on a Unified Scale," 2017. [Online]. Available: https://doi.org/10.7910/DVN/7HGFT8

[106] D. D. Das, P. C. St. John, C. S. McEnally, S. Kim, and L. D. Pfefferle, "Measuring and predicting sooting tendencies of oxygenates, alkanes, alkenes, cycloalkanes, and aromatics on a unified scale," *Combustion and Flame*, vol. 190, pp. 349–364, 2018. [Online]. Available: https://www.sciencedirect.com/science/article/pii/S0010218017304728

[107] A. Benabed and A. Boulbair, "Pm10, pm2.5, pm1, and pm0.1 resuspension due to human walking," *Air quality, atmosphere and health*, vol. 15, no. 9, pp. 1547–1556, 2022.

[108] E. A. Ubogu, "Non-conventional pollutant species measurement and prediction from a gas turbine," March 2016. [Online]. Available: https://etheses.whiterose.ac.uk/13304/

[109] E. Ubogu, J. Cronly, B. Khandelwal, and R. S, "Determination of the effective density and fractal dimension of pm emissions from an aircraft auxiliary power unit," *Journal of Environmental Sciences*, vol. 74, 2018.

[110] J. BORAK, G. SIRIANNI, H. J. COHEN, S. CHEMERYNSKI, and R. WHEELER, "Comparison of niosh 5040 method versus aethalometer to monitor diesel particulate in school buses and at work sites," *AIHAJ - American Industrial Hygiene Association*, vol. 64, no. 2, pp. 260–268, 2003.

[111] U. EPA, "Method 5i - determination of low level particulate matter emissions," *Air Emission Meaurement Center*, 2019.

[112] B. A. Almohammadi, P. Singh, S. Sharma, S. Kumar, and B. Khandelwal, "Impact of alkylbenzenes in formulated surrogate fuel on characteristics of compression ignition engine," *Fuel*, vol. 266, p. 116981, 2020. [Online]. Available: https://www.sciencedirect.com/science/article/pii/S0016236119323749

[113] S. Sharma, P. Singh, B. A. Almohammadi, B. Khandelwal, and S. Kumar, "Testing of formulated fuel with variable aromatic type and contents in a compression-ignition engine," *Fuel Processing Technology*, vol. 208, p. 106413, 2020. [Online]. Available: https://www.sciencedirect.com/science/article/pii/S0378382020301752

[114] P. Singh, S. Sharma, B. A. Almohammadi, B. Khandelwal, and S. Kumar, "Applicability of aromatic selection towards newer formulated fuels for regulated and unregulated emissions reduction in ci engine," *Fuel Processing Technology*, vol. 209, p. 106548, 2020. [Online]. Available: https://www.sciencedirect.com/science/article/pii/S0378382020308390

Appendix A

A.1 Candidate Aromatics Summary

Common Name	Alternate Name	Chemical Formula	Price [$£kg^{-1}$]	Status	Notes
Benzene	Phenane	C_6H_6	68.99	Rejected	Carcinogenic
Toluene	Methylbenzene	$C_6H_5CH_3$	43.01	Selected	
Styrene	Ethenylbenzene	$C_6H_5CH=CH_2$	37.90	Selected	
o-Xylene	1,2-Dimethylbenzene	$C_6H_4(CH_3)_2$	64.09	Selected	
m-xylene	1,3-Dimethylbenzene	$C_6H_4(CH_3)_2$	80.81	Considered	
p-Xylene	1,4-Dimethylbezene	$C_6H_4(CH_3)_2$	91.99	Considered	
Ethylbenzene		$C_6H_5CH_2CH_3$	94.17	Selected	
Indene	1H-indene	C_9H_8	133.53	Selected	
Indan	2,3-Dihydro-1H-indene	C_9H_10	296.37	Selected	
Cyclopropylbenzene	Phenylcyclopropane	$C_6H_5C_3H_5$	9560.00	Rejected	Expensive
α-Methylstyrene	Phenylpropene	$C_6H_5CH=CHCH_3$	46.87	Selected	
Hemelitene	1,2,3-Trimethylbenzene	$C_6H_3(CH_3)_3$	1814.32	Rejected	Expensive
Pseudocumene	1,2,4-Trimethylbenzene	$C_6H_3(CH_3)_3$	57.30	Selected	
Mesitylene	1,3,5-Trimethylbenzene	$C_6H_3(CH_3)_3$	46.30	Considered	
2-Ethyyltoluene		$C_2H_5C_6H_4CH_3$	4420.00	Rejected	Expensive
3-Ethyltoluene		$C_2H_5C_6H_4CH_3$	5720.00	Rejected	Expensive
4-Ethyltoluene		$C_2H_5C_6H_4CH_3$	1075.00	Rejected	Expensive
Propylbenzene		$C_6H_5C_3H_7$	250.58	Considered	
Cumene	Isopropylbenzene	$C_6H_5CH(CH_3)_2$	21.81	Selected	
1,2-Dihydronapthalene		$C_{10}H_{10}$	8840.00	Rejected	Expensive
2-Methylindene		$C_{10}H_{10}$	34800.00	Rejected	Expensive
Tetralin	1,2,3,4-Tetrahydronapthalene	$C_{10}H_{12}$	84.38	Selected	Cycoaromatic

Common Name	Alternate Name	Chemical Formula	Price [£kg^{-1}]	Status	Notes
1,2,3,5-Tetramethylbenzene		$C_6H_2(CH_3)_4$	40400.00	Rejected	Expensive
1,2,4,5-Tetramethylbenzene		$C_6H_2(CH_3)_4$	105.80	Considered	Saturation Concerns
1,2-Diethylbenzene		$C_6H_4(C_2H_5)_2$	17760.00	Rejected	Expensive
1,3-Diethylbenzene		$C_6H_4(C_2H_5)_2$	5219.91	Rejected	Expensive
1,4-Diethylbenzene		$C_6H_4(C_2H_5)_2$	6880.00	Rejected	Expensive
Di-ethylbenzene		$C_6H_4(C_2H_5)_2$	50.46	Selected	Combination of Isomers
Butylbenzene	1-Phenylbutane	$C_6H_5C_4H_9$	365.12	Considered	
Isobutylbenzene	2-Methyl-1-phenylpropane	$C_6H_5CH_2CH(CH_3)_2$	227.43	Considered	
m-Cymene	3-Isopropyltoluene	$CH_3C_6H_4CH(CH_3)_2$	525.00	Rejected	Expensive
o-Cymene	2-Isopropyltoluene	$CH_3C_6H_4CH(CH_3)_2$	317.50	Considered	
p-Cymene	4-Isopropyltoluene	$CH_3C_6H_4CH(CH_3)_2$	45.81	Selected	
sec-Butylbenzene	2-Phenylbutane	$C_6H_5CH(CH_3)CH_2CH_3$	246.81	Considered	
tert-Butylbenzene	2-Methyl-2-phenylpropane	$C_6H_5C(CH_3)_3$	68.86	Selected	
1-Methylnapthalene		$C_{10}H_7CH_3$	68.60	Selected	Polycyclic Aromatic
1-eth-1-ynyl-4-propylbenzene		$CHCC_6H_4C_3H_7$	404.00	Considered	
4-isopropylphenyl aceltylene		$CHCC_6H_4CH(CH_3)_2$	161.60	Considered	Unavailable
Neopentylbenzene	2,2-Dimethyl-1-propylbenzene	$C_6H_5CH_2C(CH_3)_3$	4370.63	Rejected	Expensive
Butyltoluene	4-tert-Butyltoluene	$(CH_3)_3CC_6H_4CH_3$	119.00	Considered	
Isoamylbenzene	(3-Methyl-1-butyl)benzene	$C_6H_5CH_2CH_2CH(CH_3)_2$	23146.85	Rejected	Expensive
Pentylbenzene	1-Phenylpentane	$C_6H_5(CH_2)_4CH_3$	1345.00	Rejected	Expensive
1-Ethylnapthalene		$C_{10}H_7CCH$	31400.00	Rejected	Expensive
1,5-Dimethyltetralin	1,2,3,4-Tetrahydro-1,5-dimethylnaphthalene	$C_{10}H_9(CH_3)_2$	459.21	Rejected	Expensive

Common Name	Alternate Name	Chemical Formula	Price [$£kg^{-1}$]	Status	Notes
Cyclohexylbenzene	Phenylcyclohexane	$C_6H_5C_6H_{11}$	628.00	Rejected	Expensive
1,3,5-Triethylbenzene		$C_6H_3(C_2H_5)_3$	5000.00	Rejected	Expensive
3-Isopropylcumene	1,3-Diisopropylbenzene	$C_6H_4[CH(CH_3)_2]2$	138.80	Selected	
1,4-Diisopropylbenzene		$C_6H_4[CH(CH_3)_2]_2$	831.97	Rejected	Expensive
5-tert-Butyl-m-xylene	1-tert-Butyl-3,5-dimethylbenzene	$(CH_3)_3CC_6H_3(CH_3)_2$	324.00	Selected	
Hexamethyldewar-benzene	1,2,3,4,5,6-Hexamethylbicyclo-hexa-2,5-diene	$C_6(CH3)_6$	Unknown	Rejected	Saturation Concerns
Hexylbenzene	1-Phenylhexane	$C_6H_5(CH_2)_5CH_3$	1295.00	Rejected	Expensive
Heptylbenzene	1-Phenylheptane	C˙6H˙5(CH˙2)˙6CH˙3	1580.00	Rejected	Expensive
1,3,5-Triisopropylbenzene		$C_6H_3[CH(CH_3)_2]_3$	717.00	Rejected	Expensive
3,5-Di-tert-butyltoluene		$CH_3C_6H_3[C(CH_3)_3]_2$	2244.00	Rejected	Expensive
Nonylbenzene	1-Phenylnonane	$C_6H_5(CH_2)_8CH_3$	4450.00	Rejected	Expensive
Undecylbenzene	1-Phenylundecane	$C_6H_5(CH_2)_{10}CH_3$	7368.42	Rejected	Expensive
Dodecylbenzene	1-Phenyldodecane	$C_6H_5(CH_2)_{11}CH_3$	3184.00	Rejected	Expensive

Appendix B

B.1 Calculated Specific Energy

- 3-isopropylcumene

$$C_{12}H_{18} + 16.5O_2 \rightarrow 12CO_2 + 9H_2O \tag{B.1}$$

$$6(518) + 6(348) + 18(413) + 16.5(498) \rightarrow 12(2)(805) + 9(2)(463) \tag{B.2}$$

$$12,630 + 8,217 \rightarrow 19,320 + 8335 \tag{B.3}$$

$$\Delta_{c,net}H = 20,847 - 27,655 = -6,808kJmol^{-1} \tag{B.4}$$

$$SE_{3-Isopropylcumene} = \frac{1000}{162.27} \times 6,808 = 41,954.8KJkg^{-1} \tag{B.5}$$

- Tert-Butyl-m-Xylene

$$C_{12}H_{18} + 16.5O_2 \rightarrow 12CO_2 + 9H_2O \tag{B.6}$$

$$6(518) + 6(348) + 18(413) + 16.5(498) \rightarrow 12(2)(805) + 9(2)(463) \tag{B.7}$$

$$12,630 + 8,217 \rightarrow 19,320 + 8335 \tag{B.8}$$

$$\Delta_{c,net}H = 20,847 - 27,655 = -6,808kJmol^{-1} \tag{B.9}$$

$$SE_{Tert-Butyl-m-Xylene} = \frac{1000}{162.27} \times 6,808 = 41,954.8KJkg^{-1} \tag{B.10}$$

Appendix C

C.1 GCMS Results

C.1.1 3-isopropylcumene

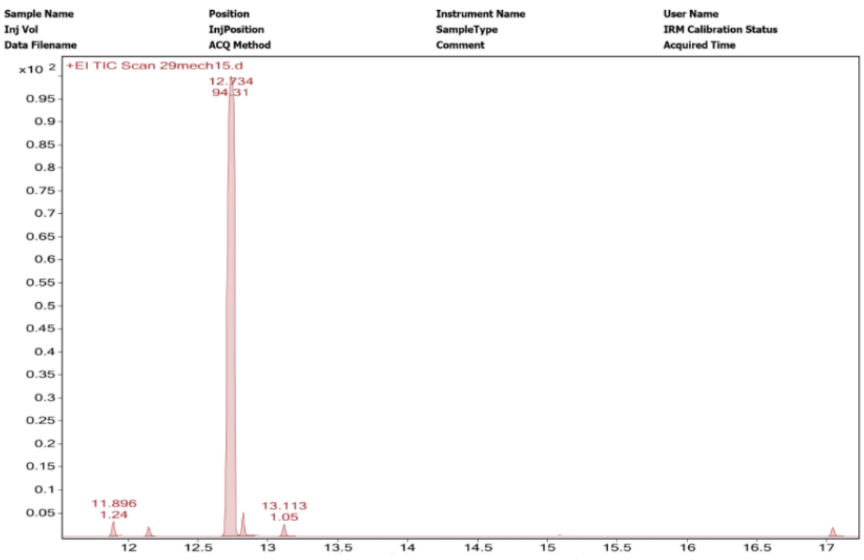

Figure C.1.1: GCMS Results for 3-Isopropylcumene

C.1.2 α-Methylstyrene

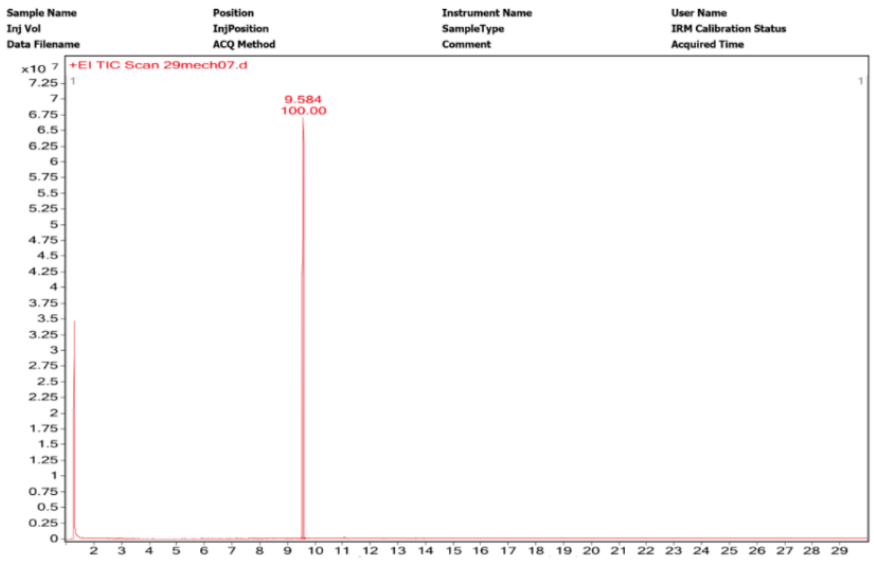

Figure C.1.2: GCMS Results for α-Methylstyrene

C.1.3 Cumene

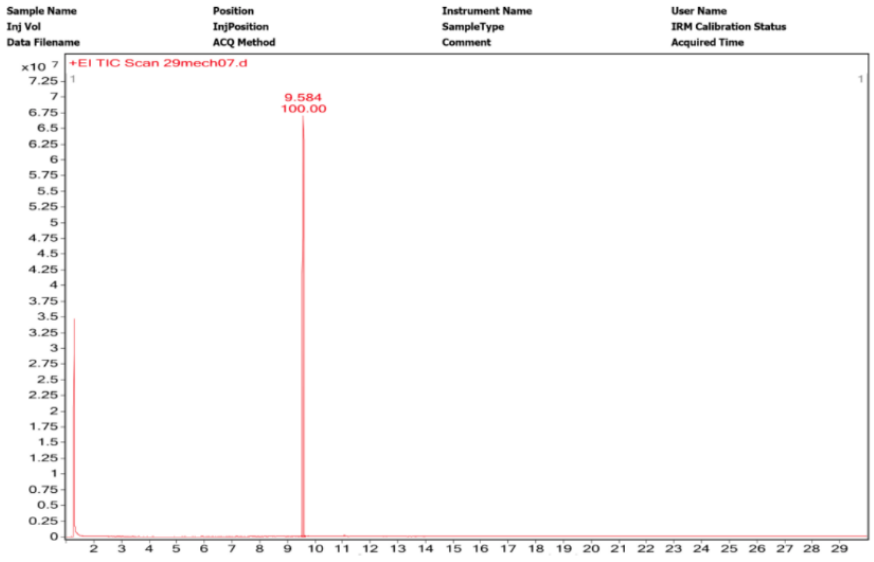

Figure C.1.3: GCMS Results for α-Methylstyrene

C.1.4 Diethylbenzene

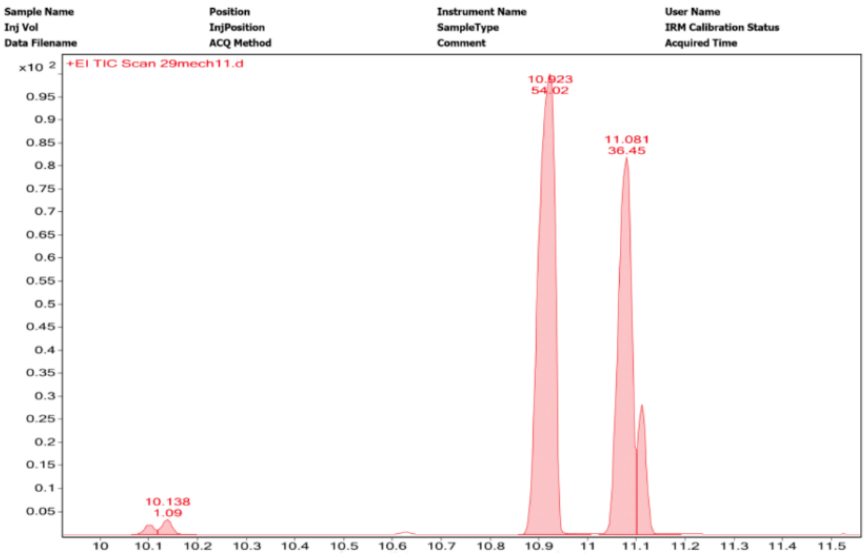

Figure C.1.4: GCMS Results for Diethylbenzene

C.1.5 Ethylbenzene

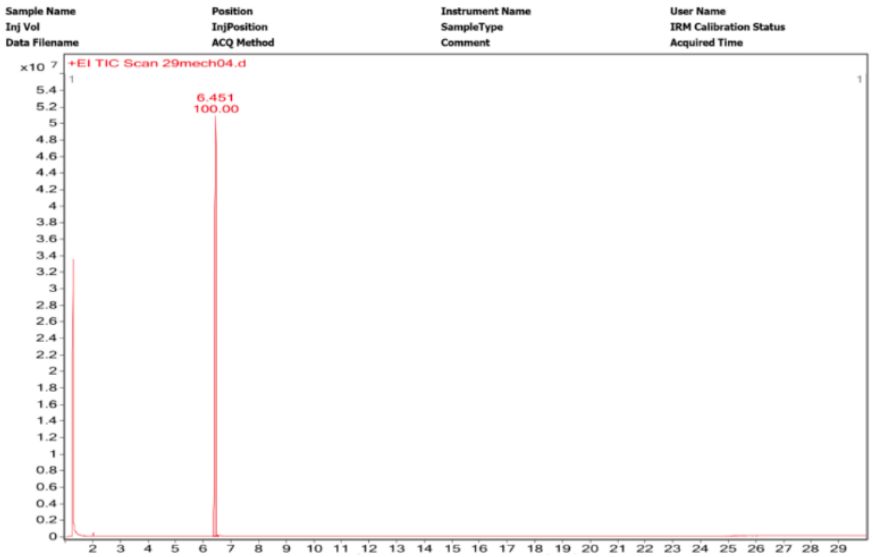

Figure C.1.5: GCMS Results for Ethylbenzene

C.1.6 Indan

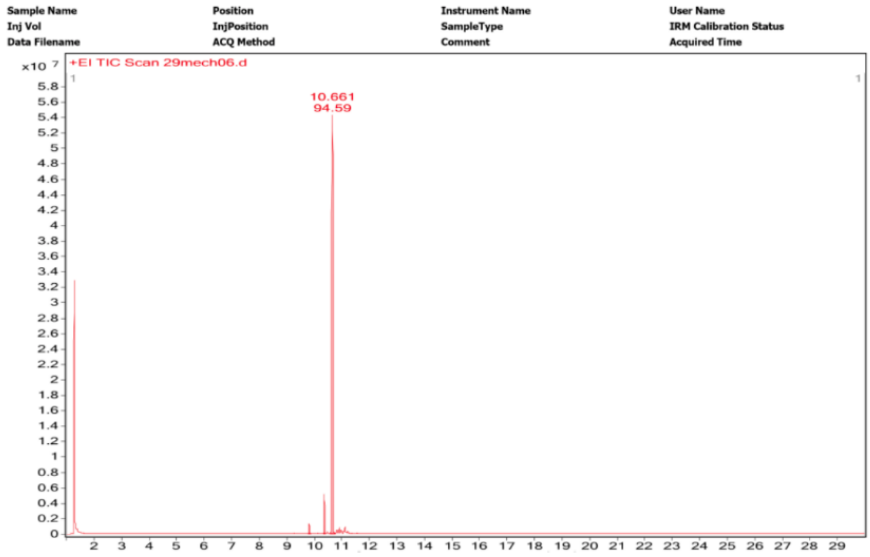

Figure C.1.6: GCMS Results for Indan

C.1.7 Indene

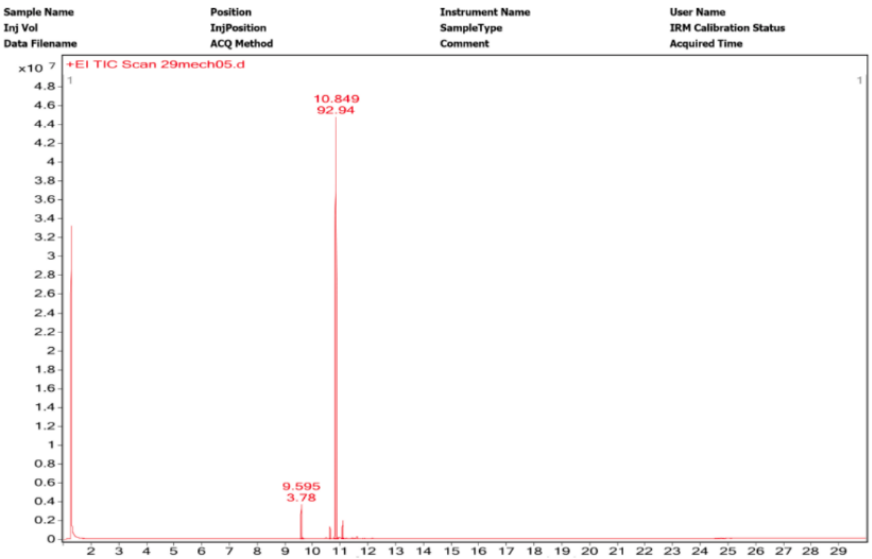

Figure C.1.7: GCMS Results for Indene

C.1.8 Methylnapthalene

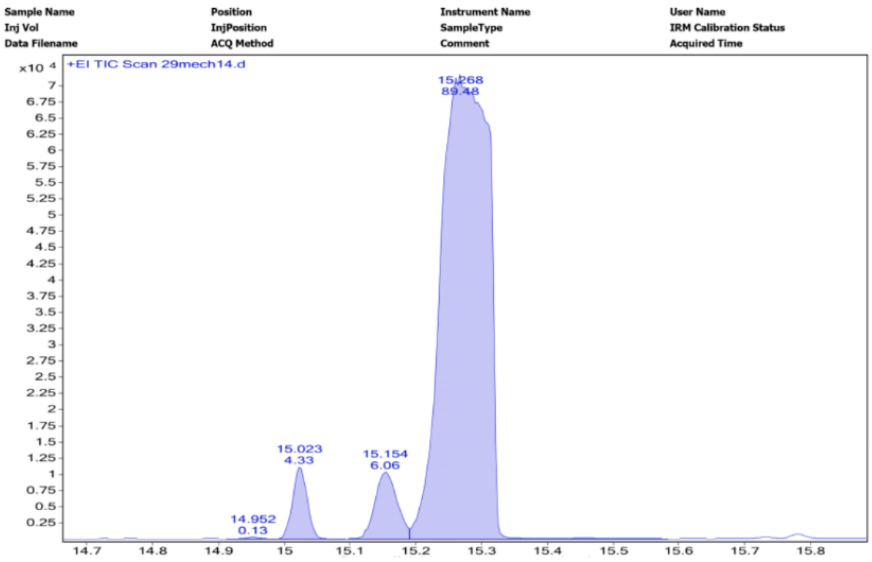

Figure C.1.8: GCMS Results for Methylnapthalene

C.1.9 o-Xylene

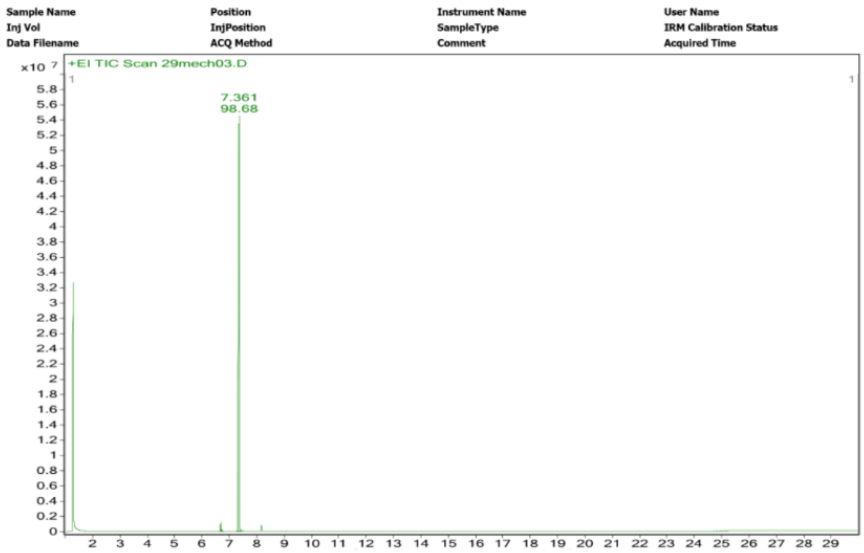

Figure C.1.9: GCMS Results for o-Xylene

C.1.10 p-Cymene

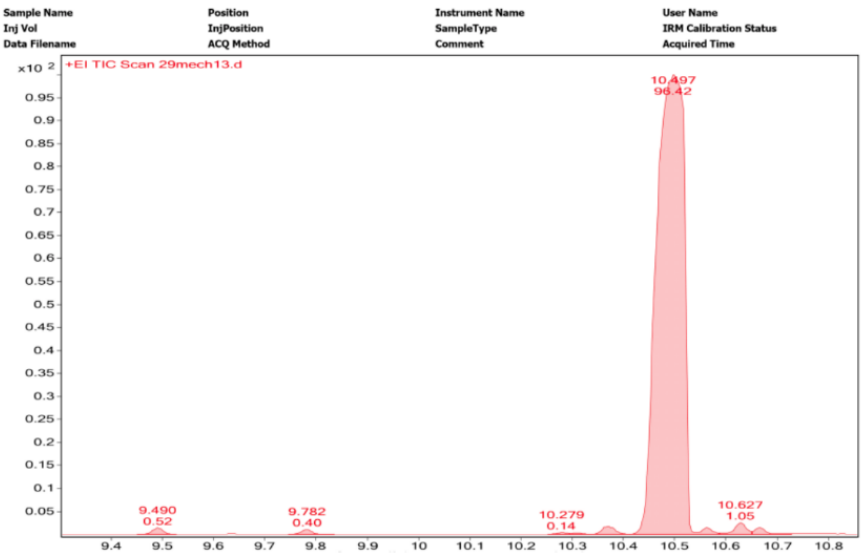

Figure C.1.10: GCMS Results for p-Cymene

C.1.11 Pseudocumene

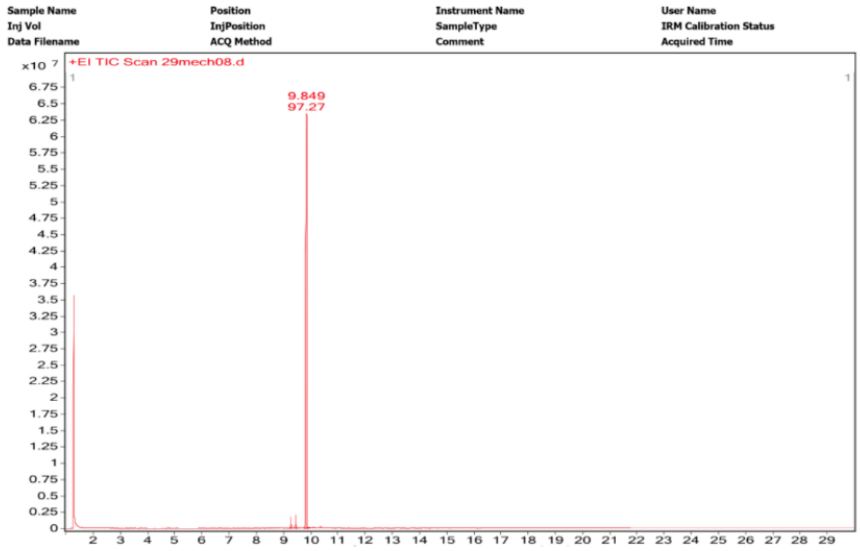

Figure C.1.11: GCMS Results for Pseudocumene

C.1.12 Styrene

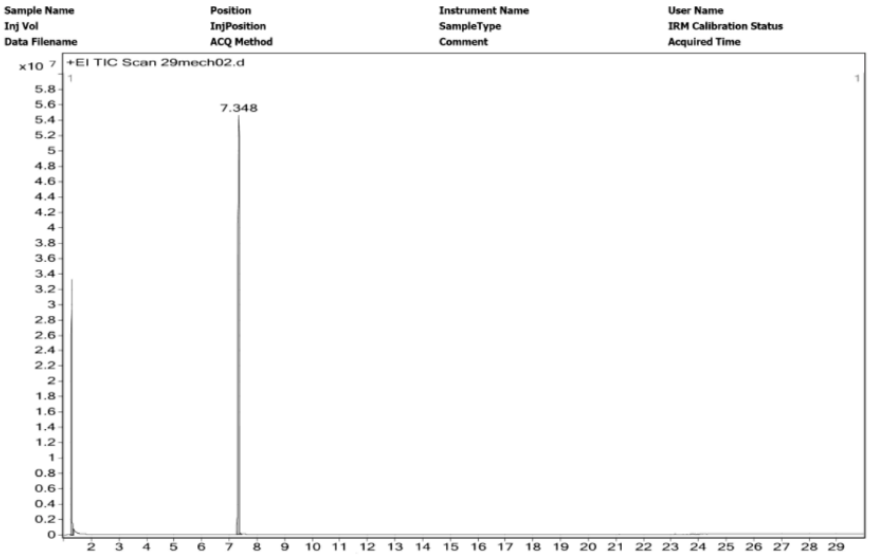

Figure C.1.12: GCMS Results for Styrene

C.1.13 Tertbutylbenzene

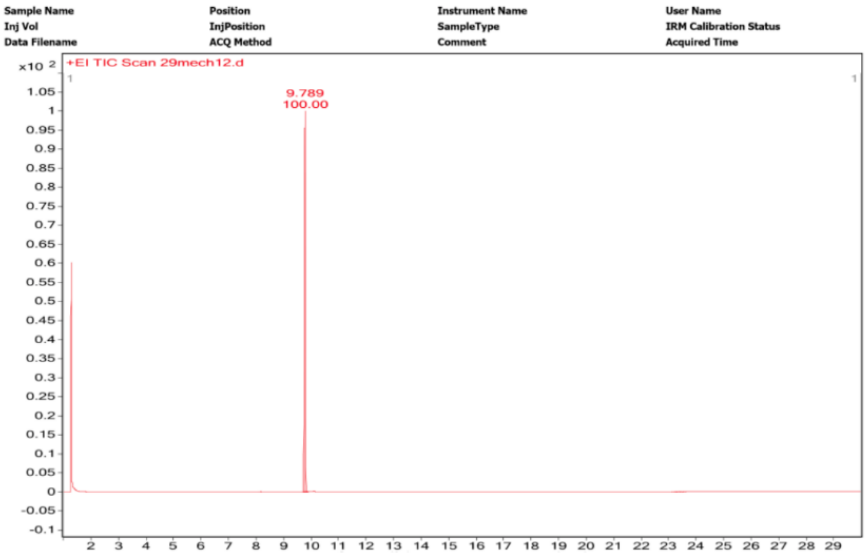

Figure C.1.13: GCMS Results for Tertbutylbenzene

C.1.14 Tetralin

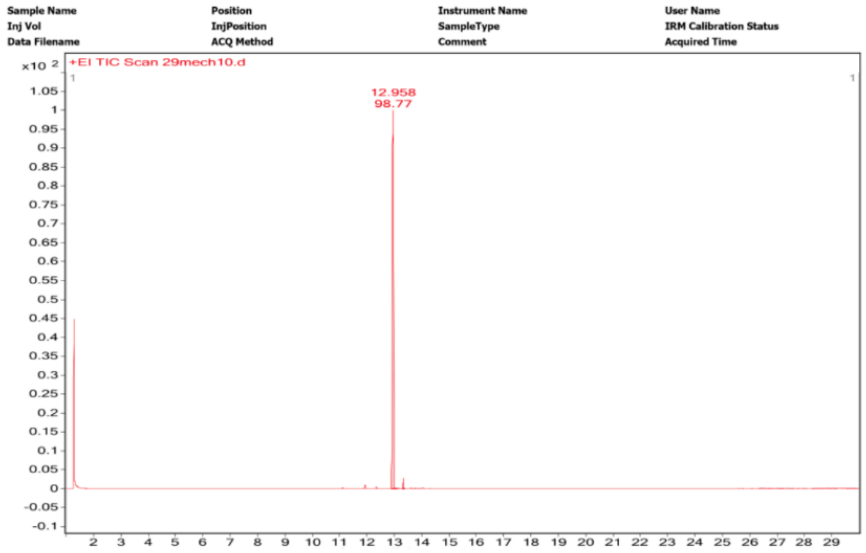

Figure C.1.14: GCMS Results for Tetralin

C.1.15 Toluene

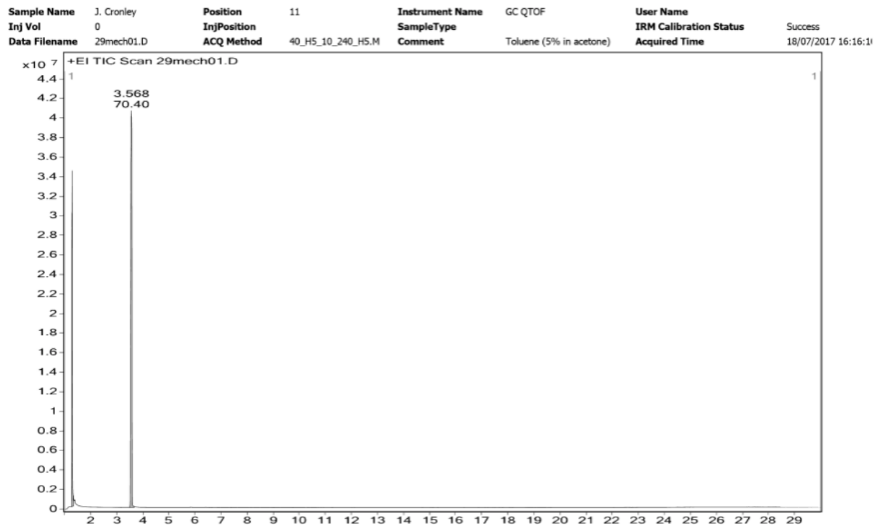

Figure C.1.15: GCMS Results for Toluene

Appendix D

D.1 LII Individual Aromatic Regression Results

D.1.1 Toluene

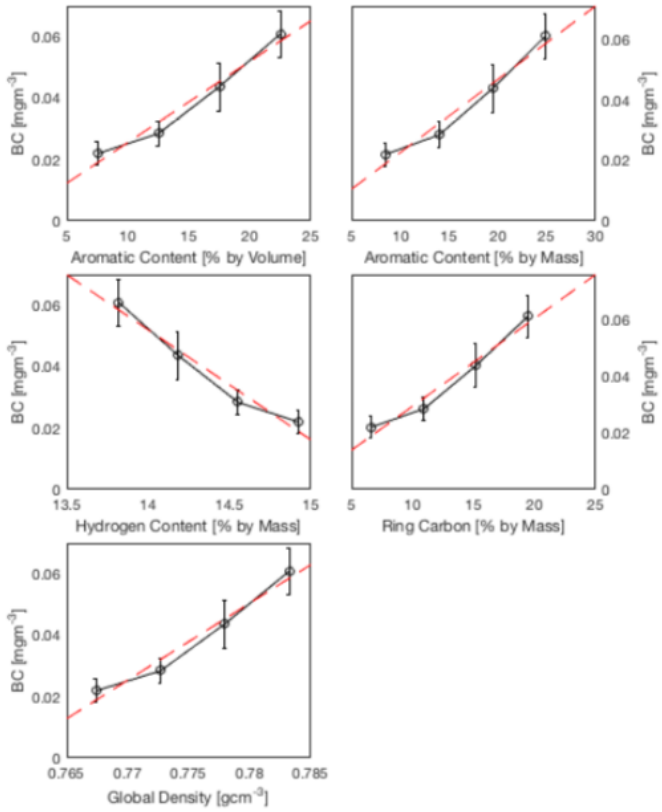

]

Figure D.1.1: Toluene BC vs a) Vol b) Mass c) Hydrogen % d) Ring Carbon % e) Global Density

	y = mx + c	R^2
Aromatic Content [% vol/vol]	0.00265x – 0.000965	0.96604
Aromatic Content[% mass/mass]	0.00168x + 0.00403	0.98153
Hydrogen Content [% mass/mass]	-0.0249x + 0.390	0.98153
Ring Carbon [% mass/mass]	0.00214x + 0.00403	0.98153
Global Density [gcm^{-3}]	2.51x – 1.91	0.96604

Figure D.1.2: Toluene Linear Regressions equations and Coefficients of Determination

D.1.2 Styrene

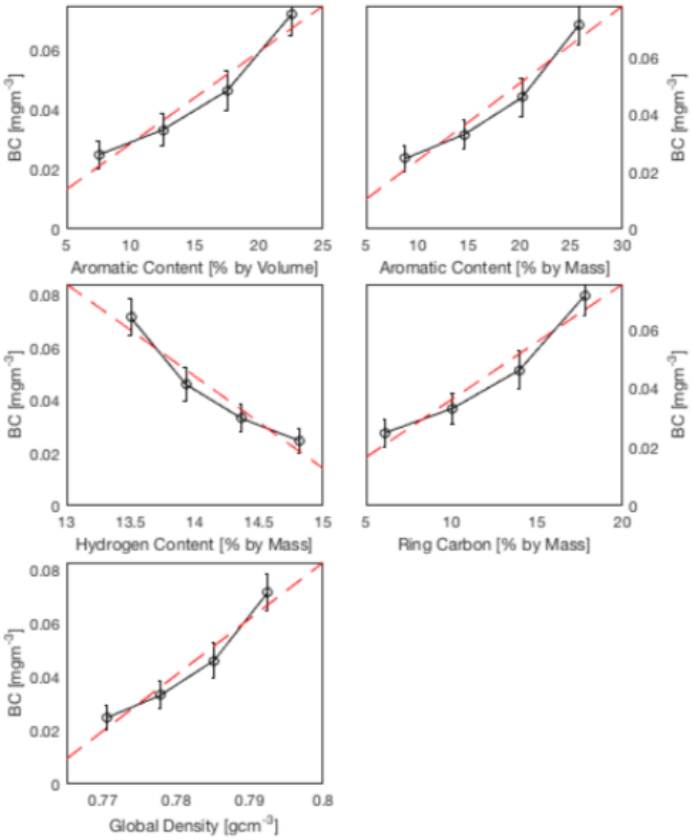

]

Figure D.1.3: Styrene BC vs a) Vol b) Mass c) Hydrogen % d) Ring Carbon % e) Global Density

	y = mx + c	R^2
Aromatic Content [% vol/vol]	0.00307x – 0.00207	0.93986
Aromatic Content[% mass/mass]	0.00272x – 0.00311	0.93589
Hydrogen Content [% mass/mass]	-0.0950x + 0.54	0.93589
Ring Carbon [% mass/mass]	0.00393x – 0.00311	0.93589
Global Density [gcm^{-3}]	2.09x – 1.59	0.93986

Figure D.1.4: Styrene Linear Regressions equations and Coefficients of Determination

D.1.3 o-Xylene

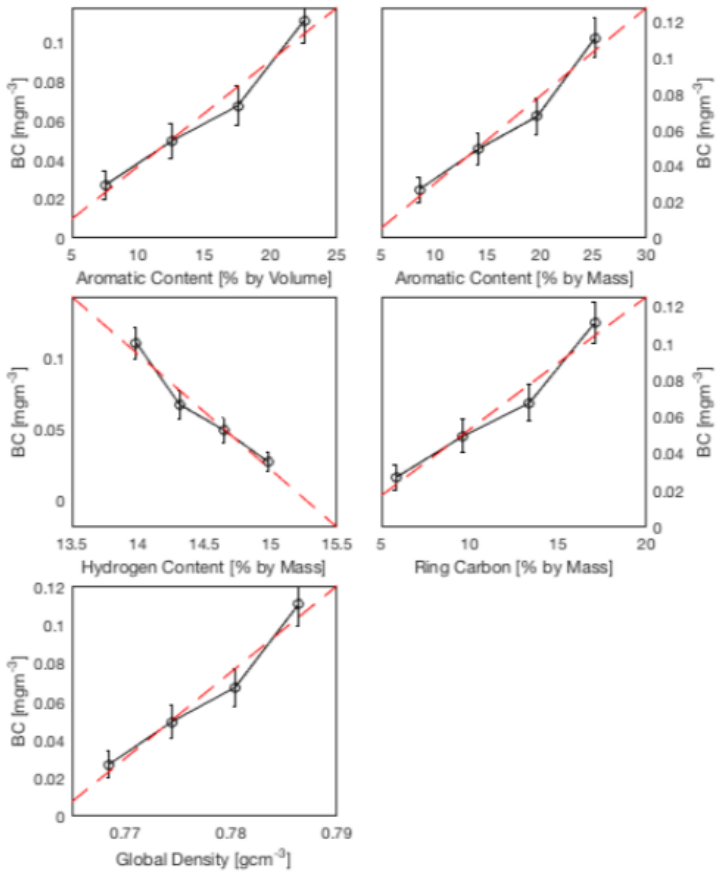

]

Figure D.1.5: o-Xylene BC vs a) Vol b) Mass c) Hydrogen % d) Ring Carbon % e) Global Density

	$y = mx + c$	R^2
Aromatic Content [% vol/vol]	0.00542x – 0.0173	0.95944
Aromatic Content[% mass/mass]	0.00490x – 0.0188	0.95711
Hydrogen Content [% mass/mass]	-0.0817x + 1.25	0.95711
Ring Carbon [% mass/mass]	0.00722x – 0.0188	0.95711
Global Density [gcm^{-3}]	4.54x – 3.46	0.95944

Figure D.1.6: o-Xylene Linear Regressions equations and Coefficients of Determination

D.1.4 Ethylbenzene

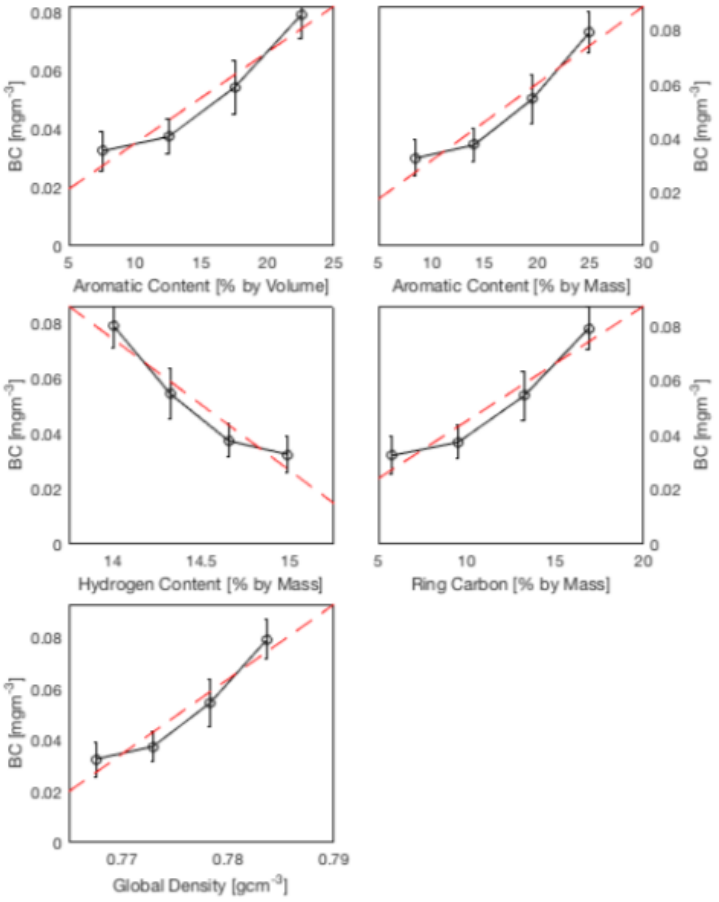

]

Figure D.1.7: Ethylbenzene BC vs a) Vol b) Mass c) Hydrogen % d) Ring Carbon % e) Global Density

	y = mx + c	R^2
Aromatic Content [% vol/vol]	0.00388x – 0.0115	0.95847
Aromatic Content[% mass/mass]	0.00354x – 0.0124	0.95613
Hydrogen Content [% mass/mass]	-0.0590x + 0.902	0.95613
Ring Carbon [% mass/mass]	0.00522x – 0.0124	0.95613
Global Density [gcm^{-3}]	3.61x – 2.75	0.95847

Figure D.1.8: Ethylbenzene Linear Regressions equations and Coefficients of Determination

D.1.5 Indan

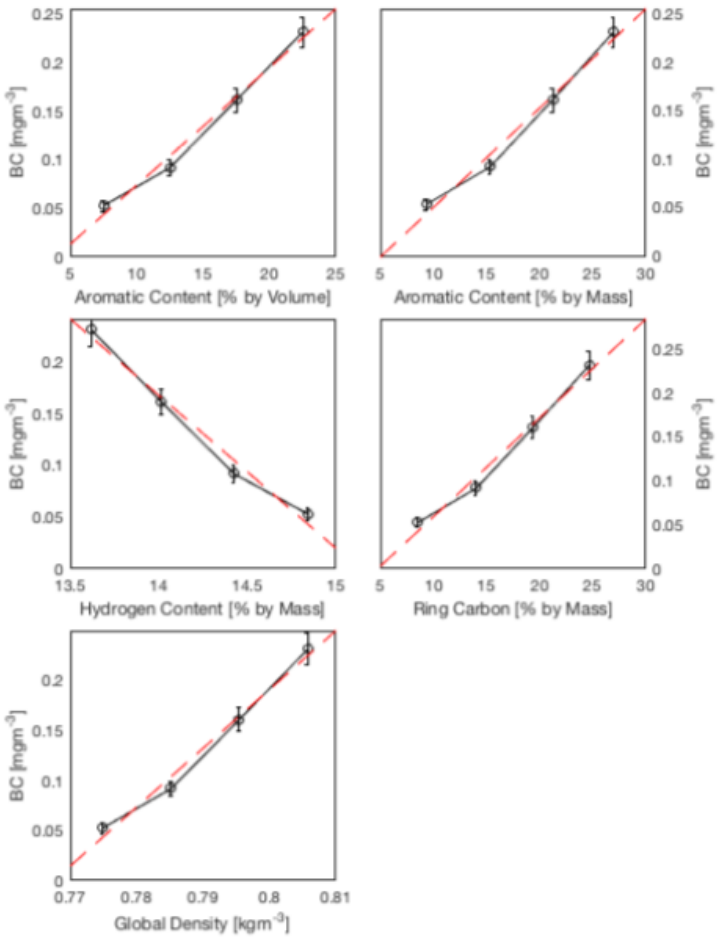

]

Figure D.1.9: Indan BC vs a) Vol b) Mass c) Hydrogen % d) Ring Carbon % e) Global Density

	y = mx + c	R^2
Aromatic Content [% vol/vol]	0.0121x – 0.0471	0.98477
Aromatic Content[% mass/mass]	0.0103x – 0.0532	0.98200
Hydrogen Content [% mass/mass]	-0.147x + 2.23	0.98200
Ring Carbon [% mass/mass]	0.0112x – 0.0543	0.98200
Global Density [gcm^{-3}]	5.88x – 4.51	0.98477

Figure D.1.10: Indan Linear Regressions equations and Coefficients of Determination

D.1.6 α-Methylstyrene

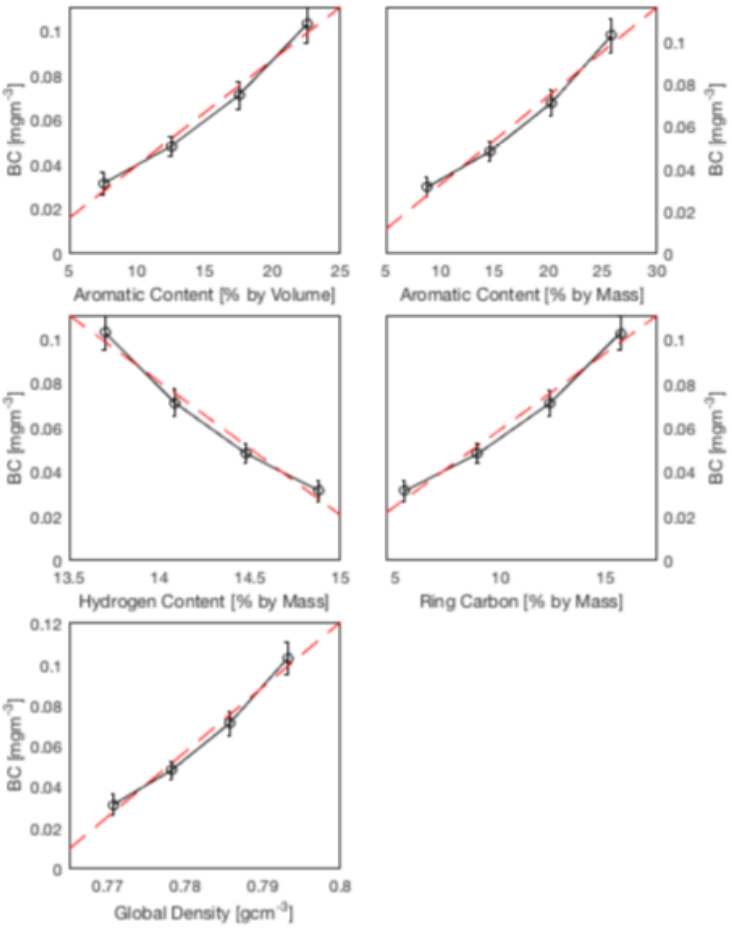

]

Figure D.1.11: α-Methylstyrene BC vs a) Vol b) Mass c) Hydrogen % d) Ring Carbon % e) Global Density

	y = mx + c	R^2
Aromatic Content [% vol/vol]	0.00475x – 0.00762	0.98020
Aromatic Content[% mass/mass]	0.00420x – 0.00933	0.97775
Hydrogen Content [% mass/mass]	-0.0603x + 0.925	0.97775
Ring Carbon [% mass/mass]	0.00689x – 0.00933	0.97775
Global Density [gcm^{-3}]	3.18x – 2.42	0.98020

Figure D.1.12: α-Methylstyrene Linear Regressions equations and Coefficients of Determination

D.1.7 Trimethylbenzene

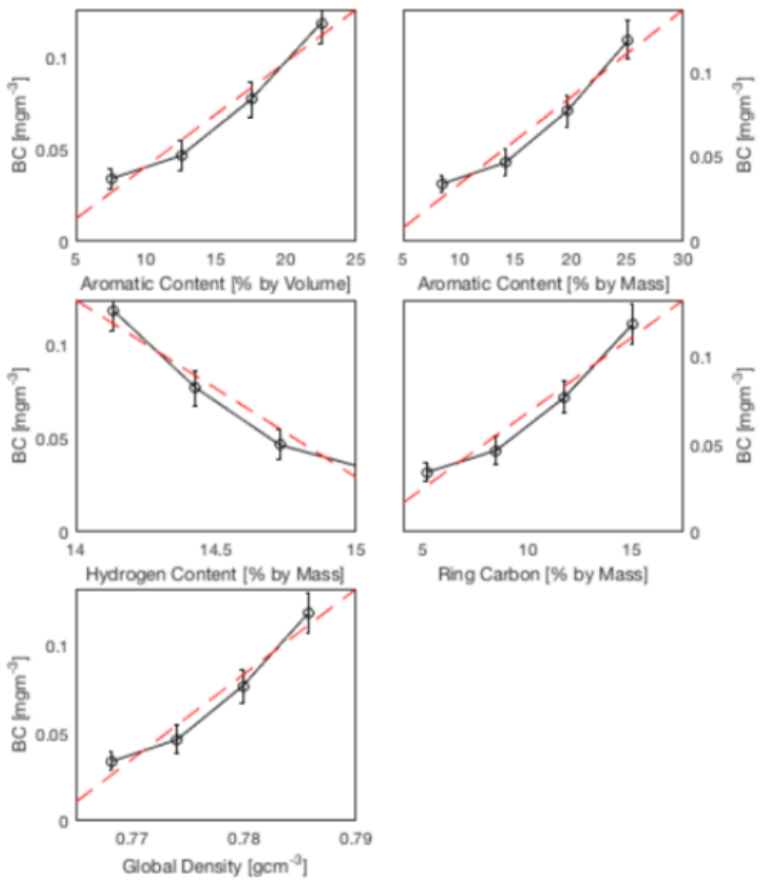

]

Figure D.1.13: Trimethylbenzene BC vs a) Vol b) Mass c) Hydrogen % d) Ring Carbon % e) Global Density

	y = mx + c	R^2
Aromatic Content [% vol/vol]	0.00569x – 0.0161	0.94989
Aromatic Content[% mass/mass]	0.00516x – 0.0177	0.94694
Hydrogen Content [% mass/mass]	-0.0950x + 1.45	0.94694
Ring Carbon [% mass/mass]	0.00860x – 0.0177	0.94694
Global Density [gcm^{-3}]	4.89x – 3.73	0.94989

Figure D.1.14: Trimethylbenzene Linear Regressions equations and Coefficients of Determination

D.1.8 Cumene

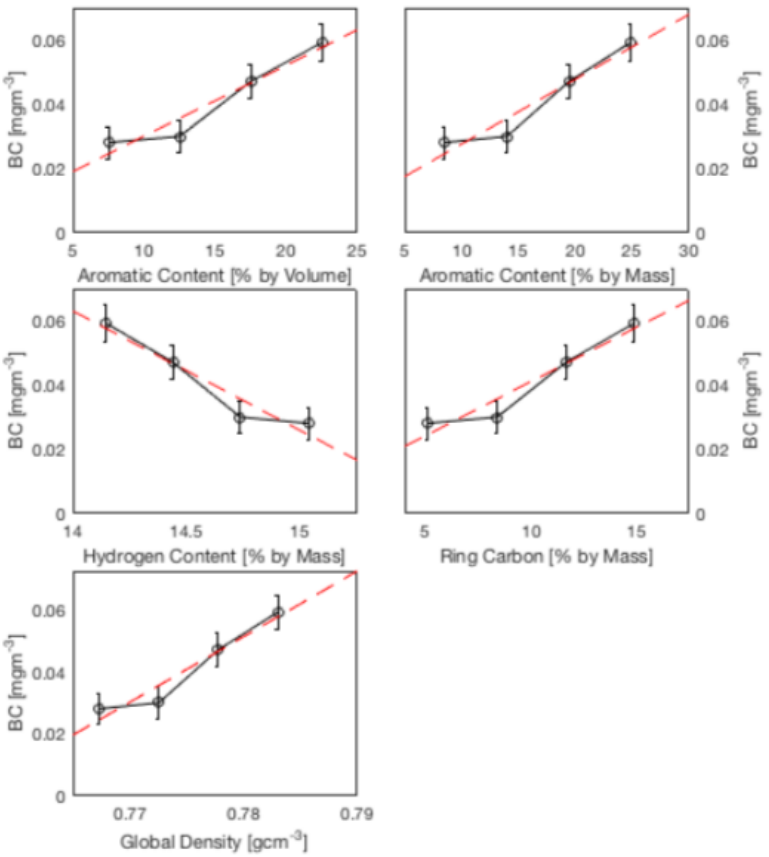

]

Figure D.1.15: Cumene BC vs a) Vol b) Mass c) Hydrogen % d) Ring Carbon % e) Global Density

	y = mx + c	R^2
Aromatic Content [% vol/vol]	0.0211x + 0.00798	0.92970
Aromatic Content[% mass/mass]	0.00202x + 0.00744	0.92734
Hydrogen Content [% mass/mass]	-0.0372x + 0.583	0.92734
Ring Carbon [% mass/mass]	0.00337x + 0.00744	0.92734
Global Density [gcm^{-3}]	2.11x – 1.6	0.92970

Figure D.1.16: Cumene Linear Regressions equations and Coefficients of Determination

D.1.9 Tetralin

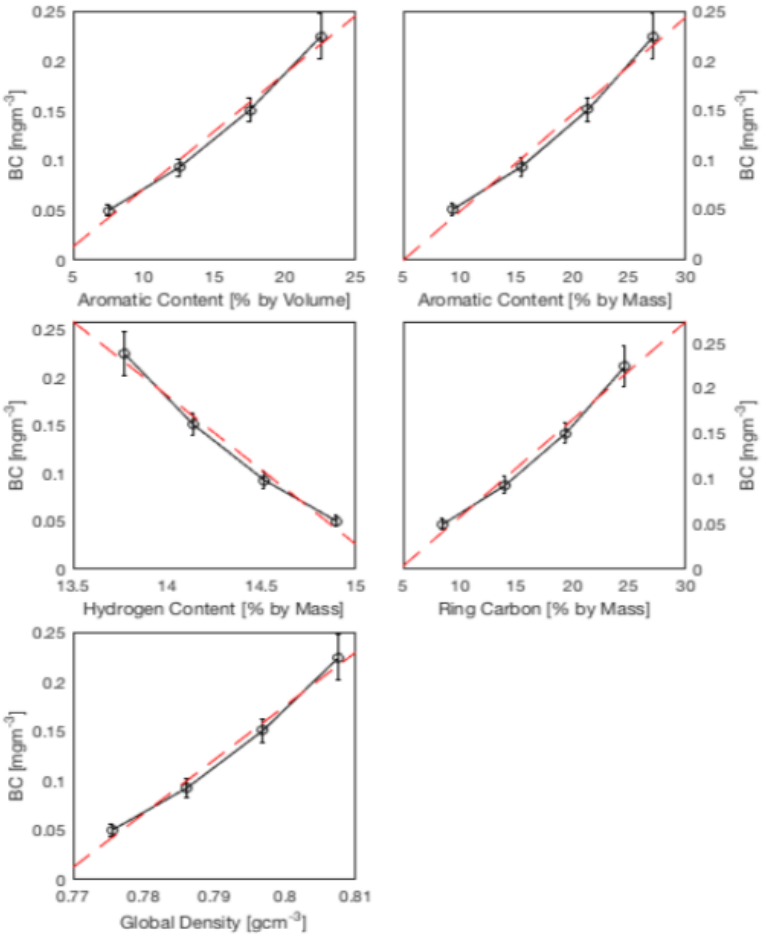

]

Figure D.1.17: Tetralin BC vs a) Vol b) Mass c) Hydrogen % d) Ring Carbon % e) Global Density

	y = mx + c	R^2
Aromatic Content [% vol/vol]	0.0116x – 0.0445	0.98628
Aromatic Content[% mass/mass]	0.00981x – 0.0506	0.98333
Hydrogen Content [% mass/mass]	-0.155x + 2.35	0.98333
Ring Carbon [% mass/mass]	0.0108x – 0.0506	0.98333
Global Density [gcm^{-3}]	5.43 x – 4.17	0.98628

Figure D.1.18: Tetralin Linear Regressions equations and Coefficients of Determination

D.1.10 Diethylbenzene

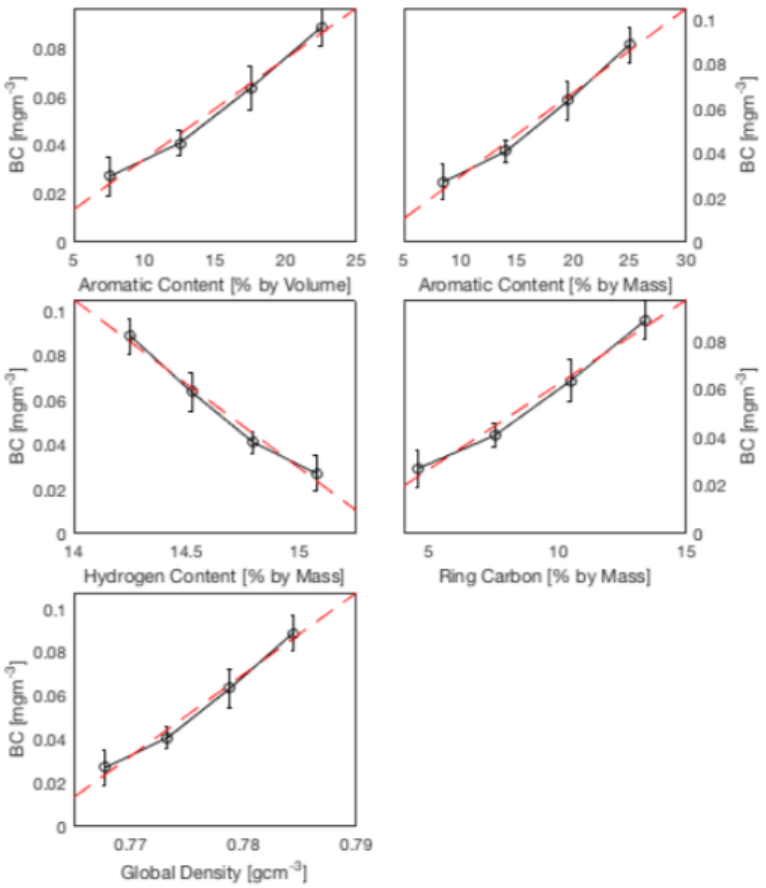

]

Figure D.1.19: Diethylbenzene BC vs a) Vol b) Mass c) Hydrogen % d) Ring Carbon % e) Global Density

	y = mx + c	R^2
Aromatic Content [% vol/vol]	0.00415x – 0.00718	0.98447
Aromatic Content[% mass/mass]	0.00378x – 0.00829	0.98290
Hydrogen Content [% mass/mass]	-0.0759x + 1.17	0.98290
Ring Carbon [% mass/mass]	0.00704x – 0.00829	0.98290
Global Density [gcm^{-3}]	3.76x – 2.86	0.98447

Figure D.1.20: Diethylbenzene Linear Regressions equations and Coefficients of Determination

D.1.11 p-Cymene

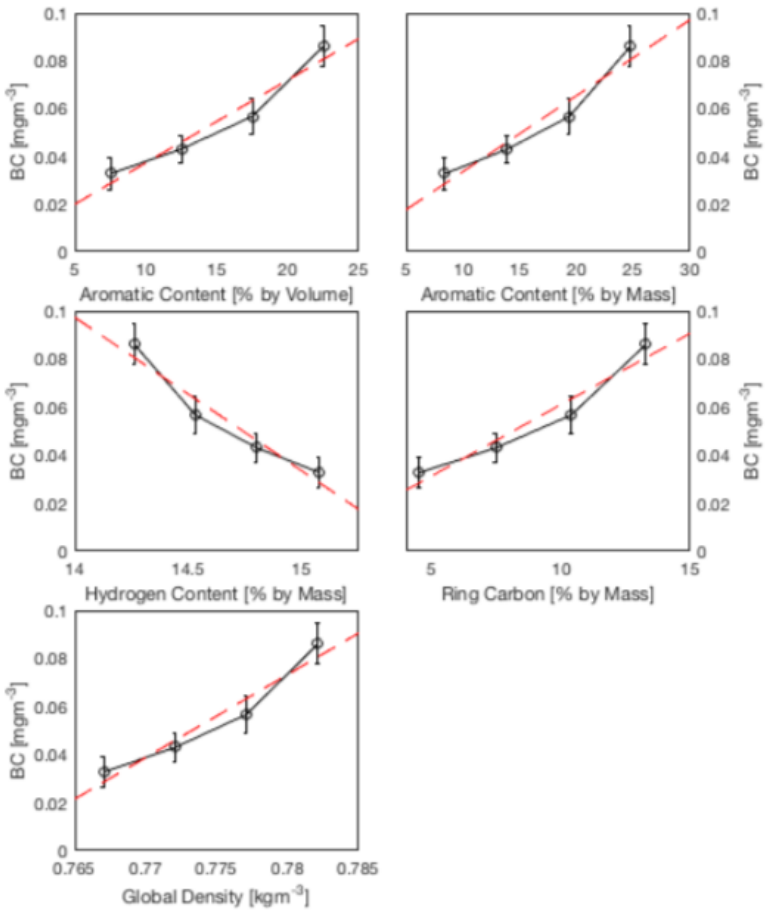

]

Figure D.1.21: p-Cymene BC vs a) Vol b) Mass c) Hydrogen % d) Ring Carbon % e) Global Density

	y = mx + c	R^2
Aromatic Content [% vol/vol]	0.00347x – 0.0252	0.93949
Aromatic Content[% mass/mass]	0.00318x + 0.00171	0.93680
Hydrogen Content [% mass/mass]	-0.0639 + 0.992	0.93680
Ring Carbon [% mass/mass]	0.00593x + 0.00171	0.93680
Global Density [gcm^{-3}]	3.45x – 2.62	0.93949

Figure D.1.22: p-Cymene Linear Regressions equations and Coefficients of Determination

D.1.12 Methylnapthalene

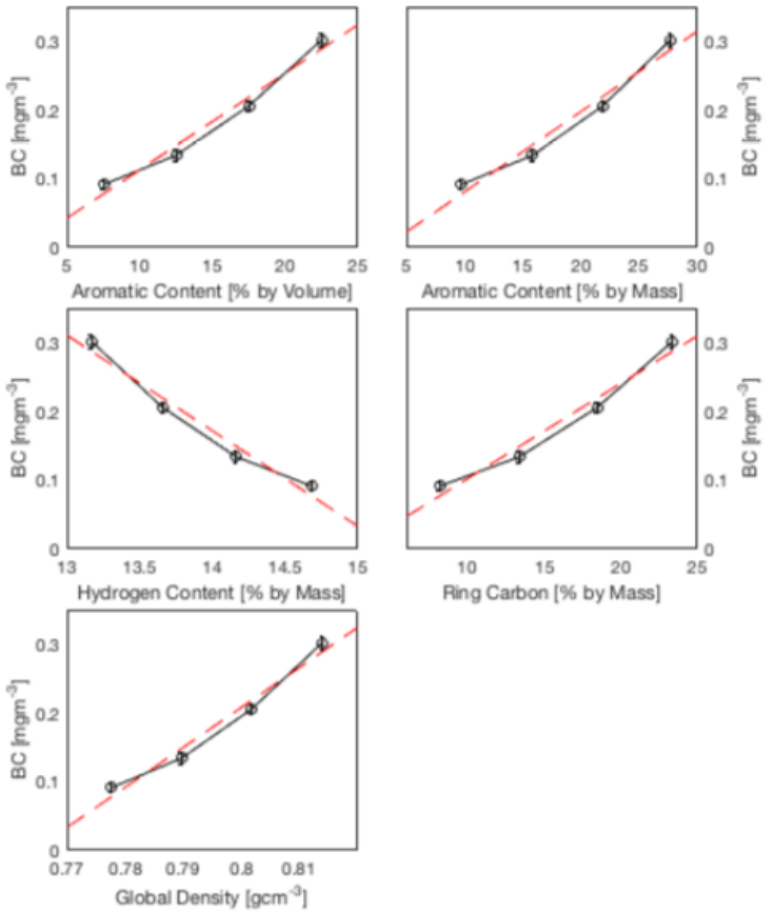

]

Figure D.1.23: Methylnapthalene BC vs a) Vol b) Mass c) Hydrogen % d) Ring Carbon % e) Global Density

	y = mx + c	R^2
Aromatic Content [% vol/vol]	0.00522x – 0.0103	0.97118
Aromatic Content[% mass/mass]	0.00434x – 0.0133	0.96722
Hydrogen Content [% mass/mass]	-0.0516x + 0.786	0.96722
Ring Carbon [% mass/mass]	0.00514x – 0.0133	0.96722
Global Density [gcm^{-3}]	2.16x – 1.65	0.97118

Figure D.1.24: Methylnapthalene Linear Regressions equations and Coefficients of Determination

D.1.13 Isopropylcumene

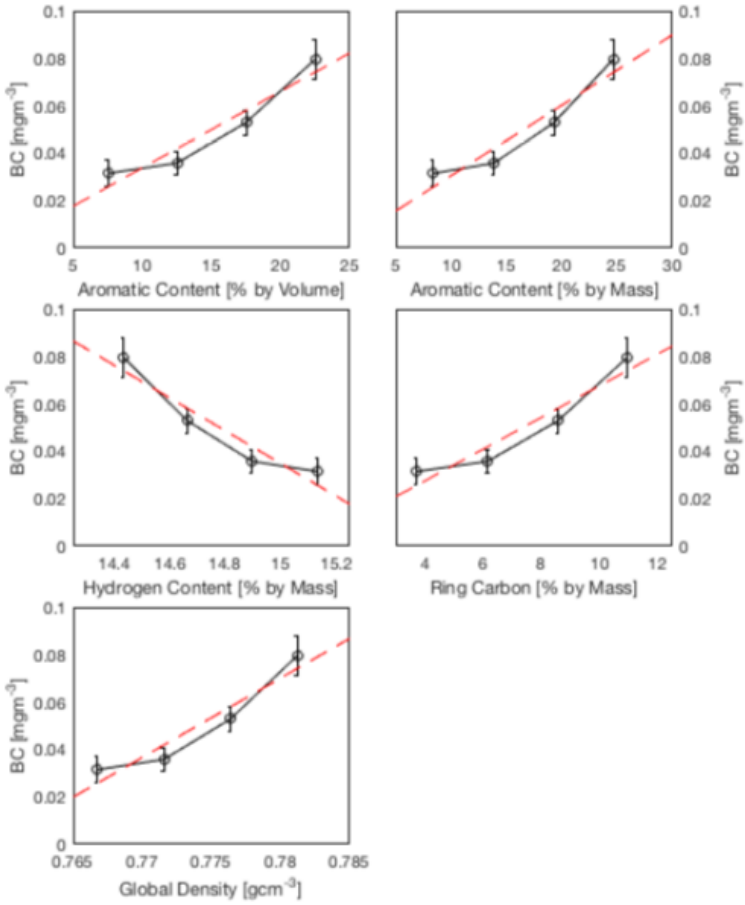

]

Figure D.1.25: Isopropylcumene BC vs a) Vol b) Mass c) Hydrogen % d) Ring Carbon % e) Global Density

	y = mx + c	R^2
Aromatic Content [% vol/vol]	0.00383x – 0.00997	0.97812
Aromatic Content[% mass/mass]	0.00352x – 0.0109	0.97651
Hydrogen Content [% mass/mass]	-0.0817x + 1.25	0.97651
Ring Carbon [% mass/mass]	0.00794x – 0.0109	0.97651
Global Density [gcm^{-3}]	3.97x – 3.02	0.97812

Figure D.1.26: Isopropylcumene Linear Regressions equations and Coefficients of Determination

Appendix E

E.1 Chapter 3 R-studio Code

```
---
title: "FuelsData2014"
author: "James Cronly"
date: "31/03/2021"
output: html_document
---

```{r}
library(xlsx)
library(dplyr)
library(ggplot2)
fuelData <- read.xlsx("./Fuels_tool_2017.xlsx", sheetIndex = 3)
df2 <- data.frame(t(fuelData))
names(df2) <- df2[1,]
df3 <- df2[-1,]
df3$`Aromatics IP 156` <- as.numeric(df3$`Aromatics IP 156`)
df3$`Smoke point` <- as.numeric(df3$`Smoke point`)
df3$pass <- df3$`Smoke point`>=25
```

```{r}
sp_hist <- ggplot(df4, aes(x = `Smoke point`)) +
        geom_histogram(colour = "black",
                       fill = "white") +
```
```

```
        geom_vline(xintercept  = 25)

sp_hist
```

```{r, fig.height=7, fig.width=7}
# Correlations

df4 <- df3

df4[,1:34] <- lapply(df4[,1:34], as.numeric)
lapply(df4[,1:34], class)

library(corrplot)

correlations <- cor(df4[,1:34], use = "pairwise.complete.obs")

corr_plot <- corrplot(correlations,
         type = "upper",
         order = "hclust",
         tl.cex = 0.5)

corr_plot

corr <- as.data.frame(correlations)

```

```{r, fig.height=5, fig.width=7}
# Bar Charts
corr <- arrange(corr, desc(corr$`Smoke point`))

sp <- ggplot(corr) +
        geom_col(aes(x= reorder(rownames(corr),`Smoke point`),y = `Smoke point`),
stat = "identity",
                 colour = 'black',
                 fill = 'white') +
        theme(axis.text.x = element_text(angle = 90)) +
        xlab('Variable') +
```

```
        ylab('Correlation Coefficient [r]')

sp

aro <- ggplot(corr) +
        geom_col(aes(x= reorder(rownames(corr),`Aromatics IP 156`),y = `Aromatics I
                 colour = 'black',
                 fill = 'white') +
        theme(axis.text.x = element_text(angle = 90)) +
        xlab('Variable') +
        ylab('Correlation Coefficient [r]')

aro
```

```
```

```
```{r}

df3$IBP <- as.numeric(df3$IBP)

plot(df3$IBP, df3$`Smoke point`)

cols <- colnames(df3)
cols[7:9] <- c("D_0.1","D_0.5","D_0.9")

colnames(df3) <- cols

df3$D_0.1 <- as.numeric(df3$D_0.1)
df3$D_0.5 <- as.numeric(df3$D_0.5)
df3$D_0.9 <- as.numeric(df3$D_0.9)
df3$FBP <- as.numeric(df3$FBP)

plot(df3$FBP, df3$`Smoke point`)
```
```

```
df3$Viscosity <- as.numeric(df3$Viscosity)

plot(df3$Viscosity, df3$`Smoke point`)
```

```{r, fig.height=5, fig.width=7}
hist(as.numeric(df3$`Aromatics IP 156`), probability = TRUE)

hist_arom <- ggplot(data = df4) +
        geom_histogram(aes(x = `Aromatics IP 156`, y = ..density..), colour = "black",
                       fill = "white",
                       bins = 30) +
        xlab("Aromatic Volume [%]") +
        geom_density(aes(`Aromatics IP 156`),
                     lwd = 0.5,
                     colour = 4)

hist_arom

mean_aro <- mean(df4$`Aromatics IP 156`)
sd_aro <- sd(df4$`Aromatics IP 156`)

lb_aro <- mean_aro - 2*sd_aro
ub_aro <- mean_aro + 2*sd_aro

library(moments)

skewness(df4$`Aromatics IP 156`)
```

```{r}
hist(as.numeric(df3$IBP))
```

```{r}
hist(as.numeric(df3$`Smoke point`),
     breaks = 20,
     probability = TRUE,
```

```
      xlab = "SP [mm]")
abline(v = 24.5,
       col = "red",
       lwd = 4,
       lty = 2)

```
```
```{r}
plot(df3$`Aromatics IP 156`,df3$`Smoke point`)
```
```{r, fig.height=6, fig.width=9}
library(ggplot2)
g1 <- ggplot(df3, mapping = aes(x = `Aromatics IP 156`,y = `Smoke point`))
g1 <- g1 + geom_point(aes(colour = pass),
                      alpha = 0.25)
g1 <- g1 + geom_density_2d(alpha = 0.5)
g1 <- g1 + labs(title = "Aromatic Volume vs Smoke Point – 2014 Jet A-1")
g1

model1 <- lm(df3$`Smoke point`~df3$`Aromatics IP 156`, df3)
aro_vs_sp <- cor(x= df3$`Aromatics IP 156`, y = df3$`Smoke point`)
```



```{r}
plot(df3$FBP,df3$`Smoke point`)
model <- lm(FBP~`Aromatics IP 156`, df3)
```


```{r}
library(dplyr)
pass <- filter(df3, `Smoke point` >= 25)
fail <- filter(df3, df3$`Smoke point` < 25)

plot(pass$`Aromatics IP 156`, pass$`Smoke point`)
```


```{r}
hist(as.numeric(df3$`Density kg/m3`), probability = TRUE, breaks = 20)
```
```

```
```
```{r}
library(ggpubr)
g2 <- ggplot(df3, aes(x= `Aromatics IP 156`, y=`Smoke point`))
g2 <- g2 + geom_point(alpha = 0.25, aes(colour = pass))
g2 <- g2 + facet_wrap(df3$pass)
g2 <- g2 + geom_smooth(method = lm)
g2 <- g2 + labs(title = "Aromatic Volume vs SP - 2014 Jet A-1")
g2 <- g2 + stat_regline_equation(label.y = 30, aes(label = ..rr.label..))
g2
```
```{r}
g3 <- ggplot(df3)
g3 <- g3 + geom_boxplot(aes(x = pass,
                            y = `Aromatics IP 156`,
                            colour = pass))
g3
```
```{r, fig.height=12, fig.width=12}
library(gridExtra)
export <- grid.arrange(g2,g3,ncol = 1)
```
```{r, fig.width=8, fig.height=5}
df3$`Density kg/m3` <- as.numeric(df3$`Density kg/m3`)
g4 <- ggplot(df3, aes(x= `Density kg/m3`, y=`Smoke point`))
g4 <- g4 + geom_point(alpha = 0.25, aes(colour = pass))
g4 <- g4 + facet_wrap(df3$pass)
g4 <- g4 + geom_smooth(method = lm)
g4 <- g4 + labs(title = "Density vs SP - 2014 Jet A-1")
g4 <- g4 + stat_regline_equation(label.y = 30, aes(label = ..rr.label..))
g4

df5 <- df4

xlab_dens <- expression(Density ~ (kgm^-3))
hist_density <- ggplot(df5) +
        geom_histogram(aes(`Density kg/m3`, y = ..density..),
                       fill = "white",
```

```
                        colour = "black") +
        geom_density(aes(`Density kg/m3`),
                     lwd = 0.5,
                     colour = 4) +
        xlab(xlab_dens)

hist_density
```
```
```{r, fig.width=8, fig.height=5}
# Density Histogram

g5 <- ggplot(df3, aes(`Density kg/m3`))
g5 <- g5 + geom_histogram(aes(colour = pass, y =..density..))
g5 <- g5 + facet_wrap(.~pass) +
        theme(panel.spacing = unit(2, "lines")) +
        xlab(xlab_dens) +
        geom_density(aes(`Density kg/m3`),
                     lwd = 0.5,
                     colour = 4)
g5

# Pass Percentage < 800

pass$`Density kg/m3` <- as.numeric(pass$`Density kg/m3`)

(nrow(filter(pass, `Density kg/m3` < 800))/nrow(pass)) *100

# Fail Percentage > 800

fail$`Density kg/m3` <- as.numeric(fail$`Density kg/m3`)

(nrow(filter(fail, `Density kg/m3` > 800))/nrow(fail)) *100

```
```
```{r, fig.height=8, fig.width=12}
density <- grid.arrange(g4, g5, ncol = 1)
density
```
```
```{r}
```
```

```
df3$IBP <- as.numeric(df3$IBP)
df3$FBP <- as.numeric(df3$FBP)


```

```{r, fig.width=8, fig.height=5}
# Napthalenes

fail$Naphthalenes <- as.numeric(fail$Naphthalenes)
g6 <- ggplot(fail, aes(x= Naphthalenes, y=`Smoke point`)) +
        geom_point(alpha = 0.25, aes(colour = pass)) +
        geom_smooth(method = lm) +
        labs(title = NULL) +
        stat_regline_equation(label.y = 30, aes(label = ..rr.label..)) +
        xlab("Naphthalenes Volume [%]") +
        ylab("SP [mm]")

g6

fail$Ratio <- fail$Naphthalenes/fail$`Aromatics IP 156`

g7 <- ggplot(fail, aes(x= Ratio, y=`Smoke point`)) +
        geom_point(alpha = 0.25, aes(colour = pass)) +
        geom_smooth(method = lm) +
        labs(title = NULL) +
        stat_regline_equation(label.y = 30, aes(label = ..rr.label..)) +
        xlab("Naphthalenes/Aromatic Volume Ratio") +
        ylab("SP [mm]")

g7
```

```{r}
# Look at specific energy

df3$`Specific Energy` <- as.numeric(df3$`Specific Energy`)
```

```
df3$Energy_Density <- df3$`Specific Energy` * df3$`Density kg/m3`

plot(df3$`Specific Energy`,df3$`Aromatics IP 156`)
```

```{r}
# Model pass/fail
library(caret)

df3_model <- df3

df3_model$pass <- as.factor(df3_model$pass)

pass_model <- train(form = pass ~ IBP + D_0.1 + D_0.5 + D_0.9 + FBP,
                    data = df3_model,
                    trControl = trainControl(method = "cv", number = 5),
                    method = "glm",
                    family = "binomial")
```

```{r}
mean_pass <- mean(pass$`Aromatics IP 156`)
mean_fail <- mean(fail$`Aromatics IP 156`)

median_pass <- median(pass$`Aromatics IP 156`)
median_fail <- median(fail$`Aromatics IP 156`)

sd_pass <- sd(pass$`Aromatics IP 156`)
sd_fail <- sd(fail$`Aromatics IP 156`)
```

```{r, fig.width=7, fig.height=5}
t.test(pass$`Aromatics IP 156`, fail$`Aromatics IP 156`)

g8 <- ggplot() +
        geom_density(aes(pass$`Aromatics IP 156`)) +
        geom_density(aes(fail$`Aromatics IP 156`))
g8
```

```
g9 <- ggplot(data.frame(x = c(10,25)), aes(x = x), colour) +
        stat_function(fun = dnorm, args = list(mean_pass, sd_pass),
                      colour = "orangered1") +
        stat_function(fun = dnorm, args = list(mean_fail, sd_fail),
                      colour = "turquoise3") +
        scale_x_continuous(name = "Aromatic Volume") +
        scale_y_continuous(name = "probability") +
        scale_color_manual(name = "pass/fail",
                           breaks = c('fail','pass'),
                           values = c('pass' = 'turquoise3', 'fail' = "orangered1"))

g9
```
```
```{r, fig.width=7, fig.height=5}
df5 <- df4

for (i in 1:nrow(df5)) {
        if(df5$`Smoke point`[i] < 20 & df5$`Smoke point`[i] >= 19) {
                df5$SP_band[i] <- "19 to 20"
        }
        if(df5$`Smoke point`[i] < 21 & df5$`Smoke point`[i] >= 20) {
                df5$SP_band[i] <- "20 to 21"
        }
        if(df5$`Smoke point`[i] < 22 & df5$`Smoke point`[i] >= 21) {
                df5$SP_band[i] <- "21 to 22"
        }
        if(df5$`Smoke point`[i] < 23 & df5$`Smoke point`[i] >= 22) {
                df5$SP_band[i] <- "22 to 23"
        }
        if(df5$`Smoke point`[i] < 24 & df5$`Smoke point`[i] >= 23) {
                df5$SP_band[i] <- "23 to 24"
        }
        if(df5$`Smoke point`[i] < 25 & df5$`Smoke point`[i] >= 24) {
                df5$SP_band[i] <- "24 to 25"
        }
        if(df5$`Smoke point`[i] < 26 & df5$`Smoke point`[i] >= 25) {
                df5$SP_band[i] <- "25 to 26"
        }
        if(df5$`Smoke point`[i] < 29 & df5$`Smoke point`[i] >=26) {
```
```

```
                df5$SP_band[i] <- "26_to_29"
        }

}

g10 <- ggplot(df5, aes(x = SP_band, y = `Aromatics IP 156`), group = SP_band) +
        geom_boxplot(aes(fill = SP_band)) +
        xlab("SP_[mm]") +
        ylab("Aromatic_Volume_[%]")

g10

aro_group_mean <- df5 %>% group_by(SP_band) %>%
        summarise(mean_aro_vol = mean(`Aromatics IP 156`),
                  sd_aro_vol = sd(`Aromatics IP 156`))

aro_group_mean$mean_aro_vol <- as.numeric(aro_group_mean$mean_aro_vol)
aro_group_mean$SP_band <- as.factor(aro_group_mean$SP_band)

g11 <- ggplot(aro_group_mean, mapping = aes(x = SP_band, y = mean_aro_vol)) +
        geom_point(shape = 9,
                   size = 3,
                   colour = "blue") +
        geom_errorbar(aes(ymin = mean_aro_vol-(2*sd_aro_vol),
                          ymax = mean_aro_vol+(2*sd_aro_vol)),
                      colour = "black",
                      alpha = 0.5) +
        scale_y_continuous(limits = c(10,25)) +
        xlab("SP_[mm]") +
        ylab("Aromatic_Volume_[%]") +
        geom_smooth(method = lm, colour = "red")

g11

```
```{r, fig.width=7, fig.height=5}
# Naphthalene Content

g12 <- ggplot(fail) +
```

```
        geom_histogram(aes(Naphthalenes, y = ..density..),
                       fill = "white",
                       colour = "black") +
        geom_density(aes(Naphthalenes),
                     lwd = 0.5,
                     colour = 4) +
        xlab("Naphthalenes Volume [%]")
```

g12

```
fail$Naphthalenes <- as.numeric(fail$Naphthalenes)

fail_no_NA <- filter(fail, !is.na(fail$Naphthalenes))

mean_napth_vol <- mean(fail_no_NA$Naphthalenes)
sd_napth_vol <- sd(fail_no_NA$Naphthalenes)
```

```{r}
# SVD

refined_var <- df5[-c(5,16,20:32)]

refined_var <- refined_var[complete.cases(refined_var),]

my_Pr <-prcomp(refined_var[,-c(20:22)],
               scale = TRUE)
summary(my_Pr)

complete_fuel <- df5[complete.cases(df5),]

my_Pr_2 <-prcomp(complete_fuel[,-c(35:37)],
               scale = TRUE)

summary(my_Pr_2)

# Barchart of PC Importance
```

```
PCA_sum <- as.data.frame(summary(my_Pr)$importance[2,])
PCA_sum$PCA <- row.names(PCA_sum)

PCA_bar <- ggplot(PCA_sum, aes(x = reorder(PCA, -`summary(my_Pr)$importance[2, ]`),
                               y = `summary(my_Pr)$importance[2, ]`)) +
        geom_bar(stat = "identity") +
        xlab("Principal Components") +
        ylab("Proportion of Variance") +
        theme(axis.text.x = element_text(angle = 90, vjust = 0.5, hjust=1))

PCA_bar



for (i in 1:nrow(PCA_sum)) {
        PCA_sum$Sum[i] <- sum(PCA_sum$`summary(my_Pr)$importance[2, ]`[1:i])
}

PCA_sum$PCA_num <- 1:19

PCA_cum_line <- ggplot(PCA_sum, aes(x = PCA_num, y = Sum)) +
        geom_line(linetype = "dashed",
                  colour = "red") +
        geom_point(type = 3) +
        xlab("Number of PCA Variables") +
        ylab("Cumulative Proportion")

PCA_cum_line

# Attach PC's to data frame

refined_var_2 <- cbind(refined_var, my_Pr$x)

head(refined_var)

# PlotsSP (pass/fail)

g13 <- ggplot(refined_var_2, aes(PC1, PC2, col = pass, fill = pass)) +
        geom_point(alpha = 0.5) +
        stat_ellipse(geom = "polygon", col = "black", alpha = 0.25) +
```

```
        theme(legend.position = "top") +
        facet_wrap(~ SP_band)

g13

g14 <- ggplot(refined_var_2, aes(PC1, PC3, col = pass, fill = pass)) +
        geom_point() +
        stat_ellipse(geom = "polygon", col = "black", alpha = 0.25) +
        theme(legend.position = "top") +
        facet_wrap(~ SP_band)

g14

g15 <- ggplot(refined_var_2, aes(PC2, PC3, col = pass, fill = pass)) +
        geom_point() +
        stat_ellipse(geom = "polygon", col = "black", alpha = 0.25) +
        theme(legend.position = "top")

g15

pca_pass_fail <- grid.arrange(g13,g14,g15, nrow = 1, ncol = 3)

plot(pca_pass_fail)

# Plot SP (bands)

g16 <- ggplot(refined_var_2, aes(PC1, PC2, col = SP_band, fill = SP_band)) +
        geom_point() +
        stat_ellipse(geom = "polygon", col = "black", alpha = 0.25) +
        theme(legend.position = "top")

g16

g17 <- ggplot(refined_var_2, aes(PC1, PC3, col = SP_band, fill = SP_band)) +
        geom_point() +
        stat_ellipse(geom = "polygon", col = "black", alpha = 0.25) +
        theme(legend.position = "top")

g17
```

```
g18 <- ggplot(refined_var_2, aes(PC2, PC3, col = SP_band, fill = SP_band)) +
        geom_point() +
        stat_ellipse(geom = "polygon", col = "black", alpha = 0.25) +
        theme(legend.position = "top")

g18

g19 <- ggplot(refined_var_2, aes(PC1, PC2, col = pass, fill = pass)) +
        geom_point() +
        stat_ellipse(geom = "polygon", col = "black", alpha = 0.25) +
        theme(legend.position = "top")

g19

g19a <- ggplot(refined_var_2, aes(PC1, PC3, col = pass, fill = pass)) +
        geom_point() +
        stat_ellipse(geom = "polygon", col = "black", alpha = 0.25) +
        theme(legend.position = "top")

g19a

pca_bands <- grid.arrange(g16,g17,g18, nrow = 2, ncol = 2)

plot(pca_bands)



# Correlations between VARS and PCS



PCA_corrplot <- corrplot(cor(refined_var[,-c(20:22)], refined_var_2[,c(22:40)]),
          tl.cex = 0.75)

corrplot(PCA_corrplot)
# PCR matrix

mat_PCR <- as.data.frame(my_Pr$rotation)
```

```
```

```{r}
# Multivariate Regression

model_regression <- lm(`Smoke point` ~ `Density kg/m3` +
                                       Colour +

                                       IBP +
                                       `0.1` +

                                       `Flash point` +
                                       Viscosity


                       , data = df5[,1:19])

summary(model_regression)

select_predict <- select(df5, `Density kg/m3`,
                         Colour,

                         IBP,
                         `0.1`,

                          `Flash point`,
                         Viscosity



                         )

predicted_values_df <- predict(model_regression, select_predict)

plot(predicted_values, df5$`Smoke point`)

complete_predict <- cbind(predicted_values, df5$`Smoke point`)
```

```
complete_predict <- as.data.frame(complete_predict)

complete_predict <- complete_predict[complete.cases(complete_predict),]

colnames(complete_predict) <- c("predicted", "actual")

g20 <- ggplot(complete_predict, aes(x= predicted, y=actual)) +
        geom_point(alpha = 0.15) +
        geom_smooth(method = "lm", se = TRUE) +
        labs(title = NULL) +
        xlab("Predicted Value") +
        ylab("Actual Value") +
        xlim(18,30) +
        ylim(18,30) +
        annotate("text", x=20, y= 27.5, label = "r2 = 0.75" )


g20

```
```{r}
# Regression Tree

# Use 10-fold validation

library(caret)
library(rpart)
library(rpart.plot)
library(rsample)

ctrl <- trainControl(method = "cv", number = 10)

refined_var$pass <- as.factor(refined_var$pass)
# What Passes SP

pass_SP <- rpart(pass~.,
                 data = refined_var,
                 method = "class"
```

```
                    )

rpart.plot(pass_SP)

# Pass SP without SP

pass_without_SP <- rpart(pass ~. -`Smoke point` -SP_band,
                    data = refined_var,
                    method = "class"
                    # trControl = ctrl,
                    # importance = TRUE
                    )

rpart.plot(pass_without_SP)
plotcp(pass_without_SP)

# What Bands

refined_var$SP_band <- as.factor(refined_var$SP_band)

what_bands <- rpart(SP_band ~. -`Smoke point` -pass,
                    data = refined_var,
                    method = "class"
                    # trControl = ctrl,
                    # importance = TRUE
                    )

fancyRpartPlot(what_bands)
plotcp(what_bands)

# Regression Tree

# Not CARET

set.seed(456)

inTrain <- createDataPartition(y=refined_var$`Smoke point`,
                               p=0.7,
                               list = FALSE)
```

```
training <- refined_var[inTrain,]
testing <- refined_var[-inTrain,]



decision_regression <- rpart(`Smoke point` ~ Colour +
                                             Acidity +
                                             `Aromatics IP 156` +
                                             `Sulphur %` +
                                             IBP +
                                             `0.1` +
                                             `0.5` +
                                             `0.9` +
                                             FBP +
                                             `Flash point` +
                                             `Density kg/m3` +
                                             `Freezing point` +
                                             Viscosity +
                                             `Specific Energy` +
                                             `Existent Gum` +
                                             MSEP +
                                             `Distillation T50-T10`+
                                             `Distillation T90-T10`
                                             ,
                                    data = training,
                                    method = "anova",
                                    control = list(cp = 0, xval = 10)
                                    )

pred <- predict(decision_regression, newdata = testing)
RMSE(pred = pred, obs = testing$`Smoke point`)

importance <- as.data.frame(decision_regression$variable.importance)

comparison <- as.data.frame(cbind(pred, testing$`Smoke point`))

g21 <- ggplot(comparison, aes(x= pred, y=V2)) +
        geom_point(alpha = 0.5) +
```

```
        geom_smooth(method = "lm", se = TRUE) +
        labs(title = NULL) +
        xlab("Predicted Value") +
        ylab("Actual Value") +
        xlim(18,30) +
        ylim(18,30) +
        annotate("text", x=20, y= 27.5, label = "" )


g21

tmp <- printcp(decision_regression)
rsq.val <- 1-tmp[,c(3,4)]
rsq.rpart(decision_regression)

importance$variables <- rownames(importance)

importance <- arrange(importance)

g22 <- ggplot(data = importance) +
        geom_bar(aes(x=reorder(variables, -`decision_regression$variable.importance`),
                     y = `decision_regression$variable.importance`),
                     stat = "identity") +
        theme(axis.text.x=element_text(angle=45, hjust=1)) +
        xlab("Variable") +
        ylab("Importance")


g22


```

E.2 Chapter 5 Code

```{r}


```

```
bannersol_percentages <- c(1.0,17.53,24.08,19.84,36.75,0.79)

bannersol_content <- c("Nonane",
                       "Decane",
                       "Undecane",
                       "Dodecane",
                       "Tridecane",
                       "Tetradecane")
bannersol_component_density <- c(0.718, 0.730, 0.740, 0.75, 0.756, 0.76)

bannersol_component_carbon <- c(9,10,11,12,13,14)

bannersol_component_hydrogen <- c(20,22,24,26,28,30)

bannersol <- data.frame(cbind(bannersol_content,
                              bannersol_percentages,
                              bannersol_component_density,
                              bannersol_component_carbon,
                              bannersol_component_hydrogen))

bannersol$hydrogen_ratio <- as.numeric(bannersol$bannersol_component_hydrogen)/as.n

bannersol_density <- 0

for (i in 1:length(bannersol$bannersol_content)) {
        bannersol_density <- bannersol_density + (as.numeric(bannersol[i,2])/100 *
}

bannersol_density <- 0.7596

bannersol_HC <- 0

for (i in 1:length(bannersol$bannersol_content)) {
        bannersol_HC <- bannersol_HC + (as.numeric(bannersol[i,2])/100 * as.numeric
}


```

```
```{r, echo = FALSE, results=FALSE, warning = FALSE, message=FALSE}
library(xlsx)

data <- read.xlsx("Aromatic_LII_for_R.xlsx", header = TRUE, sheetIndex = 1)

data$Aromatic.Mass.Percentage <- 100*((data$X..Aromatic..vol.vol.*data$Aromatic.Density)

data$Blend.Density <- data$X..Aromatic..vol.vol.*data$Aromatic.Density/100 + data$X..Ban

data$Hydrogen_Ratio_Aromatic <- data$Hydrogen.Number/data$Total.Carbon.Number

carbon_mass <- 12.011
hydrogen_mass <- 1.00797

data$aromatic_ring_carbon <- (data$Ring.Carbon.Number * carbon_mass)/
        ((data$Total.Carbon.Number*carbon_mass)+(data$Hydrogen.Number*hydrogen_mass))

data$ring_carbon_percentage <- data$Aromatic.Mass.Percentage * data$aromatic_ring_carbon

data$HC_blend <-
        (data$X..Aromatic..vol.vol./100*data$Hydrogen_Ratio_Aromatic) +
        (data$X..Bannersol..vol.vol./100*bannersol_HC)

```


```{r}
for (i in 1:length(data$Fuel.Code)) {
        if(data$Aromatic.Type[i] == "Indan" |
           data$Aromatic.Type[i] == "Tetralin" |
           data$Aromatic.Type[i] == "Methylnapthalene")
        {data$classification[i] <- "Polycylic"}
        else {data$classification[i] <- "Alkylbenzene"}

}
```


```{r, echo = FALSE, results=FALSE, warning = FALSE, message=FALSE}
```
```

```
Common_name <- c("Toluene",
                 "Styrene",
                 "o-Xylene",
                 "Ethylbenzene",
                 "Indan",
                 "alpha-Methylstyrene",
                 "Pseudocumene",
                 "Cumene",
                 "Tetralin",
                 "Diethylbenzene",
                 "p-Cymene",
                 "Methylnapthalene",
                 "Isopropylcumene")

CAS_number <- c("108-88-3",
                "100-42-5",
                "96-47-6",
                "100-41-4",
                "496-11-7",
                "98-83-9",
                "95-63-6",
                "98-82-8",
                "119-64-2",
                "25340-17-4",
                "99-87-6",
                "90-12-0",
                "99-27-7")

HC_ratio <- c(1.143,
              1,
              1.25,
              1.25,
              1.111,
              1.111,
              1.333,
              1.333,
              1.2,
              1.4,
```

```
                1.4,
                0.909,
                1.5)

specific_energy <- c(40.589,
                     42.205,
                     40.961,
                     40.938,
                     42.162,
                     40.810,
                     40.984,
                     41.217,
                     42.523,
                     43.683,
                     43.644,
                     40.668,
                     "TBD")

Boiling_Point <- c("110-111",
                   "145-146",
                   "143-145",
                   "136",
                   "175-177",
                   "165-169",
                   "169-171",
                   "152-154",
                   "206-208",
                   "180-182",
                   "177",
                   "240-243",
                   "203")

molecular_mass <- c(92.14,
                    104.15,
                    106.17,
                    106.17,
                    118.18,
                    118.18,
                    120.19,
```

```
                    120.19,
                    132.20,
                    134.22,
                    134.22,
                    142.20,
                    162.27)

density <- as.numeric(c(0.865,0.906,0.879,0.867,0.965,0.909,0.876,0.864,0.973,0.870

fuel_properties <- cbind(Common_name,
                         CAS_number,
                         density,
                         HC_ratio,
                         specific_energy,
                         Boiling_Point,
                         molecular_mass)

fuel.data.frame <- as.data.frame(fuel_properties)

names(fuel.data.frame)[1:7] <- c("Name",
                    "CAS",
                    expression("Density [g/cm\u00B3)]"),
                    "H:C",
                    "Specific Energy [MJ/kg]",
                    "Boiling Point [C]",
                    "Molecular Mass [g/mol]")

library(knitr)
library(kableExtra)

final <- fuel.data.frame %>%
        kbl(caption = "Aromatic Properties", align = "c") %>%
        kable_classic(full_width = T, html_font = "Cambria") %>%
        kable_styling(latex_options = "hold_position")

```

```{r, echo = FALSE, fig.width=2}
## Array of aromatic images
```

```
library(png)
library(EBImage)
library(magick)

AR1 <- image_read("./Images/1-Toluene.png")
AR1 <- image_annotate(AR1,
                      text = "Toluene",
                      location = "+130+50",
                      size = 30,
                      weight = 700)

AR2 <- image_read("./Images/2-Styrene.png")
AR2 <- image_annotate(AR2,
                      text = "Styrene",
                      location = "+130+50",
                      size = 30,
                      weight = 700)

AR3 <- image_read("./Images/3-o-Xylene.png")
AR3 <- image_annotate(AR3,
                      text = "o-Xylene",
                      location = "+130+50",
                      size = 30,
                      weight = 700)

AR4 <- image_read("./Images/4-Ethylbenzene.png")
AR4 <- image_annotate(AR4,
                      text = "Ethylbenzene",
                      location = "+130+50",
                      size = 30,
                      weight = 700)

AR5 <- image_read("./Images/5-Indene.png")
AR5 <- image_annotate(AR5,
                      text = "Indene",
                      location = "+130+50",
                      size = 30,
                      weight = 700)
```

```
AR6 <- image_read("./Images/6-Indan.png")
AR6 <- image_annotate(AR6,
                      text = "Indan",
                      location = "+130+50",
                      size = 30,
                      weight = 700)

AR7 <- image_read("./Images/7-alpha-Methylstyrene.png")
AR7 <- image_annotate(AR7,
                      text = "alpha-Methylstyrene",
                      location = "+130+50",
                      size = 30,
                      weight = 700)

AR8 <- image_read("./Images/8-Pseudocumene.png")
AR8 <- image_annotate(AR8,
                      text = "Pseudocumene",
                      location = "+130+50",
                      size = 30,
                      weight = 700)

AR9 <- image_read("./Images/9-Cumene.png")
AR9 <- image_annotate(AR9,
                      text = "Cumene",
                      location = "+130+50",
                      size = 40,
                      weight = 700)

AR10 <- image_read("./Images/10-Tetralin.png")
AR10 <- image_annotate(AR10,
                      text = "Tetralin",
                      location = "+130+50",
                      size = 30,
                      weight = 700)

AR11 <- image_read("./Images/11-5-tert-Butyl-m-xylene.png")
AR11 <- image_annotate(AR11,
                      text = "5-tert-Butyl-m-xylene",
                      location = "+130+50",
```

```
                        size = 30,
                        weight = 700)

AR12 <- image_read("./Images/12-Diethylbenzene.png")
AR12 <- image_annotate(AR12,
                        text = "Diethylbenzene",
                        location = "+130+50",
                        size = 30,
                        weight = 700)

AR13 <- image_read("./Images/13-p-Cymene.png")
AR13 <- image_annotate(AR13,
                        text = "p-Cymene",
                        location = "+130+50",
                        size = 30,
                        weight = 700)

AR14 <- image_read("./Images/14-tert-butylbenzene.png")
AR14 <- image_annotate(AR14,
                        text = "tert-butylbenzene",
                        location = "+130+50",
                        size = 30,
                        weight = 700)

AR15 <- image_read("./Images/15-Methylnapthalene.png")
AR15 <- image_annotate(AR15,
                        text = "Methylnapthalene",
                        location = "+130+50",
                        size = 30,
                        weight = 700)

AR16 <- image_read("./Images/16-3-isopropylcumene.png")
AR16 <- image_annotate(AR16,
                        text = "3-isopropylcumene",
                        location = "+130+50",
                        size = 30,
                        weight = 700)

aromatic_images <- c(AR1,AR2,AR3,AR4,AR6,AR7,AR8,AR9,AR10,AR12,AR13,
```

```
                        AR15,AR16)

aromatic_array <- image_montage(aromatic_images,
                                tile = "4x4",
                                geometry = "450x125 +0+25")

aromatic_array

```

```{r, fig.height=7, echo = FALSE}
library(ggplot2)
vol.labs <- c("7.5% vol/vol", "12.5% vol/vol", "17.5% vol/vol", "22.5% vol/vol")
g5 <- ggplot(data, aes(x = reorder(Aromatic.Type, LII), y = LII))
g5 <- g5 + geom_bar(aes(x = reorder(Aromatic.Type, LII), y = LII),
                    stat = "identity",
                    fill = "skyblue",
                    colour = "blue",
                    alpha = 0.5)
g5 <- g5 + geom_errorbar(data, mapping = aes(ymin = LII - 2*SD, ymax = LII + 2*SD),
                         size = 0.15)
g5 <- g5 + coord_flip()
g5 <- g5 + facet_grid(data$X..Aromatic..vol.vol.~.)
g5 <- g5 + labs(x = "Aromatic Type",
                y = "Black CarbonC [mg/m3]",
                title = "Black Carbon Mass Emissions for 10 Alkylbenzenes and 3 Po

print(g5)

```

```
\newpage

```

```{r, echo = FALSE, fig.height=2, fig.width=16, warning=FALSE,message=FALSE}
g6 <- ggplot(data, aes(X..Aromatic..vol.vol., LII))
g6 <- g6 + geom_point() + facet_grid(.~data$Aromatic.Type) + xlim(5,25)
g6 <- g6 + geom_smooth(method = "lm", lwd = 0.5, se = FALSE)
g6 <- g6 + xlab("Aromatic Content [% mass/mass]")
```

```
g6 <- g6 + ylab("mg/m\3")
g6
```

```{r echo=FALSE, fig.height=2, fig.width=16, message=FALSE, warning=FALSE}
g7 <- ggplot(data, aes(Aromatic.Mass.Percentage, LII))
g7 <- g7 + geom_point() + facet_grid(.~data$Aromatic.Type) + xlim(5,30)
g7 <- g7 + geom_smooth(method = "lm", lwd = 0.5, col="red", se = FALSE)
g7 <- g7 + xlab("Aromatic Content [% vol/vol]")
g7 <- g7 + ylab("BC [mg/m\3]")
g7
```

```{r, echo=FALSE, fig.height=2, fig.width=16, message=FALSE, warning=FALSE}
g9 <- ggplot(data, aes(HC_blend, LII))
g9 <- g9 + geom_point() + facet_grid(.~data$Aromatic.Type)
g9 <- g9 + geom_smooth(method = "lm", lwd = 0.5, col="orange", se = FALSE)
g9 <- g9 + xlab("Hydrogen:Carbon Ratio")
g9 <- g9 + ylab("BC [mg/m\3]")
g9 <- g9 + theme(axis.text.x = element_text(angle = 90, vjust = 0.5, hjust=1))
g9
```

```{r echo=FALSE, fig.height=2, fig.width=16, message=FALSE, warning=FALSE}
g8 <- ggplot(data, aes(ring_carbon_percentage, LII))
g8 <- g8 + geom_point() + facet_grid(.~data$Aromatic.Type)
g8 <- g8 + geom_smooth(method = "lm", lwd = 0.5, col="green", se = FALSE)
g8 <- g8 + xlab("Ring Carbon Content [% mass/mass]")
g8 <- g8 + ylab("BC [mg/m\3]")
g8
```

```{r echo=FALSE, fig.height=2, fig.width=16, message=FALSE, warning=FALSE}
g10 <- ggplot(data, aes(Blend.Density, LII))
g10 <- g10 + geom_point() + facet_grid(.~data$Aromatic.Type)
g10 <- g10 + geom_smooth(method = "lm", lwd = 0.5, col="purple", se = FALSE)
g10 <- g10 + xlab("Blend Density [g/cm\3]")
g10 <- g10 + ylab("BC [mg/m\3]")
g10 <- g10 + theme(axis.text.x = element_text(angle = 90, vjust = 0.5, hjust=1))
```

```
g10
```
```
```{r, fig.height= 10, fig.width= 16}
library(gridExtra)
LII_individual <- grid.arrange(g6,g7,g8,g9,g10, nrow = 5, ncol = 1)
LII_individual
```
```


```{r}
library(dplyr)
g11 <- ggplot(data, aes(HC_blend, LII))
g11 <- g11 + geom_point()
g11 <- g11 + facet_grid(.~data$X..Aromatic..vol.vol.)
g11 <- g11 +  ylab("LII BC Concentration [ mg/m^3]")
g11 <- g11 + xlab("H/C Ratio")
g11 <- g11 + geom_smooth(method = "lm",
                         lwd = 1,
                         aes(linetype = classification),
                         se = FALSE,
                         colour = "Red")
g11 <- g11 + theme(axis.text.x = element_text(angle = 90, vjust = 0.5, hjust=1))

g11
```
```


```{r}
g12 <- ggplot(data, aes(ring_carbon_percentage,
                        LII,
                        shape = classification))
g12 <- g12 + geom_point()
g12 <- g12 + facet_grid(.~data$X..Aromatic..vol.vol.)
g12 <- g12 + geom_smooth(method = "lm",
                         lwd = 1,
                         aes(linetype = classification),
                         se = FALSE,
                         colour = "Orange")
g12 <- g12 + xlab("Ring Carbon [% by Mass]")
g12 <- g12 + ylab("LII BC Concentration [ mg/m^3]")
```
```

```
g12 <- g12 + scale_fill_discrete(name = "New Legend Title")

g12
```

```{r}
g13 <- ggplot(data, aes(Blend.Density, LII,
                        shape = classification))
g13 <- g13 + geom_point()
g13 <- g13 + facet_grid(.~data$X..Aromatic..vol.vol.)
g13 <- g13 + geom_smooth(method = "lm",
                         lwd = 1,
                         aes(linetype = classification),
                         se = FALSE,
                         colour = "Green")
g13 <- g13 + xlab("Global Density [g/cm^3]")
g13 <- g13 + ylab("LII BC Concentration [mg/m^3]")
g13
```

```{r}
g13a <- ggplot(data, aes(X..Aromatic..vol.vol., LII))
g13a <- g13a + geom_point()
g13a <- g13a + geom_smooth(method = "lm", lwd = 0.5, col="purple")
g13a <- g13a + xlab("Aromatic Content [% vol/vol]")
g13a <- g13a + ylab("BC [mg/m3]")
g13a
```

```{r}
g14 <- ggplot(data, aes(Aromatic.Mass.Percentage, LII))
g14 <- g14 + geom_point()
g14 <- g14 + geom_smooth(method = "lm", lwd = 0.5, col="blue")
g14 <- g14 + xlab("Aromatic Content [% mass/mass]")
g14 <- g14 + ylab("BC [mg/m3]")
g14
```

```{r}
g15 <- ggplot(data, aes(HC_blend, LII,colour = factor(X..Aromatic..vol.vol.),
                        shape = classification))
```

```
g15 <- g15 + geom_point()
g15 <- g15 + geom_smooth(method = "lm", lwd = 0.3,
                         aes(group=classification, linetype = classification),
                         se = FALSE,
                         colour = "black")
g15 <- g15 + xlab("H/C Ratio")
g15 <- g15 + ylab("LII BC Concentration [mg/m3]")
g15
```
```
```{r}
g16 <- ggplot(data, aes(ring_carbon_percentage,
                        LII,
                        colour = factor(X..Aromatic..vol.vol.),
                        shape = classification))
g16 <- g16 + geom_point()
g16 <- g16 + geom_smooth(method = "lm", lwd = 0.3,
                         aes(group=classification, linetype = classification),
                         se = FALSE,
                         colour = "black")
g16 <- g16 + xlab("Ring Carbon Content [% mass/mass]")
g16 <- g16 + ylab("LII BC Concentration [mg/m^3]")
g16
```
```

```{r}
g17 <- ggplot(data, aes(Blend.Density,
                        LII,
                        colour = factor(X..Aromatic..vol.vol.),
                        shape = classification))
g17 <- g17 + geom_point()
g17 <- g17 + geom_smooth(method = "lm", lwd = 0.3,
                         aes(group=classification, linetype = classification),
                         se = FALSE,
                         colour = "black")
g17 <- g17 + xlab("Global Density [g/cm3]")
g17 <- g17 + ylab("LII BC Concentration [mg/m3]")
g17
```
```
```

```{r, fig.height=10, fig.width=15}
library(gridExtra)
grid <- grid.arrange(g13,g14,g15,g16,g17, nrow = 2, ncol = 3)
grid
```

```{r}
plot(data$LII[data$X..Aromatic..vol.vol.==7.5],data$LII[data$X..Aromatic..vol.vol.==12.5

plot(data$LII[data$X..Aromatic..vol.vol.==12.5],data$LII[data$X..Aromatic..vol.vol.==17.

plot(data$LII[data$X..Aromatic..vol.vol.==17.5],data$LII[data$X..Aromatic..vol.vol.==22.

plot(data$LII[data$X..Aromatic..vol.vol.==7.5],data$LII[data$X..Aromatic..vol.vol.==17.5

plot(data$LII[data$X..Aromatic..vol.vol.==7.5],data$LII[data$X..Aromatic..vol.vol.==22.5

plot(data$LII[data$X..Aromatic..vol.vol.==12.5],data$LII[data$X..Aromatic..vol.vol.==22.
```

```{r}
model1 <- lm(LII ~ X..Aromatic..vol.vol. +
                   Blend.Density +
                   HC_blend +
                   ring_carbon_percentage, data=data)

model2 <- lm(LII ~ X..Aromatic..vol.vol. +
                   Blend.Density +
                   HC_blend, data=data)

model3 <- lm(LII ~ Blend.Density +
                   HC_blend, data=data)

test <- data$Blend.Density /data$HC_blend

model4 <- lm(LII ~ Blend.Density *
                   HC_blend, data=data)

model5 <- lm(LII ~ test, data=data)
```

```
```

```{r}
TSI <- select(data, Aromatic.Type,X..Aromatic..vol.vol.,Aromatic.Mass.Percentage,Ll

TSI$Banner.Mass.Percentage <- 100 - TSI$Aromatic.Mass.Percentage

TSI_banner <- c(3.1,4.2,4.5,5.1,5.2,5.4)

TSI$molecular.mass <- c(92.14,
                        92.14,
                        92.14,
                        92.14,
                        104.15,
                        104.15,
                        104.15,
                        104.15,
                        106.17,
                        106.17,
                        106.17,
                        106.17,
                        106.17,
                        106.17,
                        106.17,
                        106.17,
                        106.17,
                        118.18,
                        118.18,
                        118.18,
                        118.18,
                        118.18,
                        118.18,
                        118.18,
                        118.18,
                        118.18,
                        120.19,
                        120.19,
                        120.19,
                        120.19,
                        120.19,
                        120.19,
```

```
                    120.19,
                    120.19,
                    132.2,
                    132.2,
                    132.2,
                    132.2,
                    134.22,
                    134.22,
                    134.22,
                    134.22,
                    134.22,
                    134.22,
                    134.22,
                    134.22,
                    142.22,
                    142.22,
                    142.22,
                    142.22,
                    162.27,
                    162.27,
                    162.27,
                    162.27)

TSI$TSI.aro <- c(44,44,44,44,
                 67,67,67,67,
                 49,49,49,49,
                 54,54,54,54,
                 62,62,62,62,
                 61,61,61,61,
                 52,52,52,52,
                 61,61,61,61,
                 61,61,61,61,
                 60,60,60,60,
                 61,61,61,61,
                 91,91,91,91,
                 51,51,51,51)

TSI$NSP.aro <- c(8.12,8.12,8.12,8.12,
                 5.27,5.27,5.27,5.27,
```

```
                    8.10,8.10,8.10,8.10,
                    5.92,5.92,5.92,5.92,
                    5.99,5.99,5.99,5.99,
                    6.09,6.09,6.09,6.09,
                    6.43,6.43,6.43,6.43,
                    6.14,6.14,6.14,6.14,
                    7.40,7.40,7.40,7.40,
                    6.11,6.11,6.11,6.11,
                    7.90,7.90,7.90,7.90,
                    5.14,5.14,5.14,5.14,
                    10.6,10.6,10.6,10.6)

TSI$YSI.aro <- c(43.5,43.5,43.5,43.5,
                    44.1,44.1,44.1,44.1,
                    50.0,50.0,50.0,50.0,
                    53.6,53.6,53.6,53.6,
                    94.9,94.9,94.9,94.9,
                    65.6,65.6,65.6,65.6,
                    69.8,69.8,69.8,69.8,
                    46.7,46.7,46.7,46.7,
                    75.1,75.1,75.1,75.1,
                    72.4,72.4,72.4,72.4,
                    74.0,74.0,74.0,74.0,
                    135.0,135.0,135.0,135.0,
                    78.4,78.4,78.4,78.4)

TSI$Unified.YSI.aro <- c(170.9,170.9,170.9,170.9,
                         174.0,174.0,174.0,174.0,
                         204.8,204.8,204.8,204.8,
                         223.7,223.7,223.7,223.7,
                         439.5,439.5,439.5,439.5,
                         286.4,286.4,286.4,286.4,
                         308.2,308.2,308.2,308.2,
                         187.6,187.6,187.6,187.6,
                         336.0,336.0,336.0,336.0,
                         322.3,322.3,322.3,322.3,
                         330.8,330.8,330.8,330.8,
                         649.1,649.1,649.1,649.1,
                         353.3,353.3,353.3,353.3)
```

```
TSI$aro.moles <- TSI$Aromatic.Mass.Percentage/TSI$molecular.mass
TSI$nonane.moles <- TSI$Banner.Mass.Percentage*0.01/128.2
TSI$decane.moles <- 0.1753*TSI$Banner.Mass.Percentage/142.29
TSI$undecane.moles <- 0.2408*TSI$Banner.Mass.Percentage/156.31
TSI$dodecane.moles <- 0.1984*TSI$Banner.Mass.Percentage/170.33
TSI$tridecane.moles <- 0.3675*TSI$Banner.Mass.Percentage/184.37
TSI$tetradecane.moles <- 0.0079*TSI$Banner.Mass.Percentage/198.39

TSI$total.moles <- TSI$aro.moles + TSI$nonane.moles + TSI$decane.moles + TSI$undecane.mo

TSI$aro.TSI <- TSI$aro.moles/TSI$total.moles * TSI$TSI.aro
TSI$nonane.TSI <- TSI$nonane.moles/TSI$total.moles * 3.1
TSI$decane.TSI <- TSI$decane.moles/TSI$total.moles * 4.2
TSI$undecane.TSI <- TSI$undecane.moles/TSI$total.moles * 4.5
TSI$dodecane.TSI <- TSI$dodecane.moles/TSI$total.moles * 5.1
TSI$tridecane.TSI <- TSI$tridecane.moles/TSI$total.moles * 5.2
TSI$tetradecane.TSI <- TSI$tetradecane.moles/TSI$total.moles * 5.4

TSI$blend.TSI <- TSI$aro.TSI + TSI$nonane.TSI + TSI$decane.TSI + TSI$undecane.TSI + TSI$

TSI$aro.NSP <- TSI$aro.moles/TSI$total.moles * TSI$NSP.aro
TSI$nonane.NSP <- TSI$nonane.moles/TSI$total.moles * 110
TSI$decane.NSP <- TSI$decane.moles/TSI$total.moles * 122
TSI$undecane.NSP <- TSI$undecane.moles/TSI$total.moles * 113
TSI$dodecane.NSP <- TSI$dodecane.moles/TSI$total.moles * 107
TSI$tridecane.NSP <- TSI$tridecane.moles/TSI$total.moles * 116
TSI$tetradecane.NSP <- TSI$tetradecane.moles/TSI$total.moles * 120

TSI$blend.NSP <- TSI$aro.NSP + TSI$nonane.NSP + TSI$decane.NSP + TSI$undecane.NSP + TSI$

TSI$nonane.YSI <- TSI$nonane.moles/TSI$total.moles * 30.6
TSI$decane.YSI <- TSI$decane.moles/TSI$total.moles * 41.7
TSI$undecane.YSI <- TSI$undecane.moles/TSI$total.moles * 53.3
TSI$dodecane.YSI <- TSI$dodecane.moles/TSI$total.moles * 64.2
TSI$tridecane.YSI <- TSI$tridecane.moles/TSI$total.moles * 72.2
TSI$tetradecane.YSI <- TSI$tetradecane.moles/TSI$total.moles * 82.2

TSI$banner.YSI <- TSI$nonane.YSI + TSI$decane.YSI + TSI$undecane.YSI + TSI$dodecane.YSI +
```

```
TSI$aro.Unified.YSI <- TSI$aro.moles/TSI$total.moles * TSI$Unified.YSI.aro
TSI$nonane.Unified.YSI <- TSI$nonane.moles/TSI$total.moles * 50.1
TSI$decane.Unified.YSI <- TSI$decane.moles/TSI$total.moles * 57.2
TSI$undecane.Unified.YSI <- TSI$undecane.moles/TSI$total.moles * 64.7
TSI$dodecane.Unified.YSI <- TSI$dodecane.moles/TSI$total.moles * 71.7
TSI$tridecane.Unified.YSI <- TSI$tridecane.moles/TSI$total.moles * 72.5
TSI$tetradecane.Unified.YSI <- TSI$tetradecane.moles/TSI$total.moles * 78.4

TSI$blend.Unified.YSI <- TSI$nonane.Unified.YSI + TSI$decane.Unified.YSI + TSI$unde
```

```{r}
g18 <- ggplot(TSI, aes(blend.TSI, LII,
                       shape = classification))
g18 <- g18 + geom_point()
g18 <- g18 + facet_grid(.~TSI$X..Aromatic..vol.vol.)
g18 <- g18 + geom_smooth(method = "lm",
                         lwd = 1,
                         aes(linetype = classification),
                         se = FALSE,
                         colour = "Blue")
g18 <- g18 + xlab("TSI")
g18 <- g18 + ylab("LII BC Concentration [mg/m^3]")
g18
```

```{r}
g19 <- ggplot(TSI, aes(blend.TSI,
                       LII,
                       colour = factor(X..Aromatic..vol.vol.),
                       shape = classification))
g19 <- g19 + geom_point()
g19 <- g19 + geom_smooth(method = "lm", lwd = 0.3,
                         aes(group=classification, linetype = classification),
                         se = FALSE,
                         colour = "black")
g19 <- g19 + xlab("TSI")
g19 <- g19 + ylab("LII BC Concentration [mg/m3]")
g19
```

```
```

```{r}
g20 <- ggplot(TSI, aes(blend.NSP, LII,
                       shape = classification))
g20 <- g20 + geom_point()
g20 <- g20 + facet_grid(.~TSI$X..Aromatic..vol.vol.)
g20 <- g20 + geom_smooth(method = "lm",
                         lwd = 1,
                         aes(linetype = classification),
                         se = FALSE,
                         colour = "Orange")
g20 <- g20 + xlab("NSP")
g20 <- g20 + ylab("LII BC Concentration [mg/m^3]")
g20
```
```{r}
g21 <- ggplot(TSI, aes(blend.NSP,
                       LII,
                       colour = factor(X..Aromatic..vol.vol.),
                       shape = classification))
g21 <- g21 + geom_point()
g21 <- g21 + geom_smooth(method = "lm", lwd = 0.3,
                         aes(group=classification, linetype = classification),
                         se = FALSE,
                         colour = "black")
g21 <- g21 + xlab("NSP")
g21 <- g21 + ylab("LII BC Concentration [mg/m3]")
g21
```
```{r}
g22 <- ggplot(TSI, aes(banner.YSI + YSI.aro, LII,
                       shape = classification))
g22 <- g22 + geom_point()
g22 <- g22 + facet_grid(.~X..Aromatic..vol.vol.)
g22 <- g22 + geom_smooth(method = "lm",
                         lwd = 1,
                         aes(linetype = classification),
                         se = FALSE,
```

```
                          colour = "Yellow")
g22 <- g22 + xlab("YSI")
g22 <- g22 + ylab("LII BC Concentration [mg/m^3]")
g22
```
```
```{r}
g23 <- ggplot(TSI, aes(banner.YSI+YSI.aro,
                       LII,
                       colour = factor(X..Aromatic..vol.vol.),
                       shape = classification))
g23 <- g23 + geom_point()
g23 <- g23 + geom_smooth(method = "lm", lwd = 0.3,
                         aes(group=classification, linetype = classification),
                         se = FALSE,
                         colour = "black")
g23 <- g23 + xlab("NSP")
g23 <- g23 + ylab("LII BC Concentration [mg/m3]")
g23
```
```
```{r}
g24 <- ggplot(TSI, aes(blend.Unified.YSI, LII,
                       shape = classification))
g24 <- g24 + geom_point()
g24 <- g24 + facet_grid(.~X..Aromatic..vol.vol.)
g24 <- g24 + geom_smooth(method = "lm",
                         lwd = 1,
                         aes(linetype = classification),
                         se = FALSE,
                         colour = "Pink")
g24 <- g24 + xlab("Unified YSI")
g24 <- g24 + ylab("LII BC Concentration [mg/m^3]")
g24
```
```
```{r}
g25 <- ggplot(TSI, aes(blend.Unified.YSI,
                       LII,
                       colour = factor(X..Aromatic..vol.vol.),
                       shape = classification))
g25 <- g25 + geom_point()
```
```

```
g25 <- g25 + geom_smooth(method = "lm", lwd = 0.3,
                         aes(group=classification, linetype = classification),
                         se = FALSE,
                         colour = "black")
g25 <- g25 + xlab("Unified YSI")
g25 <- g25 + ylab("LII BC Concentration [mg/m3]")
g25
```
```
```{r}
variables <- c(X..Aromatic..vol.vol. +
                       Aromatic.Mass.Percentage +
                       Blend.Density +
                       ring_carbon_percentage   +
                       HC_blend +
                       )

multi_model <- lm(LII~.,data)
```
```

```{r}
alkylbenzene <- data[data$classification == "Alkylbenzene",]
polycyclics <- data[data$classification != "Alkylbenzene",]

alkyl.7.5 <- alkylbenzene[alkylbenzene$X..Aromatic..vol.vol.==7.5,]
alkyl.12.5 <- alkylbenzene[alkylbenzene$X..Aromatic..vol.vol.==12.5,]
alkyl.17.5 <- alkylbenzene[alkylbenzene$X..Aromatic..vol.vol.==17.5,]
alkyl.22.5 <- alkylbenzene[alkylbenzene$X..Aromatic..vol.vol.==22.5,]

poly.7.5 <- polycyclics[polycyclics$X..Aromatic..vol.vol.==7.5,]
poly.12.5 <- polycyclics[polycyclics$X..Aromatic..vol.vol.==12.5,]
poly.17.5 <- polycyclics[polycyclics$X..Aromatic..vol.vol.==17.5,]
poly.22.5 <- polycyclics[polycyclics$X..Aromatic..vol.vol.==22.5,]

# Volume

summary(lm(LII~X..Aromatic..vol.vol., data = data))
summary(lm(LII~X..Aromatic..vol.vol., data = alkylbenzene))
summary(lm(LII~X..Aromatic..vol.vol., data = polycyclics))
```

```
# RC

summary(lm(LII~data$ring_carbon_percentage, data = data))
summary(lm(LII~ring_carbon_percentage, data = alkylbenzene))
summary(lm(LII~ring_carbon_percentage, data = polycyclics))

summary(lm(LII~ring_carbon_percentage, data = alkyl.7.5))
summary(lm(LII~ring_carbon_percentage, data = alkyl.12.5))
summary(lm(LII~ring_carbon_percentage, data = alkyl.17.5))
summary(lm(LII~ring_carbon_percentage, data = alkyl.22.5))

summary(lm(LII~ring_carbon_percentage, data = poly.7.5))
summary(lm(LII~ring_carbon_percentage, data = poly.12.5))
summary(lm(LII~ring_carbon_percentage, data = poly.17.5))
summary(lm(LII~ring_carbon_percentage, data = poly.22.5))


# HC

summary(lm(LII~HC_blend, data = data))
summary(lm(LII~HC_blend, data = alkylbenzene))
summary(lm(LII~HC_blend, data = polycyclics))

summary(lm(LII~HC_blend, data = alkyl.7.5))
summary(lm(LII~HC_blend, data = alkyl.12.5))
summary(lm(LII~HC_blend, data = alkyl.17.5))
summary(lm(LII~HC_blend, data = alkyl.22.5))

summary(lm(LII~HC_blend, data = poly.7.5))
summary(lm(LII~HC_blend, data = poly.12.5))
summary(lm(LII~HC_blend, data = poly.17.5))
summary(lm(LII~HC_blend, data = poly.22.5))

# Density

summary(lm(LII~Blend.Density, data = data))
summary(lm(LII~Blend.Density, data = alkylbenzene))
summary(lm(LII~Blend.Density, data = polycyclics))
```

```
summary(lm(LII~Blend.Density, data = alkyl.7.5))
summary(lm(LII~Blend.Density, data = alkyl.12.5))
summary(lm(LII~Blend.Density, data = alkyl.17.5))
summary(lm(LII~Blend.Density, data = alkyl.22.5))

summary(lm(LII~Blend.Density, data = poly.7.5))
summary(lm(LII~Blend.Density, data = poly.12.5))
summary(lm(LII~Blend.Density, data = poly.17.5))
summary(lm(LII~Blend.Density, data = poly.22.5))



TSI.alkylbenzene <- TSI[TSI$classification == "Alkylbenzene",]
TSI.polycyclic <- TSI[TSI$classification != "Alkylbenzene",]

TSI.alkylbenzene.7.5 <- TSI.alkylbenzene[TSI.alkylbenzene$X..Aromatic..vol.vol.==7.5,]
TSI.alkylbenzene.12.5 <- TSI.alkylbenzene[TSI.alkylbenzene$X..Aromatic..vol.vol.==12.5,]
TSI.alkylbenzene.17.5 <- TSI.alkylbenzene[TSI.alkylbenzene$X..Aromatic..vol.vol.==17.5,]
TSI.alkylbenzene.22.5 <- TSI.alkylbenzene[TSI.alkylbenzene$X..Aromatic..vol.vol.==22.5,]

TSI.polycyclic.7.5 <- TSI.polycyclic[TSI.polycyclic$X..Aromatic..vol.vol.==7.5,]
TSI.polycyclic.12.5 <- TSI.polycyclic[TSI.polycyclic$X..Aromatic..vol.vol.==12.5,]
TSI.polycyclic.17.5 <- TSI.polycyclic[TSI.polycyclic$X..Aromatic..vol.vol.==17.5,]
TSI.polycyclic.22.5 <- TSI.polycyclic[TSI.polycyclic$X..Aromatic..vol.vol.==22.5,]

# TSI

summary(lm(LII~blend.TSI, data = TSI))
summary(lm(LII~blend.TSI, data = TSI.alkylbenzene))
summary(lm(LII~blend.TSI, data = TSI.polycyclic))

summary(lm(LII~blend.TSI, data = TSI.alkylbenzene.7.5))
summary(lm(LII~blend.TSI, data = TSI.alkylbenzene.12.5))
summary(lm(LII~blend.TSI, data = TSI.alkylbenzene.17.5))
summary(lm(LII~blend.TSI, data = TSI.alkylbenzene.22.5))

summary(lm(LII~blend.TSI, data = TSI.polycyclic.7.5))
summary(lm(LII~blend.TSI, data = TSI.polycyclic.12.5))
summary(lm(LII~blend.TSI, data = TSI.polycyclic.17.5))
summary(lm(LII~blend.TSI, data = TSI.polycyclic.22.5))
```

```
# NSP

summary(lm(LII~blend.NSP, data = TSI))
summary(lm(LII~blend.NSP, data = TSI.alkylbenzene))
summary(lm(LII~blend.NSP, data = TSI.polycyclic))

summary(lm(LII~blend.NSP, data = TSI.alkylbenzene.7.5))
summary(lm(LII~blend.NSP, data = TSI.alkylbenzene.12.5))
summary(lm(LII~blend.NSP, data = TSI.alkylbenzene.17.5))
summary(lm(LII~blend.NSP, data = TSI.alkylbenzene.22.5))

summary(lm(LII~blend.NSP, data = TSI.polycyclic.7.5))
summary(lm(LII~blend.NSP, data = TSI.polycyclic.12.5))
summary(lm(LII~blend.NSP, data = TSI.polycyclic.17.5))
summary(lm(LII~blend.NSP, data = TSI.polycyclic.22.5))

# YSI

summary(lm(LII~blend.Unified.YSI, data = TSI))
summary(lm(LII~blend.Unified.YSI, data = TSI.alkylbenzene))
summary(lm(LII~blend.Unified.YSI, data = TSI.polycyclic))

summary(lm(LII~blend.Unified.YSI, data = TSI.alkylbenzene.7.5))
summary(lm(LII~blend.Unified.YSI, data = TSI.alkylbenzene.12.5))
summary(lm(LII~blend.Unified.YSI, data = TSI.alkylbenzene.17.5))
summary(lm(LII~blend.Unified.YSI, data = TSI.alkylbenzene.22.5))

summary(lm(LII~blend.Unified.YSI, data = TSI.polycyclic.7.5))
summary(lm(LII~blend.Unified.YSI, data = TSI.polycyclic.12.5))
summary(lm(LII~blend.Unified.YSI, data = TSI.polycyclic.17.5))
summary(lm(LII~blend.Unified.YSI, data = TSI.polycyclic.22.5))

```

```{r}

refined.one <- select(data, Aromatic.Type,
```

```
                        X..Aromatic..vol.vol.,
                        LII,
                        Aromatic.Mass.Percentage,
                        Blend.Density,
                        ring_carbon_percentage,
                        HC_blend,
                        classification)

refined.two <- select(TSI, blend.TSI,
                        blend.NSP,
                        blend.Unified.YSI)

complete <- cbind(refined.one,refined.two)

complete$hydrogen.mass.percentage <- 100*(complete$HC_blend/(complete$HC_blend + 12))

complete$carbon.mass.percentage <- 100-complete$hydrogen.mass.percentage

complete$carbon.density <- complete$Blend.Density * complete$carbon.mass.percentage/100

summary(lm(LII~., data = complete))

summary(lm(LII~X..Aromatic..vol.vol. +
                    Aromatic.Mass.Percentage +
                    Blend.Density +
                     ring_carbon_percentage +
                    HC_blend +
                     blend.TSI +
                     blend.NSP +
                     blend.Unified.YSI , data = complete))



LII.model <- lm(log(LII)~Blend.Density
                    , data = complete)

predicter <- select(complete, X..Aromatic..vol.vol., Aromatic.Mass.Percentage, classifica

predict(LII.model, predicter)
```

```
plot(complete$LII,predict(LII.model, predicter))
```
```
```{r}
g26 <- ggplot(TSI, aes(X..Aromatic..vol.vol.,
                       LII,
                       colour = factor(X..Aromatic..vol.vol.),
                       shape = classification))
g26 <- g26 + geom_point()
g26 <- g26 + geom_smooth(method = "lm", lwd = 0.3,
                         aes(group=classification, linetype = classification),
                         se = FALSE,
                         colour = "black")
g26 <- g26 + xlab("Aromatic Volume [vol/vol %]")
g26 <- g26 + ylab("LII BC Concentration [mg/m3]")
g26
```

```{r}
g27 <- ggplot(TSI, aes(Aromatic.Mass.Percentage,
                       LII,
                       colour = factor(X..Aromatic..vol.vol.),
                       shape = classification))
g27 <- g27 + geom_point()
g27 <- g27 + geom_smooth(method = "lm", lwd = 0.3,
                         aes(group=classification, linetype = classification),
                         se = FALSE,
                         colour = "black")
g27 <- g27 + xlab("Aromatic Mass [vol/vol %]")
g27 <- g27 + ylab("LII BC Concentration [mg/m3]")
g27
```

```{r}
# MAss

summary(lm(LII~Aromatic.Mass.Percentage, data = TSI))
summary(lm(LII~Aromatic.Mass.Percentage, data = TSI.alkylbenzene))
summary(lm(LII~Aromatic.Mass.Percentage, data = TSI.polycyclic))
```
```

```
```
```{r}
summary(lm(LII~., data = complete))

summary(lm(LII~X..Aromatic..vol.vol.  +
                    Aromatic.Mass.Percentage +
                    Blend.Density +
                     ring_carbon_percentage +
                    HC_blend +
                     blend.TSI +
                     blend.NSP +
                     blend.Unified.YSI , data = complete))



LII.model <- lm(LII~.
                     , data = complete)



predict(LII.model, complete)

plot(complete$LII,predict(LII.model, complete))

summary(lm(LII~blend.TSI + blend.NSP + blend.Unified.YSI, data = complete))

summary(lm(LII~X..Aromatic..vol.vol.  +
                    Aromatic.Mass.Percentage +
                    Blend.Density +
                     HC_blend +
                     blend.Unified.YSI , data = complete))

final <- (lm(LII~

                    Blend.Density *
                     HC_blend   , data = complete))

plot(complete$LII,predict(final, complete))
```

```
model.alkyl <- complete[complete$classification == "Alkylbenzene",]
model.poly <- complete[complete$classification != "Alkylbenzene",]

# Alkylbenzenes

 a <- (lm(LII~

                    Blend.Density +
                     # HC_blend +
                     # blend.TSI +
                     # blend.NSP +
                     blend.Unified.YSI,
          data = model.alkyl))

plot(model.alkyl$LII,predict(a, model.alkyl))

model.alkyl <- cbind(model.alkyl, predict(a, model.alkyl))

g28 <- ggplot(model.alkyl, aes(`predict(a, model.alkyl)`,
                           LII,
                           colour = factor(X..Aromatic..vol.vol.)
                           ))
g28 <- g28 + geom_point()
g28 <- g28 + geom_smooth(method = "lm", lwd = 0.3,
                         aes(group=classification, linetype = classification),
                         se = FALSE,
                         colour = "black")
g28 <- g28 + xlab("Predicted BC")
g28 <- g28 + ylab("Actual BC")
g28

standard_res_alkyl <- rstandard(a)

model.alkyl <- cbind(model.alkyl, standard_res_alkyl)

model.alkyl$conc <- paste(model.alkyl$Aromatic.Type,model.alkyl$X..Aromatic..vol.v

g29 <- ggplot(model.alkyl)
g29 <- g29 + geom_bar(aes(x = conc, y = standard_res_alkyl), stat = "identity", fil
```

```
g29 <- g29 + theme(axis.text.x = element_text(angle = 90, vjust = 0.5, hjust=1))
g29 <- g29 + xlab("Blend") + ylab("Standardised Residual")
g29

# Polycyclics

 b <- (lm(LII~

                    Blend.Density ,
                     # HC_blend +
                     # blend.TSI +
                     # blend.NSP +
                     # blend.Unified.YSI,
          data = model.poly))

plot(model.poly$LII,predict(a, model.poly))

model.poly <- cbind(model.poly, predict(b, model.poly))

g30 <- ggplot(model.poly, aes(`predict(b, model.poly)`,
                          LII,
                          colour = factor(X..Aromatic..vol.vol.)
                          ))
g30 <- g30 + geom_point()
g30 <- g30 + geom_smooth(method = "lm", lwd = 0.3,
                         aes(group=classification, linetype = classification),
                         se = FALSE,
                         colour = "black")
g30 <- g30 + xlab("Predicted BC ")
g30 <- g30 + ylab("Actual BC")
g30

standard_res_poly <- rstandard(b)

model.poly <- cbind(model.poly, standard_res_poly)

model.poly$conc <- paste(model.poly$Aromatic.Type,model.poly$X..Aromatic..vol.vol., sep =

g31 <- ggplot(model.poly)
```

```
g31 <- g31 + geom_bar(aes(x = conc, y = standard_res_poly), stat = "identity", fill
g31 <- g31 + theme(axis.text.x = element_text(angle = 90, vjust = 0.5, hjust=1))
g31 <- g31 + xlab("Blend") + ylab("Standardised Residual")
g31 <- g31 + ylim(-2,4)
g31

# Unified

c <- (lm(LII~

                    Blend.Density +
                     # HC_blend +
                     # blend.TSI +
                     # blend.NSP +
                     blend.Unified.YSI,
          data = complete))

plot(complete$LII,predict(c, complete))

complete <- cbind(complete, predict(c, complete))

g32 <- ggplot(complete, aes(`predict(c, complete)`,
                            LII,
                            colour = factor(X..Aromatic..vol.vol.)
                            ))
g32 <- g32 + geom_point()
g32 <- g32 + geom_smooth(method = "lm", lwd = 0.3,

                             se = FALSE,
                             colour = "black")
g32 <- g32 + xlab("Predicted BC ")
g32 <- g32 + ylab("Actual BC")
g32

standard_res_complete <- rstandard(c)

complete <- cbind(complete, standard_res_complete)

complete$conc <- paste(complete$Aromatic.Type,complete$X..Aromatic..vol.vol., sep =
```

```
g33 <- ggplot(complete)
g33 <- g33 + geom_bar(aes(x = conc, y = standard_res_complete), stat = "identity", fill =
g33 <- g33 + theme(axis.text.x = element_text(angle = 90, vjust = 0.5, hjust=1))
g33 <- g33 + xlab("Blend") + ylab("Standardised_Residual") + ylim(-3,4)
g33


write.table(complete, file = "LII.complete")
```

E.3 Chapter 6 Code

```
---
title: "Aromatic_Paper_2"
author: "James_Cronly"
date: "08/04/2021"
output: html_document
---


```{r}
library(xlsx)

eight_percent <- read.xlsx("Aromatic_DMS_for_R.xlsx", header = FALSE, sheetIndex = 4)
thirteen_percent <- read.xlsx("Aromatic_DMS_for_R.xlsx", header = FALSE, sheetIndex = 5)
eighteen_percent <- read.xlsx("Aromatic_DMS_for_R.xlsx", header = FALSE, sheetIndex = 6)

size <- names(eight_percent)

transpose_eight <- t(eight_percent)
transpose_thirteen <- t(thirteen_percent)
eighteen_transpose <- t(eighteen_percent)

names <- c("Toluene",
           "Styrene",
           "O–Xylene",
```
```

```
            "Ethylbenzene",
            "Indene",
            "Indan",
            "alpha-Methylstyrene",
            "Pseudocumene",
            "Cumene",
            "Tetralin",
            "5-tert-m-butyl-xylene",
            "Diethylbenzene",
            "p-Cymene",
            "Tertbutylbenzene",
            "Methylnapthalene",
            "Isopropylcumene")
```

```{r}
template <- data.frame(Aromatic = as.character(),
                       Size = as.numeric(),
                       Number = as.numeric(),
                       Vol = as.character())

temp <- data.frame(Aromatic = as.character(),
                   Size = as.numeric(),
                   Number = as.numeric(),
                   vol = as.character())

for(i in 1:16) {

        Aromatic <- rep(names[i],38)
        Size <- transpose_eight[,1]
        Vol <- rep("8",38)
        Number <- transpose_eight[,(i+1)]

        temp <- cbind(Aromatic, Size, Vol, Number)

        template <- rbind(template, temp)
}

for(i in 1:16) {
```

```
        Aromatic <- rep(names[i],38)
        Size <- transpose_eight[,1]
        Vol <- rep("13",38)
        Number <- transpose_thirteen[,(i+1)]

        temp <- cbind(Aromatic,Size,Vol,Number)

        template <- rbind(template,temp)
}

for(i in 1:16) {

        Aromatic <- rep(names[i],38)
        Size <- transpose_eight[,1]
        Vol <- rep("18",38)
        Number <- eighteen_transpose[,(i+1)]

        temp <- cbind(Aromatic,Size,Vol,Number)

        template <- rbind(template,temp)
}

```
```{r}
library(ggplot2)
library(dplyr)

toluene <- filter(template, Aromatic == "5-tert-m-butyl-xylene")
toluene$Size <- as.numeric(toluene$Size)
toluene$Number <- as.numeric(toluene$Number)

g2 <- ggplot(toluene, aes(Size,Number))
g2 <- g2 + geom_point(aes(colour = Vol,
                          shape = Vol))
g2 <- g2 + scale_x_log10()
g2 <- g2 + geom_line(aes(colour = Vol,
                         shape = Vol),
                     linetype = 2)
```

```
g2
```
```
```{r, fig.height=10, fig.width=15}
template$Size <- as.numeric(template$Size)
template$Number <- as.numeric(template$Number)

g3 <- ggplot(template, aes(Size,Number))
g3 <- g3 + facet_wrap(~Aromatic, nrow = 4, ncol = 4)
g3 <- g3 + geom_point(aes(colour = Vol,
                          shape = Vol),
                      size = 1)
g3 <- g3 + scale_x_log10()
g3 <- g3 + geom_line(aes(colour = Vol,
                         shape = Vol),
                     linetype = 2)
g3 <- g3 + theme_bw()
g3
```


```{r}
DMS_data <- read.xlsx("DMS_Number_and_GMD.xlsx", header = TRUE, sheetIndex = 1)
library(dplyr)
library(ggplot2)
library(knitr)
library(kableExtra)
library(png)
library(EBImage)
library(magick)

# classification

for (i in 1:length(DMS_data$Aromatic.Type)) {
        if(DMS_data$Aromatic.Type[i] == "Indan"|
           DMS_data$Aromatic.Type[i] == "Tetrahydronapthalene"|
           DMS_data$Aromatic.Type[i] == "Methylnapthalene" |
           DMS_data$Aromatic.Type[i] == "Indene")

        {DMS_data$classification[i] <- "Polycylic"}
        else {DMS_data$classification[i] <- "Alkylbenzene"}
```
```

```
}
```
```

```{r}
library(ggplot2)
vol.labs <- c("8% vol/vol", "13% vol/vol", "18% vol/vol")
g5 <- ggplot(DMS_data, aes(x = reorder(Aromatic.Type, Total.N.cc), y = Total.N.cc))
g5 <- g5 + geom_bar(aes(x = reorder(Aromatic.Type, Total.N.cc), y = Total.N.cc),
                    stat = "identity",
                    fill = "skyblue",
                    colour = "blue",
                    alpha = 0.5)
g5 <- g5 + geom_errorbar(DMS_data, mapping = aes(ymin = Total.N.cc - 0.05*Total.N.cc,
                                                 ymax = Total.N.cc + 0.05*Total.N.cc),
                                                    size = 0.15)
g5 <- g5 + coord_flip()
g5 <- g5 + facet_grid(DMS_data$Aromatic.Volume)
g5 <- g5 + labs(x = "Aromatic Type",
                y = "Total Number [N/cc^3]",
                cex.main = 0.5)

g5
```
```

```{r}
g6 <- ggplot(DMS_data, aes(Aromatic.Volume,
                           Total.N.cc,
                           shape = classification,
                           color = classification))
g6 <- g6 + geom_point()
g6 <- g6 + geom_smooth(method = "lm",
                       lwd = 0.5,
                       col="black",
                       aes(linetype = classification),
                       se = FALSE)
g6 <- g6 + xlab("Aromatic Content [% vol/vol]")
g6 <- g6 + ylab("BC Number Concentration [N/cc^3]")
```

```
g6
```

```{r}
# ring carbon

g7 <- ggplot(DMS_data, aes(Ring.Carbon, Total.N.cc, shape = classification))
g7 <- g7 + geom_point()
g7 <- g7 + facet_grid(.~Aromatic.Volume)
g7 <- g7 +  ylab("BC Number Concentration [N/cc^3]")
g7 <- g7 + xlab("Ring Carbon Content [% mass/mass]")
g7 <- g7 + geom_smooth(method = "lm",
                       lwd = 1,
                       aes(linetype = classification),
                       se = FALSE,
                       colour = "orange")
g7 <- g7 + theme(axis.text.x = element_text(angle = 90, vjust = 0.5, hjust=1))

g7
```

```{r}
g8 <- ggplot(DMS_data, aes(Ring.Carbon,
                           Total.N.cc,
                           shape = classification,
                           colour = factor(Aromatic.Volume)))
g8 <- g8 + geom_point()
g8 <- g8 + geom_smooth(method = "lm",
                       lwd = 0.5,
                       col="black",
                       aes(linetype = classification),
                       se = FALSE)
g8 <- g8 + xlab("Ring Carbon Content [% mass/mass]")
g8 <- g8 + ylab("BC Number Concentration [N/cc^3]")

g8
```

```{r}
# H/C

g9 <- ggplot(DMS_data, aes(Hydrogen.Content, Total.N.cc,shape = classification))
g9 <- g9 + geom_point()
g9 <- g9 + facet_grid(.~Aromatic.Volume)
g9 <- g9 +  ylab("BC Number Concentration [N/cc^3]")
g9 <- g9 + xlab("Hydrogen Content [% mass/mass]")
g9 <- g9 + geom_smooth(method = "lm",
                       lwd = 1,
                       aes(linetype = classification),
                       se = FALSE,
                       colour = "Red")
g9 <- g9 + theme(axis.text.x = element_text(angle = 90, vjust = 0.5, hjust=1))

g9
```
```{r}
g10 <- ggplot(DMS_data, aes(Hydrogen.Content,
                            Total.N.cc,
                            shape = classification,
                            colour = factor(Aromatic.Volume)))
g10 <- g10 + geom_point()
g10 <- g10 + geom_smooth(method = "lm",
                         lwd = 0.5,
                         col="black",
                         aes(linetype = classification),
                         se = FALSE)
g10 <- g10 + xlab("Hydrogen Content [% mass/mass]")
g10 <- g10 + ylab("BC Number Concentration [N/cc^3]")

g10
```
```{r}
# Density

g11 <- ggplot(DMS_data, aes(Density, Total.N.cc, shape = classification))
g11 <- g11 + geom_point()
g11 <- g11 + facet_grid(.~Aromatic.Volume)
```

```
g11 <- g11 +  ylab("BC Number Concentration [N/cc^3]")
g11 <- g11 + xlab("Global Density [g/cm^3]")
g11 <- g11 + geom_smooth(method = "lm",
                         lwd = 1,
                         aes(linetype = classification),
                         se = FALSE,
                         colour = "green")
g11 <- g11 + theme(axis.text.x = element_text(angle = 90, vjust = 0.5, hjust=1))

g11
```
```
```{r}
g12 <- ggplot(DMS_data, aes(Density,
                            Total.N.cc,
                            shape = classification,
                            colour = factor(Aromatic.Volume)))
g12 <- g12 + geom_point()
g12 <- g12 + geom_smooth(method = "lm",
                         lwd = 0.5,
                         col="black",
                         aes(linetype = classification),
                         se = FALSE)
g12 <- g12 + xlab("Global Density [g/cm^3]")
g12 <- g12 + ylab("BC Number Concentration [N/cc]")

g12
```


```{r}
# TSI and YSI
library(dplyr)

grouped <- DMS_data[order(DMS_data$Aromatic.Type, DMS_data$Blend),]

grouped$molecular.mass <- c(162.27,162.27,162.27,
                            118.18,118.18,118.18,
                            120.19,120.19,120.19,
                            134.22,134.22,134.22,
                            106.17,106.17,106.17,
```
```

```
                    118.176,118.176,118.176,
                    116.16,116.16,116.16,
                    142.20,142.20,142.20,
                    106.17,106.17,106.17,
                    134.22,134.22,134.22,
                    104.15,104.15,104.15,
                    162.27,162.27,162.27,
                    134.22,134.22,134.22,
                    132.20,132.20,132.20,
                    92.14,92.14,92.14,
                    120.29,120.29,120.29)

grouped$TSI.aro <- c(51,51,51,
                     NA,NA,NA,
                     61,61,61,
                     60,60,60,
                     54,54,54,
                     NA,NA,NA,
                     62,62,62,
                     91,91,91,
                     49,49,49,
                     61,61,61,
                     67,67,67,
                     NA,NA,NA,
                     84,84,84,
                     61,61,61,
                     44,44,44,
                     52,52,52)

grouped$YSI.aro <- c(78.4,78.4,78.4,
                     65.6,65.6,65.6,
                     46.7,46.7,46.7,
                     72.4,72.4,72.4,
                     53.6,53.6,53.6,
                     94.9,94.9,94.9,
                     100.3,100.3,100.3,
                     135.0,135.0,135.0,
                     50.0,50.0,50.0,
                     74.0,74.0,74.0,
```

```
                        44.1,44.1,44.1,
                        112.6,112.6,112.6,
                        89.4,89.4,89.4,
                        75.1,75.1,75.1,
                        43.5,43.5,43.5,
                        69.8,69.8,69.8)

grouped$NSP.aro <- c(10.6,10.6,10.6,
                        6.09,6.09,6.09,
                        6.14,6.14,6.14,
                        6.11,6.11,6.11,
                        5.92,5.92,5.92,
                        5.99,5.99,5.99,
                        5.99,5.99,5.99,
                        5.14,5.14,5.14,
                        8.10,8.10,8.10,
                        7.9,7.9,7.9,
                        5.27,5.27,5.27,
                        NA,NA,NA,
                        4.37,4.37,4.37,
                        7.40,7.40,7.40,
                        8.12,8.12,8.12,
                        6.43,6.43,6.43
                        )

grouped$Unified.YSI.aro <- c(353.3,353.3,353.3,
                                286.4,286.4,286.4,
                                187.6,187.6,187.6,
                                322.3,322.3,322.3,
                                223.7,223.7,223.7,
                                439.5,439.5,439.5,
                                468.0,468.0,468.0,
                                649.1,649.1,649.1,
                                204.8,204.8,204.8,
                                330.8,330.8,330.8,
                                174.0,174.0,174.0,
                                413.8,413.8,413.8,
                                410.8,410.8,410.8,
                                336.0,336.0,336.0,
```

```
                                    170.0,170.9,170.9,
                                    308.2,308.2,308.2)

grouped$Banner.Mass.Percentage <- 100 - grouped$Mass

TSI_banner <- c(3.1,4.2,4.5,5.1,5.2,5.4)

grouped$aro.moles <- grouped$Mass/grouped$molecular.mass
grouped$nonane.moles <- grouped$Banner.Mass.Percentage*0.01/128.2
grouped$decane.moles <- 0.1753*grouped$Banner.Mass.Percentage/142.29
grouped$undecane.moles <- 0.2408*grouped$Banner.Mass.Percentage/156.31
grouped$dodecane.moles <- 0.1984*grouped$Banner.Mass.Percentage/170.33
grouped$tridecane.moles <- 0.3675*grouped$Banner.Mass.Percentage/184.37
grouped$tetradecane.moles <- 0.0079*grouped$Banner.Mass.Percentage/198.39

grouped$total.moles <- grouped$aro.moles + grouped$nonane.moles + grouped$decane.moles +

grouped$aro.TSI <- grouped$aro.moles/grouped$total.moles * grouped$TSI.aro
grouped$nonane.TSI <- grouped$nonane.moles/grouped$total.moles * 3.1
grouped$decane.TSI <- grouped$decane.moles/grouped$total.moles * 4.2
grouped$undecane.TSI <- grouped$undecane.moles/grouped$total.moles * 4.5
grouped$dodecane.TSI <- grouped$dodecane.moles/grouped$total.moles * 5.1
grouped$tridecane.TSI <- grouped$tridecane.moles/grouped$total.moles * 5.2
grouped$tetradecane.TSI <- grouped$tetradecane.moles/grouped$total.moles * 5.4

grouped$blend.TSI <- grouped$aro.TSI + grouped$nonane.TSI + grouped$decane.TSI + grouped

grouped$aro.NSP <- grouped$aro.moles/grouped$total.moles * grouped$NSP.aro
grouped$nonane.NSP <- grouped$nonane.moles/grouped$total.moles * 110
grouped$decane.NSP <- grouped$decane.moles/grouped$total.moles * 122
grouped$undecane.NSP <- grouped$undecane.moles/grouped$total.moles * 113
grouped$dodecane.NSP <- grouped$dodecane.moles/grouped$total.moles * 107
grouped$tridecane.NSP <- grouped$tridecane.moles/grouped$total.moles * 116
grouped$tetradecane.NSP <- grouped$tetradecane.moles/grouped$total.moles * 120

grouped$blend.NSP <- grouped$aro.NSP + grouped$nonane.NSP + grouped$decane.NSP + grouped

grouped$nonane.YSI <- grouped$nonane.moles/grouped$total.moles * 30.6
grouped$decane.YSI <- grouped$decane.moles/grouped$total.moles * 41.7
```

```
grouped$undecane.YSI <- grouped$undecane.moles/grouped$total.moles * 53.3
grouped$dodecane.YSI <- grouped$dodecane.moles/grouped$total.moles * 64.2
grouped$tridecane.YSI <- grouped$tridecane.moles/grouped$total.moles * 72.2
grouped$tetradecane.YSI <- grouped$tetradecane.moles/grouped$total.moles * 82.2

grouped$banner.YSI <- grouped$nonane.YSI + grouped$decane.YSI + grouped$undecane.YS

grouped$aro.Unified.YSI <- grouped$aro.moles/grouped$total.moles * grouped$Unified.
grouped$nonane.Unified.YSI <- grouped$nonane.moles/grouped$total.moles * 50.1
grouped$decane.Unified.YSI <- grouped$decane.moles/grouped$total.moles * 57.2
grouped$undecane.Unified.YSI <- grouped$undecane.moles/grouped$total.moles * 64.7
grouped$dodecane.Unified.YSI <- grouped$dodecane.moles/grouped$total.moles * 71.7
grouped$tridecane.Unified.YSI <- grouped$tridecane.moles/grouped$total.moles * 72.5
grouped$tetradecane.Unified.YSI <- grouped$tetradecane.moles/grouped$total.moles *

grouped$blend.Unified.YSI <- grouped$nonane.Unified.YSI + grouped$decane.Unified.YS
```

```{r}
g13 <- ggplot(grouped, aes(blend.TSI, Total.N.cc, shape = classification))
g13 <- g13 + geom_point()
g13 <- g13 + facet_grid(.~Aromatic.Volume)
g13 <- g13 +  ylab("BC Number Concentration [N/cc^3]")
g13 <- g13 + xlab("TSI")
g13 <- g13 + geom_smooth(method = "lm",
                         lwd = 1,
                         aes(linetype = classification),
                         se = FALSE,
                         colour = "blue")
g13 <- g13 + theme(axis.text.x = element_text(angle = 90, vjust = 0.5, hjust=1))

g13
```

```{r}
g14 <- ggplot(grouped, aes(blend.TSI,
                           Total.N.cc,
                           shape = classification,
                           colour = factor(Aromatic.Volume)))
```

```
g14 <- g14 + geom_point()
g14 <- g14 + geom_smooth(method = "lm",
                         lwd = 0.5,
                         col="black",
                         aes(linetype = classification),
                         se = FALSE)
g14 <- g14 + xlab("TSI")
g14 <- g14 + ylab("BC Number Concentration [N/cc]")

g14
```

```{r}
g15 <- ggplot(grouped, aes(blend.NSP, Total.N.cc, shape = classification))
g15 <- g15 + geom_point()
g15 <- g15 + facet_grid(.~Aromatic.Volume)
g15 <- g15 +  ylab("BC Number Concentration [N/cc^3]")
g15 <- g15 + xlab("NSP")
g15 <- g15 + geom_smooth(method = "lm",
                           lwd = 1,
                           aes(linetype = classification),
                           se = FALSE,
                           colour = "purple")
g15 <- g15 + theme(axis.text.x = element_text(angle = 90, vjust = 0.5, hjust=1))

g15
```

```{r}
g16 <- ggplot(grouped, aes(blend.NSP,
                             Total.N.cc,
                             shape = classification,
                             colour = factor(Aromatic.Volume)))
g16 <- g16 + geom_point()
g16 <- g16 + geom_smooth(method = "lm",
                         lwd = 0.5,
                         col="black",
                         aes(linetype = classification),
                         se = FALSE)
```

```
g16 <- g16 + xlab("NSP")
g16 <- g16 + ylab("BC Number Concentration [N/cc]")

g16
```

```{r}
# YSI

g17 <- ggplot(grouped, aes(blend.Unified.YSI, Total.N.cc, shape = classification))
g17 <- g17 + geom_point()
g17 <- g17 + facet_grid(.~Aromatic.Volume)
g17 <- g17 +  ylab("BC Number Concentration [N/cc^3]")
g17 <- g17 + xlab("Unified YSI")
g17 <- g17 + geom_smooth(method = "lm",
                         lwd = 1,
                         aes(linetype = classification),
                         se = FALSE,
                         colour = "pink")
g17 <- g17 + theme(axis.text.x = element_text(angle = 90, vjust = 0.5, hjust=1))

g17
```

```{r}
g18 <- ggplot(grouped, aes(blend.Unified.YSI,
                           Total.N.cc,
                           shape = classification,
                           colour = factor(Aromatic.Volume)))
g18 <- g18 + geom_point()
g18 <- g18 + geom_smooth(method = "lm",
                         lwd = 0.5,
                         col="black",
                         aes(linetype = classification),
                         se = FALSE)
g18 <- g18 + xlab("Unified YSI")
g18 <- g18 + ylab("BC Number Concentration [N/cc]")

g18
```

```{r}
alkylbenzene <- grouped[grouped$classification == "Alkylbenzene",]
polycyclics <- grouped[grouped$classification != "Alkylbenzene",]

alkyl.8 <- alkylbenzene[alkylbenzene$Aromatic.Volume==8,]
alkyl.13 <- alkylbenzene[alkylbenzene$Aromatic.Volume==13,]
alkyl.18 <- alkylbenzene[alkylbenzene$Aromatic.Volume==18,]


poly.8 <- polycyclics[polycyclics$Aromatic.Volume==8,]
poly.13 <- polycyclics[polycyclics$Aromatic.Volume==13,]
poly.18 <- polycyclics[polycyclics$Aromatic.Volume==18,]


# Volume

summary(lm(Total.N.cc~Aromatic.Volume, data = grouped))
summary(lm(Total.N.cc~Aromatic.Volume, data = alkylbenzene))
summary(lm(Total.N.cc~Aromatic.Volume, data = polycyclics))

# RC

summary(lm(Total.N.cc~Ring.Carbon, data = grouped))
summary(lm(Total.N.cc~Ring.Carbon, data = alkylbenzene))
summary(lm(Total.N.cc~Ring.Carbon, data = polycyclics))

summary(lm(Total.N.cc~Ring.Carbon, data = alkyl.8))
summary(lm(Total.N.cc~Ring.Carbon, data = alkyl.13))
summary(lm(Total.N.cc~Ring.Carbon, data = alkyl.18))


summary(lm(Total.N.cc~Ring.Carbon, data = poly.8))
summary(lm(Total.N.cc~Ring.Carbon, data = poly.13))
summary(lm(Total.N.cc~Ring.Carbon, data = poly.18))


# HC
```

```
summary(lm(Total.N.cc~Hydrogen.Content, data = grouped))
summary(lm(Total.N.cc~Hydrogen.Content, data = alkylbenzene))
summary(lm(Total.N.cc~Hydrogen.Content, data = polycyclics))

summary(lm(Total.N.cc~Hydrogen.Content, data = alkyl.8))
summary(lm(Total.N.cc~Hydrogen.Content, data = alkyl.13))
summary(lm(Total.N.cc~Hydrogen.Content, data = alkyl.18))


summary(lm(Total.N.cc~Hydrogen.Content, data = poly.8))
summary(lm(Total.N.cc~Hydrogen.Content, data = poly.13))
summary(lm(Total.N.cc~Hydrogen.Content, data = poly.18))


# Density

summary(lm(Total.N.cc~Density, data = grouped))
summary(lm(Total.N.cc~Density, data = alkylbenzene))
summary(lm(Total.N.cc~Density, data = polycyclics))

summary(lm(Total.N.cc~Density, data = alkyl.8))
summary(lm(Total.N.cc~Density, data = alkyl.13))
summary(lm(Total.N.cc~Density, data = alkyl.18))


summary(lm(Total.N.cc~Density, data = poly.8))
summary(lm(Total.N.cc~Density, data = poly.13))
summary(lm(Total.N.cc~Density, data = poly.18))



TSI.alkylbenzene <- TSI[TSI$classification == "Alkylbenzene",]
TSI.polycyclic <- TSI[TSI$classification != "Alkylbenzene",]

TSI.alkylbenzene.8 <- TSI.alkylbenzene[TSI.alkylbenzene$Aromatic.Volume.==8,]
TSI.alkylbenzene.13 <- TSI.alkylbenzene[TSI.alkylbenzene$Aromatic.Volume.==13,]
TSI.alkylbenzene.18 <- TSI.alkylbenzene[TSI.alkylbenzene$Aromatic.Volume.==18,]
```

```
TSI.polycyclic.8 <- TSI.polycyclic[TSI.polycyclic$Aromatic.Volume.==8,]
TSI.polycyclic.13 <- TSI.polycyclic[TSI.polycyclic$Aromatic.Volume.==13,]
TSI.polycyclic.18 <- TSI.polycyclic[TSI.polycyclic$Aromatic.Volume.==18,]


# TSI

summary(lm(Total.N.cc~blend.TSI, data = grouped))
summary(lm(Total.N.cc~blend.TSI, data = alkylbenzene))
summary(lm(Total.N.cc~blend.TSI, data = polycyclics))

summary(lm(Total.N.cc~blend.TSI, data = alkyl.8))
summary(lm(Total.N.cc~blend.TSI, data = alkyl.13))
summary(lm(Total.N.cc~blend.TSI, data = alkyl.18))


summary(lm(Total.N.cc~blend.TSI, data = poly.8))
summary(lm(Total.N.cc~blend.TSI, data = poly.13))
summary(lm(Total.N.cc~blend.TSI, data = poly.18))


# NSP

summary(lm(Total.N.cc~blend.NSP, data = grouped))
summary(lm(Total.N.cc~blend.NSP, data = alkylbenzene))
summary(lm(Total.N.cc~blend.NSP, data = polycyclics))

summary(lm(Total.N.cc~blend.NSP, data = alkyl.8))
summary(lm(Total.N.cc~blend.NSP, data = alkyl.13))
summary(lm(Total.N.cc~blend.NSP, data = alkyl.18))


summary(lm(Total.N.cc~blend.NSP, data = poly.8))
summary(lm(Total.N.cc~blend.NSP, data = poly.13))
summary(lm(Total.N.cc~blend.NSP, data = poly.18))


# YSI
```

```
summary(lm(Total.N.cc~blend.Unified.YSI, data = grouped))
summary(lm(Total.N.cc~blend.Unified.YSI, data = alkylbenzene))
summary(lm(Total.N.cc~blend.Unified.YSI, data = polycyclics))

summary(lm(Total.N.cc~blend.Unified.YSI, data = alkyl.8))
summary(lm(Total.N.cc~blend.Unified.YSI, data = alkyl.13))
summary(lm(Total.N.cc~blend.Unified.YSI, data = alkyl.18))



summary(lm(Total.N.cc~blend.Unified.YSI, data = poly.8))
summary(lm(Total.N.cc~blend.Unified.YSI, data = poly.13))
summary(lm(Total.N.cc~blend.Unified.YSI, data = poly.18))

```

```

```{r}
# Alkylbenzenes

alkylbenzene <- grouped[grouped$classification == "Alkylbenzene",]
polycyclics <- grouped[grouped$classification != "Alkylbenzene",]

 a <- (lm(Total.N.cc~

                    Density +
                     # Hydrogen.Content +
                     # blend.TSI +
                     # blend.NSP +
                     blend.Unified.YSI,
            data = alkylbenzene))

plot(alkylbenzene$Total.N.cc,predict(a, alkylbenzene))

alkylbenzene <- cbind(alkylbenzene, predict(a, alkylbenzene))

g19 <- ggplot(alkylbenzene, aes(`predict(a, alkylbenzene)`,
                          Total.N.cc,
                          colour = factor(Aromatic.Volume)
                          ))
```
```

```
g19 <- g19 + geom_point()
g19 <- g19 + geom_smooth(method = "lm", lwd = 0.3,

                         se = FALSE,
                         colour = "black")
g19 <- g19 + xlab("Predicted BC")
g19 <- g19 + ylab("Actual BC")
g19

standard_res_alkyl <- rstandard(a)

alkylbenzene <- cbind(alkylbenzene, standard_res_alkyl)

alkylbenzene$conc <- paste(alkylbenzene$Aromatic.Type,alkylbenzene$Aromatic.Volume, sep =

g20 <- ggplot(alkylbenzene)
g20 <- g20 + geom_bar(aes(x = conc, y = standard_res_alkyl), stat = "identity", fill = "
g20 <- g20 + theme(axis.text.x = element_text(angle = 90, vjust = 0.5, hjust=1))
g20 <- g20 + xlab("Blend") + ylab("Standardised Residual")
g20

# Polycyclics

alkylbenzene <- grouped[grouped$classification == "Alkylbenzene",]
polycyclics <- grouped[grouped$classification != "Alkylbenzene",]

 b <- (lm(Total.N.cc~

                  Density +
                  # Hydrogen.Content +
                  # blend.TSI +
                  # blend.NSP +
                  blend.Unified.YSI,
          data = polycyclics))

plot(polycyclics$Total.N.cc,predict(b, polycyclics))

polycyclics <- cbind(polycyclics, predict(b, polycyclics))
```

```
g21 <- ggplot(polycyclics, aes(`predict(b, polycyclics)`,
                               Total.N.cc,
                               colour = factor(Aromatic.Volume)
                               ))
g21 <- g21 + geom_point()
g21 <- g21 + geom_smooth(method = "lm", lwd = 0.3,

                                se = FALSE,
                                colour = "black")
g21 <- g21 + xlab("Predicted BC ")
g21 <- g21 + ylab("Actual BC")
g21

standard_res_poly <- rstandard(b)

polycyclics <- cbind(polycyclics, standard_res_poly)

polycyclics$conc <- paste(polycyclics$Aromatic.Type, polycyclics$Aromatic.Volume, se

g22 <- ggplot(polycyclics)
g22 <- g22 + geom_bar(aes(x = conc, y = standard_res_poly), stat = "identity", fill
g22 <- g22 + theme(axis.text.x = element_text(angle = 90, vjust = 0.5, hjust=1))
g22 <- g22 + xlab("Blend") + ylab("Standardised Residual") + ylim(-3,3)
g22

# Unified

complete.use <- grouped

c <- (lm(Total.N.cc~

                    Density +
                     # Hydrogen.Content +
                     # blend.TSI +
                     # blend.NSP +
                     blend.Unified.YSI,
          data = complete.use))

plot(complete.use$Total.N.cc, predict(c, complete.use))
```

```
complete.use <- cbind(complete.use, predict(c, complete.use))

g23 <- ggplot(complete.use, aes(`predict(c, complete.use)`,
                          Total.N.cc,
                          colour = factor(Aromatic.Volume)
                          ))
g23 <- g23 + geom_point()
g23 <- g23 + geom_smooth(method = "lm", lwd = 0.3,

                           se = FALSE,
                            colour = "black")
g23 <- g23 + xlab("Predicted BC ")
g23 <- g23 + ylab("Actual BC")
g23

standard_res_unified <- rstandard(c)

complete.use <- cbind(complete.use, standard_res_unified)

complete.use$conc <- paste(complete.use$Aromatic.Type,complete.use$Aromatic.Volume, sep =

g24 <- ggplot(complete.use)
g24 <- g24 + geom_bar(aes(x = conc, y = standard_res_unified), stat = "identity", fill =
g24 <- g24 + theme(axis.text.x = element_text(angle = 90, vjust = 0.5, hjust=1))
g24 <- g24 + xlab("Blend") + ylab("Standardised Residual")
g24

write.table(complete.use, "DMS.complete")

```
```
```{r}
# GMD vs BC Number

plot(complete.use$GMD, complete.use$Total.N.cc)

complete.use[complete.use$classification=="Polycylic"]
complete.use[complete.use$classification=="Alkylbenzene"]
```
```

```
g25 <- ggplot(complete.use, aes(GMD,
                                Total.N.cc,
                                shape = classification,
                                colour = factor(Aromatic.Volume)))
g25 <- g25 + geom_point()
g25 <- g25 + geom_smooth(method = "lm",
                         lwd = 0.5,
                         col="black",
                         aes(linetype = classification),
                         se = FALSE)
g25 <- g25 + xlab("GMD")
g25 <- g25 + ylab("BC Number Concentration [N/cc]")

g25

summary(lm(Total.N.cc~GMD, data = complete.use))

summary(lm(Total.N.cc~GMD, data = complete.use[complete.use$classification=="Alkylb

summary(lm(Total.N.cc~GMD, data = complete.use[complete.use$classification=="Polyc
```